

THE WILD GOOSE ASSOCIATION



PROCEEDINGS OF THE
NINTH ANNUAL TECHNICAL SYMPOSIUM
22-24 OCTOBER 1980
BOSTON, MASSACHUSETTS



PUBLISHED BY
THE WILD GOOSE ASSOCIATION
P.O. BOX 413A
ACTON, MASSACHUSETTS 01720

THE WILD GOOSE ASSOCIATION

The Wild Goose Association (WGA) is a professional organization of individuals and organizations having an interest in loran (long range navigation). It is named after the majestic birds that navigate thousands of miles with unerring accuracy. The WGA was organized in 1972 and its membership now includes hundreds of professional engineers, program managers, scientists and operational personnel from all segments of government, industry, and the user community throughout the world, working for the advancement of loran.

CONVENTION COMMITTEE

W.F. Rice Chairman
B.J. Uttam Guest Speakers
C.A. Ippolito Administration
Cdr. D. Amos Technical Program
L.D. Higginbotham Hospitality

BOARD OF DIRECTORS 1979-80

B.J. Uttam President
V.L. Johnson Vice President
B. Ambroseno Secretary
C.S. Andren Treasurer

R. Abraczinskas
P.D. Abramson
W.N. Dean
L.F. Fehlner
G.A. Gutman
G.C. Haroules
L.D. Higginbotham
W.H. Hilbun, III
E.L. McGann
W.F. Rice
W.F. Roland
J.P. Van Etten
V.I. Weihe

BOARD OF DIRECTORS 1980-81

B. Ambroseno President
W.N. Dean Vice President
L.F. Fehlner Secretary
C.S. Andren Treasurer

R. Abraczinskas
P.D. Abramson
J.M. Beukers
G.C. Haroules
L.D. Higginbotham
J.D. Illgen
V.L. Johnson
E.L. McGann
B.J. Uttam
J.P. Van Etten
V.I. Weihe

TABLE OF CONTENTS

	<u>Page No.</u>
BIOGRAPHIES	1
SESSION I - COMMERCIAL MARINE APPLICATIONS	11
SAVINGS IN ENERGY AND TIME THROUGH ADVANCED TECHNIQUES IN LORAN C NAVIGATION, by Bernard Ambrosino and Heinz Buhrig	12
ST. MARYS RIVER LORAN-C MINI-CHAIN--- THE BOTTOM LINE, by Jack M. Ligon and Lt. David Olsen, USCG	22
ERROR ANALYSES OF LORAN-BASED BUOY POSITION AUDITING SYSTEM, by J.M. Foltz, L.M. DePalma, and J.A. Wolfson	29
SESSION II - POSITIONING TECHNOLOGY	41
PERFORMANCE REQUIREMENTS FOR RADIO NAVIGATION SYSTEMS IN HARBORS AND HARBOR WATERWAYS, by W.R. Bertsche, R.B. Cooper, D.A. Feldman, and Karl R. Schroeder	42
QUANTIFICATION OF ST. MARYS RIVER LORAN-C TIME DIFFERENCE GRID INSTABILITY, by L.M. DePalma, P.M. Creamer, and E. Anderson	51
STOCHASTIC INVESTIGATION ON THE SEARCH PROCESS OF A LORAN-C RECEIVER, by Kiyohiko Tatebayashi, Mikio Nakamura, and Tadayuki Yamada	62
LORAN-C/D APPLICATION TO TACTICAL RECONSTRUCTION INFORMATION POD (TRIPOD), by John J. Hopkins	72
LORAN-C FLIGHT TESTING IN THE WESTERN UNITED STATES, by Edwin D. McConkey and Thomas E. Scalise	80
SESSION III - SIGNAL QUALITY ASSURANCE	93
A LORAN-C TRANSMITTER SIMULATOR, by Kiyoshi Tamura, Kiyohiko Tatebayashi and Tadayuki Yamada	94
OPERATION OF A REMOTE CONTROL SYSTEM AT LORAN STATION PORT HARDY, BC, CANADA, by LCDR Ron Frazier, LT George Gunther, and LT Richard Sellers, USCG	103
SESSION IV - LAND VEHICLE APPLICATIONS	113
HYBRID LORAN-C FOR AUTOMATIC VEHICLE LOCATION, by Dr. John Hovorka	114
"CAR 54 - WHERE ARE YOU?", by Bahar Uttam and William O'Halloran	117
TWO LAND VEHICLE TRACKING SYSTEMS, by Jacob Parness	121
A HYBRID LORAN / DIFFERENTIAL ODOMETER SYSTEM FOR LAND VEHICLE NAVIGATION, by W.M. Bowles and R.R. Hildebrandt	138
LORAN-C POSITIONING TESTS IN NEW YORK, by Walter N. Dean	146
CONVENTION SCENE AND AWARDS	159
REGISTERED ATTENDANCE	167

THE AUTHORS



Biographical Sketch of Bernard Ambroseno

Mr. Ambroseno is Product Manager for Navigation Systems at EPSO, Inc. Prior to this he was a member of the technical staff, Applied Science Lab., at Harvard University, designing Ionospheric Sounder and Radar Countermeasure equipments. During employment with Northrup Nortronics Marine Equipment Div. he was Senior Engineer-Chief of the Radiometric Navigation and Communications Group, designing navigation and communications equipment, and the design and study of hardened and underwater communications system. At Pickard and Burns (Div. of LTV), he was principal engineer, specializing in navigation and timing equipment, antenna systems including submarine VFL antenna and a scale model of an Omega transmitting antenna for ONR. He also conducted FAA studies on Omega Lane Resolution in the Western Hemisphere. Mr. Ambroseno is presently on the Board of Directors for the International Omega Assoc., Secretary of the Wild Goose Association (V.P. of the New England Chapter), member of I.O.N. and R.T.C.M. Minimum Performance Standards for LORAN-C receiving equipments, Special Committee No. 70.

Biographical Sketch of Everett Anderson

Everett Anderson is currently responsible for radio aids to navigation projects at the U.S. Coast Guard Research and Development Center in Groton, Conn. Since joining the Center in 1973, he has directed design and development of remote monitor instrumentation systems, evaluation of microwave ranging systems, and directed testing, evaluation and analysis of LORAN-C propagation characteristics for short base-line chains. Prior to employment at the Research and Development Center in 1973, Mr. Anderson directed design and development of aircraft instrumentation systems at G.E. and Simonds Precision Products. His background also includes development of biomedical, nuclear, sound and vibration analysis and control systems. Mr. Anderson received a B.S. in Physics from Trinity College; B.E.E. in Electronic Engineering from Rensselaer Poly. Institute; and did graduate studies at the University of Connecticut.

Biographical Sketch of William R. Bertsche



Mr. Bertsche is Director of Engineering at Eclectech Associates, Inc. In this capacity he has conducted a wide range of research projects for the U.S. Coast Guard and U.S. Maritime Administration ranging from port design problems to the design of standardized bridges and bridge equipments for U.S. merchant ships. Mr. Bertsche has directed a number of experiments at the Computer Aided Research Facility (CAORF), Kings Point, New York.

Mr. Bertsche is project director of the U.S. Coast Guard's Performance of Aids to Navigation Program which is evaluating radio and visual aids to navigation systems and their impact on the safety of navigating in narrow channels. Mr. Bertsche is a member of the Society of Naval Architects and Marine Engineers and the Permanent International Association of Navigation Congresses (PIANC).



Biographical Sketch of Professor W. Michael Bowles

Professor Bowles joined the faculty of M.I.T. after receiving his Doctor of Science degree from the Department of Aeronautics and Astronautics at M.I.T. in 1980. His Sc.D. thesis was on "Correlation Tracking". He is the first occupant of the C. Stark Draper Chair at M.I.T. in that department. Prior to receiving his degree, Prof. Bowles worked as a staff engineer and Research Associate at the C.S. Draper Laboratory. Professor Bowles has been teaching courses in modern control theory and conducts research in vehicle navigation and estimation. He has written several publications and contract reports, including ones on perturbation approximations and density approximations for nonlinear filtering problems and efficient hardware configurations for tracking loops with deformable nonlinearities.

Professor Bowles fields of interest include nonlinear estimation, automatic control, hybrid navigation, and optimal control.



Biographical Sketch of Heinz Buhrig

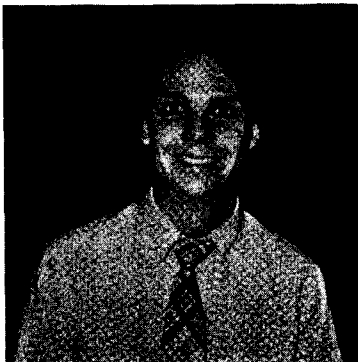
Mr. Heinz Buhrig was born in Braunschweig, Germany, where he received his college training in electronics. While attending Canterbury College, in England, he was employed in the design evaluation of radar and autopilot systems. At Canterbury he specialized in ONC mechanics. After graduation he was design engineer for autopilots and later became technical director of an autopilot manufacturing company. He is employed by EPSCO Marine of Westwood, Mass., as both Design Engineer for Autopilots and Autopilot Product Manager. He is a member of ASEE.



Biographical Sketch of Richard B. Cooper

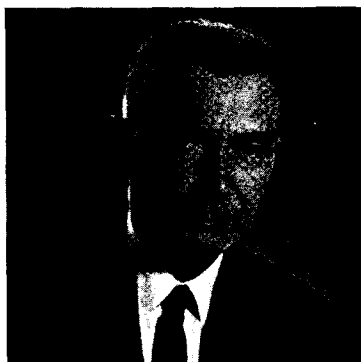
Mr. Cooper is a human factors engineer at Eclectech Associates, Inc., specializing in the design and simulator evaluation of shipboard navigation, communications and automatic radar plotting displays. Since his mid-1960s work on human factors in ship control, Mr. Cooper has been involved in the advanced bridge design program of the U.S. Maritime Administration. This project evaluates proposed and developmental bridge concepts using both the Eclectech Associates' SIMSHIP simulator and CAORF, the Computer Aided Operations Research Facility at Kings Point, New York. Mr. Cooper is presently conducting evaluations of electronic radio aids to navigation displays. This project being performed for the U.S. Coast Guard will ultimately lead to a specification of performance requirements for radio navigation systems in harbors and harbor waterways.

Mr. Cooper is a member of the Human Factors Society and the Society for Information Display.



Biographical Sketch of Paul M. Creamer

In the past two years, Paul M. Creamer has been involved in a number of radionavigation studies at The Analytic Sciences Corporation. In the St. Marys River LORAN-C data analysis effort, he designed and implemented a data-base management system which was successfully used to maintain, edit and display large volumes of data. Previously, he was involved in the development of a TD grid prediction model for the U.S. West Coast LORAN-C chain. In addition, Mr. Creamer has participated in several Omega Navigation System studies, including the development of a signal amplitude prediction model and the subsequent production of signal coverage diagrams. Mr. Creamer received his B.S. degree in Mathematics from Trinity College in 1977 and is currently pursuing an M.S. degree in Systems Engineering at Boston University.



Biographical Sketch of Walt Dean

Walt Dean has been involved in the development of LORAN-C, its predecessors and its offspring, for over 30 years. Although deeply involved in system concept and design, his major activity has been in test and evaluation of operating systems to understand better their peculiarities, and finding new ways to utilize the system. Mr. Dean retired from Magnavox in 1974 and formed his own consulting company, Verdes Engineering Co. He has since done work for the U.S. Coast Guard, New York State, and several private firms, including Magnavox, on LORAN and GPS studies.

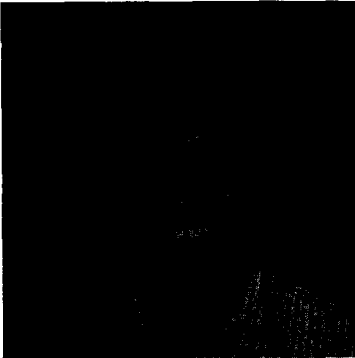
Some of his earlier activities included non-paying jobs as Chief Engineer of Fort Wayne Public Television, and Chairman of the Fort Wayne Section of IEEE. He has published over 15 papers and has 10 issued patents on LORAN and radar.



Biographical Sketch of Leon DePalma

Dr. Leon DePalma has been engaged in studies of the LORAN-C radionavigation system for three years at The Analytic Sciences Corporation. These studies include data-oriented and theoretical analyses of low-frequency signal propagation, and evaluation of proposed LORAN-C system applications. His efforts related to signal propagation have involved Time Difference grid calibration for the St. Marys River and Mediterranean Sea LORAN-C chains. System studies have included applications of LORAN-C to buoy position auditing and civil aircraft navigation.

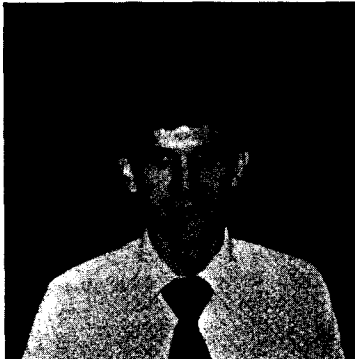
In 1972, Dr. DePalma received the B.S. degree in Electrical Engineering from the University of Pittsburgh. He received the Ph.D. degree in Computer, Information and Control Engineering from the University of Michigan in 1977.



Biographical Sketch of CAPT Don Feldman

Capt Don Feldman is a graduate of the Coast Guard Academy and MIT. He has worked for seventeen years in the field of radio navigation, primarily LORAN-C and more recently other systems such as GPS and visual aids-to-navigation. He headed the Navigation Branch of the Coast Guard's R&D program during the period of the research reported here.

Capt Feldman is currently assigned to a task force which is studying better ways to use computers in the management of the Coast Guard.



Biographical Sketch of James M. Foltz

Dr. James M. Foltz has been engaged in modeling and analysis of various navigation aids and integrated navigation systems since joining The Analytic Sciences Corporation in 1974. His experience has been in the areas of doppler sonar, sonar transponders, ocean current modeling, and the Omega and LORAN-C radionavigation systems. In the Buoy Position Auditing System Study, he developed interactive graphics for analysis of candidate system configurations. In the Alaskan Differential Omega Program, he developed a detailed random-propagation-anomaly model to estimate the navigation error induced by Omega phase errors. Dr. Foltz received the B.S. degree in engineering from Swarthmore College, and the M.S. and Ph.D. degrees in electrical engineering from Rice University.



Biographical Sketch of LCDR Ron Frazier

LCDR Ron Frazier was commissioned in the U.S. Coast Guard in 1971 after graduating from the U.S. Coast Guard Academy. After two years of sea duty he attended MIT and received SM(EE) and EE degrees in 1975.

He is presently assigned to the Systems Development Branch at Coast Guard Headquarters and is the Project Manager for the Remote Control System Project. Prior to his present assignment, he was assigned to Electronics Engineering Center in Wildwood, New Jersey as a Project Manager.

He has been a member of the Wild Goose Association since 1976.



Biographical Sketch of LT Tom Gunther

Lt Tom Gunther is a 1973 graduate of the U.S. Coast Guard Academy. He has served aboard the USCG Icebreaker STATEN ISLAND and Cutter BOUTWELL for his duties which ranged from Student Engineer to Damage Control/Assistant Engineering Officer. Following these tours, Lt Gunther was selected for Coast Guard postgraduate training. In 1977 Lt Gunther received a BS and MS degree in Electronics Engineering from the University of Michigan.

Since this period in time Lt Gunther has been stationed at the U.S. Coast Guard Electronics Engineering Center, Wildwood, New Jersey, where he has been involved in the installation and certification of the NEUS, SEUS, and CWC Solid State Transmitter, and also the RCS and various other LORAN-C projects.



Biographical Sketch of Richard Hildebrant

Dr. Richard Hildebrant is a member of the Research Staff at the C.S. Draper Laboratory in Cambridge, Massachusetts. He received his B.S. degree in Engineering from the State University of New York, at Buffalo, in 1970; his M.S. and Ph.D. were received from the Massachusetts Institute of Technology, in the Department of Aeronautics and Astronautics in 1972 and 1980, respectively.

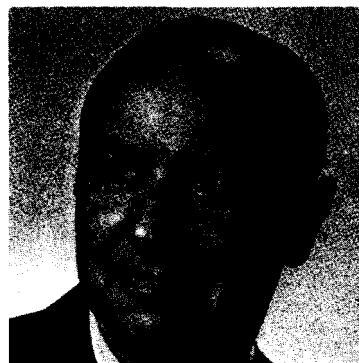
In addition to the application of modern control and estimation theory, his research interests include the application of Operations Research techniques to large scale manufacturing systems.



Biographical Sketch of John Hopkins

John Hopkins has been active in land, sea and air navigation systems and flight instrumentation and controls for 30 years. Before beginning his practice as an independent consultant in 1980, he was General Manager of Navigation Products for Teledyne Systems Company and Assistant to the President for New Product Development. At Teledyne responsibilities included LORAN C and Omega design, development, manufacturing and worldwide sales and service; also responsibility for proposals for various integrated navigation systems (LORAN-Inertial, Doppler-LORAN-Inertial, LORAN-Omega and NAVSTAR GPS). Prior experience included 15 years with Sperry Gyroscope Company. Various assignments were Manager of Marketing and Contracts for inertial, doppler and compass systems and flight and engine instruments, marketing flight and engine instruments, and flight control field engineering.

He received a BEE degree from Manhattan College in New York in 1951, and completed the UCLA Graduate School of Management Executive Program in 1977. He is an active member of the Institute of Navigation and has authored many papers on the subject which have been published in industry journals.



Biographical Sketch of John Hovorka

Dr. John Hovorka is Professor of Physics and Chairman of the Division of Sciences and Mathematics at Curry College in Milton, Massachusetts. Prior to this he was Associate Director of the Measurement Systems Laboratory at MIT, where he was engaged in navigation experiments for the Naval Oceanographic Office, and also in a space-conducted experiment to test the principle of equivalence in Einstein's general theory of relativity.

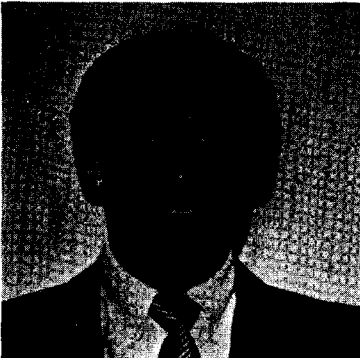
Dr. Hovorka holds a BS degree from Queens College, MS from the University of Illinois, and ScD degree in engineering from MIT.



Biographical Sketch of Jack Ligon

Mr. Jack Ligon has been the Radio Aids to Navigation Project Area Manager for the U.S. Coast Guard Office of Research and Development for the past two years. The focus of his present efforts are precision use of LORAN-C and civil-marine use of NAVSTAR-GPS. His twenty years of Coast Guard service have been devoted to both communications and radio aids to navigation. His work with LORAN has covered the entire spectrum from precision simulation to treatment as a source of interference. He is presently a member of RTCM Study Commission SC-75 "MPS--Automatic Coordinate Conversion Systems".

Mr. Ligon holds a MSE degree from the University of Pennsylvania and a BSEE degree from Virginia Polytechnic Institute. He is a registered Professional Engineer in the State of Virginia, a member of the Institute of Navigation, and a fellow honker. His outside interests include church activities, carpentry, sailing, and camping.



Biographical Sketch of Edwin D. McConkey

Mr. Edwin D. McConkey received his B.S. degree in Electrical Engineering and Mathematics from the University of Michigan in 1963, and received his B.S. in Electrical Engineering in 1964. He continued graduate studies in Automatic and Optimal Control Systems in partial fulfillment of Ph.D. requirements. His professional experience as a systems engineer in navigation includes the Institute of Science and Technology at the University of Michigan, Polhemus Navigation Sciences, Inc., and his current position as a Senior Engineer at the Champlain Technology Industries Division of Systems Control, Inc. (Vt). Recently he has been program manager or project engineer for several programs concerned with the use of area navigation in civil aviation. These programs include the Microwave Landing System and LORAN-C.

Mr. McConkey is a member of TAU BETA PI and ETA KAPPA NU, and he is a registered professional engineer in the State of Florida.



Biographical Sketch of Mikio Nakamura

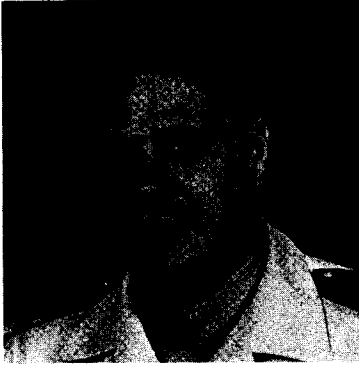
Mr. Mikio Nakamura was born in Kobe, Japan, in 1952. He received the B.S. degree in pure and applied sciences from the University of Tokyo, Japan, in 1975. He then became employed by Japan Radio Company, Ltd., where he is presently involved in the research and development of navigation systems.

Mr. Nakamura is presently a member of the IEE, the IECE, and the SICE of Japan.



Biographical Sketch of William F. O'Halloran

Mr. William F. O'Halloran is currently Technical Director of JAYCOR's Systems Engineering Division. He has fourteen years experience in the application of modern estimation and control concepts. He is currently investigating the impact of navigation and communications systems on Navy Task Force command and control. His previous experience includes error modeling, simulation, test design, performance evaluation, model validation and software development for navigation systems. He has been involved in all facets of radionavigation systems including LORAN-C. Mr. O'Halloran has authored 12 papers in the application of modern estimation and control techniques to a variety of navigation and weapon systems problems. He was also a contributing editor to a text book "Applied Optimal Estimation," (MIT Press, 1974). Mr. O'Halloran is a member of the IEEE, AIAA, Society of Photo-Optical Instrumentation Engineering, the Institute of Navigation and Wild Goose Association.



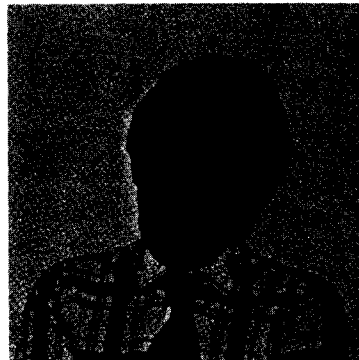
Biographical Sketch of LCDR Dave Olsen

LCDR Dave Olsen has been involved with the LORAN-C navigation system since the start of his Coast Guard career in 1971. He spent his first tour of duty at the Coast Guard's Electronics Engineering Center in Wildwood, New Jersey, where he worked on the automation of LORAN-C monitor and control equipment. From 1975 to 1980, LCDR Olsen was assigned to the Office of Research and Development at Coast Guard Headquarters where he was responsible for the development of LORAN-C user equipment for precision navigation, and for chain stability studies. He is presently assigned to the Icebreaker Support Facility in Seattle, where he is responsible for the shore-side support of electronic systems for the Coast Guard's newest and largest Polar-Class icebreakers. LCDR Olsen holds Bachelor and Master of Science degrees in Electrical Engineering from Iowa State University at Ames and the University of Illinois at Urbana. He is a member of the Wild Goose Association and the Institute of Navigation.



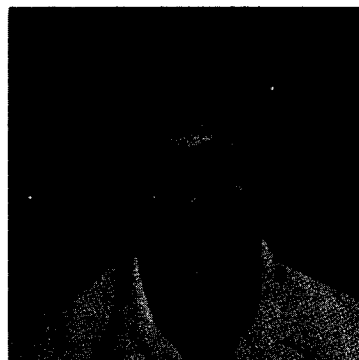
Biographical Sketch of Jacob Parness

Mr. Jacob Parness received his BEE degree from City College New York in 1963, and his MEE from Polytechnic Institute of Brooklyn in 1968. Mr. Parness joined the MITRE Corp. in 1969 and is presently a Senior Systems Engineer in the Defense Systems Evaluation Department involved with advanced submarine communication concepts. Recent assignments include the development of vehicle tracking systems, application of geostationary satellites to the land-mobile user, and the design and development of a microprocessor-based military data link evaluator system. He previously was employed by the Airborne Instrument Laboratory for 7 years and was involved in the development and flight evaluation of synthetic aperture radars. Mr. Parness recently completed a series of projects sponsored by the Department of Transportation, the Philadelphia Fire Department, the Washington Area Metropolitan Transit Authority and the Drug Enforcement Administration, involving the development of terrestrial LORAN-C receivers and their technical performance characteristics for use in tracking ambulances, buses and law enforcement vehicles.



Biographical Sketch of Thomas E. Scalise

Mr. Thomas E. Scalise received his B.S. in Advertising from the University of Florida in 1964, and his B.A.S. (Bachelor of Applied Science) in computer systems from Florida Atlantic University in December 1978. Mr. Scalise holds an FAA Commercial Pilot License for single and multi-engine, is instrument rated, has a type rating for Boeing 707/720 aircraft, and a Flight Engineers License for turbojet aircraft. While in the U.S. Air Force he flew as a co-pilot/instructor in the KC135A, and as an aircraft commander on C-123K aircraft. Mr. Scalise joined the staff of the Champlain Technology Industries Division of SCI (Vt.) in 1978. At SCI he has performed an operational analysis of RNAV/MLS cockpit procedures and developed a series of candidate MLS flight profiles for a variety of sites and procedures. Mr. Scalise recently served as an experimental subject pilot for an SCI/FAA flight test program involving the evaluation of LORAN-C as an approach aid in the mountainous West Coast terrain. He performed much of the data processing and report preparation for that program.



Biographical Sketch of Karl R. Schroeder

Mr. Karl R. Schroeder is now the Short Range Aids to Navigation Section Chief for the U.S. Coast Guard Office of Research and Development. He has been involved with the development of aircraft and marine navigation systems for 29 years, and in particular, LORAN-C and Omega receivers for 15 years at Sperry Gyroscope Company and Litton Industries. His specialty is systems engineering and managing programs.

Mr. Schroeder received a B.S.E.E. from Lafayette College in 1949 and an M.S.E.E. from Northwestern University in 1951. He is a member of Tau Beta Pi, Sigma Xi, Eta Kappa Nu, a Senior Member of I.E.E.E. and Charter Member of the Wild Goose Association.



Biographical Sketch of LT Richard J. Sellers

Lt. Sellers is a 1972 graduate of the U.S. Coast Guard Academy. After graduation he served as First Lieutenant aboard the USCGC ACUSHNET in Gulfport, Mississippi. He then commanded the USCGC CAPE KNOX in Miami, Florida. In 1976 he received his MSEE from the University of Michigan and is now stationed at the U.S. Coast Guard Electronics Engineering Center in Wildwood, New Jersey.

Lt. Sellers is a native of Colorado. He has been a project engineer on the Port Hardy, B.C. Remote Control System since its conception. Installation of transmitting timing equipment for the Canadian East Coast, Great Lakes, and LORAN Station Port Hardy have been other projects Lt. Sellers has been involved with while at the Electronics Center.

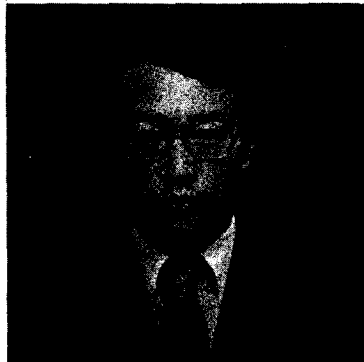


Biographical Sketch of Kiyoshi Tamura

Mr. Kiyoshi Tamura was born at Oyama, Japan, in 1948. He joined Japan Radio Co., Ltd., in 1966, and received the B.S. Degree in Electrical Engineering from CHUO University, Tokyo, in 1971.

From 1974 to 1975 he worked with The Institute of Industrial Science, University of Tokyo, and studied Digital Processing of Meteorological Satellite (NOAA) Imagery. He is now engaged in the research and development of image processing systems.

He is a member of the IECE and the SICE of Japan.



Biographical Sketch of Kiyohiko Tatebayashi

Mr. Kiyohiko Tatebayashi was born in Yaizu, Japan, in 1947. He received the B.S. degree in Electrical Engineering from the University of Tohoku, Japan, in 1970. He then joined Japan Radio Co., Ltd., Tokyo, in 1970. From 1976 to 1978, he studied the stochastic signal processing in the Faculty of Engineering, University of Tokyo. He is now engaged in the research and development of navigation systems and industrial measurement systems.

Mr. Tetebayashi is a member of the SICE of Japan.



Biographical Sketch of Bahar J. Uttam

Mr. Bahar J. Uttam is Vice President and Director of JAYCOR's Systems Engineering Division. He has had fourteen years experience in all facets of navigation systems for both military and civil applications. He has also been involved in definition and design of C³ systems. Some of the studies he has been involved in include Grid Data Management System Design for USAF tactical operations, design of integrated navigation systems for onboard (airborne and shipboard) use and a large number of radionavigation system analysis and design efforts. He is currently involved in defining navigation requirements for civil users at the state and local levels.

Mr. Uttam has been on the Board of Directors of the WGA for the past four years including two years as President. He was the founder and associate editor of the Radionavigation Journal. Mr. Uttam has authored fifteen papers on the application of modern estimation to navigation problems.



Biographical Sketch of Joseph A. Wolfson

Mr. Joseph A. Wolfson is currently an electronic engineer on the technical staff at the DOT/Transportation Systems Center. His work includes project/system engineering of advanced telecommunications, navigation and surveillance systems encompassing terrestrial-based and satellite technology. Prior to joining TSC in 1971, Mr. Wolfson was with Laboratory for Electronics for twenty years doing program management, project engineering and system development and test in the fields of HF, VHF, and UHF communications; MTI radar surveillance; radar altimetry; and Doppler radar, LORAN and Decca navigation. Previous to LFE, his work included design and test of AM, FM and TV broadcast stations and communications antenna development and test.

Mr. Wolfson received his BSEE in 1947 from Northeastern University and completed numerous graduate engineering and management courses.



Biographical Sketch of Tadayuki Yamada

Mr. Tadayuki Yamada was born in Hiroshima, Japan, in 1935, and received the B.S. Degree in Electrical Engineering from Nagoya Institute of Technology, Nagoya, Japan, in 1960. He joined Japan Radio Co., Ltd., Tokyo, in 1960. He is now engaged as Assistant Manager of JRC Laboratory, in the research and development of navigation systems, industrial measurement systems, and image processing systems, and is also interested in digital signal processing.

SESSION I
COMMERCIAL MARINE APPLICATIONS

SAVINGS IN ENERGY AND TIME THROUGH ADVANCED TECHNIQUES IN LORAN C NAVIGATION

BERNARD AMBROSENO
HEINZ BUHRIG

EPSCO MARINE
Division of EPSCO, INCORPORATED
411 Providence Highway
Westwood, Massachusetts 02090

ABSTRACT

Continuing advances in LORAN C navigation techniques are having greater impact on the fishing industry through conservation of energy, savings in time and money, and improved safety conditions. The advances in LORAN C have already revolutionized the fishing industry, where LORAN C is now the most preferred navigation system (over Satellite and Omega) because of its high degree of accuracy and repeatability attainable in real-time continuous navigation. The recent innovation of an XY microprocessor plotter has enhanced the LORAN C system by providing continuous position information in a graphic display. And now, by combining these recent advances with the new LORAN C controlled Auto-Pilot, the fisherman has a complete, compact, and precise navigation system.

INTRODUCTION

Hyperbolic navigation systems yield position data as the intersection of selected hyperbolas where the identification and shape of the hyperbolic line in any local area are a function of the system geometry. Navigators must therefore use charts bearing the hyperbolic line set or have the computational capability to convert hyperbolic data

to the familiar latitude/longitude coordinate system. In order to enhance the utility of hyperbolic navigation data, an electromechanical plotter which permits a non-technical navigator to see and track his position on a two-dimensional chart was developed (Figures 1 and 2). Using a microprocessor, the plotter transforms the hyperbolic data into corresponding north-south or east-west position changes.

Present receivers (Figure 11) utilize the same hyperbolic information to determine speed over ground. Since currents and winds have adverse effects when using RPM as an indicator of speed, present emphasis is on the greater reliance on LORAN C for speed indication.

Using LORAN C data to control ship heading to a destination is now possible through the complementing of the conventional autopilot with a LORAN C autopilot, EPSCO's C-Pilot (Figure 16). These innovations illustrate that LORAN hyperbolic navigation is finding application beyond the mere indication of present position.

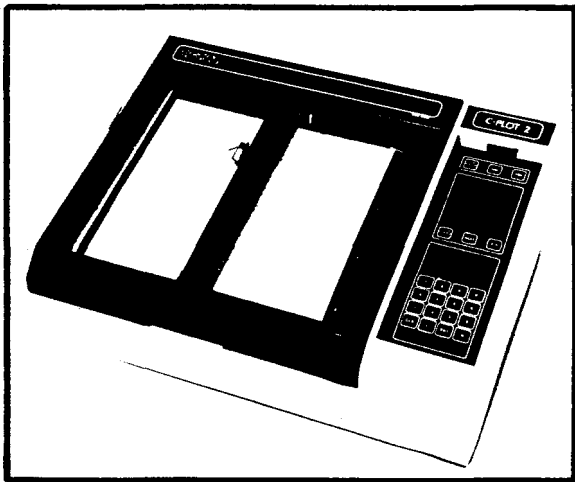


Figure 1. LORAN C Position Plotter

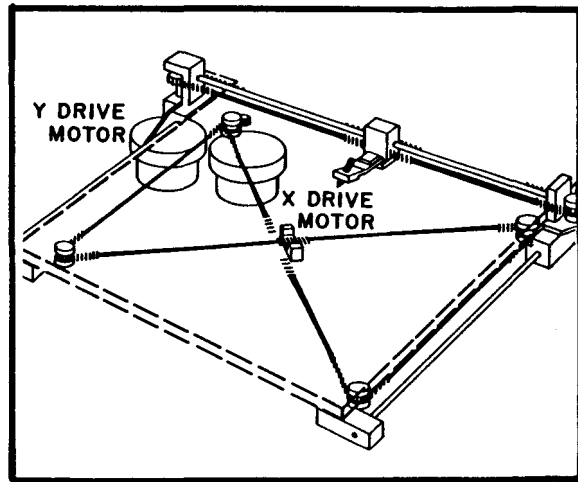


Figure 2. Pen Drive System

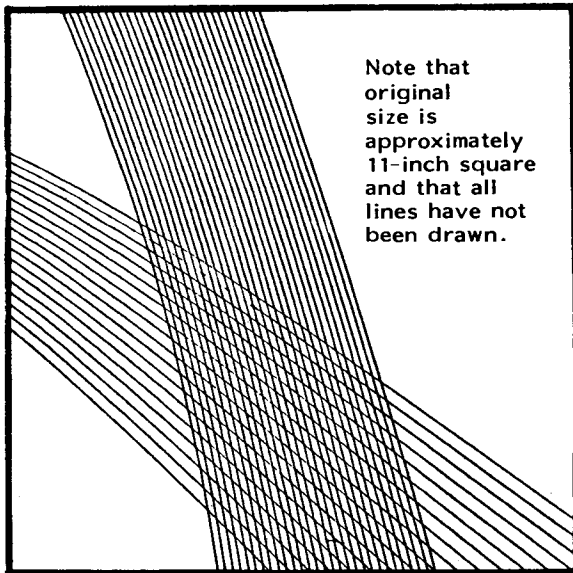


Figure 3. Time Difference Plot

LORAN PLOTTERS

THEORY OF OPERATION

The plotter records the track of a vessel or of a vehicle on an 11-3/4-inch square of chart paper. The pen position is determined from radio navigation data. TD (time difference) data are automatically transformed to north-south and east-west components to allow track plotting with a Mercator map projection.

A set of TD lines can be automatically drawn for each of two LORAN C Master/Secondary station pairs. The number of lines and the line-spacing is selectable by the operator. The track of the vessel is shown with respect to a "reference" position which is selectable by the operator and is inserted into the plotter via its keyboard before plotting begins.

A computer within the plotter transforms LORAN data to produce a plot on the equivalent of a Mercator equidistant map projection. The program used to draw the LORAN C grids is the same as that used by N.O.A.A. and the Coast Guard. A section of any chart may therefore be inserted in the plotter, and, by using the correct scale, the LORAN grid on the chart will coincide with the grid drawn by the plotter. Figure 3 illustrates a time difference section of a plot scaled to 200 nautical miles with a 25-microsecond spacing and displaying the characteristic bending and spreading of the TD lines.

In providing a true LORAN C grid, as well as readouts in both LORAN coordinates and latitude and longitude, the plotter facilitates operation by presenting plots and readouts in terms familiar to the operator.

A point on the plot area made by the pen in a certain position will be plotted in exactly the

same place when the vessel returns to that position. The course of a vessel, plotted on a clear day, may be retraced in poor visibility to allow a return to harbor.

Remote Initialization. Remote initialization permits the operator to use as a reference point any known location within the chain that is at a distance from his starting position. Referring to Figure 4, remote initialization is the procedure by which Point B is designated the reference point while the vessel is still at Point A.

With the coordinates of point B entered into the plotter, the vessel's present position will be beyond the scale of the chart (see Figure 4), and the pen will lie against the edge of the plotter chart at the point at which the moving vessel will enter the chart area.

The plotter's ability to display distance and heading to a destination can be utilized as an aid in directing the vessel to point B. By considering the coordinates of point B as a destination, the plotter can be made to display instantaneous distance and heading to point B. This display can be used by the operator to compensate for any variation from true course to point B.

If, as shown in the extreme example of Figure 4, the vessel is so much off course that it must now approach the destination from an easterly direction, the pen will move to that point on the chart at which the moving vessel will enter the area of chart coverage.

Destinations (Way Points). The plotter is designed to allow insertion of up to nine way points and will provide both audible and visual alarms as the vessel approaches each way point. As noted above, the display will indicate, on command, the range to destination and the course to destination. Although tides and winds may vary a ship's course, the plotter will continually update the bearing indication. Way points may be entered into the plotter in either TD's or latitude and longitude.

North-Up Presentation. This feature is the plotter's ability to provide a plot of the vessel's movements with a minimum distortion and present it in a North-Up manner. By using a microprocessor, the plotter is able to transform the hyperbolic positional data (lines of constant time difference) into a corresponding Cartesian coordinate system.

Each new set of time difference readings is received by the plotter, converted to Cartesian coordinates, and the new pen position is computed relative to the initial reference position. It is possible to plot track directly on a standard Mercator chart with distortion minimized to an acceptable level.

Flexibility of Scale. If plotting is to be performed on an actual chart, the scale of that chart may be inserted into the plotter. Since the mechanical resolution of the plotter is 0.005 inches along both the X and Y axes, the limitation on choice of usable scale is normally receiver performance, as expressed in terms of RMS noise.

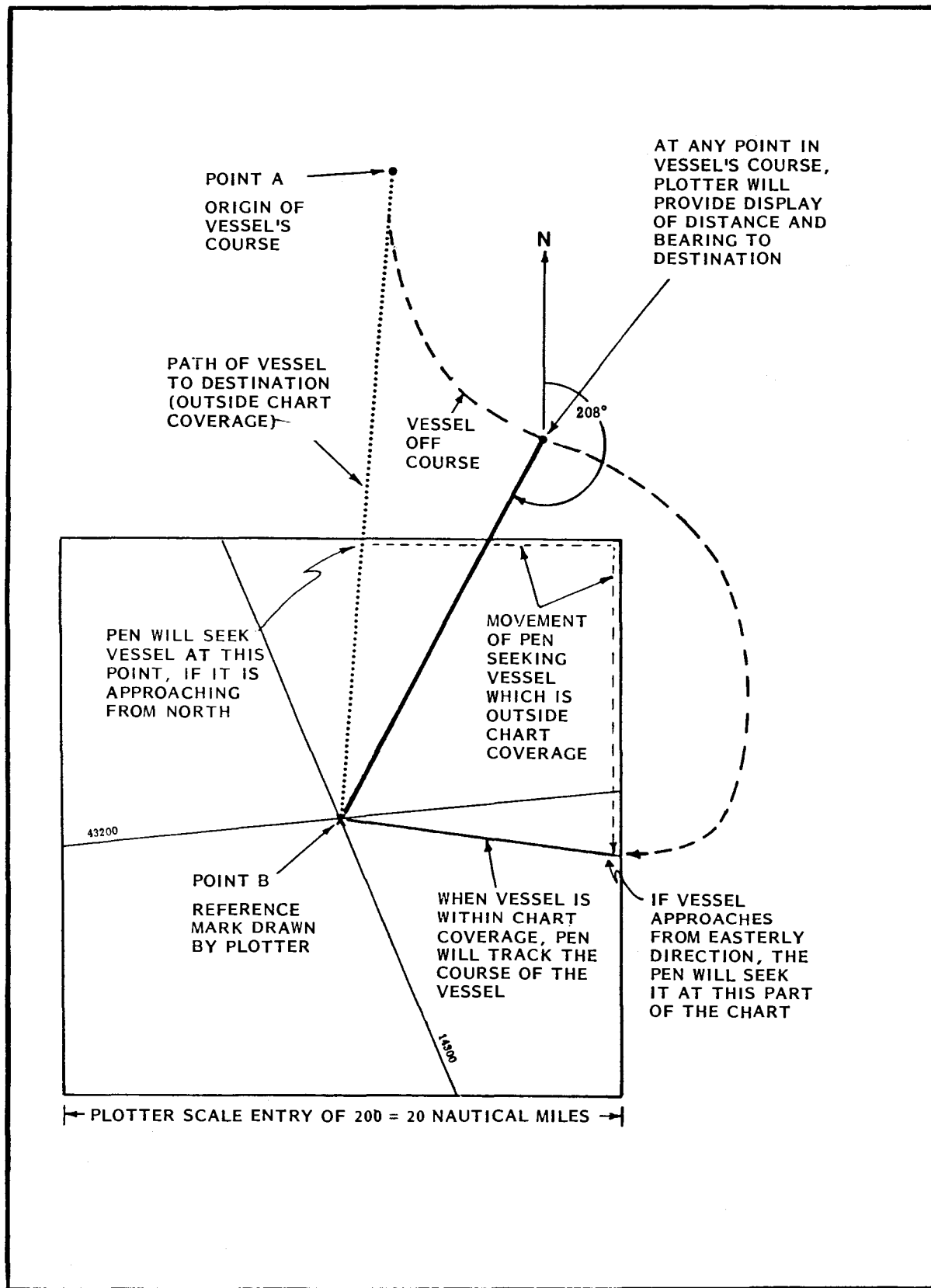


Figure 4. Tracking in a Remote Initialized Area

The plotter can be used with any scale between 1 and 999 nautical miles. The precise dimensions of the plotter will vary minutely due to mechanical limitations but are approximately 10.94 inches by 10.94 inches.

Flexibility of Drawing LORAN C Grid Lines. -

A set of two LORAN C lines for each station, or a complete LORAN C grid, may be drawn. When working with an actual chart, grid lines are generally not necessary. On plain plotting paper, however, the LORAN C grid lines are an extremely useful tool.

Image Area. - In order to retain the entire plotting surface for "safe operation", an arithmetic image space is provided. This image space increases the area in which the vessel's position is computed and tracked to one which is 15 times the physical plotting surface. If the pen should be driven off the plotting surface, it will automatically re-enter at the appropriate position and resume normal plotting operation.

Running Average. - The plotter normally responds directly to the data provided from the receiver. The quality of data varies depending on signal strength, receiver errors, receiver resolution, and many other external factors. Obviously, if the output data are noisy, and if the data were plotted directly, a noisy trace would result. This problem is further exaggerated when the vessel is operating well off the baseline in areas where the distance represented by microseconds is large, and the operator wishes to plot on an expanded scale.

The operator may select the running average feature of the plotter to smooth the recorded track by averaging the last eight sets of time difference readings received and by computing vessel position based on these average inputs. This feature allows the user to take full advantage of the wide range of scaling provided by the plotter.

The running average feature introduces a velocity lag of approximately eight seconds. This lag in pen position versus the ship's actual position is greatest when traveling along the baseline. At speeds of 20 knots along the baseline, the lag would be less than 300 feet, or 0.6 microseconds. In physical terms, the pen would lag by approximately 0.3 inches for a scale of 10,000:1. For larger/smaller scales, the actual pen lag would be less.

Velocity Filtering. - Sudden and momentary LORAN C data errors associated with weak signals or a peculiar local environment will be disregarded, if the operator elects to use the velocity filtering feature of the plotter. A smooth and continuous track is assured even in the presence of noisy receiver data by filtering circuits which will not respond to any changes in input data which represent a ship's velocity that is greater than 50 knots.

An additional mode of operation combines the advantages of velocity filtering with the running average feature. The effect of using the velocity filter and the running average is shown in Figure 5.

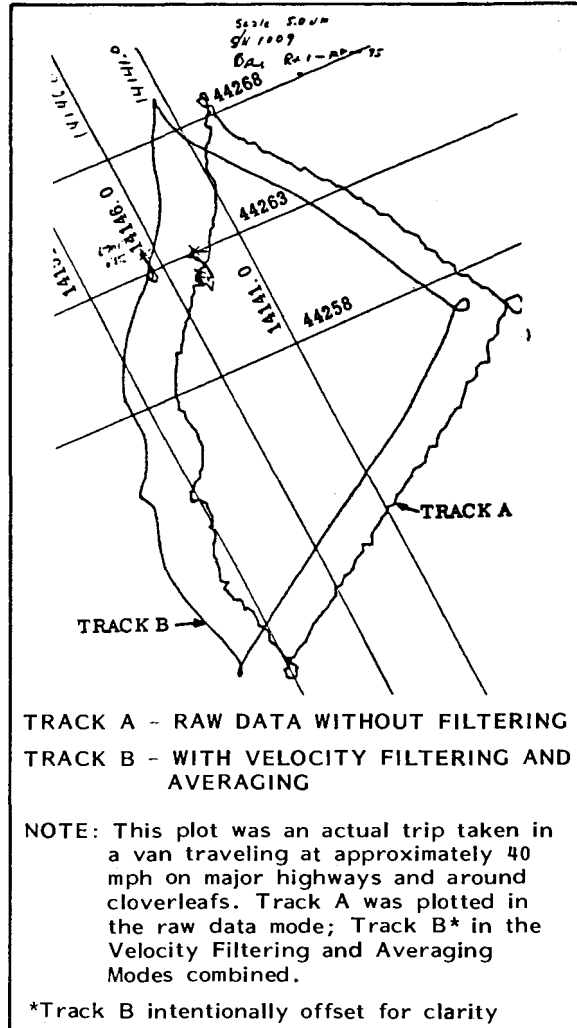


Figure 5. Effect of Velocity Filtering and Averaging

Inserting LORAN Corrections. - There may be occasions when, because of the vessel's location within a LORAN chain, the receiver's present position display is incorrect by a few microseconds. While the correction of this error may not be critical to plotter operation by fishermen or to the majority of plotter users, there is a method in the plotter for correcting such errors for those users who require the greatest degree of accuracy. Scientific users, such as geographical survey units, national fisheries, and offshore technology people, will find the C-PLOT 2 capability for entering corrections (from 0.1 to 9.9 microseconds) a most valuable feature.

COMMERCIAL FISHING APPLICATIONS.

Trawlers and Dragners. When fish are found, the plotter is set into operation to draw the vessel's course line. When the fish yield ceases, the vessel comes about and is able to traverse the exact course line in the opposite direction. All of the combined methods of LORAN-A, radar fixes, and reciprocal compass courses have never been able

to duplicate this feat with such accuracy because of tides, currents, wind sets, and heavy seas.

Figure 6 illustrates a search pattern made by a trawler using the C-PLOT 2 together with sonar (fishfinding) equipment. The trawler follows a random, criss-crossing course over an area suspected of containing fish. As this random course is traced on the plotter, the operator makes an X on the plotter track whenever the sonar indicates the presence of fish. The totality of X's, and their distribution, establishes the "pattern" which indicates not only the presence of fish in great quantity but also their general direction of travel. The vessel can now retrace the pattern (direction shown by dotted line) with its net deployed for a maximum catch.

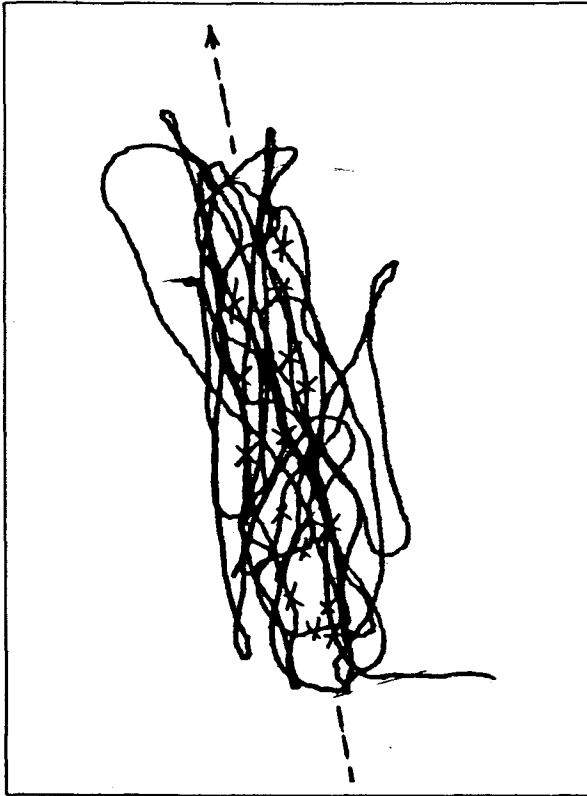


Figure 6. Trawler Search Pattern

A good plotter will allow a shrimper to operate in areas that would normally be inoperable because of treacherous sea bottom, hazardous to both net and vessel. As in the previous example, the shrimper, using a plotter and sonar, follows a random course over a particular area. In the plot of Figure 7, taken by a shrimp boat in the Gulf of Mexico, the operator darkened the plot manually whenever the sonar indicated banks (labelled N.W Bank, S.W Bank, South End, and East Side). The darkened lines now form the outline of an area in which the net can be deployed, they also indicate areas to be avoided. Since some of the banks were as high as 30 feet, the basin or canyon formed by these banks offered shelter to the shrimp. To the shrimper, such a plot indicates not only areas of high yield but also areas in

which he can operate safely without snagging or losing his net. Moreover, the plot, once made, may be used at any time to enable the shrimper to return to the same spot.

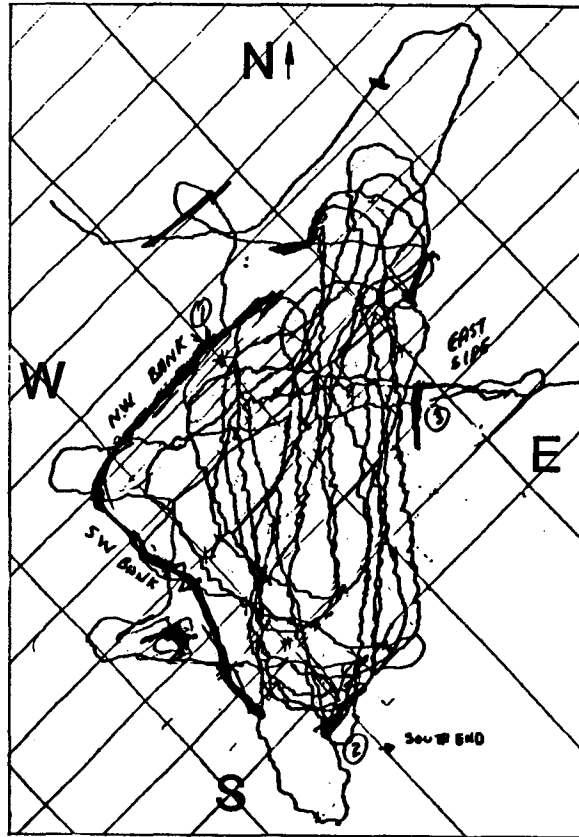


Figure 7. Shrimper Survey Plot, Gulf of Mexico (3-Mile Scale)

Lobster Boats and Crabbers. Figure 8 illustrates a crabbing operation as it is used in the area of Dutch Harbor and the Pribilof Islands. The plotter is first set to plot a course from Dutch Harbor to the crab area, in this case approximately 100 miles. This same plot can then be used to return to Dutch Harbor after the crab operation is complete. In the initial setup, the navigator sets the destination into the plotter to the crabbing area. Once there, he immediately changes the plotter paper and the scale in which he will operate. When setting a pot line, he records the first pot position, marking an X and the Reference TD or Lat-Long position. He then lays pots along a line marking X's as he sets the pots. For each line of pots, the procedure is repeated. The traps or pots can then be located for hauling at any time with pinpoint accuracy under any conditions (darkness, fog, heavy seas) using the same chart which was drawn when the traps were set. The helmsman simply follows his way back to each previously marked site by retracing the original plot. He can just as easily re-enter and pick up the traps/pots in the reverse order, or in any desired order.

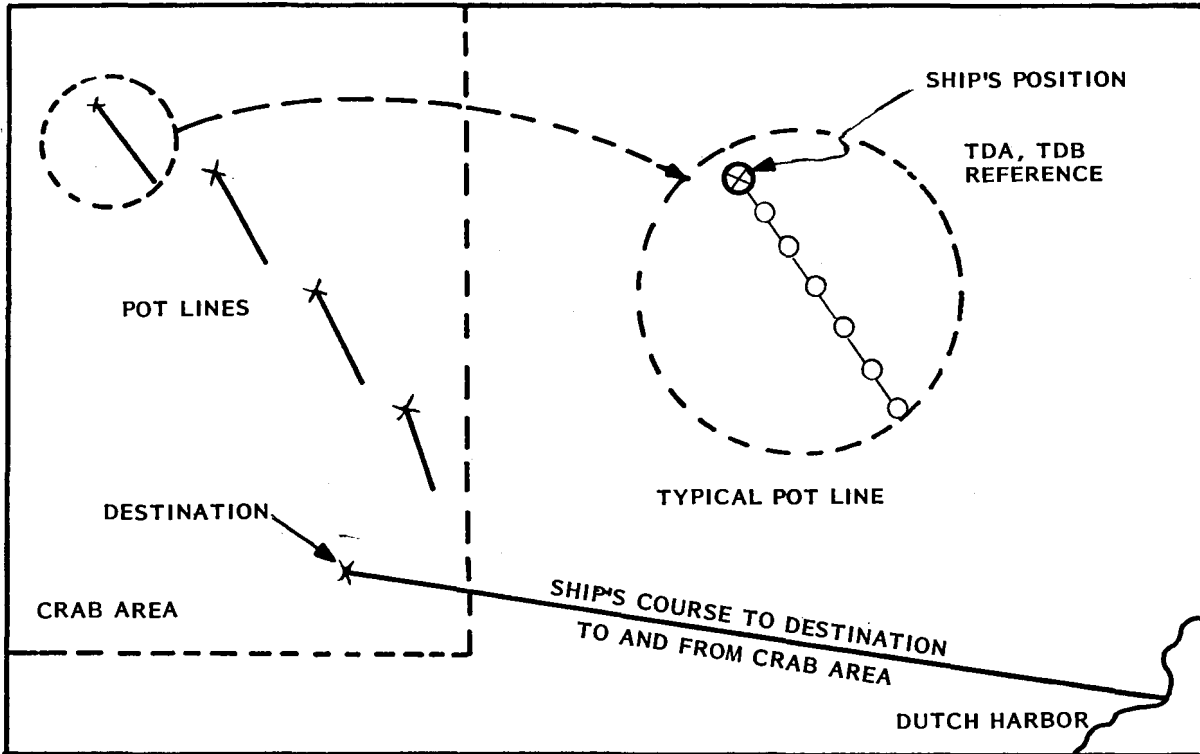


Figure 8. Plotter Used in Crabbing Operation

Tuna Fishing. A new plotter application has emerged recently in the tuna fishing industry. The tuna fishermen first find the bait fish in an area where tuna have been sighted then follow their movements in a circular pattern (see Figure 9) with the aid of the plotter. When the tuna move in to feed, the tuna boat is accurately positioned for maximum catch.

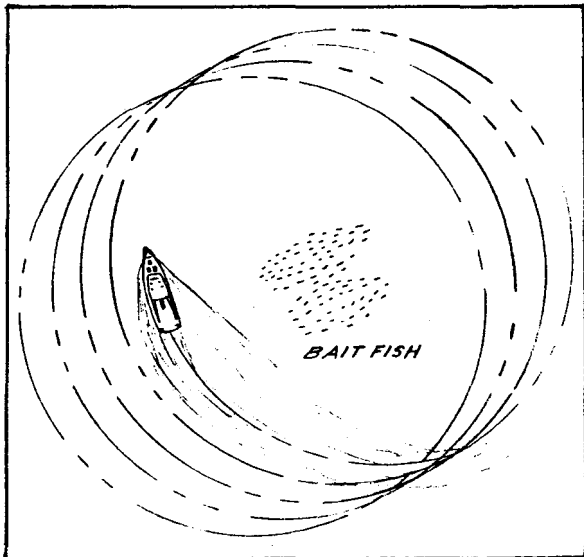


Figure 9. Tuna Fishing with EPSCO's C-Plot 2 Plotter

Long-Range Navigating. The plotter is extremely useful in navigating from one port to another on a permanent schedule such as on a ferry boat. The plot, either derived from a trip or preplotted can be retraced in bad weather when it may become difficult to pick up buoys by radar because of sea clutter. A plot of this type of navigation is shown in Figure 10. During the trip, the vessel PRINCESS MARGUERITE sailed from Seattle Washington to Victoria, British Columbia plotting a course and returned by navigating on a course parallel to the previous trip.

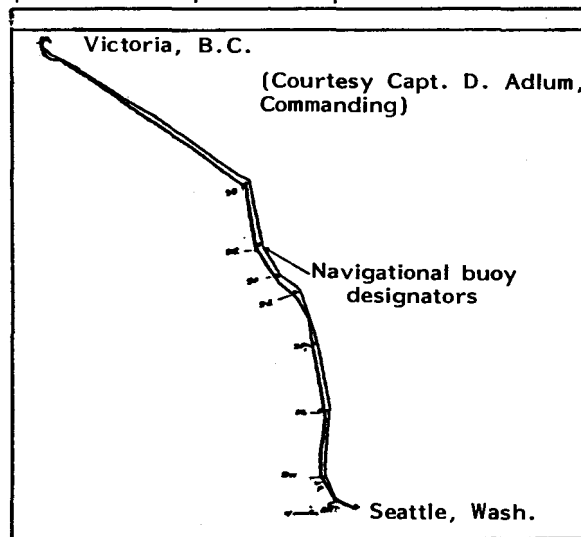


Figure 10. Plot of PRINCESS MARGUERITE

LORAN RECEIVERS

The fishing industry has been somewhat reluctant to accept LORAN C as a replacement for LORAN A; however, time changes all things, LORAN C is now accepted in many areas and is proving to be a blessing in disguise. The fishermen have always needed a speed indicator over ground (SPD) and a destination entry capability (DEST) which would allow the operator to enter positions he would like to go to and be able to read from his display the bearing in degrees and the range in nautical miles. These two features, among many others such as latitude /longitude (Lat/Lon) are also available in the new sophisticated sets like the EPSCO C-NAV XL, Figure 11.

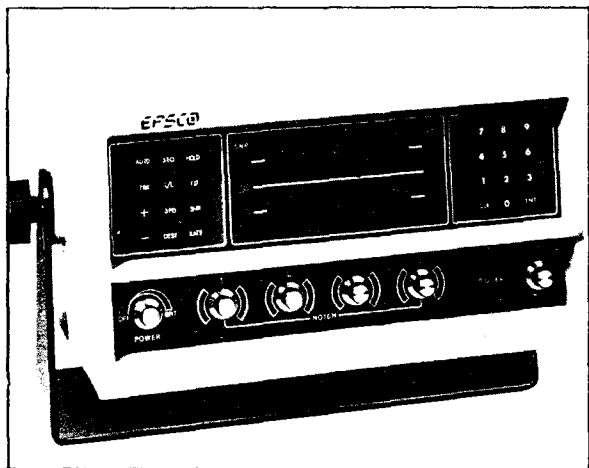


Figure 11. EPSCO's C-NAV XL LORAN Receiver

The speed indicator (SPD) is extremely important in the clamming industry. They need to know their vessel speed over ground because when towing a dredge, it is important that vessel speed be kept at approximately 1.5 to 2.0 knots. If the speed is too high, the dredge will bounce and will be digging only part of the time. What would have been a 1/2-mile tow, for example, would actually only be a portion of that, resulting in a smaller catch or possibly leaving a good area thinking that it had been fished out. Going too slow fills the dredge with mud and prevents the intake of more clams, Figure 12.

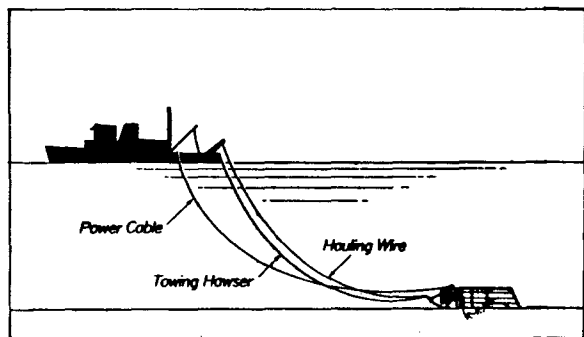


Figure 12. Proper Speed in a Clamming Operation.

Bottom Trawling. For the bottom trawler, the speed indicator is also extremely essential. Here again, if the speed of the vessel is too slow, the net will not retain fish netted; the fish will either swim out if in the net, or swim away from it.

Midwater Trawling. In midwater trawling, speed is a very essential indicator because the net must be positioned at a specific depth (Figure 13) for maximum catch; if vessel speed is too fast, the net will be too shallow, if vessel speed is too slow, the net will be too deep.

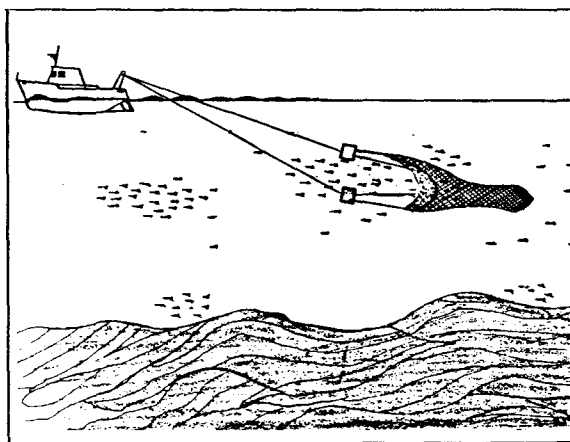


Figure 13. Midwater Trawling

Scallop Dragging. A scalloper now finds LORAN C indispensable for, like the clammer, he also needs speed information because of his type of gear. The dragger must maintain vessel speed accurately between 4.4 to 4.8 knots. The scalloper will not go out (for economic reasons) if his LORAN C and plotter combination are not working perfectly even though at the present time LORAN A is still operating and the dragger may have LORAN A aboard. This is an indication of the superiority of LORAN C because of its advanced technology.

The destination feature (DEST) in the LORAN C Receiver allows the navigator to go to a selected fishing area by steering a course indicated by the receiver and will also confirm when he has arrived. If they are setting lobster pots or crab pots, the use of the DEST feature will provide savings in time and energy. The feature also permits the integration of the EPSCO C-Pilot discussed in the next section.

C-PILOT

DESCRIPTION.

The C-Pilot is actually an interface between the EPSCO LORAN C XL receiver and the Cetrek Autopilot. The C-Pilot design interfaces the receiver to the Autopilot through a Model 504 or a modified Model 506 Autopilot sensor. A block diagram of the complete system is shown in Figure 14; Figure 16 is a photograph of the C-Pilot.

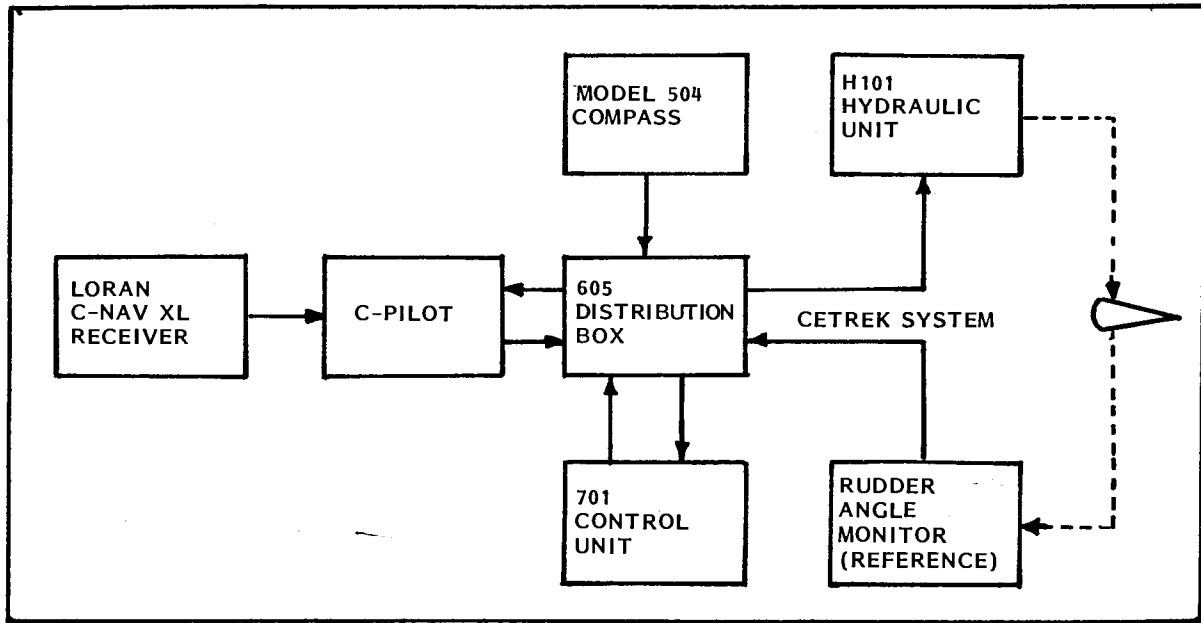


Figure 14. Block Diagram, Complete LORAN C System

The C-Pilot has two modes of operation. In the autopilot (A/P) mode, the Cetrek Autopilot will operate in a normal manner, maintaining a constant heading for the vessel without regard to set and drift. In the C-NAV mode, the combination of the C-NAV XL and the C-Pilot monitors the vessel's present course and continuously computes and compensates for course error.

When first turned on, the C-Pilot operates in the C-NAV mode. When an alarm condition arises, and the alarm is sounded, the C-Pilot automatically switches the system to the A/P mode, and the vessel will maintain a heading based on the last valid course computation.

OTHER PILOT INTERFACES.

Unlike the C-Pilot, some pilot interfaces operate on cross track error, but they introduce the additional distortion of bounding the intended track in terms of LORAN time differences. When one expresses cross track error in terms of microseconds, the actual width between boundaries varies as a function of vessel position within the chain. A boundary of ± 0.2 microsecond represents a cross track error of a minimum of 100 feet to greater than 400 feet either side of the intended track. Since cross track error is expressed in microseconds rather than feet, one cannot optimize the time response. These circumstances virtually ensure that the vessel will continuously weave around its intended track, as shown in sketch a of Figure 15.

EPSCO'S APPROACH.

The C-Pilot continuously monitors the vessel's current course and compares it to the intended course. When the difference between these two courses (angle a in sketch b of Figure 15) exceeds a preset limit, the vessel's heading is

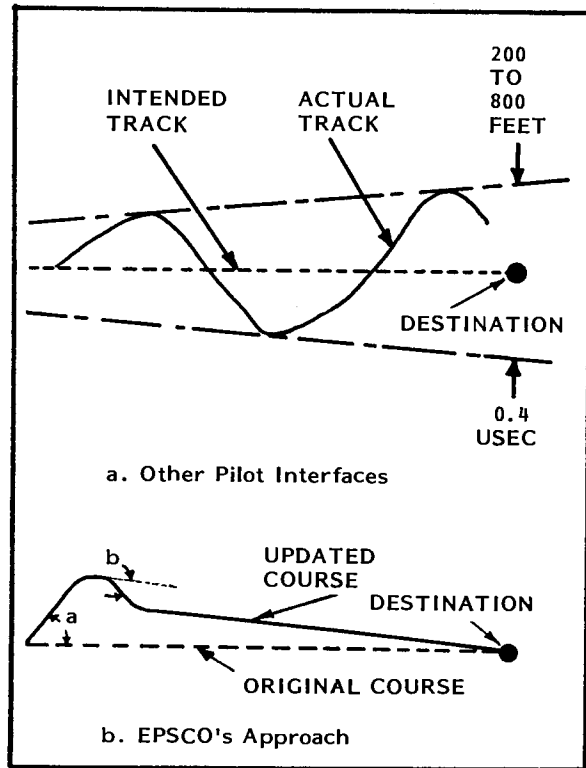


Figure 15. EPSCO's C-Pilot Approach to Tracking

altered by an amount (angle b) calculated to assure its reaching its intended destination.

If the factors which influence set and drift change, the C-Pilot would detect these changes within approximately three minutes and would alter the vessel's heading. This continuous

monitoring and updating of course-to-destination results in the shortest actual track from origin to destination.

If the original heading is within 10° of the intended course, the maximum departure from original course would not exceed 160 feet. Even if the vessel heading was 90° off course, the maximum deviation from intended course would not exceed 920 feet.

For the first six minutes of operation, the heading will be checked and corrected when necessary every 0.15 nautical miles. The time interval between updates is thus governed by the speed over ground. Cross-track error can not exceed 160 feet, even if the pilot has been set 10° off the heading to destination at the outset. After the first six minutes, the updating will occur regularly at 0.3 nautical miles over ground, provided 3 minutes have elapsed since the last update. The heading will be corrected only if the error is greater than $\pm 3^\circ$. The system, consisting of the Cetrek autopilot, the C-Pilot, and the C-NAV XL receiver, is capable of providing full steering automation for up to 10 waypoints, a task that cannot be achieved with any other commercially available system at this time.

Various alarms and safeguards are provided by the C-Pilot. A LORAN SNR or cycle light will also actuate an audible and visual alarm as well as automatic switching to full auto-pilot control. Full autopilot control will be realized around zero output of the deviation monitor at last update. This switching function assures that, for all practical purposes, the pilot will still be set to the most efficient heading to destination at the time of loss of LORAN control.

Other available systems, working on cross-track error correction and associated course trim, will revert back to original heading to destination. It is obvious that, in these systems, the original heading must be set well within $\pm 20^\circ$ and, preferably, as close as possible, since the setting will also affect the accuracy of heading to destination in the case of LORAN control failure. With the C-Pilot system, the original heading adjustment is of no consequence in the event of LORAN control failure.

The C-Pilot will alert the helmsman when the vessel is 0.4 nautical miles off destination and, at the same time, revert back to normal autopilot function. If the operator desires to turn immediately to the next destination, he depresses the NEW LEG pushbutton. The alarm will stop, and the LORAN computer will take over long-term control. If the NEW LEG pushbutton is not depressed and no other action is taken, the system will revert back to LORAN control using the new heading to the next destination. This action will take place provided the helmsman has entered more than one destination. The helmsman must remember that it is his responsibility to be at the helm during course changes.

It can be seen that only the basic functions are the same for the C-Pilot system and other systems which compute cross-track error. The autopilot carries out its normal functions. The autopilot

takes its short-term heading from the deviation monitor, whose setting or signal is modified by LORAN C information for long-term efficiency.

THEORY OF OPERATION.

EPSCO has developed a LORAN-C controlled autopilot driven by an EPSCO LORAN XL computerized receiver interfaced to a Cetrek 701 or 901 system. The interface is called the C-Pilot, and the system uses an auto-following type sense unit (Model 504). The Model 504 is a motor-driven deviation monitor which lends itself to the C-Pilot interface because of its remote course-changing ability.

The system is a proportional follow-up type which employs the deviation monitor to provide either on-course (null) information or off-course information of direction and magnitude and a rudder angle monitor which provides similar (though 180° reversed) information. The information from both monitors are compared in a bridge circuit.

Assuming all resistors of the bridge circuit are equal, a 10° deviation from course will unbalance the bridge circuit; a 10° deviation from rudder amidships to the appropriate side will rebalance the circuit. Thus, the ratio of course error to rudder applied is 1:1.

Under normal cruising conditions of a typical 85-foot fishing vessel, the ratio required to prevent either over-steering or under-steering may be in the order of 1/3 to 1, which means that two degrees of corrective helm will be applied for six degrees of course error. A RUDDER control is provided on the control unit to facilitate ratio changes from typically 1/6:1 to 1:1. The setting of the control, which depends on type of vessel, speed, and sea conditions, is generally lower when the speed of the vessel increases.

The deviation monitor has an output which rises in linear fashion up to $\pm 40^\circ$ deviation from zero. Maximum output is thus achieved at 40° , and a greater deviation will give no further rise. When a course is dialed which is, say, 180° off present course, the error output will be at maximum positive or negative-going, depending on whether the course was reset to provide a turn to port or to starboard. Helm will be applied until the bridge circuit is rebalanced, and this will be at:

$$\frac{40^\circ (\text{deviation})}{3 (\text{ratio } 1/3:1)} = 13^\circ.$$

Once the vessel has turned by about 140° , the output from the deviation monitor will start to decrease and thus unbalance the bridge circuit in the opposite direction. The unbalance will cause the drive unit to move the helm in a direction that will decrease the rudder angle proportionally to the decrease in the monitor output and thus move the vessel to a new heading.

Thus, it can be seen that the pilot is in full proportional control of up to 40° before the vessel comes onto the new heading. The rate of turn is reduced gradually, and the vessel will settle on her new course heading with a minimum of overshoot and oscillation.

The C-Pilot interface is designed to retain this full control and it is capable of making a full turn when a new destination is required. The C-Pilot simply instructs a motor to turn the deviation monitor by the desired number of degrees in the desired direction, just as the helmsman would have normally hand-dialed the new destination.

Other systems, working on cross track error elimination, apply "Course Trim" signals to the deviation monitor signal. With a deviation monitor of typically $\pm 40^\circ$ control range, the maximum "trim" offset range has to be limited to, say, $\pm 20^\circ$ in order to maintain enough range for normal pilot operation. It can be seen that the automatic new waypoint selection cannot be achieved in these systems as it can with the C-Pilot system.

The autopilot receives and evaluates heading information only; it cannot, by itself, initiate action to compensate for set and drift and other changing factors.

A TRIM control may be used for short-term compensation for those external forces that are continuously trying to change the vessel's heading to one side. This is standing helm, or rudder bias, and, if used correctly, it will balance the vessel's steering action and thus enhance both course-holding and fuel efficiency. When performed as noted, it is a relatively short-term adjustment; it should be altered at intervals to compensate for varying conditions. Again, drift and set may render the vessel on a parallel to intended course, and the magnitude of this cross-track error can be kept to an acceptable level only by regular computation of position and resultant new heading to destination and manual readjustment of the deviation monitor.

The C-Pilot fulfills these functions at very short intervals automatically. The C-NAV XL computer continuously monitors geographical position of the vessel; it is also aware of the true course of the vessel since its last update. Since the geographic point of destination is known to the computer, the number of degrees of heading required can be readily computed and realized. The deviation monitor is not required to be corrected for deviation, and variation is of no consequence, since the C-

Pilot needs only to reset the deviation monitor by the appropriate number of degrees from null in the required direction.

As can be seen, the C-Pilot system does not work on cross-track error correction. Instead, it computes and sets heading for the shortest distance to destination.

COST EFFECTIVE ADVANTAGES OF THE C-PILOT.

The autopilot was designed to relieve the helmsman of the tedious duty of maintaining an average magnetic heading manually. In inshore work, where the helmsman may be steering by landmarks, savings in fuel by using the autopilot would be insignificant. However, even in inshore work, the autopilot allows the helmsman to be free periodically to attend other tasks and be the "other crewman" to the fishermen.

In offshore work, a good autopilot generally saves transit time and thus saves fuel. These savings may be up to 30% of normal fuel expenditures.

A helmsman, on a four-hour watch, trying to maintain a good average magnetic heading, will gradually tire. The sheer strain of maintaining a sharp lookout, attending his charts, radar, LORAN, and keeping his eyes on a continuously moving compass card, will cause him to let the vessel yaw at $\pm 10^\circ$ and more about its intended heading, depending on weather and fatigue.

The autopilot is a non-tiring machine and will hold a tighter average heading than most experienced helmsmen for long intervals.

It is expected that the C-Pilot system will save an extra 5% to 25% of time and therefore fuel over a conventional autopilot and over long distances. The impact of these developments on the shipping industry in these times of high fuel costs will be tremendous. If used correctly, this further aid to navigation will also increase safety at sea by making more time available for monitoring collision avoidance systems and for all other safety and navigational duties of the men on the bridge.

CONCLUSION.

The advanced technology in LORAN-C equipment such as plotters, receivers, and autopilots will continue to prove their worth to the LORAN-C user in the fishing industry in terms of time saved, fuel conserved, and greater catches. Only the more obvious applications have been described; others have not been presented, and more uses will suggest themselves.

With the availability of new LORAN chains assuring stronger signals and improved grid geometry, the usefulness of the plotter will be enhanced in ability to provide smoother plots. LORAN receivers will supply the user with more sophisticated data such as speed over ground (SPD) and destination (DEST) which will provide range and bearing to a particular location and also provide more accurate information to control a LORAN-C autopilot.



Figure 16. EPSCO's C-Pilot

St. Marys River Loran-C Mini-Chain -- The Bottom Line

Mr. Jack M. Ligon LT David L. Olsen
United States Coast Guard
2100 Second Street, S.W.
Washington, D.C. 20593

The U.S. Coast Guard had an experimental Loran-C minichain installed on the St. Marys River at the Michigan Upper Peninsula in 1975. The minichain was instrumented with three monitor sites and was operated to best Coast Guard standards during the period May 1979 to May 1980 to establish the ultimate signal stability and determine its suitability for use as an all-weather year round radionavigation aid. A preliminary assessment, a description of the experiment, and the analysis procedure were given by Lt. Olsen in his paper presented at the 1979 WGA Technical Symposium. This paper presents the full data and attempts to assess its meaning, and concludes that the minichain will provide position information to within 20 meters 2DRMS in the critical portions of the river when operated with relatively infrequent differential offsets.

INTRODUCTION

In recognition of the potential benefits of an extended navigation season on the Great Lakes and St. Lawrence Seaway, Congress authorized a Winter Navigation Program which included several Demonstrations. The goal of the Demonstrations was to test concepts and, at the same time, progressively extend the navigation season.

The St. Marys River is a vital water link between Lakes Superior and Huron. For years, navigation on this river during icy winter months and during periods of low visibility has been a problem of great concern for mariners. The river has many channels with a minimum width of 300 feet, and is regularly traversed by vessels up to 1000 feet long and 105 feet in beam. In the past, ore carriers have been forced to reduce shipping services during the winter ice season, partly due to reduced floating navigation aids.

The concept of a Loran-C "mini-chain" of low-powered transmitters seemed ideally suited to the St. Marys River situation, and such an installation was proposed by the Coast Guard. Since the original position accuracy goal of ± 10 feet (1 sigma) was clearly unobtainable with Loran-C, discussions were held with the Lake Carrier's Association to better determine actual system requirements. Many ship's masters felt that a reliable "100-foot system" (30 meters) could help them through the St. Marys River. The Coast Guard proposal for a mini-chain was thus adopted by the Winter Navigation

Board. The objective of the Coast Guard program was to provide a Loran-C mini-chain and shipboard user equipment for demonstration, with an accuracy suitable for navigating in the St. Marys River.

GROUND STATION EQUIPMENT

A four-station chain arranged in a diamond pattern provides the coverage for the river. A monitor is installed approximately two miles south of the Coast Guard Base at Sault Ste. Marie, Michigan. Only the monitor station is manned, with control of the transmitting stations over dedicated telephone lines. Site selection and preparation were completed in late September, 1975 and building construction was completed in early January, 1976.

USER EQUIPMENT

Several generations of user equipment were developed for evaluation with the mini-chain. The original St. Marys program planned two different sets of equipment, designated User I and User II. These were evaluated aboard Coast Guard and commercial vessels operating in the St. Marys River and the Great Lakes through the summer of 1978. To determine the short-term navigational accuracy of this equipment, dynamic testing was performed using a microwave positioning system for reference. Ninety-five percent of the user equipment's off-track indications were within 11 meters of the reference system's values in one test area, and within 14 meters in another area.

User II had demonstrated the precision use of Loran-C in the repeatable mode. However, it was primarily an R&D tool and was impractical, expensive and non-reproducible as an operational radionavigation equipment. In the fall of 1978 the Coast Guard began an effort to produce a commercially realizable precision Loran-C navigator, termed the PILOT (Precision Intracoastal Loran Translocator). The system was initially tested on the St. Marys River in October 1979. Overall performance was excellent, combining receiver TDs with survey data and ship's gyro heading to provide accurate position and situation information. The PILOT system was also installed aboard the U.S. Coast Guard Cutter Katmai Bay for operational deployment during the winter of 1979-1980. PILOT was shown to be useful in thick fog and for starting turns based upon the distance to go. The consensus was that PILOT should be a useful aid in breaking channel edges not marked with buoys.

TIME DIFFERENCE SURVEYING

Accurate navigation with Loran-C must rely upon the repeatability inherent in the system. This requires that the points or areas of interest be "visited" or surveyed with a loran receiver so that TDs can be measured and stored for future reference. A "static" survey method was used during the initial surveys, with the test vessel holding position at each waypoint while TDs were recorded on the user equipment. Later, an attempt was made to use a microwave positioning system to locate several waypoints. The method proved ultimately unsuccessful due to discrepancies -- as large as 80 meters for the few points tried -- between the visual aids and the reference-system-determined waypoints. The vessel was not lined up with the visual ranges when the reference said it was at the true channel intersection. Waypoint TD prediction using a force-fit algorithm proved unsuitable for the St. Marys River for the same basic reason as the microwave survey method, as it depended on knowing the precise latitude and longitude of the waypoints. Unfortunately, the vast majority of the aids the mariner successfully depends upon are not precisely charted on any common reference grid.

A Time Difference Survey Set (TDSS) was developed as a calibration tool for PILOT. The TDSS is comprised of a monitor receiver interfaced to a calculator, with several algorithms

to facilitate the visual survey of a waterway. The TDSS permits dynamic measurement and accurate estimation of the waypoint time differences using regression techniques.

PRELIMINARY GRID STABILITY

Data were collected at 23 shore sites during September/October 1977 for the development of the grid prediction algorithm. This was followed by a wintertime collection effort from November 1977 to March 1978 for input to a seasonal sensitivity analysis of the mini-chain. The predictions of grid instability computed in a theoretical seasonal analysis could not explain the TD variations recorded at several data collection sites during the winter collection period. The TD variations were unusually large at several sites, with an average of 300 nanoseconds and a maximum of 850 ns.

TRANSITIONAL PERIOD

The large temporal variations observed during the winter data collection, if true, could render the mini-chain unusable for precision navigation on the St. Marys River. Although reasonable care was taken in performing the measurements, the data remained suspect due to the equipment and methodology used. While the TD variability seemed most probably equipment and operationally caused, plans for making the mini-chain operational could not proceed until the question of grid stability was resolved. A careful data collection effort was deemed necessary to verify the mini-chain's performance and to definitively judge its navigation capabilities.

Preparations for a one-year in-depth study of stability were begun in the fall of 1978. The equipment at the SAM was switched to the the 35-foot whip antenna and Austron 5000-CALOC system that is becoming standard equipment for long-baseline Loran-C chains. The mini-chain was staffed with professional Loran people. The Master and Xray station designations were interchanged to improve Master station availability.

Three fixed monitor sites were established along the river. These sites were located on the south end of the river at DeTour Village, mid-river at Dunbar Forest, and at Point Iroquois near the river's northern end. Each site was equipped with a Coast Guard standard 35-foot whip antenna. DeTour and Dunbar were each equipped with a Magnavox

AN/BRN-5 receiver plus an Internav LC-204 DCU. Point Iroquois had two LC-204 DCUs installed. This setup enabled each site to monitor all three mini-chain baselines. The sites were visited on a regular basis to insure proper equipment operation and to collect the data. The Coast Guard study discussed in this report utilized twice-daily "system samples" -- one-hour averages taken once around noon and once around midnight.

DATA CHARACTERIZATION

A year's worth of data was collected in a limited but carefully-controlled study of the mini-chain TD grid. The following conclusions can be made concerning the TD data:

The data show more stable performance than the 850 ns worst case variation indicated in some earlier reports. After removing SAM offsets to eliminate chain control effects (although with a control tolerance of + 15 ns, these offsets were insignificant), peak-to-peak TD variations range from 211 ns to 353 ns. After adjusting the TD records for identified transmitter casualty effects, remaining peak-to-peak TD variations range from 128 ns to 319 ns.

Forty-nine percent of the variance in the TD records can be removed by correction terms which are common at all sites, while only six percent of the variance is removed by corrections based upon uniform changes in propagation velocity. These results are indicative of nonhomogeneous propagation effects.

The greatest portion of the variations are seasonal in nature and show a high correlation with temperature. These seasonal variations show significant correlation for up to 40 days, and the method of twice-daily system samples is entirely adequate to characterize these variations. The seasonal variations are of roughly the same magnitude as was predicted in a contracted study of seasonal effects.

Short-term TD variations are essentially uncorrelated with temperature, and are essentially uncorrelated with each other from site-to-site and from baseline-to-baseline. The short-term variations show insignificant correlation after one to four hours, but the twice-a-day system sample frequency is inadequate for study of

these short-term variations.

The following conclusions can be made regarding the possible causes for the observed seasonal-TD effects:

Neither the monitor sites nor the SAM show any identifiable equipment-related reason for the observed seasonal TD variations.

Ground systems at both Point Iroquois and DeTour present unusually high resistance to "earth," but there does not appear to be significant biasing of the data records.

Side-by-side receivers of different types (linear vs hard-limited) show basically similar TD variations. Experiments with these side-by-side receivers show different TD response to pulse shape effects. The presumed monitor of pulse shape effects, ECD observed on the Austron 5000 receiver at SAM, is not an all-inclusive indicator of pulse shape effects.

The transmitter sites are located in areas where there is relatively high ground resistivity.

Rapid spatial variations in magnetic and geological properties are indicative of the area's non-homogeneous nature.

From these observations, we draw the following basic conclusions as to the source of the seasonal TD variations:

They are not principally caused by hardware variations at the monitor sites (receivers, couplers, antennas).

They are not principally caused by uniform changes in the velocity of radio wave propagation over the entire area.

They are not totally caused by transmitter pulse shape variations.

They can only be explained by some combination of changing conductivity in the very non-homogeneous geology of the area, and possible impedance effects at the transmitting antenna due to high ground resistivity.

Further analysis of the seasonal TD variations would require a far more detailed knowledge of the area's geology, or equivalently a far denser spatial sampling of TD history. The data and analysis presented here represents about as far as one can

TABLE 1. TD RESIDUALS (NANOSECONDS) AND PERCENT REDUCTION IN VARIANCE FOR SEVERAL COMMON-TERM DIFFERENTIAL CORRECTION SCHEMES

SITE	TD	REAL TIME		14-DAY SMOOTHED		REAL-TIME OPTIMIZED	
		RMS	Var Red	RMS	Var Red	RMS	Var Red
Iroquois	X	32	63%	35	52%	41	17%
	Y	23		30		44	
	Z	36		40		53	
Dunbar	X	19	51%	23	35%	18	75%
	Y	19		26		17	
	Z	35		37		20	
DeTour	X	20	65%	23	52%	21	21%
	Y	43		50		66	
	Z	14		18		25	
SAM	X	23	N/A	21	N/A	18	N/A
	Y	39		35		17	
	Z	14		8		20	

reasonably go.

UTILITY OF THE MINI-CHAIN FOR NAVIGATION

The TD fluctuations seem large, but must be considered in light of the resulting position fixes and the margin of error available to a navigator on the St. Marys River. A close look shows that, in the narrow portions of the river near the SAM, the mini-chain can provide the 30-meter performance desired by some mariners. Through implementation of a differential correction scheme or an equivalent distributed control policy, a considerable margin of safety can be provided for even the largest vessels in the river's tightest channels.

half-width curve at Dunbar, leaving the largest vessels only a one meter margin for guidance error. Without differential corrections, the margin of error is clearly unacceptable for the largest ships in the river's most narrow channels. The mini-chain does, however, meet the requirements of a "100-foot system," and with 99 percent probability, but only in the vicinity of the SAM. The chain's performance would seem useful in the river's wider channels, and perhaps even for smaller vessels operating in some of the river's more critical areas.

Real-Time Differential Corrections from Common Error Model. Also shown in Figure 1 are the position errors a

Table 2. MAY 1979 TO MAY 1980 RADIAL ERROR STATISTICS (METERS) FOR THREE COMMON-TERM DIFFERENTIAL CORRECTION SCHEMES

SITE	REAL TIME		14-DAY SMOOTHED		REAL-TIME OPTIMIZED	
	AVG	99%	AVG	99%	AVG	99%
Iroquois	12	36	14	43	16	51
Dunbar	6	16	7	20	5	14
DeTour	8	26	9	29	10	34
SAM	5	14	4	11	5	14

The 99 percent radial error values calculated from the TD records at the three monitor sites are Plotted on Figure 1. These records represent the fix quality for a "repeatable-mode" user of Loran-C who is operating without the benefit of differential corrections, under the policy of single-point control of the mini-chain from the SAM. Also plotted is the half-width of the navigation channel along the downbound summer route through the St. Marys River. Although the points are below the curve, the comparison does not allow for the 16 meter half-width of the largest vessels on the river, nor does it allow for guidance errors -- a user's inability to perfectly follow a desired trackline. Only 17 meters separate the data from the

navigator would have observed had his user equipment obtained real-time corrections over a data link, showing a significant improvement in comparison to half-channel width.

Smoothed Differential Corrections from Common Error Model. The "smoothed" correction points in Figure 1 represent the fix quality for a repeatable-mode user of Loran-C who is operating with a "daily" differential correction passed to him as he enters the river, under the policy of singlepoint control of the mini-chain from the SAM. The correction algorithm used here is both non-responsive and physically non-realizable, since it uses 14-day-smoothed moving window TD records, which have the benefit of future

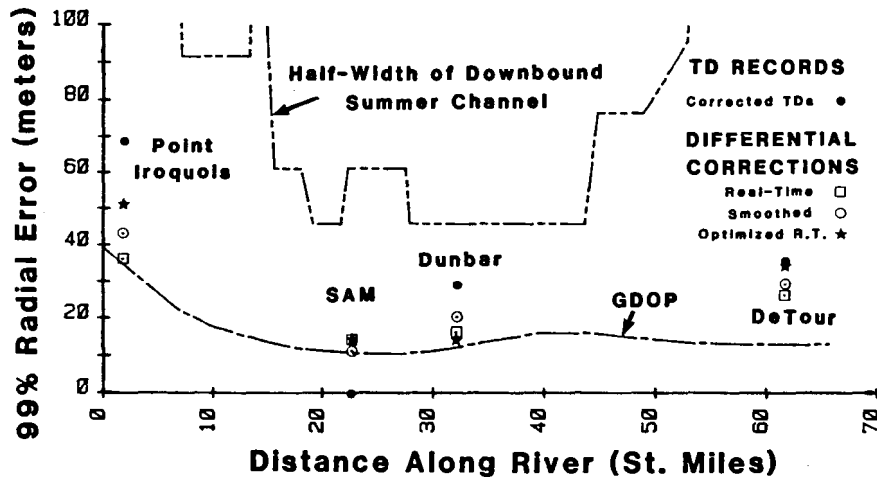


FIGURE 1- 99 PERCENT RADIAL ERRORS AND DIFFERENTIAL CORRECTIONS COMPARED TO ST. MARYS RIVER HALF-CHANNEL WIDTHS

knowledge of the TDs. Almost equivalent performance could be expected with a real-time filter algorithm, which could be made responsive to present values and recent history at the monitor sites, yet allow a reading to be "missed" if a monitor site were inoperative at sample time. A margin of 25 meters remains at Dunbar, allowing a guidance error of 9 meters for the largest ships.

Optimization to Narrow Channels. Plotted in Figure 1 are the 99 percent errors which result when the differential corrections are optimized to SAM and Dunbar. Here Dunbar's performance has improved at the expense of the other sites. However, considering the available channel widths, the degradation in performance at Iroquois, and particularly at DeTour, has been minimal.

Differential Correction through control. Chain control policy could be implemented using differential corrections instead of having SAM control to a CSTD. This scheme could effectively implement real-time corrections chainwide, obviating the requirement for a communications channel to the user. The resulting distributed control strategy shows performance superior to that of a single-point control policy, when implemented for a non-homogeneous area.

Geometric Analysis. The smooth dashed curve drawn on Figure 1 is the relative error expected at each way-point along the downbound channel in the St. Marys River, and is useful as a guide for interpolating between the plotted monitor points. It shows the

effect of GDOP (geometric dilution of precision) along the river. Obviously, it is only a "weak" interpolator since the variations have been shown to result from non-homogeneity.

Conclusions. The following conclusions can be made concerning the mini-chain's potential for providing precision navigation service for the St. Marys River:

The repeatable-mode user of the mini-chain will experience errors which are below 30 meters, with 99 percent probability, in the river's narrower channels. The 99 percent errors degrade to 35 meters at the river's south end and to 70 meters at the north end. However, the channels are wider in these areas. While the 99 percent errors do not exceed the river's half-channel width, they do not allow an acceptable margin of error for the largest ships in the narrower channels.

A differential correction scheme could be implemented using data from several shoreside monitor receivers. These "corrections" could be either passed to the users or applied in chain control. A single set of corrections passed to the user upon entering the river could reduce the 99 percent error to 20 meters in the tightest channels, allowing a guidance error margin of 9 meters for the largest ships. This is the technical "bottom line".

Even better differential corrections could be implemented -- showing an improvement to 16 meters in the narrower channels - by sending corrections directly into the

user's equipment over a realtime data link. The communications problems for this improvement certainly exceed the benefits. The real-time differential correction scheme could also be implemented through a distributed control policy, as opposed to the presently

used single-point SAM control policy, precluding the need for any communications with the user. However, this will only work for one such precision navigation area in a large Loran-C chain that serves numerous harbors.

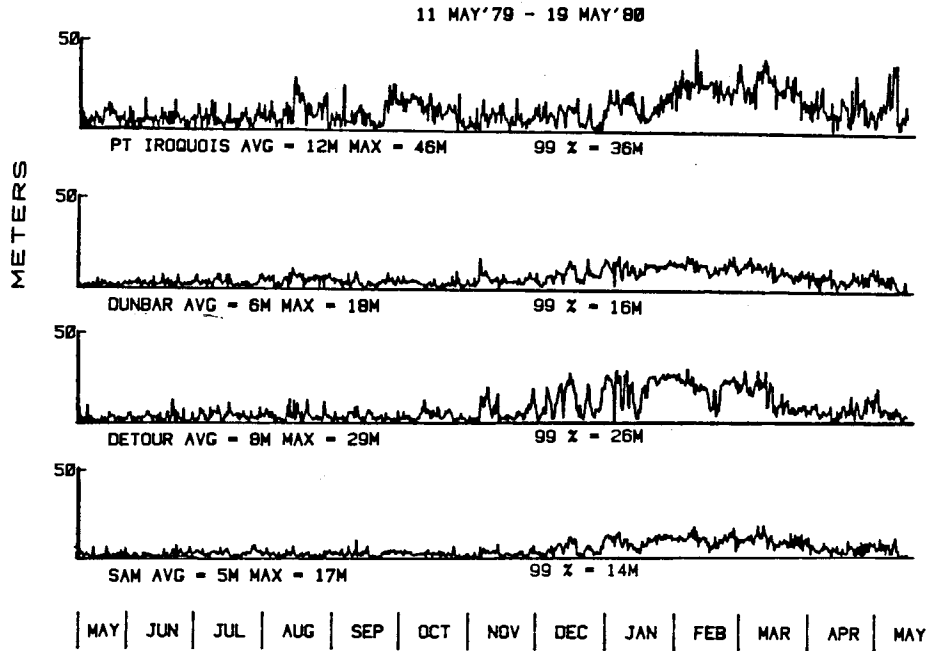


FIGURE 2. RADIAL ERRORS AT FOUR SITES USING REAL-TIME COMMON TERM DIFFERENTIAL CORRECTIONS

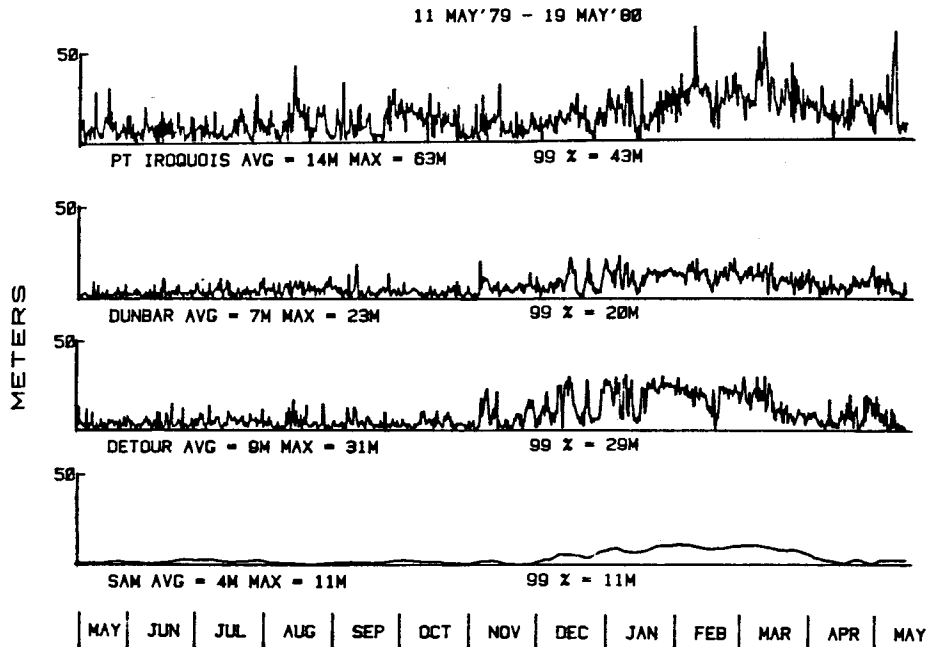


FIGURE 3. RADIAL ERRORS AT FOUR SITES USING 14-DAY SMOOTHED COMMON TERM DIFFERENTIAL CORRECTIONS

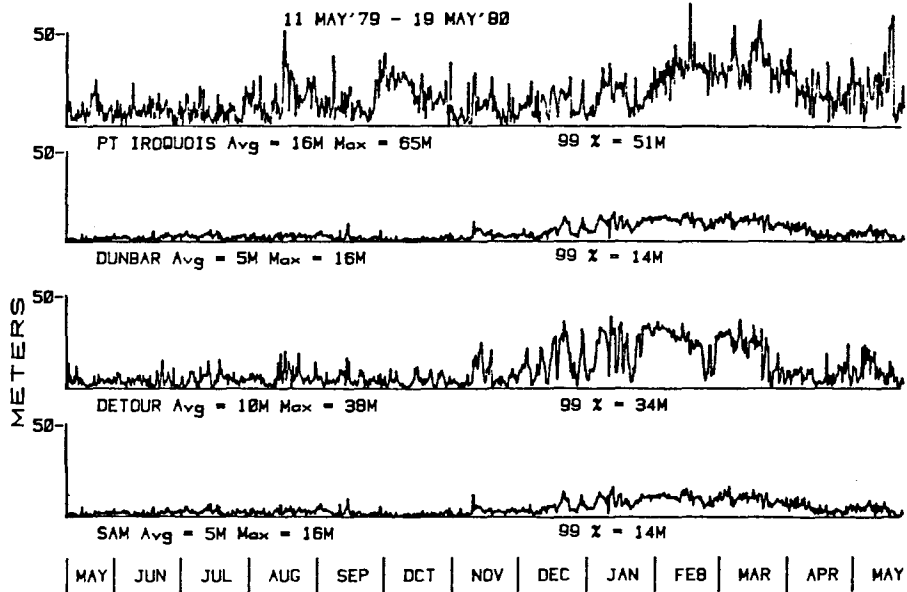


FIGURE 4. RADIAL ERRORS AT FOUR SITES USING REAL-TIME DIFFERENTIAL CORRECTIONS OPTIMIZED TO DUNBAR AND SAM

ERROR ANALYSES OF LORAN-BASED BUOY POSITION AUDITING SYSTEMS

By

J.M. Foltz and L.M. DePalma
The Analytic Sciences Corporation
One Jacob Way
Reading, Massachusetts 01867

J.A. Wolfson
U.S. Department of Transportation
Research and Special Programs Administration
Transportation Systems Center
Cambridge, Massachusetts 02142

ABSTRACT

Error analyses of two Buoy Position Auditing System (BPAS) configurations which utilize differential Loran-C are presented. The candidate BPAS configurations include: transmission of digital Time Difference (TD) data from a Loran-C receiver on the buoy, and processing of helicopter Loran-C data and helicopter-to-buoy microwave ranging data in a "variable geometry" solution. A model is developed to characterize differential Loran-C errors, accounting for the expected effect of the land/sea water conductivity interface. The error model is utilized alone, or with a microwave ranging system error model, to estimate BPAS accuracy for selected buoys in Boston Harbor. Analyses are conducted to determine the sensitivity of BPAS accuracy to changes in pattern monitor receiver location, helicopter flight pattern, error model parameter values, and Loran-C chain geometry. It is concluded that the variable geometry BPAS configuration is more accurate than the TD transmission configuration because of calibration of Loran-C errors by processing of redundant data. However, advantages of simplicity and low cost make the TD transmission configuration preferable for experimental verification. The TD transmission BPAS error analysis results are indicative of the performance expected in the planned application of differential Loran-C to harbor and harbor entrance navigation.

INTRODUCTION

Background and Objectives

The U.S. Coast Guard maintains a network of moored buoys (aids to navigation) to control coastal and inland maritime traffic. The buoys can drag anchor or break their moorings in severe storms or ice floes. Delays presently encountered in identifying off-station buoys can result in property damage and potential government liability.

To remedy this problem, the U.S. Coast Guard is considering implementation of an electronic Buoy Position Auditing System (BPAS). An evaluation of two candidate BPAS configurations is presented herein:

- Transmission of digital Time Difference (TD) data from a Loran-C receiver on the buoy to a shore station or helicopter
- Combination of helicopter position data (from a Loran-C receiver and an altimeter) and helicopter-to-buoy range data (from a microwave ranging system), in a variable geometry solution.

The configurations are referred to as "TD Transmission" and "Variable Geometry," respectively.

The objectives of the study reported herein are to estimate system accuracy and to identify critical hardware parameters and operational restrictions. A theoretical error analysis approach is adopted.

System Descriptions

Both BPAS configurations employ differential Loran-C to minimize errors caused by TD grid instability. Specifically, corrections are applied to the TDs measured on the buoy or helicopter, based on TDs measured at a centrally-located pattern monitor. The BPAS application does not require that differential Loran-C be implemented in real time.

In the TD Transmission configuration, a Loran-C receiver is installed on each buoy (see Fig. 1). On command, buoy TD data are transmitted over a VHF telemetry link to a shore station, where the data are processed with pattern monitor TD data to determine the buoy position. Alternatively, buoy TD data may be transmitted to a helicopter and stored on magnetic tape for delivery to the shore station. The TD Transmission

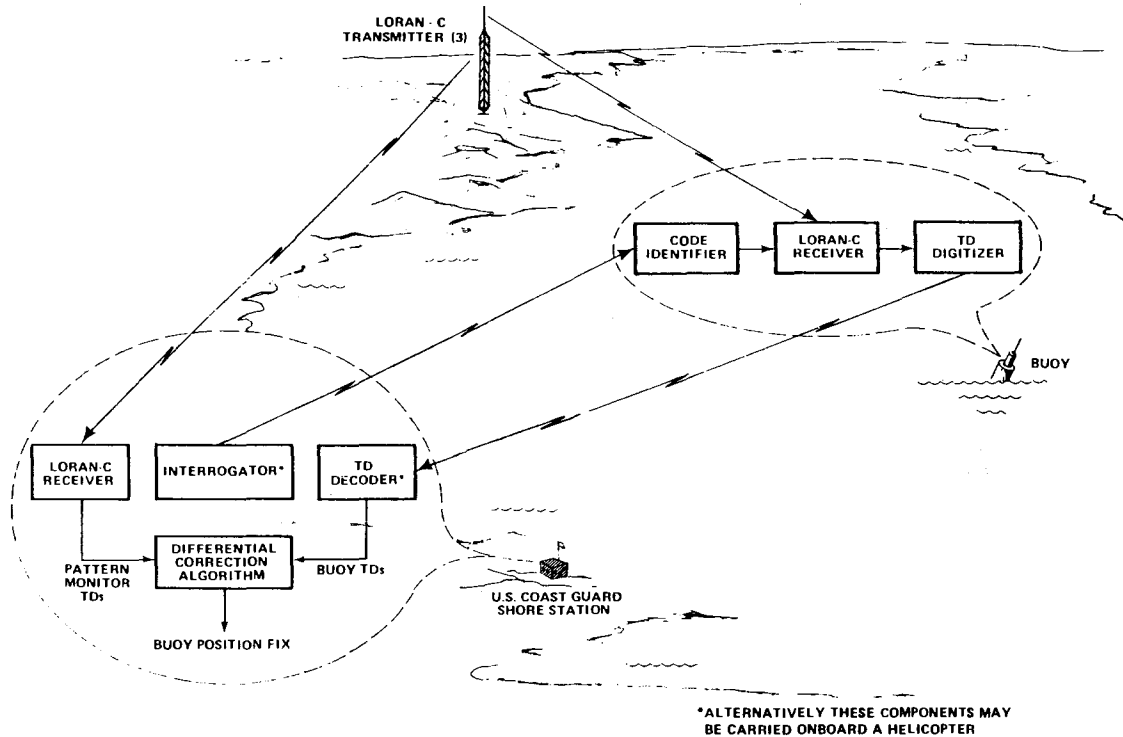


Figure 1 TD Transmission BPAS Configuration

configuration is conceptually simple and requires only minor modifications to existing equipment (Ref. 1).

In the Variable Geometry configuration, the audit is conducted from a helicopter equipped with a Loran-C receiver, a microwave ranging system, and an altimeter (see Fig. 2). The microwave ranging system serves to measure helicopter-to-buoy ranges. Active ranging is assumed, thereby requiring a transponder on each buoy. Synchronous TD, range, and altitude data are stored on magnetic tape and delivered to a shore facility for processing. The helicopter position at discrete points on the flight path is determined by differential Loran-C, and buoy positions are then estimated in a least-squares algorithm. The Variable Geometry BPAS configuration is more complex than the TD Transmission configuration, but still does not require major equipment development (Ref. 1).

ERROR ANALYSIS APPROACH

Buoy and Loran-C Scenarios

Seventeen buoys and three fixed aids (lights) in Boston Harbor are selected for analysis. (Fixed aids are considered for their possible use as pattern monitors.) The common names and approximate coordinates of the buoys and fixed aids are listed in

Table 1. Loran-C coverage for Boston Harbor is provided by the following transmitters of the Northeast U.S. chain: Seneca, NY; Caribou, ME; and Nantucket, MA. Hyperbolic Loran-C geometry is excellent in Boston Harbor, as quantified by a Geometric Dilution of Precision (GDOP) near unity.

TD Transmission Error Model

In the TD Transmission configuration, buoy position errors result from atmospheric noise and from propagation approximations made in the TD-to-position coordinate conversion (i.e., the TD grid). The latter errors are reduced significantly in differential Loran-C, because the grid is known precisely at the pattern monitor. It is only necessary to extrapolate the grid to the buoy. It is assumed that TDs are measured on the buoys when the Loran-C equipment is installed. These measurements define the grid at the desired buoy locations, at a specific time. If the relationship (difference) between the TD grid at the pattern monitor and other harbor locations is constant in time, the grid extrapolation can be performed exactly. However, the relationship is generally time-varying because TD variations are range-dependent.

The error model is based on idealized signal paths with:

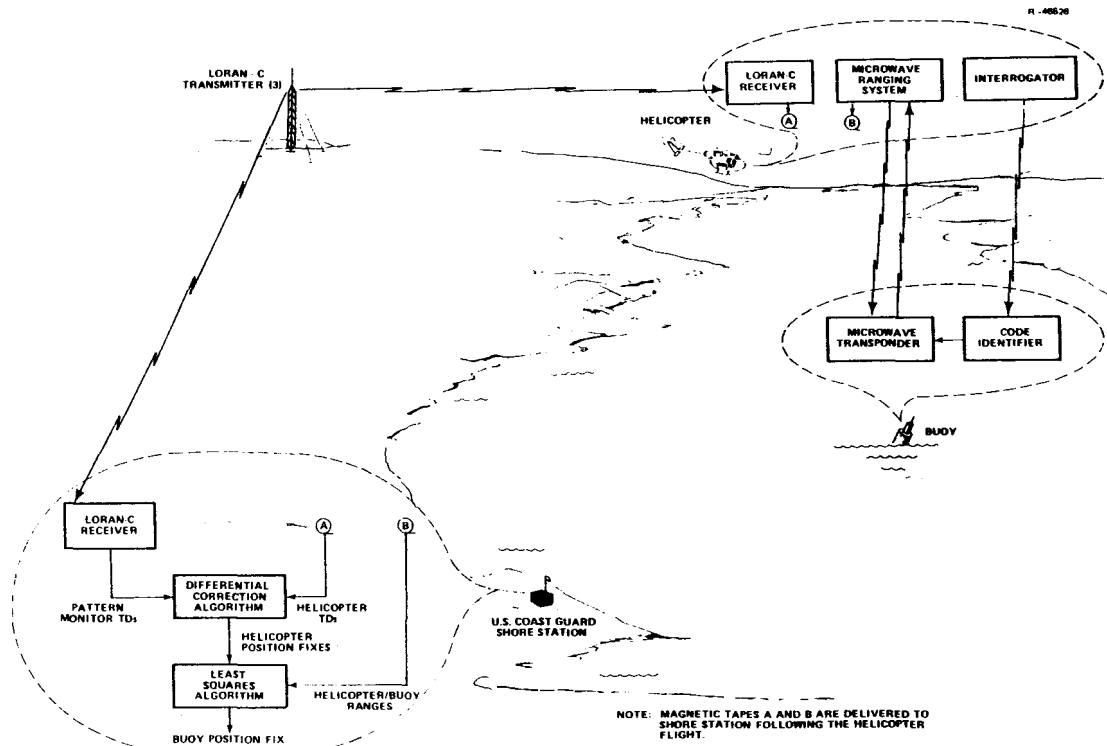


Figure 2 Variable Geometry BPAS Configuration

TABLE 1

SELECTED BUOYS AND FIXED AIDS IN BOSTON HARBOR*

TASC NUMBER	U.S. COAST GUARD NUMBER	COMMON NAME	LOCATION	APPROXIMATE LATITUDE (North)	APPROXIMATE LONGITUDE (West)
1	431	Lighted Bell Buoy 2	Boston North Channel	42°22.2'	70°55.2'
2	432	Lighted Buoy 1	Boston North Channel	42°21.9'	70°55.2'
3	437	Lighted Bell Buoy 10	Boston North Channel	42°20.6'	70°56.6'
4	438	Lighted Buoy 9	Boston North Channel	42°20.5'	70°56.2'
5	445	Lighted Buoy 2	Boston Main Channel	42°20.1'	70°59.0'
6	448.50	Light 5 (Fixed Aid)	Boston Main Channel	42°20.0'	71° 0.1'
7	41.52	Lighted Bell Buoy 2	3½ Fathom Ledge	42°21.1'	70°50.5'
8	461	Channel Lighted Bell Buoy 3	Nantasket Roads	42°19.1'	70°52.8'
9	462	Channel Lighted Buoy 4	Nantasket Roads	42°19.2'	70°54.0'
10	463	Channel Lighted Buoy 7	Nantasket Roads	42°19.0'	70°54.5'
11	464	Channel Lighted Buoy 8	Nantasket Roads	42°18.9'	70°55.0'
12	465	Channel Lighted Buoy 11	Nantasket Roads	42°18.7'	70°55.3'
13	466	Channel Lighted Buoy 12	Nantasket Roads	42°18.3'	70°55.6'
14	479.40	Lighted Buoy 4	Hull Gut Channel	42°17.9'	70°55.5'
15	480	Lighted Buoy 5	Hull Gut Channel	42°17.7'	70°55.4'
16	481	Harrys Rock Light 10 (Fixed Aid)	Hingham Bay Channel	42°17.2'	70°55.9'
17	430	Entrance Lighted Gong Buoy NC	Boston North Channel	42°22.5'	70°54.3'
18	38	The Graves Lighted Whistle Buoy 5	The Graves	42°22.5'	70°51.5'
19	42.10	Boston Lighted Horn Buoy B	Massachusetts Seacoast	42°22.7'	70°47.0'
20	43	Boston Light (Fixed Aid)	Little Brewster Island	42°19.7'	70°53.4'

* From Refs. 2 and 3.

- Homogeneous atmospheric refractive index and vertical lapse rate
- Two homogeneous-conductivity path segments -- land for the transmitter end of the path and sea water for the receiver end.

Loran-C signal phase delay is related to the path parameters by classical propagation theory and Millington's method (Refs. 4 and 5). A strong correlation between surface refractive index and vertical lapse rate is used to express the atmospheric effects by a linear function of refractive index alone (Refs. 1 and 6). The nonlinear phase/range relationship near the land/sea water conductivity-interface is the key element of the error model.

The nonlinear effect is shown in Fig. 3, a plot of secondary phase delay (SF) versus range for various land path lengths. SF decreases upon crossing from land to sea water. The shape of the SF function on the sea water path segment is important in the buoy application. The shape is independent of land path length (see Fig. 3), but depends on land conductivity. In Fig. 4, SF is shown relative to its value at the coastline, for various land conductivities. The slope of the SF function near the coastline (termed the scale factor) is sensitive to changes in land conductivity; far from the coastline, the slope approaches the constant slope for an all sea water path. With this in mind, three path types are defined in terms of the sea water path length, R_S :

- Type I: $R_S < 15$ km
- Type II: 15 km $< R_S < 200$ km
- Type III: $R_S > 200$ km

The path type may be transmitter-dependent, as illustrated for a hypothetical harbor in Fig. 5. The results contained herein are based entirely on Type I paths, representing a worst case.

In Ref. 1, it is shown that differential Loran-C errors are caused by the difference between the scale factors existing at the equipment installation time and buoy audit time. The rms scale factor error listed in Table 2 is based on a doubling of conductivity from winter to summer (Ref. 7). The refractive index error listed in Table 2 is based on seasonal meteorological data for the northeast United States. Loran-C measurement noise for the buoy and pattern monitor receivers

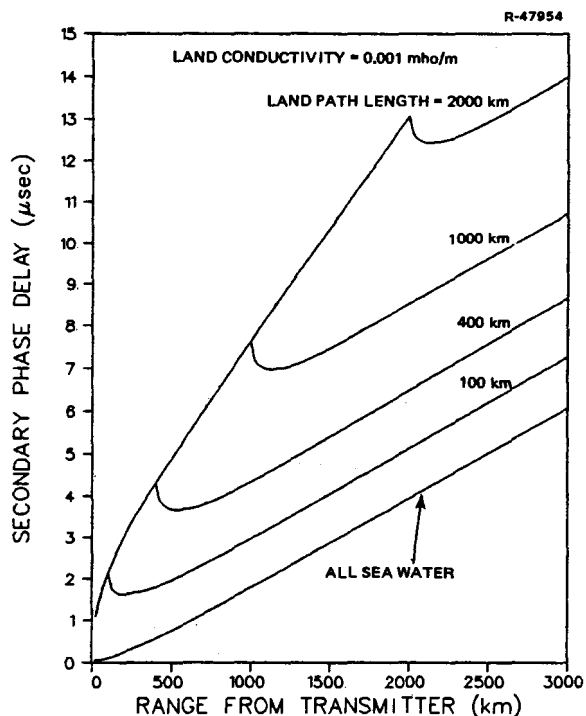


Figure 3 Secondary Phase Delay for a Mixed Land and Sea Water Signal Path

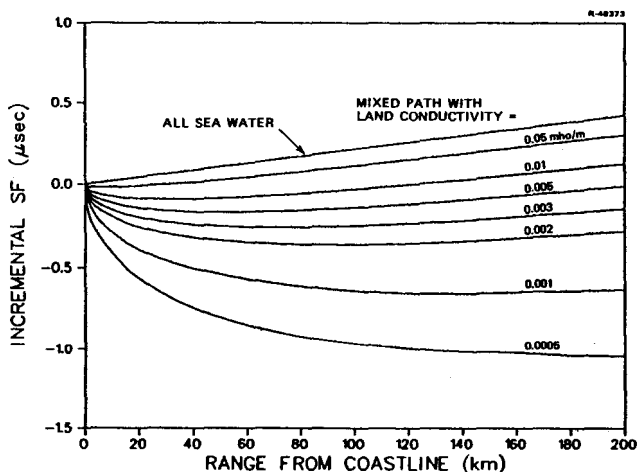


Figure 4 Incremental Secondary Phase Delay on Sea Water Path Segment

is set to 0.02 μ sec rms, consistent with available equipment and a 5-min averaging time.

Variable Geometry Error Model

The Variable Geometry BPAS error model includes components for Loran-C, the microwave ranging system, and the altimeter. The Loran-C error model is similar to the TD transmission error model (see Table 3). However, the scale factor error is assigned a larger standard deviation, because TD data

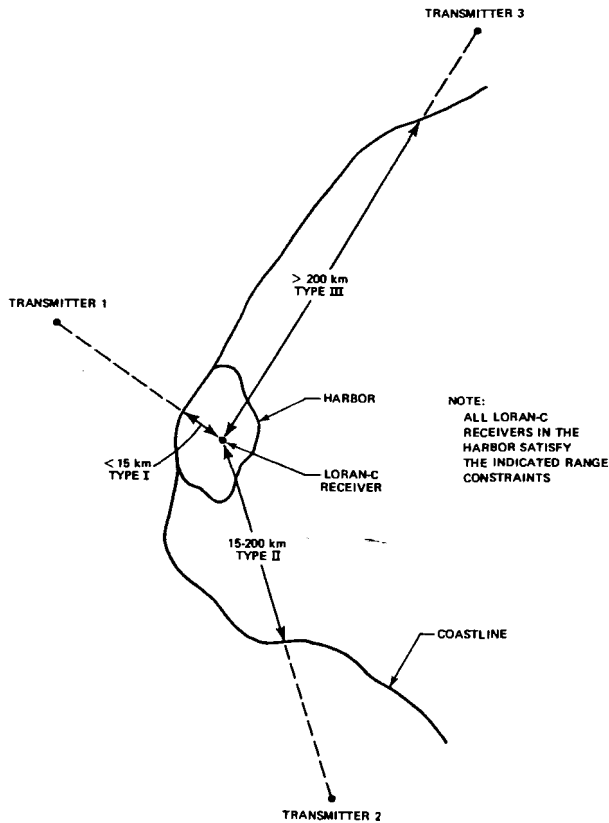


Figure 5 Definition of Signal Path Types For A Hypothetical Harbor

are assumed not to be available prior to the audit. In this case, scale factor error is caused both by seasonal conductivity variations and uncertainty in the yearly average conductivity. A nominal Loran-C measurement noise of 0.02 $\mu\text{sec rms}$ is assumed, although this value is probably not achievable in a wide-bandwidth airborne receiver. Sensitivity analyses are performed to study the effect of increased measurement noise.

The microwave ranging system error model includes the following error sources:

- Propagation velocity error -- the difference between actual and assumed microwave signal propagation velocities
- Common timing error (same for all buoys) -- uncompensated bias in round-trip signal travel time; could arise from helicopter receiver bias or common temperature-dependent transponder delay
- Independent timing errors (one per buoy) -- uncompensated bias in round-trip travel time; could arise from differences in transponder delays from

TABLE 2
NOMINAL ERROR LEVELS FOR
TD TRANSMISSION

ERROR SOURCE	VARIABILITY DURING AUDIT	NOMINAL STANDARD DEVIATION
Scale Factor Error	Constant	$12 \times 10^{-6} \mu\text{sec/m}$
Refractive Index Error	Constant	50 N-units
Buoy Measurement Noise	Random	0.02 μsec
Pattern Monitor Measurement Noise	Random	0.02 μsec

TABLE 3
NOMINAL ERROR LEVELS FOR
VARIABLE GEOMETRY

ERROR SOURCE	VARIABILITY DURING AUDIT	NOMINAL STANDARD DEVIATION
<u>LORAN-C ERRORS</u>		
Scale Factor Error	Constant	$33 \times 10^{-6} \mu\text{sec/m}$
Refractive Index Error	Constant	50 N-units
Helicopter Measurement Noise	Random	0.02 μsec
Pattern Monitor Measurement Noise	Random	0.02 μsec
<u>MICROWAVE ERRORS</u>		
Propagation Velocity Error	Constant	0.015 m/ μsec
Common Timing Error	Constant	0.02 μsec
Independent Timing Error	Constant	0.02 μsec
Measurement Noise	Random	0.01 μsec
Altitude Error	Constant	10 m

buoy to buoy, caused by manufacturing tolerances

- Measurement noise -- includes all random timing errors.

Nominal standard deviations for the microwave error sources are listed in Table 3. Propagation velocity error is based on seasonal variations in refractive index. The common and independent timing errors and measurement noise are based on use of a C-band or X-band microwave ranging system. Although the assumed values are consistent with the ranging errors reported for existing systems (i.e., less than 10 m rms; Ref. 8), individual contributions of the error components cannot be readily deduced from manufacturer specifications.

A three percent altitude error is assumed, based on the APN-171 radar altimeter. A typical 300 m helicopter altitude results in an rms error of 10 m.

TD TRANSMISSION ERROR ANALYSIS RESULTS

Sensitivity to Pattern Monitor Location

The buoy position error* ellipses (lo) for the 17 buoys in Boston Harbor are shown in Fig. 6 for a pattern monitor located at Boston Light. Note that the major axis of each error ellipse is oriented in the direction of the pattern monitor. Buoy position error increases with increasing distance from the pattern monitor, from approximately 10 m rms for the closest buoys to over 30 m rms for the farthest buoy.

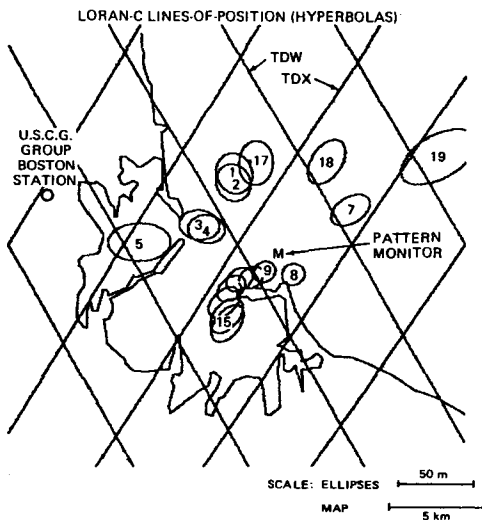


Figure 6 Nominal Error Ellipses (TD Transmission)

*Measurement error; not distance from desired location.

Buoy position error is a function of the geometry of the Loran-C stations as well as the location of the pattern monitor with respect to the buoy. However, in the case that the Loran-C lines-of-position (hyperbolas) cross nearly at right angles, as in Boston Harbor, rms buoy position error is a function of only the range to the pattern monitor, in the manner shown in Fig. 7. The 10 m rms position error for a buoy coincident with the pattern monitor is contributed by measurement noise.

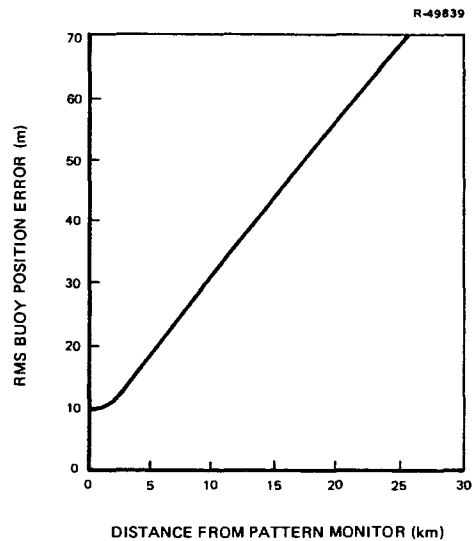


Figure 7 Dependence of Buoy Position Error on Distance from Pattern Monitor (TD Transmission)

The above results show the importance of locating the pattern monitor as near as possible to all buoys. For large harbors, multiple pattern monitors could be used. If a U.S. Coast Guard facility near the center of the buoy network is not available, buoy position error will degrade accordingly. For example, if the pattern monitor for Boston harbor were located at the U.S. Coast Guard Group Boston Station (see Fig. 6), the maximum rms buoy position error would increase from 31.5 m to 60 m.

Nominal Error Budget

Buoy position error is caused by the following Loran-C error sources:

- Scale factor error
- Refractive index error
- Buoy and pattern monitor measurement noises.

The individual contribution of each of these sources to buoy position error is shown in Table 4 for four selected buoys. Measurement noise is the same for all buoys and is composed of equal contributions for the buoy receiver and the pattern monitor receiver. The contribution of scale factor error to buoy position error increases with increasing buoy-to-pattern monitor range, starting from zero when the buoy is coincident with the pattern monitor. At a range of approximately 3 km from the pattern monitor, measurement noise and scale factor error contribute equally to rms buoy position error. Nominal refractive index error makes a negligible contribution to buoy position error.

TABLE 4
NOMINAL ERROR BUDGET FOR TD TRANSMISSION

ERROR SOURCE	CONTRIBUTION TO RMS BUOY POSITION ERROR (m)			
	BUOY 5	BUOY 15	BUOY 17	BUOY 19
Scale Factor Error	22.5	13.5	16.5	29.9
Measurement Noise	9.9	9.9	9.9	9.9
Refractive Index Error	0.3	0.2	0.2	0.5
Total Error	24.6	16.8	19.2	31.5

Sensitivity to Error Model Parameter Values

Accuracy is very sensitive to an increase or decrease in scale factor error, relative to the assumed nominal value (Fig. 8).* The nominal scale factor error standard deviation is computed based on Type I propagation paths for all three transmitters and a factor of two seasonal change in land conductivity. If scale factor error is reduced to the value associated with Type II or Type III propagation paths, the residual buoy position error is contributed almost entirely by measurement noise. Sensitivity of buoy position error to refractive index error is negligible for any physically reasonable increases or decreases in that error source. Sensitivity to measurement noise can be summarized as follows: a decrease in measurement noise below nominal does not improve performance significantly for the assumed Type I paths because of the dominance of the nominal scale factor error.

*This sensitivity curve has a logarithmic abscissa scale, offset by the nominal value of the error source.

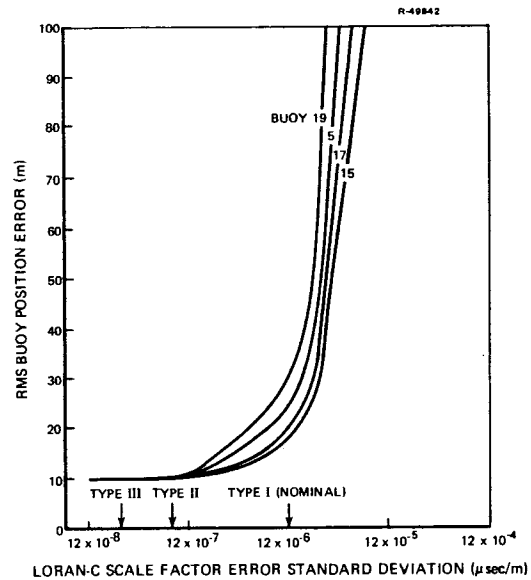


Figure 8 Buoy Position Error Sensitivity to Loran-C Scale Factor Error (TD Transmission)

Accuracy is relatively sensitive to increases in measurement noise, but the nominal value is expected to be achievable.

Effect of Loran-C Geometry

The impact of Loran-C transmitter geometry on buoy position accuracy at harbors other than Boston Harbor is evaluated using the scalar index GDOP. For the TD Transmission configuration, GDOP can be considered as the index by which buoy position error is scaled to determine BPAS accuracy for another harbor location, when TD errors in the two locations are equal (Ref. 1). GDOP is displayed for each location along the U.S. coastline in Fig. 9. The Loran-C secondary pair which gives the minimum GDOP is selected for each point on the coastline, after selecting the Loran-C chain which provides the maximum signal levels. Figure 9 shows that GDOP is nearly a minimum at Boston Harbor (1.17) and for most of the East Coast. The position errors reported in the previous sections should be scaled by GDOP (e.g., the position errors for San Francisco Harbor are approximately four times the position errors for Boston Harbor, given equal TD errors).

VARIABLE GEOMETRY ERROR ANALYSIS RESULTS

Sensitivity to Helicopter Trajectory and Pattern Monitor Location

Figure 10 shows the significant effect that helicopter trajectory

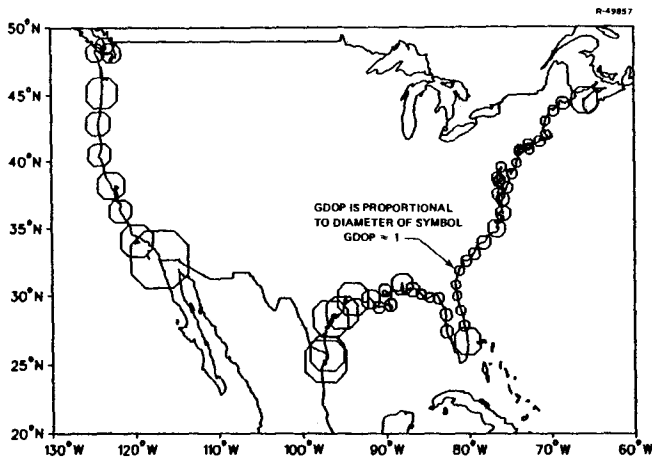


Figure 9 Loran-C GDOP Along U.S. Coastline

and east) of buoy position error. Position error for buoy 17 is reduced from 135 m rms after fix 2 (error ellipse not shown) to 87 m rms after fix 3, but additional fixes along the path are not effective. For example, fix 4 only reduces the error to 85.1 m rms. A deviation from the straight-line trajectory (fix 5), however, results in a substantial reduction to 20.4 m rms, and the final fix reduces the error to 6.3 m rms. A straight-line trajectory is ineffective in reducing buoy position error because of limited observability of constant error sources by the least-squares algorithm.

Results shown in Fig. 10 are relatively insensitive to the precise shape of the trajectory as long as a significant deviation from a straight line path is made. Studies have shown that a "rectangular" trajectory which penetrates the buoy field at least 10 km and deviates at least 3 km from a straight line will lead to rms buoy position errors of 10 m or less (see Fig. 11).

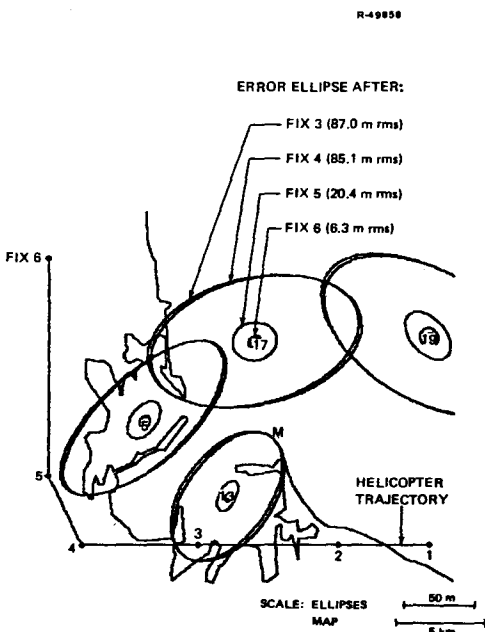


Figure 10 Buoy Position Error Ellipses for a Peripheral Trajectory (Variable Geometry)

geometry can have on buoy position error in the Variable Geometry BPAS configuration. Fixes 1 through 4 are taken along a straight-line path. Note that after the first fix, no estimate of buoy position can be computed from the least-squares algorithm, because at least two fixes are required to solve for the two components (north

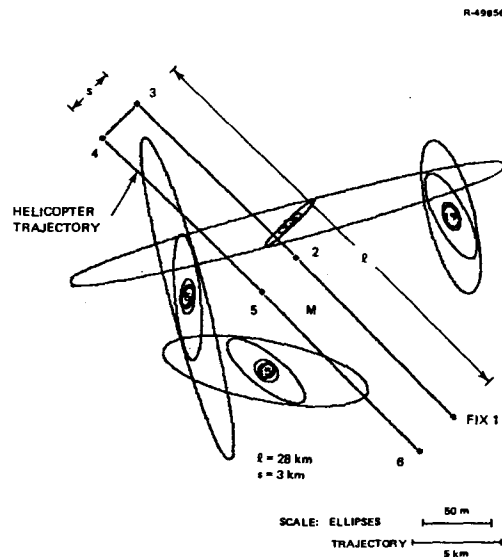


Figure 11 Buoy Position Error Ellipses for a Rectangular Trajectory (Variable Geometry)

The relation of buoy position error to pattern monitor location is more complex in the Variable Geometry configuration than in the TD Transmission configuration. The position of the helicopter trajectory with respect to both the buoys and the pattern monitor must be considered because of its relationship to observability of Loran-C errors in the least-squares algorithm. Since the helicopter would fly near the buoys to make microwave range measurements, a pattern monitor located in

the center of the buoy network is preferred. Figure 12 shows that moving the pattern monitor 94 km east of Boston Light (its nominal location) results in an increase in rms buoy position error from approximately 10 m to 80 m. This increase is much less than in the TD Transmission configuration (see Fig. 7) because of error calibration by the least-squares algorithm. As the pattern monitor is moved from its nominal central location, accuracy not only degrades, as shown in Fig. 12, but accuracy becomes more sensitive to helicopter trajectory. Figure 13 shows that buoy position error is extremely sensitive to the orientation of the trajectory when the pattern monitor is remotely located. (Orientation angle is measured to the long axis of the rectangular trajectory assumed for these studies, clockwise from north.) When the trajectory is rotated by 90 deg, rms buoy position error increases from 80 m to 175 m. There is little sensitivity to trajectory orientation for the nominal pattern monitor location. The cause of high sensitivity to the helicopter trajectory with a remote pattern monitor is explained by the ability (or inability) of the least-squares algorithm to calibrate the Loran-C scale factor error.

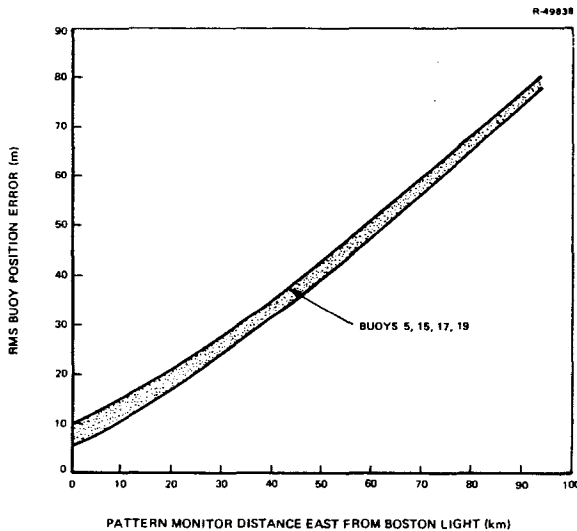


Figure 12 Buoy Position Error Sensitivity to Pattern Monitor Location (Variable Geometry)

Sensitivity to Error Model Parameter Values

Buoy position error in the Variable Geometry configuration is not

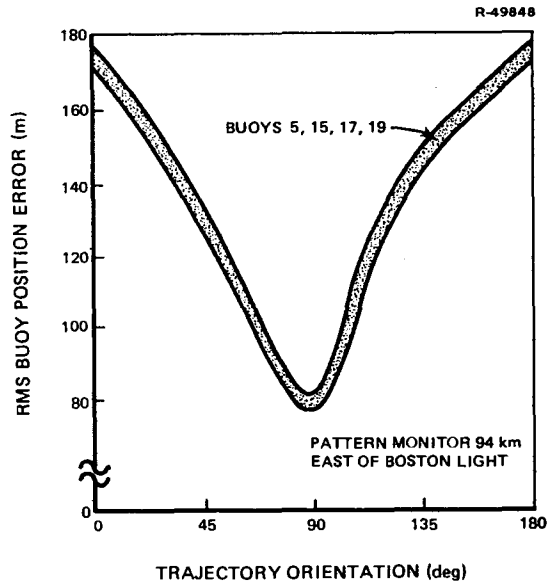


Figure 13 Buoy Position Error Sensitivity to Trajectory Orientation with Remote Pattern Monitor (Variable Geometry)

sensitive to the following parameters over a factor of 1,000 on either side of nominal (sensitivity to each parameter is determined with all other parameters at their nominal values):

- Loran-C scale factor error
- Loran-C refractive index error
- Helicopter altitude error
- Microwave common timing error.

The least-squares algorithm can effectively calibrate each of these error sources even from very large initial values.

Buoy position error is more sensitive to the following error sources:

- Microwave propagation velocity error
- Microwave independent timing error
- Microwave measurement noise
- Loran-C measurement noise.

An increase in microwave propagation velocity error by more than a factor of 10 is required to affect accuracy.

Sensitivity to the independent component of the microwave timing error is moderate for a factor of 10 increase in the error source. For larger microwave timing errors, buoy error increases rapidly and then levels off; the least-squares algorithm can calibrate the independent timing errors when they are large with respect to other error sources. Recall that sensitivity to the common microwave timing error is small; an error which is common to all buoys is more observable to the algorithm.

Buoy position error exhibits a large sensitivity to measurement noise, in both the microwave ranging and Loran-C systems. This large sensitivity is expected since measurement noise impedes the ability of the least-squares algorithm to calibrate the constant error sources. Sensitivity to helicopter Loran-C measurement noise (Fig. 14) is especially important because of the dynamic environment of the helicopter. The nominal standard deviation of the helicopter Loran-C noise was chosen to be the same as for the pattern monitor. However the increased bandwidth of the Loran-C phase-locked loops, required to compensate for helicopter motion, increases the measurement noise. While Fig. 14 shows performance to be quite sensitive to an increase in noise relative to the assumed nominal value, this sensitivity may be reduced by processing additional measurements. When helicopter Loran-C measurement noise is a factor of 10 above nominal, Fig. 15 shows that rms buoy position error can be reduced to 10 to 20 m by processing 100 measurements.

CONCLUSIONS

A comparison of the accuracy of the TD Transmission and Variable Geometry BPAS configurations is presented in Table 5. Under the nominal conditions assumed for this study (in particular, worst-case path conditions), the Variable Geometry configuration is more accurate than the TD Transmission configuration. Nominal buoy position-fix error is less than 10 m rms in the Variable Geometry configuration, while errors range from 10 m rms to 30 m rms in the TD Transmission configuration. The TD Transmission configuration has the advantage of minimal impact on U.S. Coast Guard operations, but the requirements of the Variable Geometry configuration are not severe. Only six microwave ranging fixes, taken along a 3 km by 10 km rectangular helicopter trajectory, are required to achieve a 10 m rms buoy position-fix accuracy in the Variable Geometry configuration.

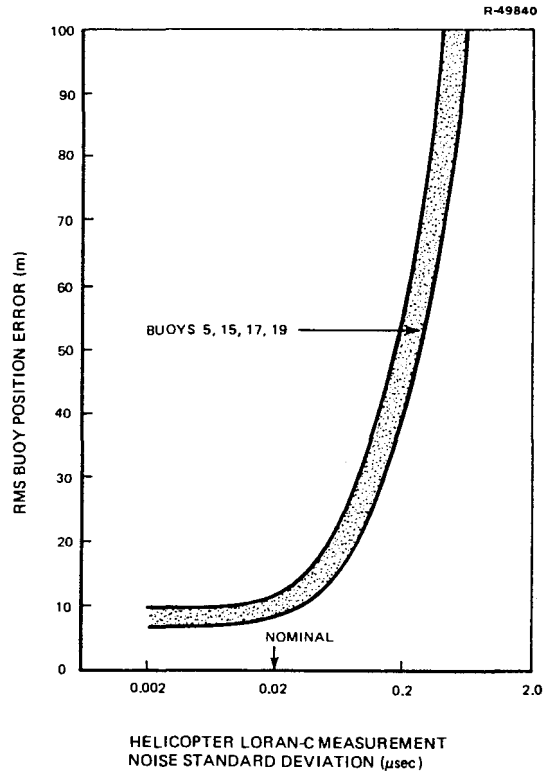


Figure 14 Buoy Position Error Sensitivity to Helicopter or Pattern Monitor Loran-C Measurement Noise (Variable Geometry)

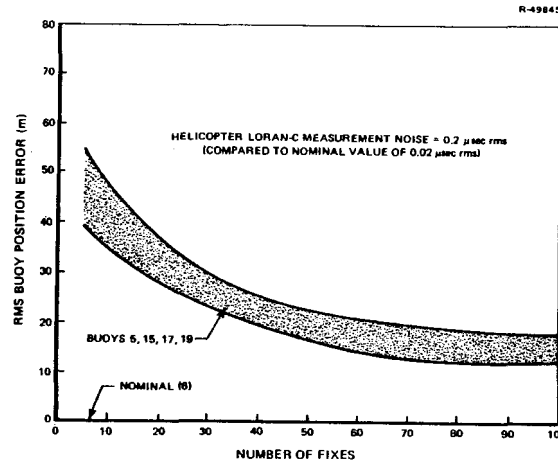


Figure 15 Buoy Position Error Sensitivity to Number of Fixes With Large Helicopter Loran-C Measurement Noise (Variable Geometry)

TABLE 5
TD TRANSMISSION AND VARIABLE GEOMETRY ACCURACY
FOR WORST-CASE PATH CONDITIONS

CONSIDERATION	TD TRANSMISSION	VARIABLE GEOMETRY
Nominal rms Error	10-30 m	<10 m
Operational Requirements	Minimal	3 km By 10 km Rectangular Trajectory With Six Fixes
<u>LORAN-C ERRORS</u>		
Scale Factor Error	Initial Calibration When Equipment Is Installed; BPAS Errors Sensitive To Scale Factor Error	No Initial Calibration; BPAS Errors Not Sensitive To Scale Factor Error Because Of Calibration By Least-Squares Algorithm
Pattern Monitor Measurement Noise	BPAS Errors For Both Configurations Sensitive To An Increase In Pattern Monitor Measurement Noise; Nominal Should Be Achievable, However	
Buoy Or Helicopter Measurement Noise	Factor Of Five Increase In Measurement Noise Produces 50 m rms BPAS Error; Subject To Extremes In Buoy Environment	Factor Of Five Increase In Measurement Noise Produces 30 m rms BPAS Error; Dependent On Receiver Tracking-Loop Bandwidth
Refractive Index Error	Negligible Impact On BPAS Error For Both Configurations	
<u>MICROWAVE ERRORS</u>		
Propagation Velocity Error	The TD Transmission Configuration Is Not Subject To Microwave Ranging And Altimeter Errors	Factor of 10 Increase In Propagation Velocity Error Produces Negligible Increase In BPAS Errors
Common Timing Error		BPAS Errors Not Sensitive To An Increase In Common Timing Error
Independent Timing Error		Factor Of 10 Increase In Independent Timing Error Produces 30 m rms Buoy Position Error
Measurement Noise		Factor Of Five Increase In Measurement Noise Produces 30 m rms Buoy Position Error
Altimeter Error		BPAS Errors Not Sensitive To Altimeter Error
Pattern Monitor Location	BPAS Errors Sensitive To Distance Of Pattern Monitor From Buoys	Less Sensitive Than TD Transmission; Sensitivity Can Be Further Reduced By Additional Fixes And/Or Improved Helicopter Trajectory
Potential For Improved Accuracy	Multiple Pattern Monitors	BPAS Error Estimates Significantly Less Than 10 m rms Are Unrealistic Because Of Potential Impact Of Unmodeled Error Sources
Loran-C Geometry (GDOP)	Very Sensitive; Proportional to GDOP	Relatively Insensitive

The most important distinction between the TD Transmission and Variable Geometry configurations affecting accuracy is the availability of redundant information in the Variable Geometry configuration. The Variable Geometry configuration is more accurate than the TD Transmission configuration primarily because of calibration of the Loran-C scale factor error by the least-squares algorithm at the time of the audit. Redundant information also makes the Variable Geometry configuration more adaptable in the event of adverse system constraints, such as a remote pattern monitor. Accuracy can normally be improved under adverse conditions by increasing the number of fixes or altering the helicopter trajectory. TD Transmission accuracy can be improved by employing multiple pattern monitors. Multiple monitors can be utilized conventionally or in a scale-factor estimation scheme. The latter is recommended for future study.

BPAS cost and complexity issues are discussed in Ref. 1. There it is concluded that the TD Transmission configuration per-buoy cost is less than half the cost for the Variable Geometry configuration. Based on its lower cost per buoy unit and relative simplicity, the TD Transmission configuration is recommended over the Variable Geometry configuration for experimental verification.

ACKNOWLEDGMENT

This project was sponsored by the U.S. Coast Guard Office of Research and Development under Transportation Systems Center Contract No. DOT-TSC-1723. BPAS hardware availability and associated cost studies were conducted by Joseph A. Wolfson and Peter D. Engels of the Transportation Systems Center and Martin C. Poppe, Jr. of Cambridge Engineering, and are documented in Ref. 1.

REFERENCES

1. Wolfson, J.A., Engels, P.D., Poppe, M.C., Jr., Foltz, J.M., and DePalma, L.M., "Loran-Based Buoy Position Auditing Systems -- Analytical Evaluation," Transportation Systems Center, Report No. CG-D-09-80, February 1980.
2. "Light List, Volume I, Atlantic Coast, St. Croix River, Maine to Little River, South Carolina," U.S. Coast Guard, CG-158, December 1978.
3. Nautical Chart of Boston Harbor, National Oceanic and Atmospheric Administration, National Ocean Survey, Chart Number 13270, 43rd Ed., March 1979.
4. Johler, J.R., Keller, W.J., and Walters, L.C., "Phase of the Low Radio Frequency Groundwave," National Bureau of Standards Circular 573, June 1956.
5. Millington, G., "Ground Wave Propagation over an Inhomogeneous Smooth Earth," Proceedings of the Institute of Electrical Engineers, Vol. 96, Pt. III, January 1949.
6. Bean, B.R., and Thayer, G.D., "On Models of the Atmospheric Refractive Index," Proc. IRE, Vol. 47, May 1959, pp. 740-755.
7. DePalma, L.M., and Gupta, R.R., "Seasonal Sensitivity Analysis of St. Marys River Loran-C Time Difference Grid," The Analytic Sciences Corporation, Technical Information Memorandum TIM-1119-3 (U.S. Coast Guard Report No. CG-D-33-80), June 1978.
8. Munson, R.C., "Positioning Systems," presented at International Congress of Surveyors (Stockholm, Sweden), June 1977.

SESSION II
POSITIONING TECHNOLOGY

PERFORMANCE REQUIREMENTS FOR RADIO NAVIGATION SYSTEMS IN HARBORS AND HARBOR WATERWAYS

William R. Bertsche and Richard B. Cooper
Eclectech Associates, Inc., North Stonington Professional Center, North Stonington, Connecticut 06359

Donald A. Feldman and Karl R. Schroeder
Office of Research and Development, U.S. Coast Guard, Washington, D.C. 20590

ABSTRACT

The provision of accurate radio navigation in U.S. harbors and harbor waterways will ultimately permit safe pilotage of vessels with the assistance of radio navigation displays. The safety of such operations is integrally dependent on the radio signal noise characteristics, the radio receiver filtering methods and characteristics and the method of information display. Quantification of these relationships is required to provide the system designer with standards for performance. This paper describes a series of experiments which parametrically addressed each of the above issues and attempted to identify the sensitivity of navigational safety to each of the above elements. All experiments were conducted on the SIMSHIP ship's bridge simulator using qualified pilots as subjects. The facility simulated high fidelity response characteristics of a 30,000 dwt tanker through a 35-degree left turn of a 500-foot wide channel in arduous but realistic wind and current conditions. Initially, four unique radio aids to navigation concepts, each with a number of individual design variables, were evaluated with ownship positioned by "perfect" information. From this, a benchmark display was selected and reexamined in a simulated noise environment. The project identified a graphic display with track-up, true motion, and a heading vector to be the more effective presentation of radio aids to navigation information. Further, while pilots were found to adaptively filter a broad range of noise on the display, bias errors caused immediate difficulty. Without filtering, pilots' performance was unchanged by display errors between 4 and 12 meters. With basic filtering techniques, 16 to 32 meter errors were acceptable. With from 16 to 32 meter rms noise, simple $\alpha - \beta$ trackers and gyro aided trackers resulted in nearly equivalent pilotage performance. For the $\alpha - \beta$ trackers, the best rise time fell near 12 seconds at rms signal noise of 16 to 32 meters. Results were inconclusive at the time this paper was written.

INTRODUCTION

The safe and effective implementation of radio aids to navigation systems for piloting in restricted waters continues as a major pursuit of the United States Coast Guard. Recent advances in electronic information processing and display technology have created new potentials for shipboard navigation systems. Increased accuracy, repeatability and reliability, as well as miniaturization and reduced cost of hardware, have led developers to promote these systems for use in restricted waterways. While many of these systems are inherently different in the way position information is derived, all pursue the common objectives of an effective display presentation,

suitable accuracy and minimal cost. Acknowledging these objectives, the U.S. Coast Guard program has focused on no one particular navigation system but instead is concentrating on how any system's information could be displayed and what effect the system's errors, tracker filter operation and tracker filter aiding technique would have on its overall usefulness.

The research employed the SIMSHIP ship's bridge simulator located at the Eclectech Associates, Incorporated facility in North Stonington, Connecticut. It was conducted in three experiments. The first two selected a benchmark display from among 20 alternative designs. This benchmark display was concluded to be easily understood, relevant to the immediate task, clearly and concisely formatted within perceptual limits and capable of instilling confidence in the user.* The final experiment evaluated the benchmark display under conditions of simulated system noise, filter design characteristics such as rise time and the effects of gyro aiding to the filter.

The project implicitly addresses the restricted waterway environment in which the watch officer is faced with a plethora of task demands in addition to navigation. Here the possibility of reduced visibility, removal or relocation of floating aids and difficulties in shiphandling could severely encumber his performance. In such an environment, the radio navigation system, pilot and ship must function together in a complex interaction which at present cannot be modeled. This research uses simulation as the means of parametrically and functionally studying the interaction, with results evidenced in a subsequent design specification. By acknowledging that information provided to the user is only as effective as the interface through which it is implemented, the research not only reveals criteria for the design of an effective system, but it provides cost tradeoffs with anticipated performance and demonstrates performance measures and analyses uniquely suitable for evaluating other displays.

THE SIMULATION EXPERIMENT

The simulator used for all three experiments was developed by Eclectech Associates in conjunction with a U.S. Coast Guard program for evaluating

*R.B. Cooper and K.L. Marino. Simulator Evaluation of Electronic Radio Aids to Navigation Displays, The Miniexperiment. Washington, D.C., United States Coast Guard, March 1980.

R.B. Cooper, K.L. Marino, and W.R. Bertsche. Simulator Evaluation of Electronic Radio Aids to Navigation Displays, The RA-1 Experiment. Washington, D.C., United States Coast Guard, August 1980.

visual aids to navigation systems. The simulated radar and navigation displays were driven by a Digital Equipment Corporation GT-44 computer graphics system with PDP-11/40 central processor and VT-11 graphic generation hardware. The computer CRT display is mounted in a free-standing pedestal and equipped with required controls/indicators and bearing rings to simulate a PPI type bridge display or various radio aids to navigation formats. Other computers control both the electronic bridge display and visual system although visuals were not used during the radio aids evaluation. The computer program reflects ownship characteristics, maneuverability, hydrodynamic influences, and individual scenario (i.e., waterway and environment) conditions. In the case of the benchmark display evaluation which included a simulated noise environment, the program also modeled navigation system noise, system filter characteristics, and filter aiding techniques. The computer facility provides a continuous automatic recording of ship position, ship status, and bridge control manipulations for subsequent data reduction, graphic and statistical analysis. —

The scenario selected for all radio aids to navigation experiments had been used in other U.S. Coast Guard research projects* and was selected to provide a means of comparing and validating resulting performance. Simulated ownship was a 30,000 dwt tanker, with 595-foot LOA, 84-foot beam, and 28-foot draft. A qualified helmsman familiar with the handling characteristics of the ship was assigned as quartermaster. All necessary charts, ship maneuvering data and thorough instructions on the use of displays were provided.

Initially both wind and current were from astern making trackkeeping relatively easy, but requiring a continuous determination of speed over the ground in order to properly execute the turn. In the second leg, current was initially strong on the port quarter but gradually weakened and shifted astern. Wind speed and direction remained strong and gusting on the port quarter which tended to weathervane the ship. Trackkeeping in the second leg required the pilot to initially steer about 300 degrees true to make good 306 degrees. By the finish, steering 306 degrees true made good the course. All this time the helmsman was required to hold from 3 to 5 degrees right rudder for the wind. This provided a very challenging but not unrealistic scenario for determining the sufficiency of navigation information and the pilotage.

A variety of performance measures were applied in the experiments not only to identify which displays were effective during the pilotage, but also to determine suitable measures for use in subsequent navigation display evaluations. Prior to each run, subjects were instructed to remain on the centerline of the channel as much as possible. Establishing this goal was somewhat artificial to those pilots who

*M. Smith and W. Bertsche. Aids to Navigation Presimulation Report, AN-CAORF Experiment. Washington, D.C.: United States Coast Guard, September 1979.

M. Smith. Aids to Navigation Presimulation Report, AN-VISUAL Experiment. Washington, D.C.: United States Coast Guard, October 1979.

otherwise might have chosen to keep to the right. This was necessary, however, to define a baseline of performance and in the end was considered reasonable by most pilots in light of the narrow channel width. Two major categories of performance were analyzed; the ability to keep on the channel centerline well within the channel, and the ability to avoid excessive control actuations such as hard rudder or full propulsion power. Ownship initially started 92 feet to the right of the centerline requiring the pilot to maneuver back to the centerline as he might after passing an outbound traffic ship.

SELECTION OF BENCHMARK DISPLAY

The benchmark display was selected by evaluating pilots' shiphandling and trackkeeping performances as they used each different display to navigate through a narrow, simulated waterway. The selection process first screened 18 display variables using brief 15-minute simulations requiring maneuvering through a 35-degree turn in a 500-foot wide channel. From this experiment, five displays which resulted in the best performance, plus two additional steering displays were selected for a second, full-length simulation. The second scenario included maneuvers within the channel, transit of straight legs with wind and current effects and, again, the 35 degree left turn. Both selection experiments were conducted with ownship situated on the display using perfect position information. In other words, no navigation system noise error or filter effects (i.e. lag or jitter) were simulated. This second experiment not only selected the benchmark display, but, as a result of using perfect position information, it provided a baseline of performance to which the display could be compared when tested with noise and a filter.

Initially, three basic display concepts were evaluated; a DIGITAL display or alphanumeric presentation of navigation parameters, a GRAPHIC or plan position type of display, and a PERSPECTIVE presentation similar to the view from the forward windows. These different display concepts and the systems requirements necessary to produce them, represented major cost categories which were traded off against each display's operational effectiveness. In the second experiment a STEERING display concept representative of proposed predictive steering systems was introduced. A brief description of the display variables follows for each of the basic concepts evaluated.

DIGITAL DISPLAY

Figure 1 shows one example of the six different DIGITAL display formats evaluated. For commercial applications, the information could be presented using LED, liquid crystal, plasma panel or multiple-projection type displays. For the experiment, all display concepts were presented on a CRT screen. The DIGITAL display variable included what information was presented and, to some extent, how and when it was presented. Displayed information consisted of the following:

1. Crosstrack distance and direction of ownship from the channel centerline.
2. Crosstrack velocity and direction of velocity.

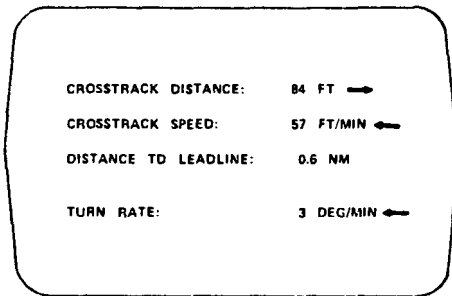


Fig. 1. Example of a DIGITAL Display

3. Course error and direction, which is the angular difference between ownship course and the channel leg.
4. Heading to steer for ownship to make good the channel leg.
5. Actual turn rate of ownship and direction.
6. Recommended turn rate and direction to arrive on the centerline of the next leg (used only at intersections).
7. Distance to the intersection leadline or waypoint.
8. Time to the intersection leadline or waypoint.

In addition to what information was displayed, the experiment also evaluated two methods governing when it was displayed. Since the display was intended to provide both trackkeeping and turnmaking guidance, turning information such as recommended turn rate and distance to new centerline were either precomputed and displayed automatically by the system or prompted manually by the individual pilot. The appropriateness of this timing, of course, would affect the outcome of the turn; as a result, the method of prompting for the information became a display design variable. Cost estimates for the display system excluding up-front receiver hardware are expected to range up to \$1,000 for each unit. Aside from display hardware, the system would require a microcircuit position resolver or microprocessor and RAM memory. If turn initiation is prompted automatically, development costs for describing the waterway would be incurred.

The experiment evaluated all practical combinations of displayed information for the DIGITAL display from the simplest with only crosstrack distance, crosstrack velocity and time or distance to the waypoint, to the most comprehensive, including heading to steer and turning instructions. The experiments concluded with recommendations for implementing this type of display and perhaps incorporating it with other display concepts. In general however, the DIGITAL display did not yield the superior performance exhibited by some of the other concepts, particularly during maneuvers within the channel and at the turn. Major performance deficiencies of the DIGITAL displays, regardless of which variables were used, were continuous overshoots when steadying up on the centerline, at the 35-degree bend and when steadying up beyond the bend. There was also high crosstrack variability (i.e., large crosstrack standard deviations) entering the bend, through the

bend and well into the second leg. This indicated highly inconsistent trackkeeping performance among the pilots, a detrimental characteristic under such circumstances. The DIGITAL display was not recommended as the benchmark display for subsequent experiments in a simulated noise environment

GRAPHIC DISPLAY

Figure 2 shows one example of the ten different GRAPHIC display formats which were evaluated. As a shipboard system, the information would be presented on a CRT or flat panel display, possibly superimposed over a radar PPI or automatic radar plotting aid (ARPA) display. The GRAPHIC display variable included display orientation (head up or track up), display motion (true or relative), ownship's vector (heading flash or course vector) and ownship's designation (a scaled ship image or symbolic cross). Cost estimates for such a system would, of course, depend upon its integration with other systems if that were desired. A standalone system excluding up front receiver hardware is expected to range up to \$5,000 for each unit. This would include capabilities for adding alphanumeric to the display, a variable not investigated in the study. The GRAPHIC system as it was simulated would require a microprocessor, RAM memory, control and display unit, and perhaps gyro interface. Such a system is presently under development by the Applied Physics Laboratory, Johns Hopkins University for the U.S. Coast Guard. It is scheduled for at-sea operational evaluation on the St. Mary's River later this year (1980). This particular system, called PILOT, was the subject of a previous paper.*

While additional costs could be incurred for unique display features such as color, zoom or variable range capabilities and selection of operating modes, the greatest cost will probably result from the development and maintenance of the computerized description of the waterway that would be required. Accuracy and feature details for this waterway model were not addressed in the research, though it is acknowledged that all of the display concepts evaluated will require some degree of waterway description.

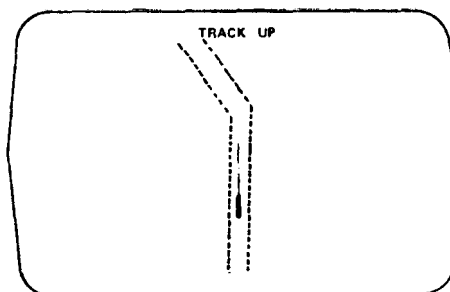


Fig. 2. Example of a GRAPHIC Display

*C.R. Edwards and J.M. Ligon. PILOT: Precision Intracoastal LORAN Translocation - Exploiting LORAN-C in the Harbor and River Environment. Paper delivered at the Wild Goose Association Eighth Annual Technical Symposium, Williamsburg, Virginia, 17 to 19 October 1979.

The GRAPHIC display presented a plan view with ownship always situated in the center of the screen during relative motion operation, and moving across the screen in the true motion mode. Channel boundaries were shown as dashed lines. Range scale for the experiment was 0.75 nautical miles (screen radius). In the track-up mode the channel leg always reset to the top of the screen either when ownship had traveled three-quarters of the way across the screen (true motion only) or when ownship had penetrated more than one ship length into a new leg. This characteristic enabled a smooth transition through lengthy straight legs as well as when turning from one leg to another. Overall operation was quite similar to the PILOT system.

The variable of greatest interest on the GRAPHIC display was the presentation of ownship's vector. Two types were evaluated: a heading vector, which corresponded to gyro heading and appeared similar to a PPI heading flash, and a course vector, which represented the course-being-made-good of ownship. The course vector was drawn for a distance ownship would travel in 1.5 minutes.

The experiments concluded that the track-up, true motion displays with scaled ship's image were both well received by the subjects and provided overall superior pilotage performance. Results of the track-keeping analysis showed that pilots did best in the straight legs when they used the course vector, and best in the turns when they used the heading vector. Both performances were superior to other display concepts. Due primarily to its wide acceptance by pilots and its overall cost-effectiveness, the heading vector, GRAPHIC display was recommended for benchmark display evaluation.

PERSPECTIVE DISPLAY

Figure 3 shows one of the two different PERSPECTIVE formats tested. The PERSPECTIVE display represents what the pilot would see out the forward windows if channel boundaries were visible. These boundaries, shown as dashed lines, only identified boundary location. They were not affixed to the world and consequently did not appear to pass by ownship as it transited through the waterway. This lack of a velocity cue, plus difficulty in "seeing" abeam and astern made use of the display difficult for many pilots.

Variables selected for the experiment were 60-degree and 90-degree fields of view. The 60-degree display provided considerably less visibility abeam and made determining position within the channel very difficult for the pilot. Cost estimates for the PERSPECTIVE display were up to \$5,000 due to

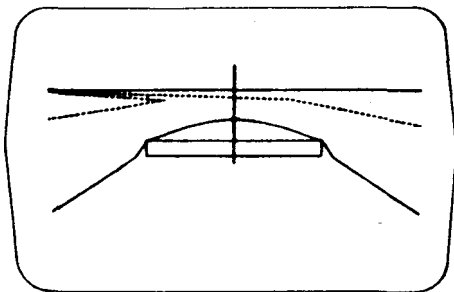


Fig. 3. Example of a PERSPECTIVE Display

graphic transformation requirements, the need to model ownship as well as the waterway, and the cost of suitable display hardware.

Analysis of performance showed that the pilots had difficulty steadying on the channel centerline, both before the bend and beyond it. While trackkeeping through the turn was acceptable, pilots also had difficulty in determining when to apply check rudder and the amount of set by the wind and current. The PERSPECTIVE display was not recommended as a benchmark display for subsequent experiments.

STEERING DISPLAY

Figure 4 shows one of the two predictor STEERING display formats evaluated. Both displays are intended to predict for the pilot what his ship's track will be, given its present motion and state of ship control. The two different STEERING displays selected for evaluation were representative of diverse design sophistication. One format, the Predictor Steering Display, used ownship's hydrodynamic equations to continuously recompute and redraw its projected track from inputs of rudder, rpm, ship motions and forces acting upon ownship. Whenever rudder or throttle actuations were initiated, a resultant projected trackline was displayed. In addition to the projected track, a projected ownship image was drawn at the end of the vector. This image showed the computed attitude (or drift angle) of ownship by the time it would reach the full prediction. For the experiment, "prediction time" was fixed at 1.5 minutes, a length suitable for use given ownship's speed, display range scale, and angle of the bend in the channel.

Hardware and development costs for this type of display would be high, well in excess of \$10,000. Analysis of trackkeeping and shiphandling measures from the experiment, however, demonstrated superior pilotage performance over all other concepts when the Predictor Steering Display was used. This was evidenced in both high trackkeeping consistency among pilots and an overall mean track well on the channel centerline. Such results were anticipated based on the findings of numerous other studies* relating to predictive steering systems.

A Simplified Predictor Steering Display representing lower cost and less sophistication was also evaluated in the experiment. Both STEERING displays were identical to the GRAPHIC displays in orientation, motion and spatial characteristics. The

*R.B. Cooper, W.R. Bertsche, and K.P. Logan. Standardization of the Advanced Ship's Bridge Display. Washington, D.C.: U.S. Maritime Administration, July 1978.

R.B. Cooper, W.R. Bertsche and G.J. McCue. Simulator Evaluation of Predictor Steering, Short Range Collision Avoidance and Navigation Displays. Washington, D.C.: U.S. Maritime Administration, November 1979.

W.B. Van Berlekom. "Simulator Investigations of Predictor Steering Systems for Ships," Transactions of Royal Institute of Naval Architects, Paper 2, 1977.

Kockums Automation AB. Precise Maneuvering in Confined Waters, Controlled Radial Steering. Unpublished, Malmo, Sweden.

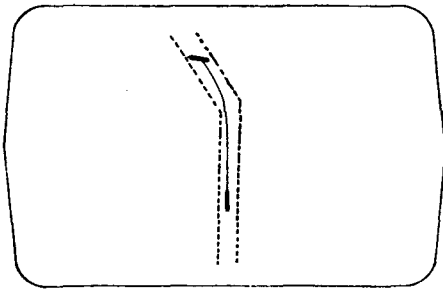


Fig. 4. Example of a STEERING Display

steering displays, however, could exhibit curved vectors to portray the curved track of ownship through a maneuver. With the simplified steering display, this vector consisted of a series of short straight vectors. The first, or closest vector to ownship, was drawn in the direction ownship was traveling (i.e., course) based on existing speed and rate of turn. Assuming a constant velocity and rate of turn for ownship, second, third and fourth, etc. vectors were then drawn and attached to each other to produce a gradually curving projected track. Since turn rate rarely remains constant through a turn maneuver, the vector updated periodically to show the newly computed track based on newly sampled turn rate information. The resultant track prediction, however, is always "behind" the actual dynamics of the ship; this is unlike the more sophisticated, but also more costly Predictor Steering Display, which indicated the future curved track even before turn rate developed.

The Simplified Predictor Steering Display is estimated to cost only a little more than the GRAPHIC display since required computational capabilities and gyro inputs would already exist. Unfortunately, pilots' performance when using the simplified display was less favorable than when using either the Predictor Steering or GRAPHIC displays. Results of the trackkeeping and shiphandling analysis conclude that while adequate training and/or experience probably would make pilots proficient with the simplified version, the performance exhibited during the experiment precludes its recommendation as a benchmark system. On the other hand, while the Predictor Steering Display promoted overall superior pilotage performance, the relative uncertainty of its future implementation and cost factors governing both its development and installation severely disadvantaged it as a viable candidate for benchmark consideration; it also was not recommended.

EVALUATION OF BENCHMARK DISPLAY WITH SYSTEM NOISE

The simulator evaluation of the benchmark display in a noise environment was conducted early in the fall of 1980. Subsequently, all conclusions reported herein are the result only of a preliminary analysis of data and of observations made during the simulations.

Evaluation of the benchmark display with system

noise required an additional simulation of a signal noise environment, a radio receiver, and a signal processing unit (filter). A digital signal processing technique was selected for this application because a survey of state of the art radio receivers showed most of them to employ microprocessor technology and digital filtering techniques. Both the receiver and signal filter characteristics were represented as a single alpha-beta (α - β) tracker. The form of the α - β tracker was a second order recursive filter that represents an optimum compromise between transient performance and noise reduction.* A two-axis orthogonal signal geometry was assumed for the implementation — north-south signal and an east-west signal. The noise in these signals was assumed to be independent over the sample interval chosen. A white noise source with a Gaussian distribution was assumed.

The basic navigation receiver system was implemented as shown in Figure 5. The α - β tracker equations implemented in each tracker are listed in reference 2. Each tracker was critically damped under the condition that:

$$\beta = \alpha^2 / (Z - \alpha) \quad (1)$$

For the experimental conditions the value of α was changed to alter the tracker's rise time. Where tracker rise time was defined to be the time period (in seconds) required for the filter output to achieve 66.7 percent of the filter input value given a step input value. Reference 2 also contains a table of α versus tracker rise time.

Fast time simulation of these tracker performances with the 30,000 dwt ship maneuvering in the test channel showed acceptable performance could be obtained in the straight legs. However, with longer rise times, a substantial lag error was introduced while the ship maneuvered through the turn. Figures 6, 7, and 8 show the tracker's performance in a 35-degree right turn with 3, 12, and 24 second rise time respectively. The smooth central track is the actual track of the simulated ship. The sequence of tracker estimated positions are also plotted for a sample

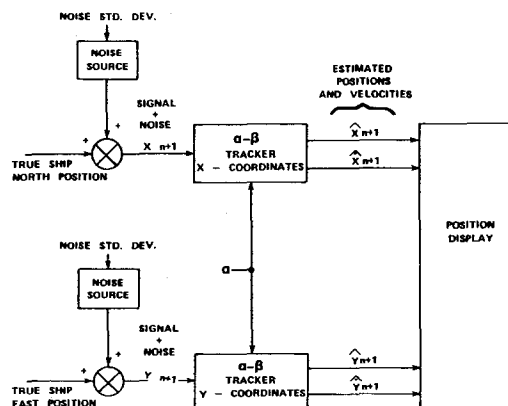


Fig. 5. Implementation of Navigation System for Experimentation

*CAPT. Donald A. Feldman. Using Alpha-Beta Trackers in Marine Piloting By Radio Navigation. Washington, D.C.: United States Coast Guard, Final Report, July 1980.

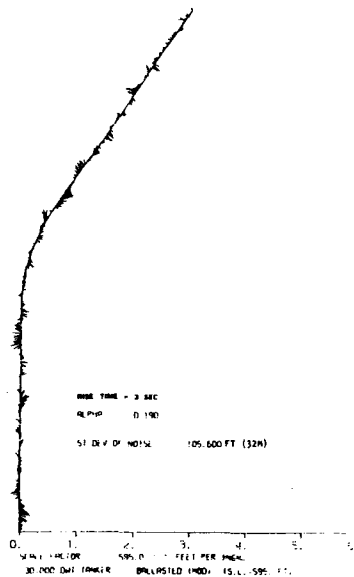


Fig. 6. Rise Time - 3 Seconds

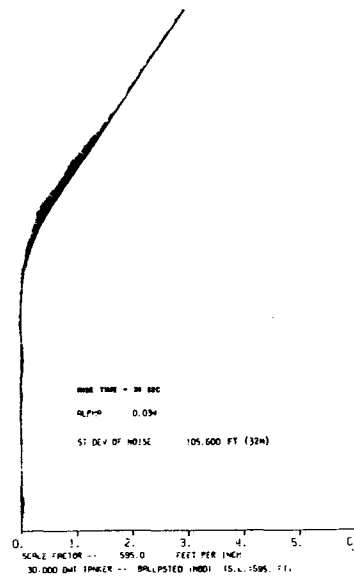


Fig. 8. Rise Time - 24 Seconds

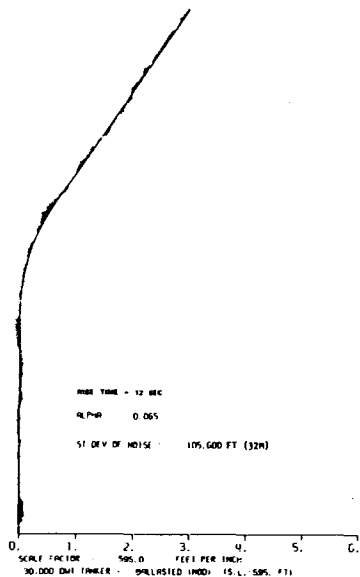


Fig. 7. Rise Time - 12 Seconds

period of $T=1$ second. Short lines connect the ship's actual position with the tracker estimated position for each sample interval. A 32-meter rms noise is added to ownship's true position "signal" for these runs.

There are several characteristics of the plots in Figures 6, 7, and 8, which are of interest with regard to the benchmark display evaluation. The errors of the estimated position for the short rise times (3 seconds) is relatively large but the pattern is somewhat random. The longest rise time (24 seconds), on the other hand, appears to have minimal errors in the straight legs, but a rather large bias error in the turn which results from filter lag. The medium rise time (12 seconds) represents a compromise between the two extremes and results in the smallest maximum position error over the entire run.

An improvement in the tracker design was sought to emulate performance of more sophisticated trackers available in certain receiving and signal processing systems. Gyro aiding was added to the basic $\alpha - \beta$ trackers to improve the trackers' estimate of velocity and to account for velocity changes that occur in turns. For each sample velocity, changes were calculated based on the assumption of constant turn rate, and constant velocity over the sample period. Figure 9 illustrates an $\alpha - \beta$ tracker system with gyro aiding. The applicable equations are provided in reference 2.

The inherent advantage of providing gyro aiding to the trackers is that the bias error is eliminated in the turn and the tracker may be operated at a higher rise time. Figure 10 illustrates a fast time digital simulation run equivalent to those in Figures 6, 7, and 8. Note that for the same noise (32 meter rms) minimum tracker errors are present with the 24 second rise time.

The combination of rise time, presence or absence of gyro aiding, and rms level of the noise provide a variety of perception problems to the observer of navigation displays. The evaluation of the benchmark display considered four basic signal noise characteristics with both 16 meter and 32 meter rms signal noise:

- 3-second rise time no aiding (high noise random)
- 12-second rise time no aiding (medium noise random)
- 24-second rise time no aiding (low noise bias errors)
- 24-second rise time with gyro aiding (minimum noise)

Conduct of the experiment as described in the presimulation plan* required eight qualified pilots as

*R. Cooper and K. Marino. Presimulation Plan for the Evaluation of Radio Aids to Navigation Displays with System Noise. Washington, D.C.: United States Coast Guard, August 1980.

BENCHMARK DISPLAY WITH 16 M AND 32 M RMS NOISE

Perhaps the most outstanding finding of the experimental runs was the fact that no significant difference in performance occurred between conditions when the noise was 16 meters versus 32 meters rms, a difference of 52 feet. In retrospect, it is considered that within certain limits of noise, man himself is a very adaptable filter and he is able to achieve good shiphandling performance relatively independent of the level and characteristics of noise he observes. This finding could have profound effects on the future development of radio navigation systems, since systems signal to noise ratio apparently has less effect on piloting performance than was previously expected.

BENCHMARK DISPLAY WITH HIGH RANDOM NOISE

In the single condition of high random noise (i.e., 32 meter rms noise, 3 second rise time, no aiding) pilots showed the largest variability in piloting performance. This behavior was indicated by a small (8 feet) but statistically significant increase in the average crosstrack standard deviation during the turn recovery. The increase was as great as 25 feet in some areas of the channel. Under this condition there appears to be a trend for the ships' tracks to oscillate about the channel centerline. Otherwise, their overall performance was nearly equivalent to other conditions. The observed performance under this condition implies that if the rms noise were to increase by other multiples (e.g., up to 64 meters), then perhaps piloting performance would decrease under high random noise conditions.

BENCHMARK DISPLAY WITH MEDIUM RANDOM NOISE

In the condition of minimum maximum errors without gyro aiding (e.g., 32 meter rms noise, 12-second rise time, no aiding), the pilots' showed a minimum crosstrack variability following the turn. Their performance in this condition appears to be equivalent to that with gyro aiding and a rise time of 24 seconds. Under this condition during the turn recovery, the crosstrack standard deviation was 25 feet less than for the previously discussed high random noise case (3-second rise time). The observed performance under this condition has some interesting implications. First, the pilots' performance with the unaided filter was best with the filter condition which had displayed the minimum maximum error in simulated evaluation of the filter. Second, while overall the unaided filter exhibited a higher level of random noise versus the aided filter, the pilots themselves were able to filter the random noise and achieved equivalent performance.

BENCHMARK DISPLAY WITH LOW NOISE/HIGH BIAS ERROR

In the condition of 32 meter rms noise the long rise time (i.e., 24 seconds) resulted in low noise but a large bias error in the turn when no gyro aiding was present. Under these conditions during the turn recovery, the ships' crosstrack standard deviations were nearly equivalent to the case of high random

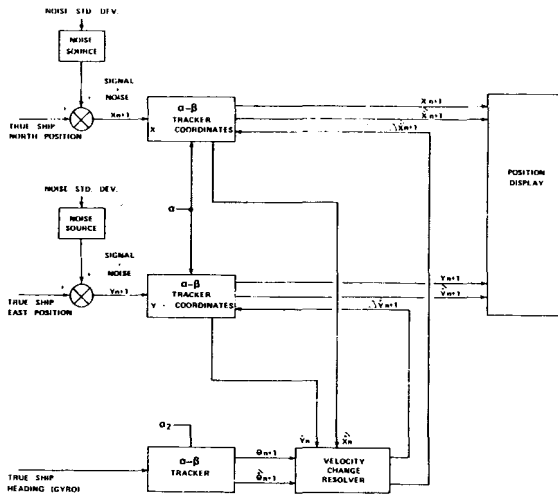


Fig. 9. Implementation of Navigation System With Gyro Aiding

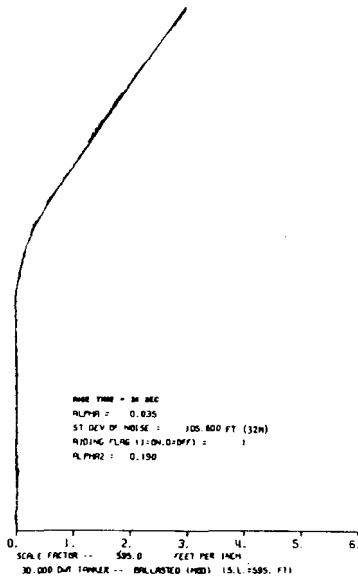


Fig. 10. Rise Time - 24 Seconds, Gyro Aided

subjects, each to use the benchmark display for eight different conditions of noise, tracker rise time, and gyro aiding. All subjects were thoroughly familiarized with the operation of the benchmark display but were unaware of position lag errors in the system as a result of the filter characteristics. They could, of course, see the display jitter when it was prevalent. The noise experiment employed the same scenario conditions and measures of performance used in selecting the benchmark display without noise. This resulted in a metric that could be used to compare baseline performance (i.e., no noise) with performance exhibited when noise and filter characteristics prevailed.

noise (3 second rise time). The crosstrack standard deviation was approximately 25 feet greater for these conditions than the case of medium random noise, no aiding, and minimum noise, with aiding. It is especially noteworthy that the performance in the turn was nearly equivalent for the 3-second and 24-second rise time cases because the maximum errors predicted in the simulation runs for these two conditions were equivalent. Thus, in the area of turn recovery, there appears to be little behavioral difference between high random noise conditions and high bias errors. It is believed, however, that high bias errors are potentially more detrimental since during these runs pilots often expressed the opinion that the ship did not appear to be handling correctly.

BENCHMARK DISPLAY WITH MINIMUM NOISE

The overall best piloting behavior with 32 meter rms noise occurred with a 24-second rise time and gyro aiding. Under these conditions the noise level was minimum throughout the run and the bias error was removed. The fact that performance in this condition was essentially equivalent to the medium noise condition (12-second rise time, no aiding) reinforces the concept that piloting performance is relatively insensitive to rms noise level especially if there are no bias errors present. As noted, however, piloting performance began to degrade in the high noise condition (3-second rise time, no aiding). Further quantification of these results must await a more thorough analysis of the experimental results; however, the crosstrack rms display errors for the four tracker conditions were calculated in the simulated runs and are shown in Table 1. The 25-foot increase in crosstrack standard deviation following the turn might be attributed to the 6 meter increase in crosstrack rms display error.

TABLE 1. CROSSTRACK RMS DISPLAY ERRORS

<u>TRACKER CONDITION</u>		<u>SIGNAL NOISE</u>	
RISE TIME GYRO		16 meter	32 meter
(SECONDS)		AIDED	
3	No	5.6 meter	12 meter
12	No	3.7 meter	6 meter
24	No	13.7 meter	10 meter
24	Yes	2.5 meter	4 meter

CONCLUSIONS

Full analysis of the experimental results has not yet been completed. Nevertheless, the emerging trends in the data permit us to draw some conclusions relative to piloting ships in very narrow channels. They are as follows:

- Within the available state of the art and the competitive price range, the most suitable navigation display appears to be a GRAPHIC display which shows in plan view the channel boundaries, the ship hull outline, and a heading vector. The preferable operating mode appears to be track-up, true motion. This display, however, tends to result in some overshoot of the turn; and piloting performance with it is at present considered inferior to visual piloting techniques.

- DIGITAL and PERSPECTIVE displays generally result in inferior piloting performance relative to the other displays which were evaluated. They could, however, be made more effective through training, redesign, or incorporation with other displays.
- Piloting performance is relatively insensitive to changes in the rms display error when the error falls between 4 to 12 meters. Given even basic filtering techniques, this may be restated in terms of 16 to 32 meter rms signal noise in orthogonal independent signals.
- Pilots appear to adaptively filter a broad range of noise on the display. Bias errors on the other hand tend to cause more immediate difficulty and should be minimized.
- In very narrow channels with signal noise on the order of 16 to 32 meter rms, simple $\alpha - \beta$ trackers or $\alpha - \beta$ trackers gyro aided with a rise time selected to achieve minimum maximum crosstrack error result in performance nearly equivalent to performance with no signal noise present.
- For a simple $\alpha - \beta$ tracker the best rise time appears to fall near 12 seconds for rms signal noise of 16 to 32 m.

REFERENCES

1. R.B. Cooper and K.L. Marino. Simulator Evaluation of Electronic Radio Aids to Navigation Displays, The Miniexperiment. Washington, D.C.: United States Coast Guard, March 1980.
2. R.B. Cooper, K.L. Marino, and W.R. Bertsche. Simulator Evaluation of Electronic Radio Aids to Navigation Displays, The RA-1 Experiment. Washington, D.C.: United States Coast Guard, August 1980.
3. M. Smith and W. Bertsche. Aids to Navigation Presimulation Report, AN-CAORF Experiment. Washington, D.C.: United States Coast Guard, September 1979.
4. M. Smith. Aids to Navigation Presimulation Report, AN-VISUAL Experiment. Washington, D.C.: United States Coast Guard, October 1979.
5. C.R. Edwards and J.M. Ligon. PILOT: Precision Intracoastal LORAN Translocation - Exploiting LORAN-C in the Harbor and River Environment. Paper delivered at the Wild Goose Association Eighth Annual Technical Symposium, Williamsburg, Virginia, 17 to 19 October 1979.
6. R.B. Cooper, W.R. Bertsche and K.P. Logan. Standardization of the Advanced Ship's Bridge Display. Washington, D.C.: U.S. Maritime Administration, July 1978.
7. R.B. Cooper, W.R. Bertsche and G.J. McCue. Simulator Evaluation of Predictor Steering, Short Range Collision Avoidance and Navigation Displays. Washington, D.C.: U.S. Maritime Administration, November 1979.

8. W.B. Van Berlekom. "Simulator Investigation of Predictor Steering Systems for Ships," Transactions of Royal Institute of Naval Architects, Paper 2, 1977.
9. Kockums Automation AB. Precise Maneuvering in Confined Waters, Controlled Radial Steering. Unpublished, Malmo, Sweden.
10. CAPT. Donald A. Feldman. Using Alpha-Beta Trackers in Marine Piloting By Radio Navigation. Washington, D.C.: United States Coast Guard, Final Report, July 1980.
11. R. Cooper and K. Marino. Presimulation Plan for the Evaluation of Radio Aids to Navigation Displays with System Noise. Washington, D.C.: United States Coast Guard, August 1980.

QUANTIFICATION OF ST. MARYS RIVER
LORAN-C TIME DIFFERENCE GRID INSTABILITY

L.M. DePalma and P.M. Creamer
The Analytic Sciences Corporation
One Jacob Way
Reading, Massachusetts 01867

E. Anderson
U.S. Coast Guard
Research and Development Center
Avery Point
Groton, Connecticut 06430

ABSTRACT

Time Difference (TD) data collected in the St. Marys River Loran-C chain coverage area between May 1979 and May 1980 are analyzed to quantify an apparent temporal TD grid instability. The data include TD-samples, nominally recorded every 15 min at three fixed-site monitors and the System Area Monitor (SAM), Local Phase Adjustment (LPA) data, and meteorological data from the National Weather Service Station at Sault Sainte Marie, Michigan. Assorted non-parametric data analyses, including spectral and correlation analyses, are conducted to separate diurnal and seasonal components of grid instability and identify relationships among the various TDs. The relative magnitude of the seasonal TD variations and the correlation of pairs of TDs are not consistent with expected weather-related variations in signal propagation time, suggesting that the grid instability may be partially transmitter- and/or receiver-related. The Loran-C data are also employed to evaluate the U.S. Coast Guard low-density (five 15-min samples, twice daily) data analysis approach. The low-density approach is found to be adequate for monitoring seasonal TD variations, but inadequate for monitoring diurnal variations. An increase in the sampling rate is recommended for low-density Loran-C data collection in harbors.

Furthermore, theoretical sensitivity analyses based on seasonal meteorological effects could not explain the instability (Ref. 3). It was recommended that the U.S. Coast Guard initiate a yearlong data collection effort. Data-base management software was subsequently designed to support the data editing and analysis.

High-density data are collected, consisting of TDs and signal-quality indicators, recorded nominally every 15 min at three fixed sites: DeTour Village, Dunbar Experimental Forest, and Pt. Iroquois (see Fig. 1). Two Internav LC-204 Loran-C receivers are located at both the DeTour and Iroquois sites, and one Internav LC-204 and one Magnavox AN/BRN-5 receiver are located at the Dunbar site. The following data are collected to support the analyses: System Area Monitor (SAM) TDs from the Austron-5000 receiver used for chain control, Local Phase Adjustments (LPAs) from the Calculator Assisted Loran Controller (CALOC) system, and meteorological data from the National Weather Service Station at Sault Sainte Marie, Michigan.

In addition, the U.S. Coast Guard collects low-density data for in-house analyses. These data consist of five 15-min samples recorded

INTRODUCTION

Background

The U.S. Coast Guard collected St. Marys River Loran-C data from May 1979 to May 1980 to quantify an apparent Time Difference (TD) grid instability. This data collection program culminated a three-year effort aimed at characterizing the mini-chain grid.

The three-year effort began with the calibration of a spatial TD grid prediction model based on data collected during September and October 1977 (Refs. 1 and 2). TD data collected monthly from November 1977 to March 1978 exhibited temporal variations as large as 0.4 μ sec peak-to-peak (p-p). Because the utility of the spatial model and the mini-chain requires a stable grid, it was important that the observed instability be confirmed. In particular, questions remained regarding the receiver installations, e.g., the antenna

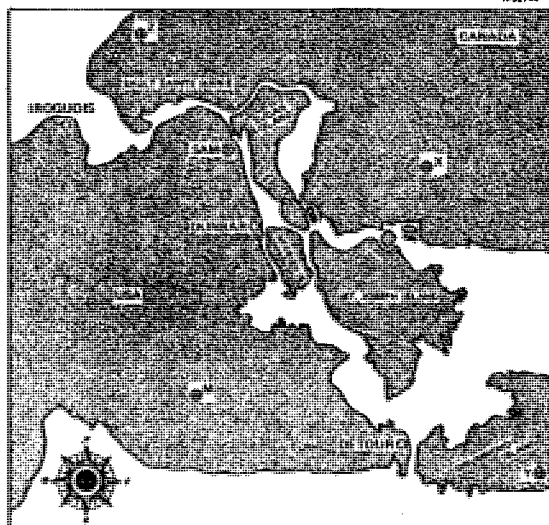


Figure 1 Locations of Data Collection Sites and Transmitters in Reconfigured St. Marys River Loran-C Mini-Chain

TABLE 1
SUMMARY OF EDITING OPERATIONS

SITE	RECEIVER TYPE/ NUMBER	TIME DIFFERENCE	TOTAL NUMBER OF SAMPLES	PERCENT OF DATA RETAINED AFTER EACH EDITING OPERATION			NUMBER OF RETAINED SAMPLES	STANDARD DEVIATION* (µsec)
				SIGNAL-QUALITY CHECK	TOLERANCE CHECK	OUTLIER EDITING		
DeTour	LC-204/1	X	17,574	90.4	93.0	97.5	14,417	0.015
		Y	19,186	92.7	69.1	92.7	11,403	0.024
DeTour	LC-204/2	Y	20,432	93.1	98.0	96.1	17,910	0.020
		Z	19,047	91.0	97.1	95.6	16,095	0.020
Dunbar	BRN-5/1	X	21,772	98.2	98.3	95.3	20,037	0.023
		Y	21,843	98.4	98.5	89.2	18,873	0.031
Dunbar	LC-204/2	Y	20,219	91.9	98.6	96.0	17,593	0.019
		Z	16,983	92.1	98.4	95.3	14,670	0.020
Iroquois	LC-204/1	X	28,650	88.2	99.2	97.8	24,527	0.017
		Z	28,485	88.0	99.2	96.4	23,959	0.020
Iroquois	LC-204/2	Y	29,344	90.3	98.3	96.2	25,052	0.020
		Z	29,642	87.7	98.8	97.6	25,041	0.018
SAM	Austron/1	X	37,486	97.6	97.4	98.1	34,995	0.016
		Y	37,484	95.6	97.9	97.4	34,135	0.019
		Z	37,363	97.2	98.0	96.9	34,463	0.018

*Standard deviation of the differences between the retained TD data and trend lines fit to daily data segments

twice daily, which are then averaged and transmitted over a telephone data link. A similar system is under development for use in the U.S. Coast Guard Loran-C Harbor Monitor Program.

Objectives

The objectives are to process and analyze the high-density data to

- Quantify TD grid instability in the St. Marys River Loran-C mini-chain
- Evaluate the low-density data analysis approach to assure an effective monitoring strategy for harbors.

The determination and modeling of cause/effect relationships is beyond the scope of the analyses discussed herein. Possible explanations for the observed instability are offered in Refs. 4 and 5.

DATA-BASE DESCRIPTION

Editing Procedure

A three-step TD editing procedure is used, which includes a signal-quality check, a tolerance check and a check for statistical outliers. The procedure is implemented by a flagging system to preserve the original data base.

Signal quality is determined from the sufficient-signal indicators output by the receivers. The signal-quality check is the only editing operation not based on the TD data itself.

Next, the TD data are compared with conservative lower and upper bounds determined from the low-density data. TDs which differ from

the seasonal mean by more than 0.5 µsec are rejected. A major purpose of the tolerance check is to detect receiver cycle jumps.

In the final editing operation, outliers are detected by comparing each TD sample to a daily trend line fit to the time series data. Samples which differ from the trend line by more than 0.15 µsec are rejected, and a new trend line is computed from the remaining samples. Only samples which lie within 0.05 µsec of the new trend line are retained (89.2 to 98.1 percent of the data; see Table 1). Data which are inconsistent with the short-term time series behavior are removed in this operation.

Data Inventory

The editing operations are summarized in Table 1 for the 15 TD time series. The quality of the edited data base is excellent. All data lie within a ±0.05 µsec band centered on the daily trend line, and the standard deviations of the TD/trend line differences are between 0.015 µsec and 0.031 µsec (see Table 1). The short-term fluctuations are consistent with those measured in the laboratory.

Large gaps spanning one to eight weeks occur in some time series. These gaps are associated with missing cassette tapes, rather than edited data. U.S. Coast Guard low-density data are available to fill the gaps (Ref. 4), but would not significantly affect the analysis results. The 46-megabyte St. Marys River Loran-C data base is the most comprehensive of its kind assembled to date.

QUANTIFICATION OF TD GRID INSTABILITY

Seasonal Variations

Seasonal TD variations are quantified by the mean and standard deviation of the data

in 3-day time windows. The seasonal time series are presented in Figs. 2, 3, and 4. An examination of these figures leads to the following conclusions:

- Seasonal TD variations are less than $0.4 \mu\text{sec}$ p-p, consistent with previous observations (Refs. 2 and 3)
- TD values in May 1979 and May 1980 are approximately equal, suggesting a meteorological effect
- TD variations during monthly periods are larger in the winter than in the summer, consistent with signal propagation theory (Refs. 3 and 6)
- The 3-day standard deviation is small ($<0.025 \mu\text{sec}$) relative to variations in the 3-day mean

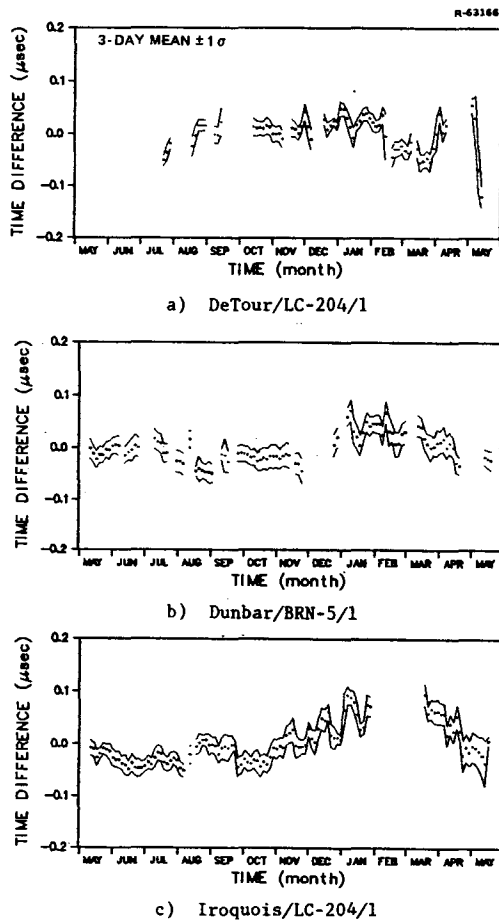


Figure 2 TDX Seasonal Time Series

*Each receiver is identified by site/receiver type/receiver number. TDs are plotted relative to the seasonal mean.

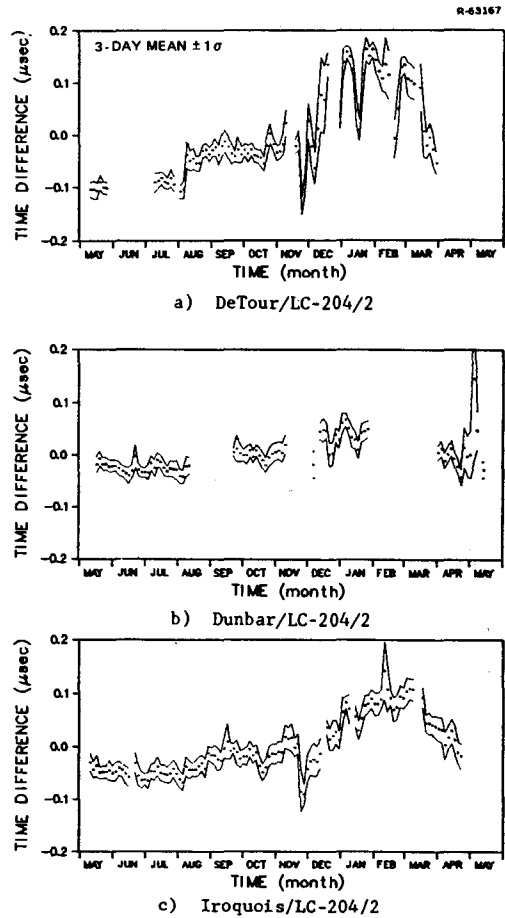


Figure 3 TDY Seasonal Time Series

- The standard deviation of the 3-day means (see Table 2) is larger for TDY than for TDX and TDZ, i.e., $0.069 \mu\text{sec}$ average compared to $0.032 \mu\text{sec}$ average.

The mini-chain is controlled to a $0.015\text{-}\mu\text{sec}$ control tolerance during the data collection period. Actual seasonal TD variations at the SAM are less than $0.02 \mu\text{sec}$ p-p.

Monthly Variations

The distinct difference between summer and winter TD variations is analyzed by focusing on July and January. Monthly TD variations are quantified in Ref. 7 by the mean and standard deviation of the data in 6-hr time windows (e.g., see Fig. 5). An examination of the monthly time series leads to the following conclusions:

- TD variations are less than $0.10 \mu\text{sec}$ p-p for July, but as large as $0.20 \mu\text{sec}$ p-p for January
- TDs often change very abruptly in January -- e.g., $0.10 \mu\text{sec}$ during a one- or two-day period

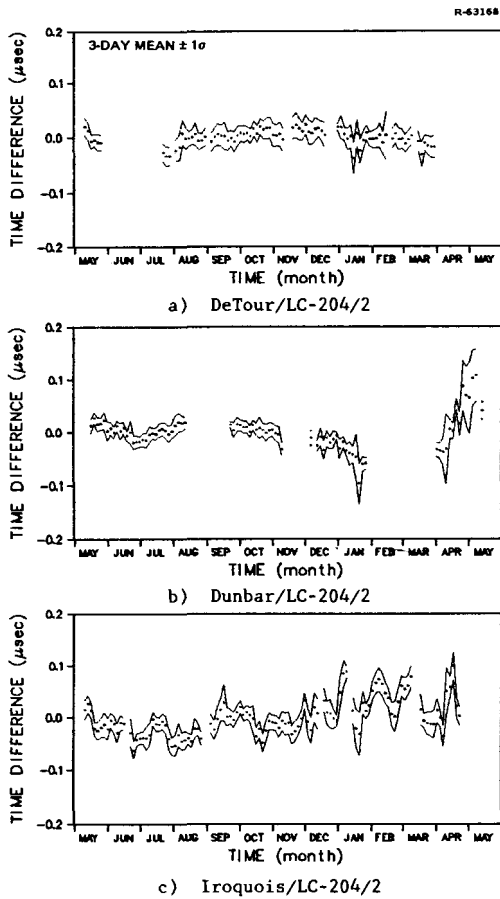


Figure 4 TDZ Seasonal Time Series

TABLE 2
SEASONAL TD STATISTICS

SITE	RECEIVER TYPE/ NUMBER	TIME DIFFERENCE	STATISTICS OF 3-DAY TD MEANS (μsec)		
			MEAN	STANDARD DEVIATION	PEAK-TO-PEAK
DeTour	LC-204/1	X	11328.261	0.032	0.174
		Y	22210.351	0.106	0.532
DeTour	LC-204/2	Y	22210.346	0.082	0.300
		Z	33416.693	0.013	0.061
Dunbar	BRN-5/1	X	11293.276	0.027	0.119
		Y	22363.361	0.045	0.180
Dunbar	LC-204/2	Y	22363.369	0.032	0.189
		Z	33290.870	0.033	0.204
Iroquois	LC-204/1	X	11325.374	0.037	0.146
		Z	33156.894	0.044	0.235
Iroquois	LC-204/2	Y	22413.893	0.052	0.232
		Z	33156.915	0.034	0.162
SAM	Austron/1	X	11259.695	0.002	0.013
		Y	22363.866	0.005	0.037
		Z	33200.397	0.003	0.015

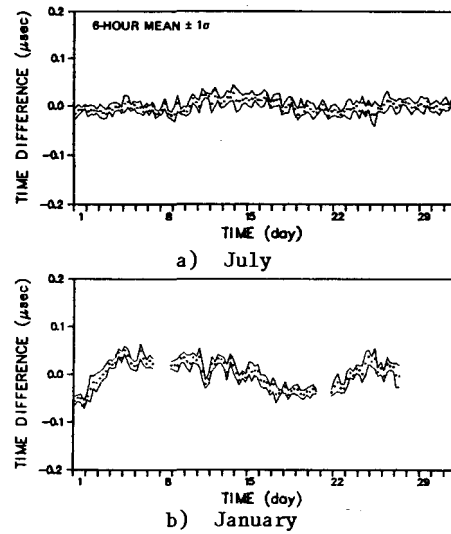


Figure 5 TDX Monthly Time Series for Iroquois/LC204/1

- Diurnal variations are smaller in July than in January, but represent a greater proportion of the overall monthly variation in July
- The 6-hr standard deviations are small relative to the variation of the 6-hr means.

Confirmation of the expected difference between summer and winter TD variations is an important contribution of the data collection program.

Diurnal Variations

Diurnal TD variations in July and January are quantified in terms of the mean diurnal cycle. The monthly data are first sorted by day, and the daily mean is subtracted to form TD residuals. The TD residuals are then sorted by time-of-day, irrespective of day-of-month, and the mean and standard deviation of the residuals in 2-hr time windows are computed.

Examples of the diurnal cycles for July and January are presented in Figs. 6 and 7, respectively.* The following conclusions are drawn:

- The diurnal cycles are small, generally less than $0.02 \mu\text{sec}$ p-p
- The diurnal cycle is obscured by random variations for many time series, but is distinct for others (e.g., see Fig. 6a)
- Some diurnal cycles exhibit a bimodal behavior (e.g., see Fig. 7a).

*The time shown is Greenwich Mean Time (GMT), where 0 hours GMT is 7 p.m. Sault Sainte Marie local time.

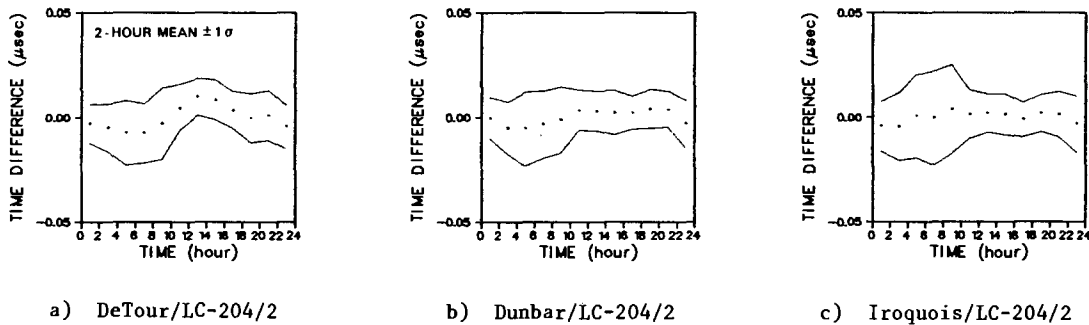


Figure 6 TDY Diurnal Cycles for July

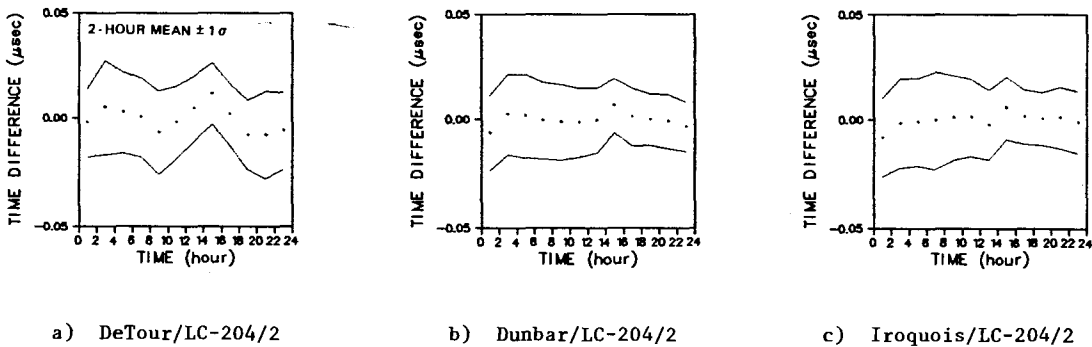


Figure 7 TDY Diurnal Cycles for January

Histograms of the random diurnal variations are approximately Gaussian with a standard deviation of 0.02 μsec (Ref. 7).

Spectral Analyses

The relative contributions of seasonal, monthly, and diurnal TD variations are given by the normalized Power Spectral Density (PSD). The procedure adopted for PSD computation is described in Refs. 7 and 8. Data pre-processing includes: 2-hr averaging to reduce computation, linear interpolation to bridge gaps, and removal of a ramp function to detrend the time series. PSD computation involves the Fast Fourier Transform and intermediate computation of the autocorrelation function.

PSDs are presented in Figs. 8, 9, and 10. The time series all contain spectral peaks at the 24-hr and 12-hr periods. The 24-hr diurnal peak is 10 to 20 dB below the zero-frequency spectral level and, in some cases, is more than 10 dB above the level at adjacent frequencies (e.g., see Fig. 10b).

The width of the 24-hr "hump" in the PSD depends on the seasonal variation (i.e., modulation) of the diurnal-cycle amplitude. (The hump would be a "spike" if the diurnal cycle were a pure sinusoid with constant amplitude.) The 12-hr component in the PSD may be partly due to the bimodal diurnal cycle identified

previously. However, such a component arises even for a unimodal diurnal cycle, because the cycle is not a pure amplitude-modulated sinusoid. Indeed, the 12-hr component is the first harmonic of the fundamental 24-hr component.

Correlation of TD Pairs

Relationships among the TDs are identified by correlating pairs of time series. The 3-day smoothed seasonal time series are used for this purpose.

Correlation coefficients (ρ) for TD pairs arranged by site are presented in Tables 3, 4, and 5. Of particular interest is the low correlation between redundant TDZ data collected with the two LC-204 receivers at Iroquois ($\rho = 0.61$). This low correlation suggests that at least one of the receivers may not be functioning properly. Redundant TDs at the other sites exhibit high correlation.

Correlation coefficients for TD pairs arranged by station are presented in Tables 6, 7, and 8. The high correlation of TDY together with the low correlations of TDZ and TDZ suggest that the TDY variations are caused by a common non-propagation mechanism. This mechanism is necessarily associated with either the TDY channel of the Austron-5000 receiver at the SAM or with transmitter Y itself.

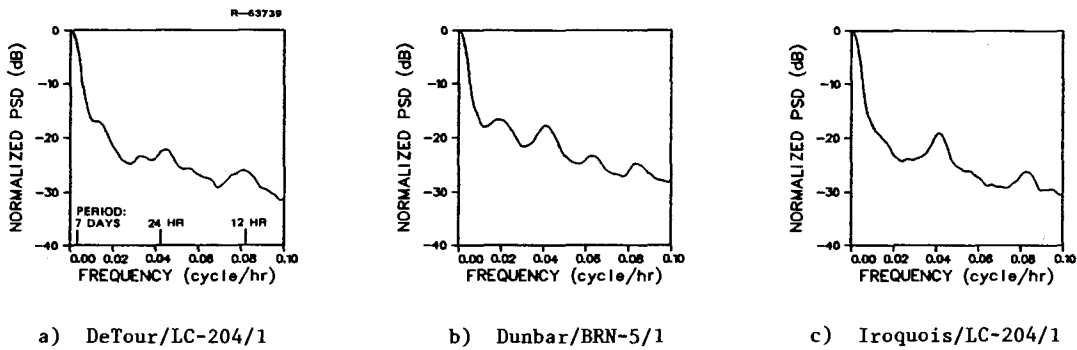


Figure 8 Power Spectral Densities for TDX

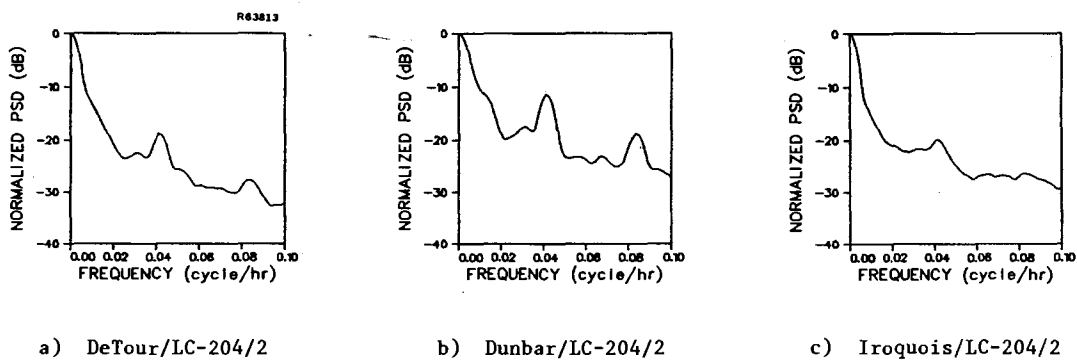


Figure 9 Power Spectral Densities for TDY

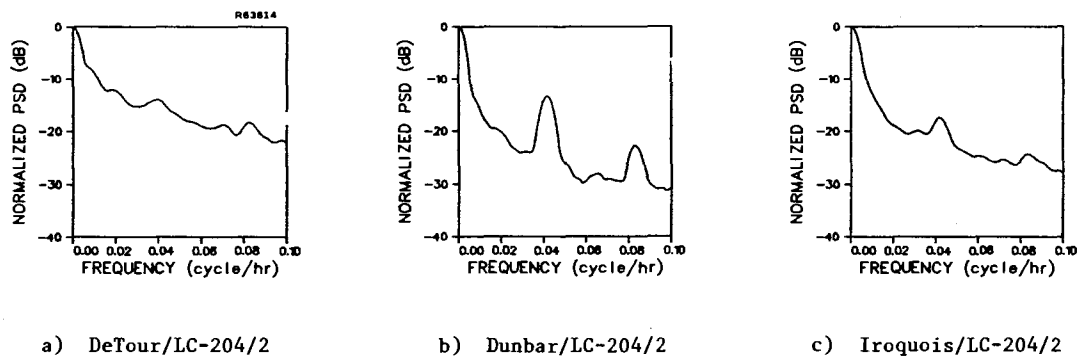


Figure 10 Power Spectral Densities for TDZ

Coherency spectra, which show the correlation coefficient as a function of frequency, are presented in Ref. 7. These spectra reveal that coherency is a maximum at zero frequency and decreases rapidly with increasing frequency. Therefore, TD/TD relationships are expected to be more pronounced on a seasonal rather than diurnal time scale.

Correlation of TDs with Temperature

Temperature data recorded at 3-hr intervals were obtained from the National Weather Service Station at Sault Sainte Marie, Michigan. Correlation coefficients based on 3-day smoothed

TD and temperature time series are presented in Table 9. These results indicate a relatively strong correlation ($\rho = -0.77$ to -0.85) between TDY and temperature for all sites and receivers. Because the TD/temperature correlation is generally stronger for TDY than for TDX or TDZ, it appears that the temperature effect may be related to something other than chain-wide propagation conditions.

Correlation coefficients for TDs vs refractivity are presented in Ref. 7. The correlation coefficients are all less than 0.61 in absolute value. This is consistent with the

TABLE 3
CORRELATION COEFFICIENTS FOR DETOUR

		LC-204/1		LC-204/2	
		TDX	TDY	TDY	TDZ
LC-204/1	TDX	+1.00	-	-	-
	TDY	+0.66	+1.00	-	-
LC-204/2	TDY	+0.36	+0.94	+1.00	-
	TDZ	+0.53	+0.07	+0.05	+1.00

TABLE 6
CORRELATION COEFFICIENTS FOR TDZ

		DETOUR	DUNBAR	IROQUOIS
		LC-204/1	BRN-5/1	LC-204/1
DETOUR	LC-204/1	+1.00	-	-
DUNBAR	BRN-5/1	+0.22	+1.00	-
IROQUOIS	LC-204/1	+0.18	+0.56	+1.00

TABLE 4
CORRELATION COEFFICIENTS FOR DUNBAR

		BRN-5/1		LC-204/2	
		TDX	TDY	TDY	TDZ
BRN-5/1	TDX	+1.00	-	-	-
	TDY	+0.89	+1.00	-	-
LC-204/2	TDY	+0.69	+0.80	+1.00	-
	TDZ	-0.69	-0.83	-0.08	+1.00

TABLE 7
CORRELATION COEFFICIENTS FOR TDY

		DETOUR	DUNBAR	IROQUOIS
		LC-204/2	LC-204/2	LC-204/2
DETOUR	LC-204/2	+1.00	-	-
DUNBAR	LC-204/2	+0.94	+1.00	-
IROQUOIS	LC-204/2	+0.87	+0.88	+1.00

TABLE 5
CORRELATION COEFFICIENTS FOR IROQUOIS

		LC-204/1		LC-204/2	
		TDX	TDZ	TDY	TDZ
LC-204/1	TDX	+1.00	-	-	-
	TDZ	+0.41	+1.00	-	-
LC-204/2	TDY	+0.84	+0.40	+1.00	-
	TDZ	+0.59	+0.61	+0.71	+1.00

TABLE 8
CORRELATION COEFFICIENTS FOR TDZ

		DETOUR	DUNBAR	IROQUOIS
		LC-204/2	LC-204/2	LC-204/2
DETOUR	LC-204/2	+1.00	-	-
DUNBAR	LC-204/2	+0.10	+1.00	-
IROQUOIS	LC-204/2	+0.07	-0.17	+1.00

TABLE 9
CORRELATION OF TDs WITH TEMPERATURE

SITE	RECEIVER TYPE/ NUMBER	TIME DIFFERENCE	CORRELATION COEFFICIENT
DeTour	LC-204/1	X	-0.22
		Y	-0.77
DeTour	LC-204/2	Y	-0.84
		Z	-0.19
Dunbar	BRN-5/1	X	-0.70
		Y	-0.80
Dunbar	LC-204/2	Y	-0.85
		Z	+0.54
Iroquois	LC-204/1	X	-0.76
		Z	-0.51
Iroquois	LC-204/2	Y	-0.80
		Z	-0.66

expected negligible impact of atmospheric variations on mini-chain signal propagation (Ref. 3).

COMPARISON OF THEORETICAL AND OBSERVED TD VARIATIONS

Signal propagation theory is employed in Ref. 3 to estimate the magnitude of St. Marys River Loran-C TD grid instability. Because the mini-chain coverage area is less than 60 nm in diameter, the propagation medium is assumed to be homogeneous. This simplifying assumption is consistent with the goal of estimating temporal TD variations.

The sensitivity of TDs to temporal variations in three propagation parameters -- atmospheric refractive index, vertical lapse rate of refractive index, and ground conductivity -- is analyzed in Ref. 3. TD sensitivity to refractive index and vertical lapse rate variations is approximately proportional to the "Double Range Difference"

$$DRD = (R_s - R_m) - (R'_s - R'_m) \quad (1)$$

where R_s and R_m are the secondary-to-site and master-to-site ranges, respectively, and R'_s and R'_m are the corresponding ranges to the SAM. DRD contours are hyperbolas, as shown for TDX in Fig. 11. The zero-sensitivity contour passes through the SAM location, because the SAM controls its TD to a constant level. TD sensitivity to conductivity variations is nonlinear in range (Ref. 9). However, the DRD provides an accurate approximation to the nonlinearity for the St. Marys River data collection sites.

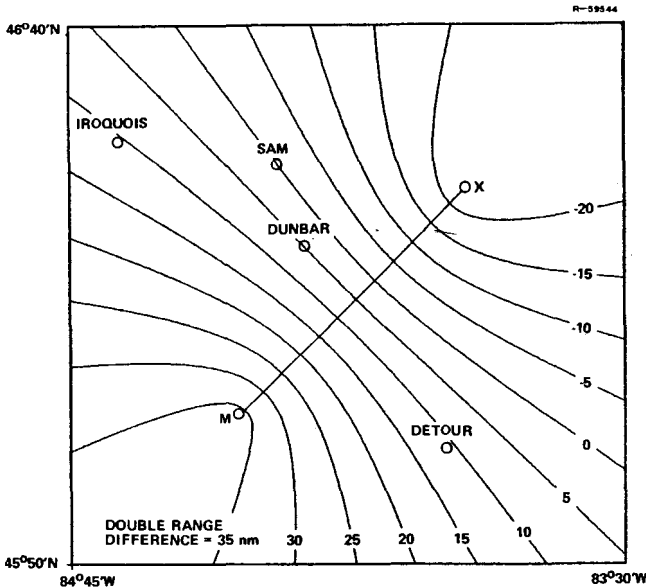


Figure 11 TDX Temporal Variation Sensitivity

Theoretical TD variations associated with particular variations in the propagation parameters are indicated below:

- Refractive Index -- 6×10^{-6} $\mu\text{sec}/\text{nm}^*$ per N-unit
- Vertical Lapse Rate -- 3×10^{-5} $\mu\text{sec}/\text{nm}$ per 0.02 α -units
- Conductivity -- 4×10^{-3} $\mu\text{sec}/\text{nm}$ per doubling of conductivity.

The maximum DRD for the data collection sites is 35 nm. Therefore, the maximum seasonal TD variation for the measured 50 N-unit refractive index variation (Ref. 7) is only 0.010 μsec . Similarly, the maximum seasonal TD variation expected for a 0.25 α -unit vertical lapse rate variation (Refs. 3 and 6) is 0.026 μsec . Clearly, the observed 0.4- μsec p-p seasonal TD variations, if propagation-related, are necessarily caused by conductivity variations. TD variations as large as 0.14 μsec p-p are expected for a potential doubling of conductivity from winter to summer (Ref. 3).

Although the maximum magnitude of the observed TD variations is more or less consistent with propagation theory, the relative

*TD variation per nm of DRD.

variations of the individual time series are not consistent with the DRD (see Fig. 12). The following are among the obvious discrepancies:

- Dunbar TDY variations are 0.189 μsec p-p, but the DRD equals zero
- DeTour TDZ variations are only 0.061 μsec p-p, but the DRD equals +35 nm
- DeTour and Iroquois TDY variations are in the same direction, but the DRDs are of opposite sign (-25 nm vs +8 nm)
- DeTour and Iroquois TDX variations differ significantly, but the DRDs are both equal to +11 nm.

It is possible that seasonal conductivity variations are spatially nonhomogeneous thereby violating the DRD model assumptions. However, it is more likely that the variations are caused by a transmitter- and/or receiver-related mechanism, which disguises the propagation mechanism.

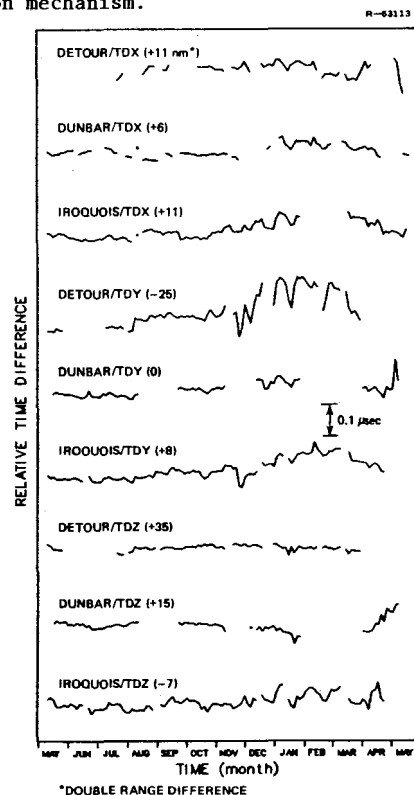


Figure 12 Comparison of Seasonal TD Time Series and Double Range Difference

LOW-DENSITY DATA ANALYSIS EVALUATION

The U.S. Coast Guard has conducted low-density data analyses which closely parallel the high-density analyses presented herein.

The reduced data volume has enabled monthly internal reports to be issued. A statistical evaluation of the low-density approach is presented here to confirm the accuracy of these monthly reports and assure an effective monitoring strategy for harbors.

Potential errors in the low-density TD data, compared to the high-density data, can be categorized as follows:

- Relatively small errors associated with computing mean TD values based on a reduced sample size
- Relatively large errors resulting from the inability to detect outliers in short segments of a time series.

The first error category is discussed here. The second error category is not a major problem because of the scarcity of outliers (see Table 1 and Ref. 7).

"Generic" low-density sampling strategies are employed to investigate the effect of sample size. Each generic strategy is defined by three parameters:

- Number of equally-spaced time windows per day, during which 15-min samples are recorded
- Width of time windows
- Phase of time windows, i.e., the time-of-day at the beginning of the first window.

The nominal U.S. Coast Guard sampling strategy involves two time windows of width equal to 1 hr, beginning at 0 hr and 7 hr GMT.

Seasonal and Monthly Variations

The utility of the low-density data in quantifying seasonal TD variations depends on the difference between the low- and high-density 3-day smoothed time series. The rms differences (i.e., errors) for the generic sampling strategies are presented as a function of window width in Fig. 13. These results are obtained by processing TDY data from the Iroquois/LC-204/2 receiver, which represents worst-case seasonal variations. TD errors are less than 0.01 μsec rms for all strategies considered. Errors can be reduced by using four 1-hr windows instead of two. However, the additional detail lends little to the quantification of seasonal variations.

The utility of the low-density data in quantifying monthly TD variations depends on the difference between the low- and high-density 6-hr smoothed time series. The low-density monthly time series is somewhat less accurate than the low-density seasonal time series but, nevertheless, is in error by less than 0.01 μsec rms.

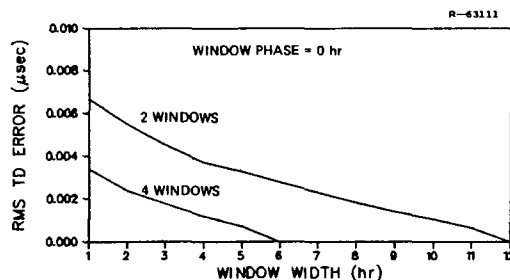


Figure 13 Accuracy of Generic Low-Density Seasonal Time Series

Diurnal Variations

Intuitively, it is difficult to accurately measure the peak-to-peak value of the diurnal TD cycle by using only two 1-hr windows. The phase of the windows is a critical parameter in this case, more so than in the measurement of seasonal and monthly TD variations. The error in the peak-to-peak value of the generic low-density diurnal cycle* is presented as a function of window phase in Fig. 14. January TDZ data from the Iroquois/LC-204/2 receiver are analyzed, because they exhibit a distinct diurnal cycle. TD cycle errors range from less than 0.001 μsec to 0.020 μsec , depending on the choice of window phase.

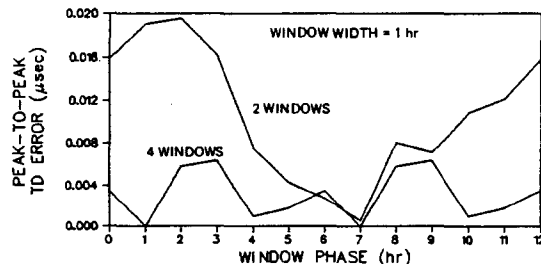


Figure 14 Accuracy of Generic Low-Density Diurnal Cycle

A direct comparison of the high-density and U.S. Coast Guard low-density diurnal cycles is presented in Fig. 15. The "trough" in the cycle is not observable with the U.S. Coast Guard sampling strategy, thereby resulting in a 50-percent error in the measured cycle amplitude. Although not a problem in the St. Marys River chain because of the small contribution of diurnal variations, a problem

*For two 1-hr windows, the diurnal "cycle" consists of only two points.

could exist if the same strategy is applied to a long-baseline chain. To increase data utility, it is recommended that four or more time windows per day be employed initially in the Loran-C Harbor Monitor Program. Alternatively, the monitoring system should provide the mean, standard deviation, and peak-to-peak values of the data in 24-hr time windows.

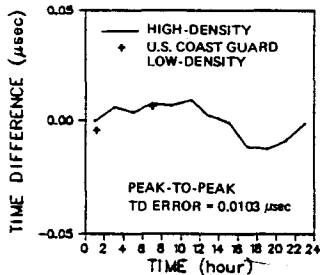


Figure 15 Comparison of High-Density and U.S. Coast Guard Low-Density Diurnal Cycles

CONCLUSIONS

The following conclusions are drawn from analyses of the St. Marys River Loran-C data:

- Seasonal TD variations are less than 0.4 μsec p-p, consistent with previous observations
- TD variations during monthly periods are larger in the winter than in the summer, consistent with signal propagation theory
- Diurnal TD cycles are generally less than 0.02 μsec p-p, which is small relative to longer-term variations
- Power Spectral Densities show that the diurnal TD cycle is 10 to 20 dB below the zero-frequency (bias) spectral component
- TDY data exhibit a relatively high negative correlation with Sault Sainte Marie temperature.

A comparison of the data analysis results to theory shows that the maximum observed TD variation is more or less consistent with expected seasonal conductivity variations. However, the relative variations of the individual time series are not consistent with theory for a homogeneous medium.

The following principal conclusions are drawn from an evaluation of the low-density data analysis approach:

- Errors in the low-density seasonal and monthly TD time series are less than 0.01 μsec rms

- Significant errors (as large as 50 percent) result if low-density data are used to compute the peak-to-peak value of the diurnal TD cycle
- The low-density diurnal-cycle measurement errors are very sensitive to the times-of-day selected for sampling
- The optimal sampling times for diurnal-cycle resolution generally differ for different months and different receiver/TD combinations.

It is recommended that the low-density sampling rate be increased in the Harbor Monitor Program to permit analysis of diurnal effects. In anticipation that different results may apply to a long-baseline chain, it appears desirable that high-density harbor monitor data be collected during both a summer month and a winter month and analyzed prior to standardizing a low-density sampling strategy.

ACKNOWLEDGMENT

This project was sponsored by the U.S. Coast Guard Research and Development Center under Contract No. DOT-CG-81-77-1785. Mr. Ernest Hunt of the Center transferred the Loran-C data base from cassette to half-inch magnetic tape. Dr. E. Michael Geyer and Mr. Irwin P. Bramson of TASC developed the spectral analysis software used in the study. The authors also appreciate the technical contributions of Mr. Ronald S. Warren, who has participated in the entire three-year mini-chain grid-characterization effort at TASC.

REFERENCES

1. Warren, R.S., Gupta, R.R., and Healy, R.D., "Design and Calibration of a Grid Prediction Algorithm for the St. Marys River Loran-C Chain," The Analytic Sciences Corporation, Technical Information Memorandum TIM-1119-2, (U.S. Coast Guard Report No. CG-D-32-80) March 1978.
2. Warren, R.S., Gupta, R.R., and Shubbuck, T.J., "Design and Calibration of a Grid Prediction Algorithm for the St. Marys River Loran-C Chain," Proc. of Seventh Annual Technical Symposium of the Wild Goose Association (New Orleans, LA), October 1978.
3. DePalma, L.M., and Gupta, R.R., "Seasonal Sensitivity Analysis of St. Marys River Loran-C Time Difference Grid," The Analytic Sciences Corporation, Technical Information Memorandum TIM-1119-3 (U. S. Coast Guard Report No. CG-D-33-80), June 1978.

4. "St. Marys River Loran-C Mini-Chain," U.S. Coast Guard, Report No. CG-D-43-80 (Draft), July 1980.
5. Ligon, J.M., and Olsen, D.L., "St. Marys River Mini-Chain -- the Bottom Line," Presented at the Ninth Annual Technical Symposium of the Wild Goose Association (Boston, MA), October 1980.
6. Campbell, L.W., Doherty, R.H., and Johler, J.R., "Loran-C System Dynamic Model: Temporal Propagation Variation Study," Analytical Systems Engineering Corporation and Colorado Research and Prediction Laboratory, Inc., Technical Report ASECR 79-107, July 1979.
7. DePalma, L.M., and Creamer, P.M., "Quantification of St. Marys River Loran-C Time Difference Grid Instability," The Analytic Sciences Corporation, Technical Report TR-1119-3-1 (to be published by U. S. Coast Guard), August 1980.
8. Rabiner, L.R., and Gold, B., Theory and Application of Digital Signal Processing, Prentice-Hall, 1975.
9. Johler, J.R., Keller, W.J., and Walters, L.C., "Phase of the Low Radio Frequency Groundwave," National Bureau of Standards Circular 573, June 1956.

STOCHASTIC INVESTIGATION ON THE SEARCH PROCESS
OF A LORAN-C RECEIVER

by

Kiyohiko Tatebayashi, Mikio Nakamura & Tadayuki Yamada
Japan Radio Co., Ltd
Laboratory
5-1-1 Shimorenjaku Mitaka-shi Tokyo Japan

ABSTRACT

The Loran-C receiver operation in the noise can be analyzed on the basis of stochastics. We have applied such investigation to the following two subjects.

Comparison is made between two different ways of the pattern matching; the procedure of master and slave identification. One is based on the cross-correlation derived from the whole coding pattern, and the other is based on the product of two cross-correlations derived from two divided parts of the coding pattern. We conclude that the rather complicated method using the product of two cross-correlations is not superior to the simpler one under poor signal-to-noise ratio conditions.

Dependence of the signal detecting power on the quantizing number of analog-to-digital conversion is analyzed by means of statistical test. The results indicate that the simple one bit analog-to-digital converter, called hard limiter, meets the performance requirements from the practical standpoint; accordingly, we may avoid the significant cost penalty involved in the introduction of analog-to-digital conversion of more than one bit.

These analyses utilizing stochastic technique will provide the essential guidance for the design of a Loran-C receiver.

INTRODUCTION

Loran-C chains are comprised of a master transmitting station and two or more slave transmitting stations. The transmitting stations of a Loran-C chain transmit groups of pulses at a specified group repetition interval (GRI). Each pulse has a 100kHz carrier and is of the shape described in Figure 1. Each station transmits one pulse group per GRI. The master pulse group consists of nine pulses and slave pulse groups contain eight pulses as shown in Figure 2. The phase of the 100kHz carrier is changed in each pulse of a group in accordance with a predetermined pattern. The phase coding pattern used in the Loran-C system is shown in Figure 3. The different phase codes for master and slave signals allow an automatic receiver to use the code for master and slave station

identification.

A position fix by the Loran-C system is obtained by measuring a difference in time of arrival between signals from the master and slave transmitters. The time difference measurements may be broken down into two major processes.

- (1) Search process
detects whether a signal of an interested chain is present or absent.
- (2) Track process
tracks the zero crossover at 30 μ s, from the beginning of the pulse, which is the most favorable one to use for tracking, when combining the requirements with respect to skywave contamination and signal-to-noise ratio (SNR).

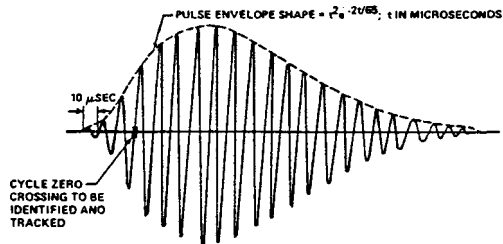


Figure 1 Loran-C pulse

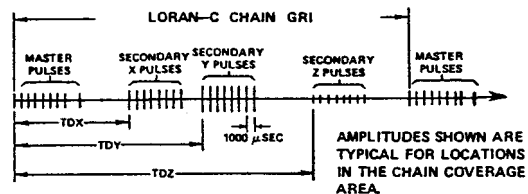


Figure 2 Loran-C pulse groups

	MASTER	each SLAVE
GRI A	+++--+ +	++++--
GRI B	---++++ -	+--+---

(+) indicates zero degree carrier phase
(-) indicates 180 carrier phase
Loran-C intervals A & B alternate in time

Figure 3 Loran-C phase code

The recent progress of digital signal processing has made it practicable to automate the above two processes required for the newest Loran-C receiver.

Now, it is important to make a study of receiver design under poor SNR conditions. Therefore, stochastic investigations with consideration of noise are necessary to design all processes for the time difference measurements.

This paper deals with two problems about Loran-C signal detection in the search process.

- (1) How does a receiver identify the master and slave signals ?
- (2) What quantizing number is suitable for a low cost digital type receiver ?

Stochastics with keywords, such as statistical test and probability distribution function, can give reasonable solutions to above problems.

MASTER AND SLAVE IDENTIFICATION

Procedure Of Identification

Master and slave identification is accomplished by pattern matching of received pulses with locally generated reference pulses. Robert L. Frank proposed the following pattern matching

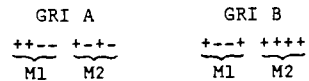


Figure 4 Master reference signal

method.²⁾

Master signal identification will be described below, and it can apply to slave signal identification. A code pattern corresponding to the first four GRI A and B reference pulses is designated as M1, and that corresponding to the second four pulses is designated as M2 as shown in Figure 4. Cross-correlation is carried out between received and reference pulses, both with signal level assumed to be +1 or -1. The results of cross-correlation for typical code alignments are summarized in Table 1.

During initial search, there are four possible conditions: the coder in the receiver and the coder at the transmitter may be either in step, or out of step by one repetition interval, and the master identification circuit may be sampling either master pulses or slave pulses. These four conditions are shown as four major rows in Table 1, and minor rows indicate possible pulse alignments. Column M1 or Column M2 indicates cross-correlation functions over two GRIs between received pulses and, M1 or M2 ref-

	Pulses Sampled (by Master Sampler)	M1	M2	M1×M2	M1+M2	
Transmitter and Receiver Coders in Step	#1-2 1-4 1-6	0	0	0	0	
		0	0	0	0	
		-4	+4	-16	0	
	Master	1-8	+8	+8	+64 (Correct Alignment)	+16
		3-8	-4	+4	-16	0
		5-8	0	0	0	0
		7-8	0	0	0	0
	Slave	#1-2	0	0	0	0
		1-4	0	0	0	0
		1-6	-4	+4	-16	0
		1-8	0	0	0	0
		3-8	+4	-4	-16	0
		5-8	0	0	0	0
		7-8	0	0	0	0
Coders Out of Step by One GRI	Master	#1-2	0	+4	0	+4
		1-4	0	0	0	0
		1-6	0	-4	0	-4
		1-8	0	0	0	0
		3-8	-4	0	0	-4
		5-8	0	0	0	0
		7-8	+4	0	0	+4
	Slave	#1-2	0	+4	0	+4
		1-4	0	+8	0	+8
		1-6	0	+4	0	+4
		1-8	0	0	0	0
		3-8	-4	0	0	-4
		5-8	+8	0	0	+8
		7-8	-4	0	0	-4

Table 1 Cross-correlation (by Frank)²⁾

erence pattern, respectively. For example, Row #1-8 shows the condition existing when the reference and received pulses are aligned; all of the detected pulses are the same polarity, and Row #1-2 shows the condition resulting from the received pulses led by six pulses with respect to the reference. Column "M1+M2" indicates simple cross-correlation functions, in which the whole master group is used.

The results show that the value of "M1+M2" is read to be +16 in a correct alignment case and +8, +4, -4 or 0 in misalignment cases. However, "M1*M2" is read to be +64 in a correct alignment case and -16 or 0 in misalignment cases. Thus, the latter procedure makes to identify the master signal more easily than the former. But the presence of noise was not taken into account in Frank's investigation.

Calculation Of Discrimination Error Rate

Definition of signal-to-noise ratio(SNR)

The received signal will be assumed to consist of the signal with DC amplitude μ and the noise with standard deviation σ , in other words, the received signal is a normally distributed random variable with mean value μ and variance σ^2 (so-called $N(\mu, \sigma^2)$). We define here SNR as follows:

$$\text{SNR} = 20 \log(\mu/\sigma) \quad (\text{dB}) \quad (1)$$

Sum and multiplication of normally distributed random variables

The probability density function of a random variable x with $N(\mu, \sigma^2)$ is

$$P(x) = \frac{1}{\sqrt{2\pi}\sigma} \exp\left\{-\frac{(x-\mu)^2}{2\sigma^2}\right\} \quad (2)$$

Let x_1 and x_2 be mutually independent normally distributed random variables with $N(\mu_1, \sigma_1^2)$ and $N(\mu_2, \sigma_2^2)$ respectively. A sum $y (=x_1+x_2)$ will also be normally distributed and the probability density function is

$$P(y) = \frac{1}{\sqrt{2\pi} \cdot \sqrt{2}\sigma} \exp\left\{-\frac{(y-\mu_1-\mu_2)^2}{2 \cdot 2\sigma^2}\right\} \quad (3)$$

, $P(y)$ is now represented by $N(\mu_1+\mu_2, 2\sigma^2)$.

Now, consider the distribution of multiplication. The joint probability density function of the combined events $x_1=\lambda$ and $x_1 \cdot x_2=y$, is

$$P(x_1, x_2) = |J|^{-1} R(\lambda) R(y/\lambda) \quad (4)$$

where J is the well-known mathematical expression for the Jacobian transformation of coordinates to determine the relation between elements of area in the two planes.

$$J = \begin{vmatrix} \frac{\partial \lambda}{\partial x_1} & \frac{\partial \lambda}{\partial x_2} \\ \frac{\partial y}{\partial x_1} & \frac{\partial y}{\partial x_2} \end{vmatrix} = \lambda \quad (5)$$

Therefore, the probability density function of y is

$$P(y) = \int_{-\infty}^{\infty} \frac{1}{|\lambda|} R(\lambda) \cdot R(y/\lambda) d\lambda \\ = \frac{1}{2\pi\sigma^2} \int_{-\infty}^{\infty} \frac{1}{|\lambda|} \exp\left\{-\frac{1}{2\sigma^2}\left\{(\lambda-\mu)^2 + (y/\lambda - \mu)^2\right\}\right\} d\lambda \quad (6)$$

Hence, the probability density functions of (M1+M2) and (M1*M2) described earlier, are given by Equation (3) and (6), respectively.

Probability distribution of the master and slave signal

In the search process, pulse groups may be obtained synchronously with a spacing of GRI. Consequently, the received signal may be treated as a static DC signal contaminated by noise. Now, let a noise strength σ be 10.0. By definition of Equation (1), the relations between SNR and the signal average value μ are listed in Table 2.

SNR (dB)	signal average value
-10	3.162
-15	1.778
-20	1.000
-25	0.562
-30	0.316

Table 2 Relations between SNR and signal average value

Calculation procedure of the probability density function

The probability density function can be calculated by using μ and σ determined in the preceding paragraph. The probability density function of multiplication represented by Equation (6) can, however, be calculated approximately by the numerical-integration using Simpson's rule instead of analytic procedure.

Furthermore, by Monte Carlo simulation studies, comparisons have been made between theoretical values and experimental values. Normally distributed random number can be obtained by applying the central limit theorem to the uniformly distributed random number generated by the multiplicative congruential method. The number of the random numbers is 5000.

Threshold level for discrimination and the error rate

Master signal identification will be considered again. The condition that the master signal is present means that the master reference and received signal are aligned, or in other words, the condition is M1=8 and M2=8 in Table 1. And the condition that the master signal is absent means all the cases of the possible pulse misalignments.

There are two error rates in discriminating between the presence and absence of the master signal. Let us define the two error rates as:

E1--- Probability of rejecting the presence of the master signal when in fact it is true.

E2--- Probability of accepting the presence of the master signal when in fact it is false.

Figure 5 indicates graphically two error rates in the form of the probability density function in Figure 5-(a), and the probability distribution function in Figure 5-(b). The distribution of the detected object means the distribution of $(M1+M2)$ or $(M1 \times M2)$ under the condition of $M1=8$ and $M2=8$. Discrimination may be carried out in such a manner that the master signal is present when a sample value is greater than a threshold level and is absent when a sample value is less than the threshold level. Thus, error rates E1 and E2 are represented by the area of the shaded portion in the form of the probability density function or the point of intersection between a threshold level and the distribution function curves.

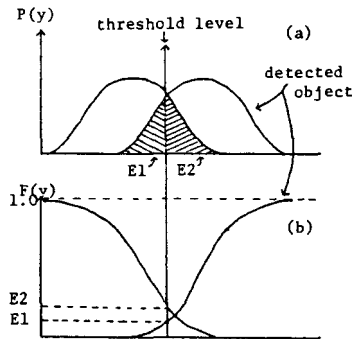
In future, the distribution of $(M1+M2)$ and $(M1 \times M2)$ will be called as the ADD

distribution and the MULT distribution, respectively. The threshold level to minimize the sum of two error rates $ET (=E1+E2)$ is called as the optimum threshold level. This threshold level is given by a point of intersection of the ADD or MULT distribution curves for presence and absence of the signal. In this paper, two kind of the optimum threshold levels in each case and the worst case are selected as threshold levels for discrimination. Besides, the threshold levels fixing E1 or E2 may be used. The 0 threshold level proposed by Frank is improper in consideration of the noise.

Evaluation Using The Discrimination Error Rate

The results of calculating the error rates in the master identification by the MULT and ADD processings over the SNR range from -10 to -30 dB are summarized in Table 3. Upper and lower values of each row in Table 3 apply to the condition using the optimum threshold level of each case and the worst case, respectively.

The probability distribution functions of each case at SNR -20 dB are illustrated in Figure 6 (a)-(e). The right-side distribution function curves in those figures show the distribution



(M1, M2)	MULT			ADD		
	E1	E2	ET	E1	E2	ET
(-4, 0)	.285	.189	.474	.085	.076	.161
(-4, 4)	.231	.140	.371	.148	.129	.277
(0, 0)	.285	.189	.474	.309	.012	.321
(0, 4)	.285	.144	.429	.309	.045	.354
(4, 0)	.285	.144	.429	.148	.129	.277
(4, 4)	.285	.184	.469	.309	.129	.438
(8, 0)	.285	.269	.554	.309	.289	.598

Table 4 Results by Monte Carlo simulation (SNR=-20dB)

Figure 5 Two error rates

(M1, M2)	-10dB			-15dB			-20dB			-25dB			-30dB			
	E1	E2	ET	E1	E2	ET	E1	E2	ET	E1	E2	ET	E1	E2	ET	
MULT	(-4, 0)	.003	.002	.005	.069	.068	.137	.230	.211	.441	.418	.284	.702	.596	.253	.849
	(-4, 4)	.000	.000	.000	.016	.018	.034	.127	.131	.258	.315	.247	.562	.596	.240	.836
	(0, 0)	.000	.000	.001	.041	.035	.076	.230	.145	.375	.418	.249	.667	.596	.249	.845
	(4, 0)	.003	.002	.005	.069	.068	.137	.230	.211	.441	.418	.284	.702	.596	.253	.849
	(8, 0)	.013	.000	.013	.106	.041	.147	.230	.211	.441	.369	.336	.705	.543	.308	.851
ADD	(-4, 0)	.000	.000	.000	.006	.006	.012	.079	.079	.158	.213	.213	.426	.327	.327	.654
	(-4, 4)	.000	.000	.000	.022	.022	.044	.129	.129	.258	.263	.263	.526	.361	.361	.722
	(0, 0)	.000	.000	.000	.022	.022	.044	.129	.129	.258	.263	.263	.526	.361	.361	.722
	(4, 0)	.003	.003	.006	.066	.066	.132	.198	.198	.396	.317	.317	.634	.394	.394	.788
	(8, 0)	.037	.037	.074	.157	.157	.314	.284	.284	.568	.375	.375	.750	.428	.428	.856

Table 3 Results of calculating the error rates

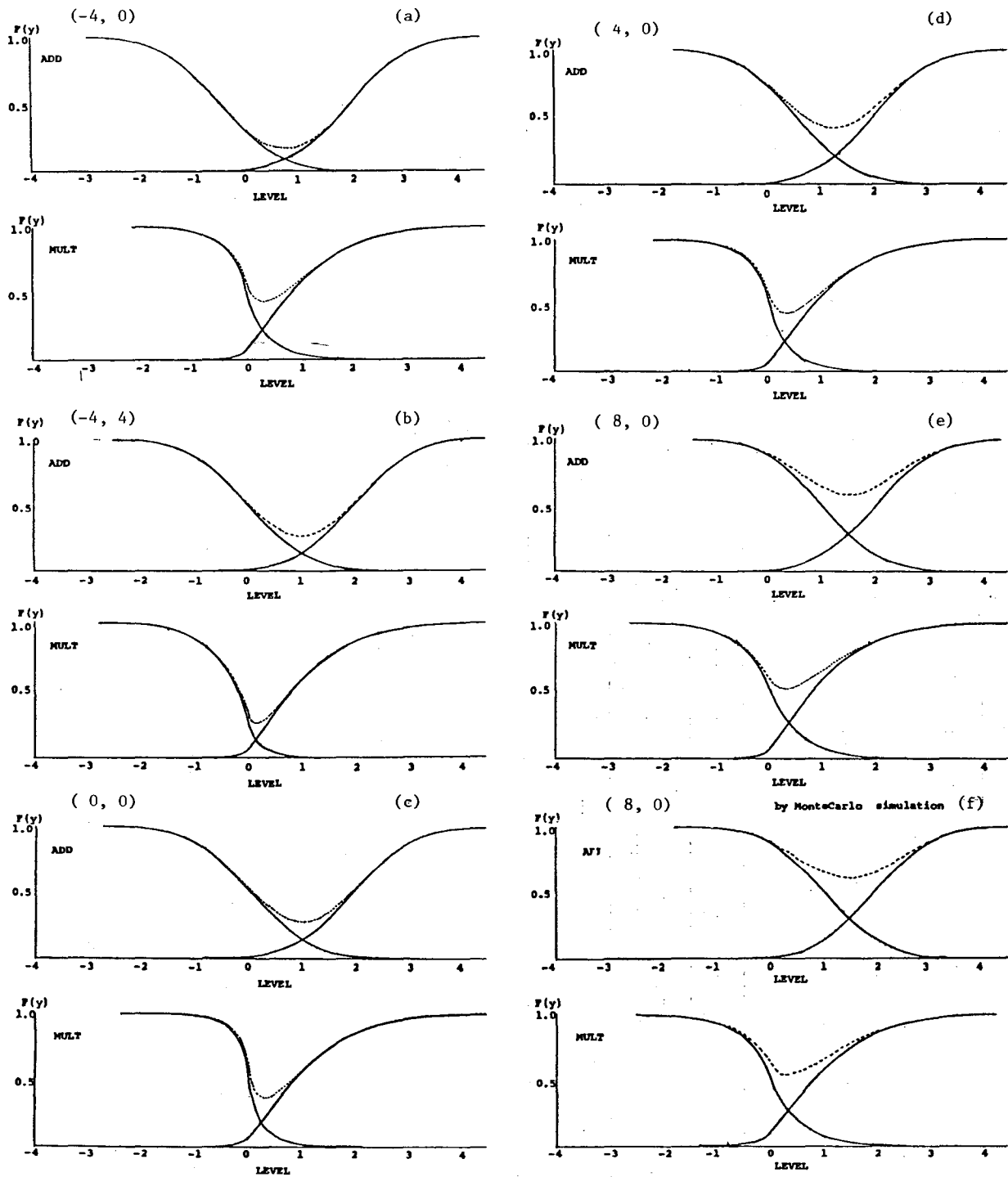


Figure 6 Probability distribution function of each case (SNR=20 dB)

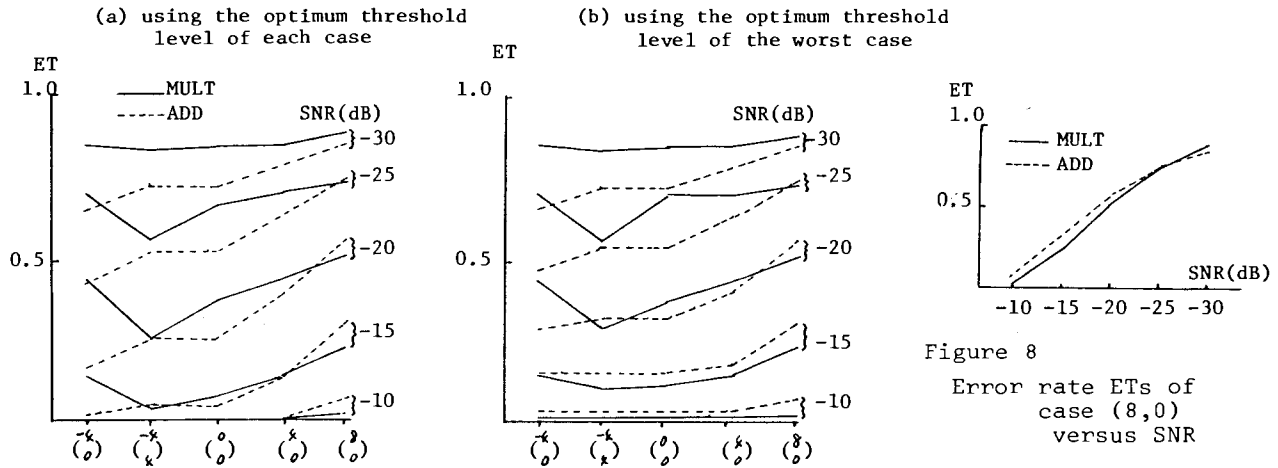


Figure 7 Error rate ETs of each case

Figure 8 Error rate ETs of case (8,0) versus SNR

of a detected object, namely (M1=8,M2=8) case, and the left-side curves show the distribution under conditions that the master signal is absent. The dotted curves show the sums of two distribution functions described above. Therefore, the minimum values of those curves are ETs, and the threshold levels bringing minimum values are the optimum threshold levels.

The results of Monte Carlo simulation at SNR -20 dB are summarized in Table 4. The results show good agreement with the theoretical values. The distribution functions of the case (8,0) obtained by Monte Carlo simulation are illustrated in Figure 6-(f). Figure 7 shows plots of ETs shown in Table 3, and Figure 8 also shows plots of ETs of the worst case (8,0) versus SNR.

The results studied above reduce to those given below:

- 1) The worst case in both the MULT and ADD processings occurs in discriminating against case (8,0).
- 2) The best case in the MULT processing occurs in case (-4,4), and in the ADD processing occurs in case (-4,0).
- 3) Based on the error rate in the worst case, the MULT processing is superior to the ADD processing up to SNR -25 dB, but is inferior beyond SNR -25 dB.
- 4) Based on the error rate except in the worst case (8,0), the ADD processing is mostly superior.

HARD LIMITING

The problem of determining the quantizing number arises in the design approach of linking a digital processor to the receiver by means of an analog-to-digital converter (ADC). This assessment requires consideration of the trade-off between the signal detecting power and the simplicity of the equipment. In this chapter, the dependence of the signal detecting power on the quantizing number of ADC will be studied by using the statistical test theory. Further, the relations among the design parameters will be investigated in the hard limiting operation, the simplest ADC.

Calculation Of Signal Detecting Power

Procedure of the test

Now, consider the following hypothesis:

Hypothesis H_0 :

In the received signal, Loran-C signal is absent and only noise is present.

Acceptance of the hypothesis H_0 means the absence of Loran-C signal. Rejection of the hypothesis H_0 means the presence of Loran-C signal.

Hypothesis H_0 may also be represented by an alternative hypothesis:

Hypothesis H_1 :

The synchronous average value of the received signals of the sample number n , is normally distributed random variable with $N(0, \sigma^2)$.

Now, consider the test of the hypothesis H_1 . Synchronous average value \bar{x} is now represented by

$$\bar{x} = \frac{1}{n} \sum_{i=1}^n x_i \quad (7)$$

where n is the sample number and x_i is a sample of received signals. Calculate

$$t = \frac{\bar{x}}{s/\sqrt{n}} \quad (8)$$

$$\text{, where } s = \sqrt{\frac{1}{n-1} \sum_{i=1}^n (x_i - \bar{x})^2} \quad (9)$$

Random variable t has the Student's t distribution function with n-1 degrees of freedom when the hypothesis H_1 holds. This property makes it possible to apply the Student's t test to the detection whether signal is present or absent.

If $|t| \leq t_{n-1, \alpha/2}$, accept H_1 .

If $|t| > t_{n-1, \alpha/2}$, reject H_1 .

$t_{n-1, \alpha/2}$ is the value of t, defined in

$$\int_{t_0}^{\infty} dx \cdot R(x) = \alpha/2 \quad (10)$$

where $R(x)$ is the probability density function of the Student's t distribution with n-1 degrees of freedom, and α is the error probability that the hypothesis might be rejected when in fact it is true and is called "level of significance" or Type 1 Error.

A good index indicating effectiveness of above mentioned method is a signal detecting power function; the probability of rejecting the hypothesis when it does not hold, in other words, the probability of accepting the presence of the signal when it is present. This function P is defined as

$$P = \text{Prob.} \left[\left| \frac{\bar{x}}{s/\sqrt{n}} \right| > t_{n-1, \alpha/2} \right] \quad (11)$$

Probability distribution of the average value processed by ADC

Loran-C signal (amplitude μ) contaminated by the noise ($N(0, \sigma^2)$) is normally distributed ($N(\mu, \sigma^2)$), but ADC operation changes it into a discrete

distribution. An average value of the discrete distributed random variables has the discrete probability density function represented by the convolution of the original discrete probability density function. For a large sample number, however, it may be regarded as the normal distribution. This average value is used for calculating the signal detecting power according to the Equation (11). This calculating process is illustrated in Figure 9.

Dependence Of The Signal Detecting Power On The Quantizing Number

Figure 10 shows the signal detecting power in the cases of the linear conversion, and the quantizing number 7, 3 or 2 for a fixed value of Type 1 Error $\alpha = 0.05$. Since σ will be 1.0, the signal level μ of the transverse is transformed into SNR, as given by

$$\text{SNR} = 20 \log(\mu) \quad (\text{dB}) \quad (12)$$

, for $\mu = 0.1$ SNR = -20 dB

Table 5 shows the signal detecting power for SNR = -20 dB and a sample number $n = 512$. The results shown in Table 5 are interpreted as follows:

quantizing number	signal detecting power
linear	0.73
7	0.72
3	0.65
2	0.57

(SNR = -20dB n = 512)

Table 5 Relations between quantizing number and signal detecting power

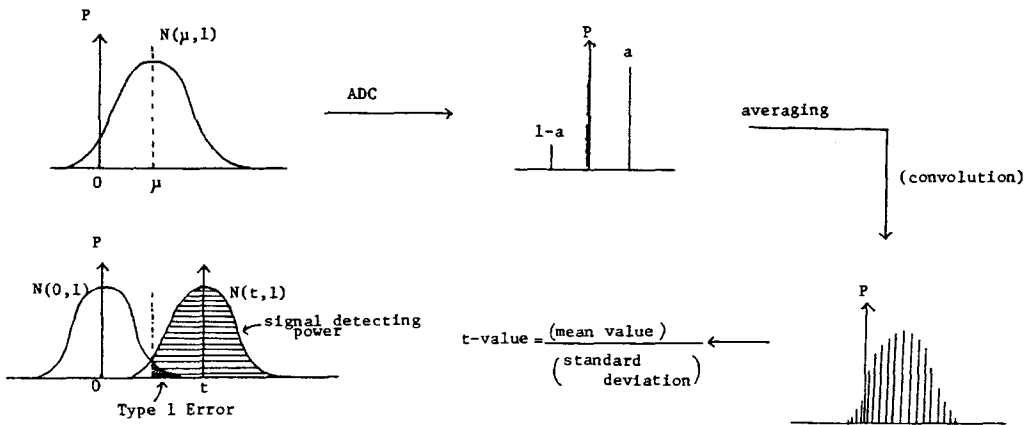


Figure 9 Process for calculating the signal detecting power

- 1) No significant difference in the signal detecting power is found between the linear conversion and ADC with the quantizing number 7 .
- 2) Hard limiting operation is inferior only about 2 dB to the linear conversion.

Compared with the hard limiting, the soft limiting, which means ADC except the hard limiter, has the following hardware loads:

- 1) Automatic gain control (AGC) is needed.
- 2) A larger capacity of data memory is needed.
- 3) ADC circuit is more complicated.

Therefore, it is suggested that the hard limiting better meets a low cost Loran-C receiver.

Relations Among Design Parameters

Determining the signal processing performance in the search process involves the considerations of the relations among design parameters, namely SNR, Type 1 Error, the signal detecting power and the sample number. Since the availability of the hard limiter has been indicated in the preceding section, the following relations will be investigated for the hard limiting operation.

- 1) Relations among the signal detecting power, SNR and the sample number for a fixed value of Type 1 Error. (shown in Figure 11 (a)-(d))
- 2) Relations among Type 1 Error, SNR and the sample number for a fixed value of the signal detecting power. (shown in Figure 12 (a) and (b))

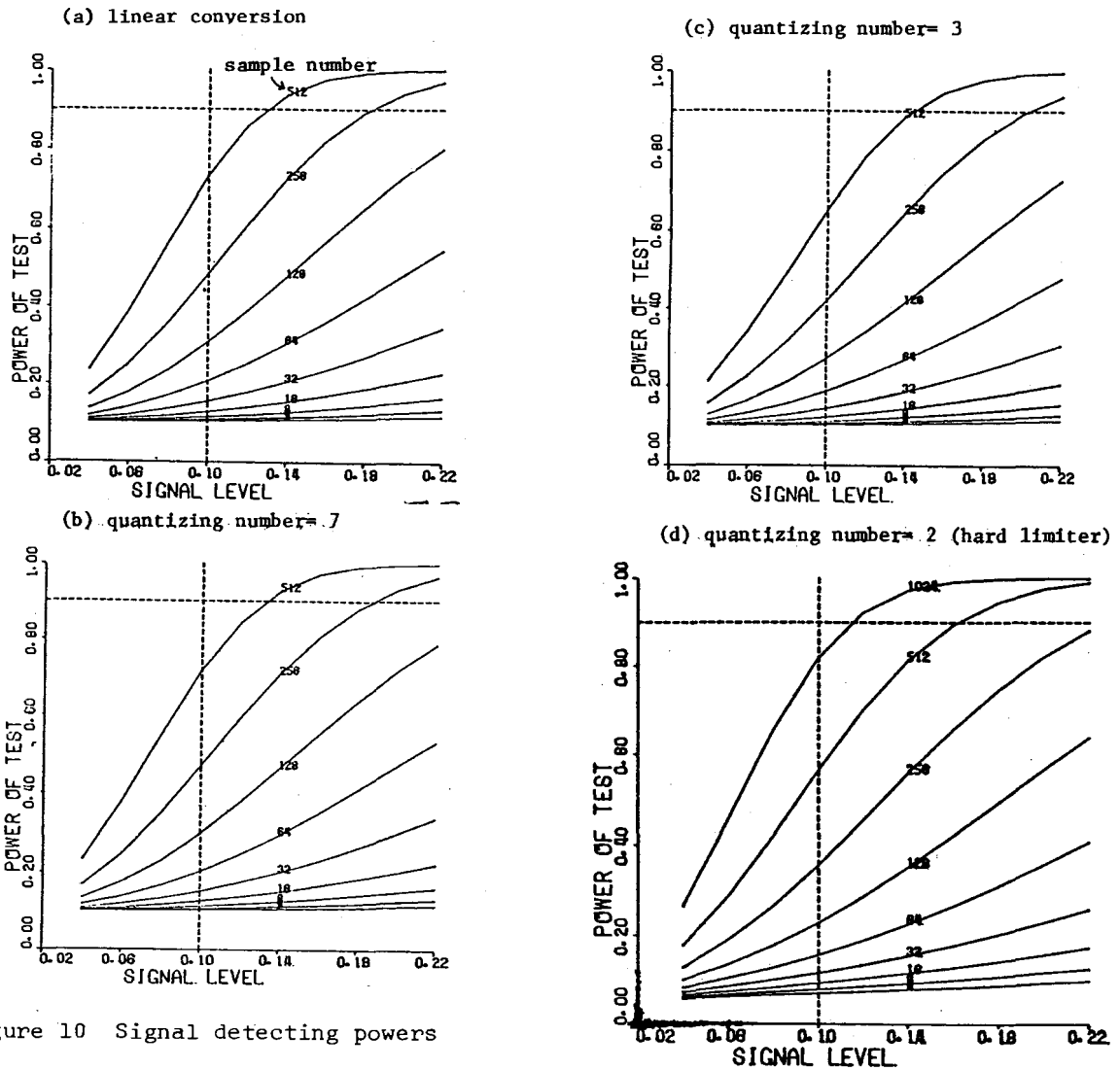


Figure 10 Signal detecting powers

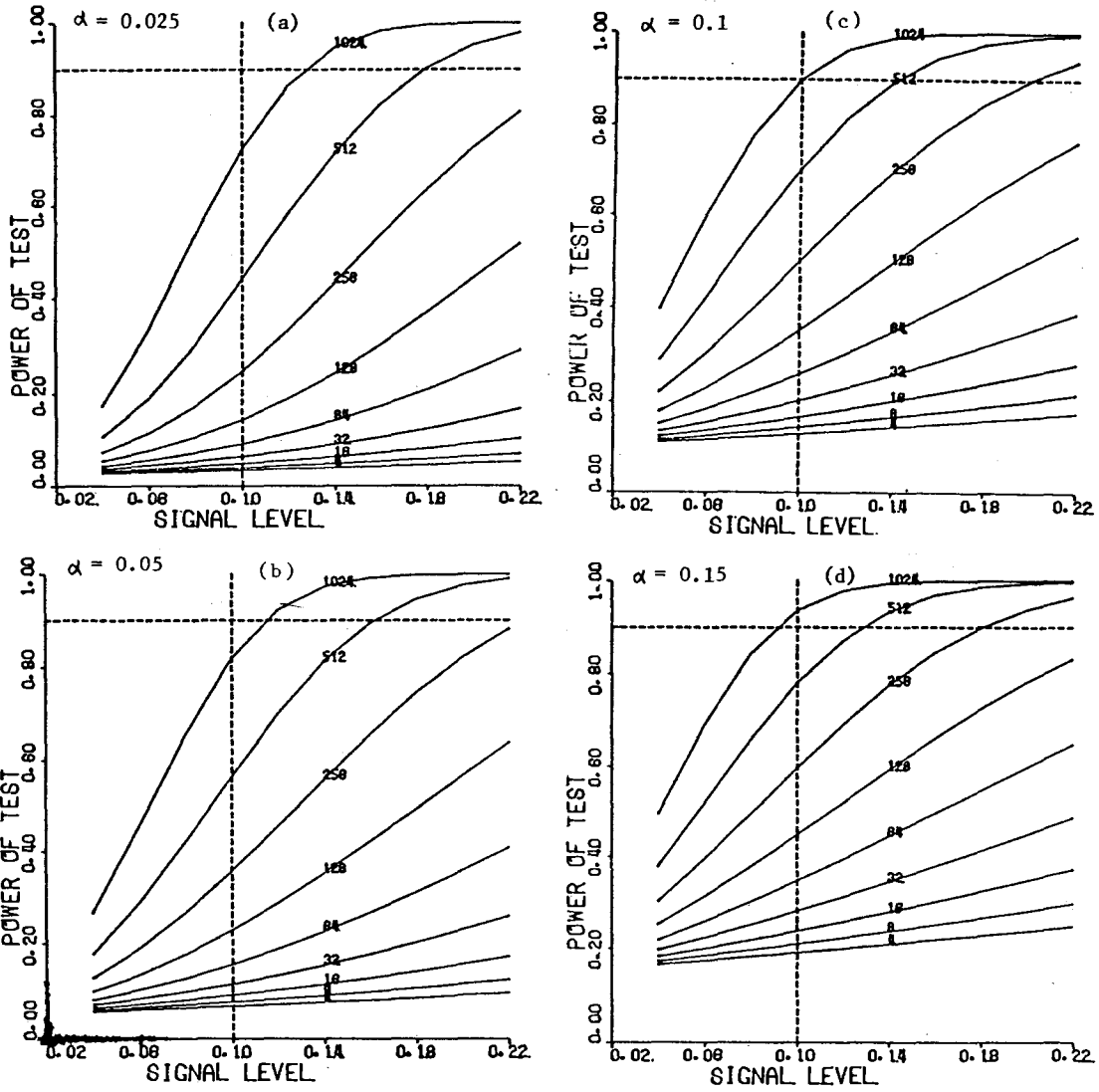


Figure 11 Relations among the signal detecting power, SNR and the sample number

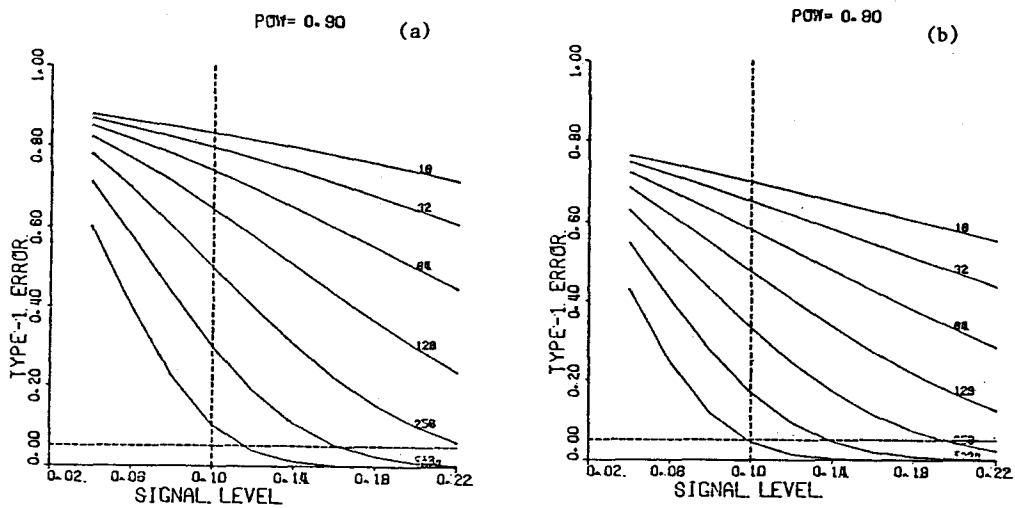


Figure 12 Relations among Type 1 Error, SNR and the sample number

For example, the results of 1) enable us to consider what sample number is needed for guaranteeing a desired signal detecting power and Type 1 Error, under a certain SNR. On the other hand, the results of 2) enable us to consider how much Type 1 Error appears at a threshold level set for guaranteeing a desired signal detecting power with a desired sample number, under a certain SNR.

For example,

- 1) SNR=-20dB, $\alpha=0.1$, P=0.9 ---n=1024
- 2) SNR=-20dB, P=0.9, n=512 --- $\alpha=0.3$

CONCLUSION

This paper has approached the problem of master and slave identification and the selection of the quantizing number in a digital type receiver. The conclusions we have reached are as follows:

- 1) Two different procedures of master and slave identification have been studied. One is based on the cross-correlation derived from the whole coding pattern, and the other is based on the product of two cross-correlations derived from two divided parts of the coding pattern. There is no significant difference in the discrimination error rate between two procedures, and under poor SNR conditions, the simpler one is superior to the complicated method that uses the MULT processing requiring a long execution time.
- 2) Although the hard limiting operation introduces a little reduction of the signal detecting power, it is available for a low cost digital receiver on account of the advantage of the simplicity and consequently low cost.
- 3) The relations among design parameters, the signal detecting power, SNR, Type 1 Error and the sample number, have been cleared.

After all, it is concluded that the analyses utilizing the stochastic technique are effectively employed in processing the signal contaminated by noise, and especially the statistical test brings powerful ability for a design of Loran-C receiver. Further, a similar stochastic investigation can be applied to approach the problems in the track process, such as cycle identification and digital phase locked loops.

REFERENCES

- 1) United States Coast Guard
" Loran-C User Handbook "
August 1974
- 2) Robert L. Frank
" Multiple Pulse and Phase Code Modulation in the Loran-C System "
IRE Trans. on Aeronautical and Navigational Electronics
June 1960
- 3) Julius S. Bendat
" Principles and Applications of Random Noise Theory "
John Wiley & Sons, Inc.
1958
- 4) Y.Taki, Y.Kaya, H.Miyagawa and Y.Sekine
" Stochastic Phenomena "
Iwanami-Shoten
1978

LORAN C/D APPLICATION TO TACTICAL RECONSTRUCTION
INFORMATION POD (TRIPOD)

John J. Hopkins
for
Teledyne Brown Engineering
and
Teledyne Systems Company
19601 Nordhoff Street
Northridge, California 91324

ABSTRACT

This paper concerns the use of Loran C/D in the TRIPOD application. TRIPOD is a training tool for pilots. It stores the location of hypothetical enemy EW or SAM sites, alerts the pilot when his aircraft comes within range of the stored phantom site and records on tape the pilot's evasive maneuver response. The TRIPOD is a pod with a self-contained Loran C/D navigation set, recorder and related equipment which can be installed on existing aircraft pod mounts. This paper specifically addresses the critical factors involved in using Loran C/D in this application. Emphasis is placed on the European Theatre because it is a difficult Loran C/D environment, caused by powerful in-band and near-band CW interference, and also because it is the area of most current interest. The paper points out those experiences which have proven it is possible to have satisfactory Loran D operation in Europe by proper selection of bandwidths, notch filters, rate aiding and antenna configurations. These issues and those related to Loran C/D coverage both in Europe and worldwide are addressed.

SUMMARY

Loran D transmitters currently installed in Europe provide adequate daytime signal-to-noise ratios for TRIPOD operation approximately 95 percent of the time. Installation of the new TRN-38 transmitters in late 1981 will improve the SNR by 8 dB which will increase the percentage of time TRIPOD would perform satisfactorily. The special Loran receiver front end and notch filter designs necessary to suppress strong European CWI are complete and proven in actual use in Europe, on the ground and in the air, even at very low altitude in mountainous terrain.

TRIPOD can be used anywhere there is adequate Loran C or D coverage. This includes a major portion of the northern hemisphere today. Plans to expand this coverage further include plans to fill the coverage gap in the western U.S. There is also serious interest in Loran C being expressed by many other countries.

LORAN C/D COVERAGE

Currently Loran C covers most of the U.S., North Atlantic, Mediterranean and portions of the Pacific and Far East. Two new stations were recently installed in Korea to expand the coverage in that area and plans are well advanced to

add a new station in British Columbia to improve the coverage in that area and to add a new station in Labrador to fill the gap in the North Atlantic coverage. Loran D (TRN-21) covers central Europe. The Soviet Union has installed two Loran C chains for its use. Figure 1 illustrates the Loran C/D coverage.

In late 1981 the new more powerful TRN-38 transmitters will replace the TRN-21 transmitters in Europe which will make the Loran C/D coverage much more solid and dependable. In the next few years expanded Loran C coverage is very probable in areas such as the mid continent of the U.S. and along the French Atlantic coast. Considerable interest in Loran C has also been expressed by many other countries including Taiwan, Australia, New Zealand, Mexico, Canada, Egypt, Saudi Arabia and several South American countries.

PERFORMANCE

This paper is concerned with low altitude performance of Loran C/D where TRIPOD is intended for use. In some areas this can be a more difficult environment than higher altitudes because of proximity to in-band RF interferences emanating from the ground. Experience with low altitude and ground operation have shown that Loran signals are usable and performance is satisfactory even in mountainous terrain and urban areas. These experiences include:

- Low altitude flights in Southeast Asia by USAF reconnaissance drones and special mission aircraft. The drones were flown well below mountain tops down in the valleys using prestored Loran waypoints. Photos taken were marked with Loran coordinates so that targets located on these photos could easily be found by Loran equipped strike aircraft. Many special mission aircraft carrying portable or installed Loran C steering systems with automatic position data links were used on low altitude missions.
- Mystic Mission in Hohenfels, Germany, by USA/USAF to demonstrate air/ground rendezvous, intrusion detection and weapon delivery. The rendezvous demonstration involved a Loran equipped helo and armoured personnel carrier. The APC Loran coordinates were transmitted to the helo and the helo crew was instructed to fly to those

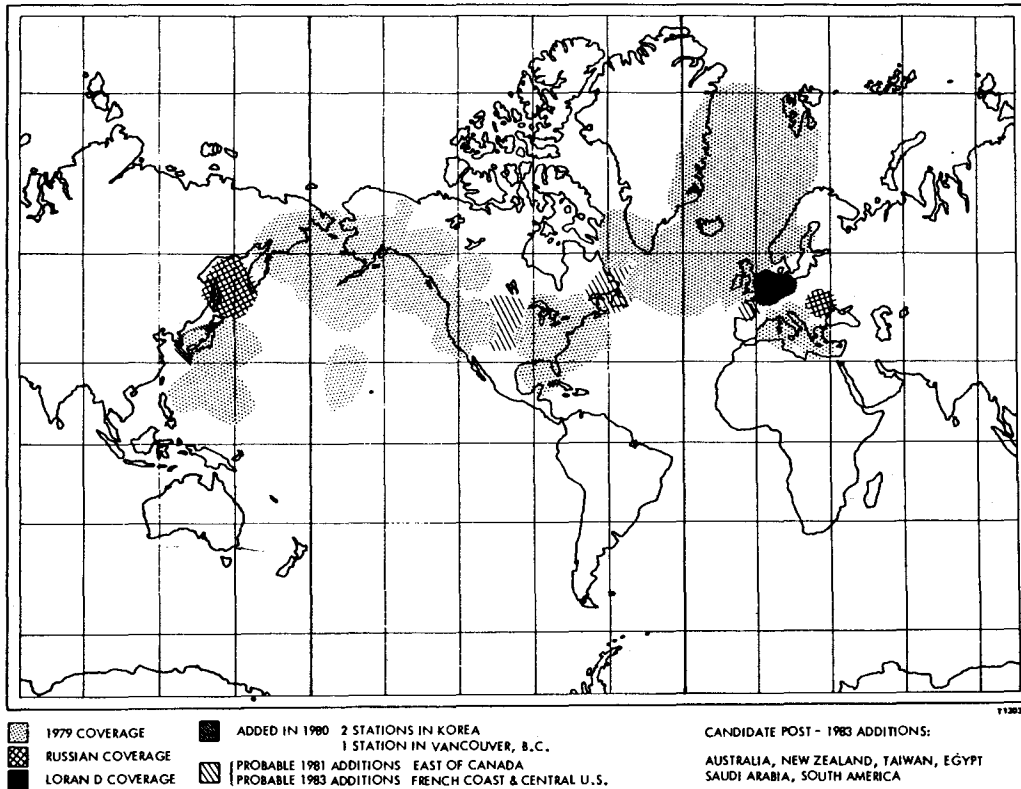


Figure 1. Worldwide Loran C/D

coordinates and drop a bag of flour. The drops were always very near the APC and in one case right on it. The other demonstrations involved intrusion detection sensors; such as, acoustic, pressure, seismic, IR and magnetic. They were implanted either by air drop or hand placed and Loran position recorded. When these sensors were activated Loran equipped strike aircraft, flying at very low altitude, made drops on the Loran coordinates dictated by the activated sensors. All these demonstrations were successful.

- State of Vermont flight tests sponsored by DOT/NASA which covered low altitude performance in mountainous terrain. Accuracy was demonstrated of better than 100 meters. Following is a quotation from the March 24, 1980, issue of AVIATION WEEK, page 51. "Preliminary data indicates that both as an enroute R-Nav aid and, particularly, during terminal and final approach phases of flight, Loran C can confer significant benefits as a supplement or complement to existing Vortac and nondirectional beacon procedures functioning right down to minimum descent altitude and below, even in this mountainous terrain."
- Automatic vehicle monitoring demonstrations in numerous urban environments including Philadelphia, Washington, DC, Salt Lake City, Las Vegas, and Los Angeles. See Figure 2. Results indicate usable Loran C signals are available in all but the most dense high-rise portions of these cities. Typically,

where buildings are more than ten stories high and streets are narrow Loran C signals are too weak and noise is too great for reliable operation. This usually amounts to less than 1 percent of the urban area. In the remaining 99 percent of the area the signals are usable.

The overall conclusion from all the foregoing experiences is that Loran C will operate satisfactorily at low altitudes even in areas where there are mountains or other obstructions.

Interference to Loran C/D

Generally, atmospheric noise is the principal source of interference in the Loran band (90 to 110 KHz). This is burst interference characterized by high spikes. It is 8 db to 20 db more severe at night than in the daytime hours between 0800 and 1600. In Europe there is also man-made high power CW transmissions in and near the Loran band that require special notch filters. A supplemental notch filter has been built and successfully demonstrated. This filter assembly provides manual notches which when added to the existing notches, see Figure 3, enables satisfactory operation in Europe with the TDL-424 and the AN/ARN-129 Loran C/D Navigation Systems.

Also, very important in the rejection of out-of-band interference, is the bandwidth and cutoff characteristics of the front end bandpass filter. The filter must be wide enough to pass the needed Loran signal energy and have steep

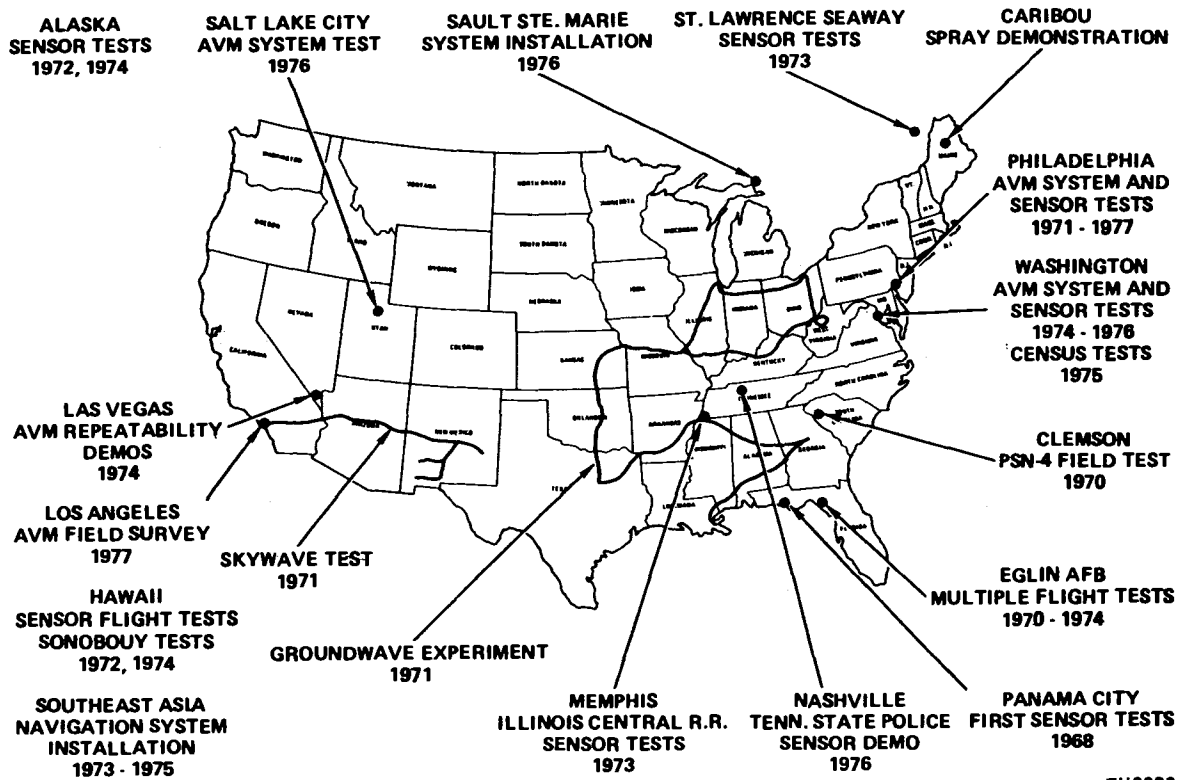


Figure 2. National and Worldwide Loran C Sensor And System Demonstrations

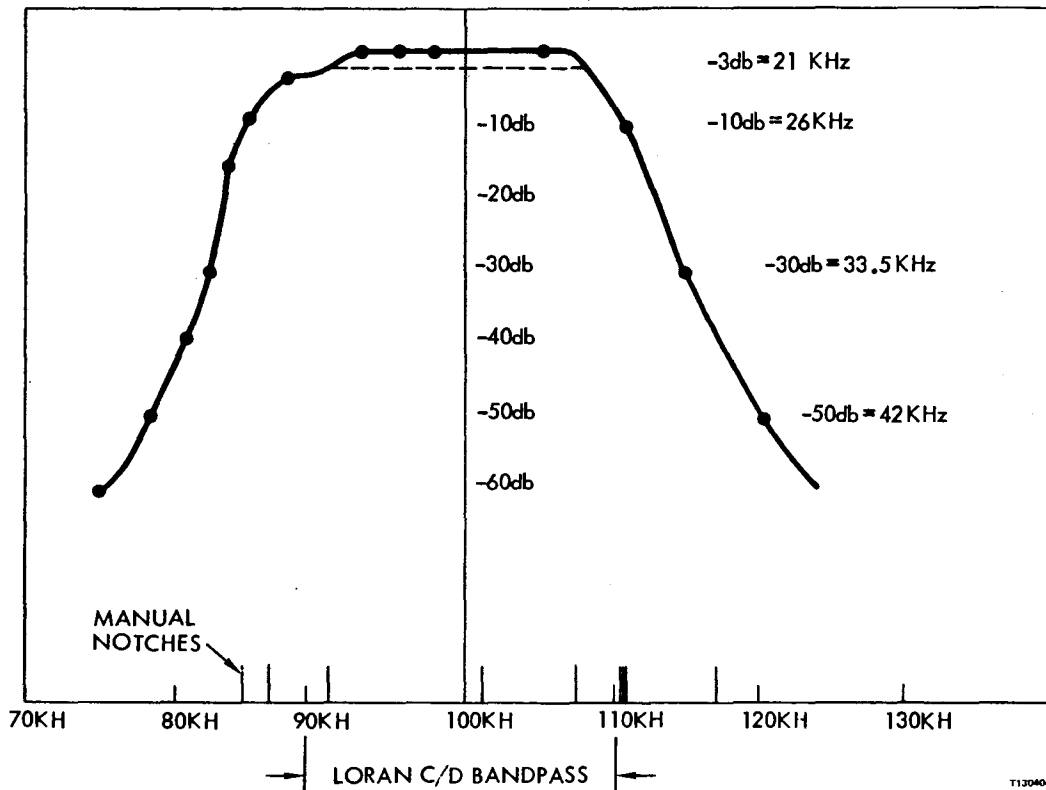


Figure 3. Bandpass of 8 Pole Filter and Notch Filters for European Operation (Manual Notches as Shown Plus 2 Auto Notches)

roll-off to suppress out-of-band interference. Figure 3 also shows the characteristics of the 8-pole filter used in the AN/ARN-129 which has successfully performed in Europe.

In the U.S. there is very little man-made interference. No notches are required in most places. Exceptions are Washington, DC, and San Francisco areas where two notches are required to suppress Navy communication transmissions at 88 KHz and 120 KHz.

Signal-to-Noise Considerations in Europe

The signal to noise ratio is the most important single factor in Loran C/D performance. Although Loran C/D receivers can operate in today's SNR conditions in Europe the signal strength is barely adequate to compete against the man-made CWI, especially at night. When the front end bandpass filter is narrowed and supplementary notch filters are added to suppress the CWI they also cause a signal loss of about 10 db in SNR.

Fortunately, there are plans to replace the current 5 KW TRN-21 Loran D transmitters with 30 KW TRN-38 transmitters in late 1981. This six-fold increase in power will add 8 db to the SNR. Also, since there is no skywave to contend with because of the relatively short range of Loran D as compared to Loran C, the receivers can track deeper into the pulse and pick up 6 db over a long baseline Loran C installation. Furthermore, in the TRIPOD application most of the low altitude training flights will be flown in the daytime when the noise is 8 db to 20 db less than nighttime noise.

The TRIPOD Loran C receiver acquisition threshold is -10 db. Above this SNR, the receiver can be turned on and it will search and find the correct tracking cycle. Once in track it will actually track to lower SNR's (-16 db) but if it should lose lock it will not reacquire and find the correct tracking cycle unless the SNR is above -10 db.

Now considering all the SNR improvements mentioned above, what could cause the SNR to fall so low that the receiver loses lock? Several things. First, the atmospheric noise can increase to much higher levels than the averages on which most coverage maps are based. When this happens the receiver will lose lock unless the signal is more than enough to maintain an adequate SNR. The stronger the signal the less likely it is that atmospheric burst noise will cause loss of lock. Other potential causes for a drop in SNR are changes in antenna effective height when the aircraft changes attitude and P-static. These effects can be minimized by proper antenna design. This will be discussed further in a later section. Another place SNR would degrade is at very long range from the transmitter, but it is unlikely that this would be a concern with a short (250 to 350 NM) baseline Loran D system because the geometry limits the useful range, not the signal strength, i.e., the lines of position crossing angles become very small before the signal gets too weak to use. This is called geometric dilution of precision or GDOP.

To illustrate the effects of atmospheric noise on receiver performance please refer to Figure 4. This figure plots atmospheric noise as a variable on the X-axis, and then using the signal strengths from the 5 KW transmitters at 300 NM and 500 NM ranges, it indicates the resultant SNR on the Y-axis. The atmospheric noise was taken from a sample noise calculation for 40° latitude based on CCIR* data. The noise levels indicated in the table are 4 hour averages which are not exceeded 95 percent of the time according to the CCIR source. The table shows the wide disparity between daytime, 0800 to 1600 hours, and nighttime noise levels. The average daytime and nighttime noise levels are:

$$\frac{\Sigma \text{ of } 0800 \text{ to } 1600 \text{ hours noise averages}}{\text{Number of Measurements}} = \frac{307}{8} = 38.4 \text{ db}$$

$$\frac{\Sigma \text{ of } 1600 \text{ to } 0800 \text{ hours noise averages}}{\text{Number of Measurements}} = \frac{807}{16} = 50.4 \text{ db}$$

In this case the average nighttime noise is 12 db greater than the average daytime noise.

For reliable Loran operations it is desirable to maintain the SNR well above the -10 db acquisition threshold to allow for the degradations caused by atmospheric noise bursts and aircraft attitude changes. A 10 to 20 db margin is desirable and will insure reliable operation. The plot shows that this margin is available at 300 NM using daytime average noise. This would be adequate for the TRIPOD application. The added power provided by the TRN-38 transmitters will provide 8 db greater margin. This additional margin can be traded off against simplifications in the antenna configuration if desired or it can be retained to insure even more reliable Loran performance.

Figure 5 is a computer derived plot of accuracy attainable in the Loran D coverage area with the installed TRN-21 transmitters. Actual data confirms these predictions. The Electronic Systems Division Field Measurement Program conducted from 1976 to 1979 indicates latitude/longitude repeatable accuracy of better than 150 feet in the prime coverage area.

Figure 6 shows areas lying within 360 NM and 500 NM of three transmitters. Inside the 360 NM range line the SNR is better than 0 db (based on the 24 hour average noise). Inside the 500 NM range line the SNR is better than -10 db, the receiver acquisition threshold.

The conclusion is that the TRN-21 transmitters furnish adequate signal power for most noise conditions but with little margin to spare. The additional power of the TRN-38 will insure reliable Loran operation in Europe.

*International Radio Consultative Committee Dynamic Effects

Loran C/D receivers must smooth the error samples to extract the signal. This takes time.

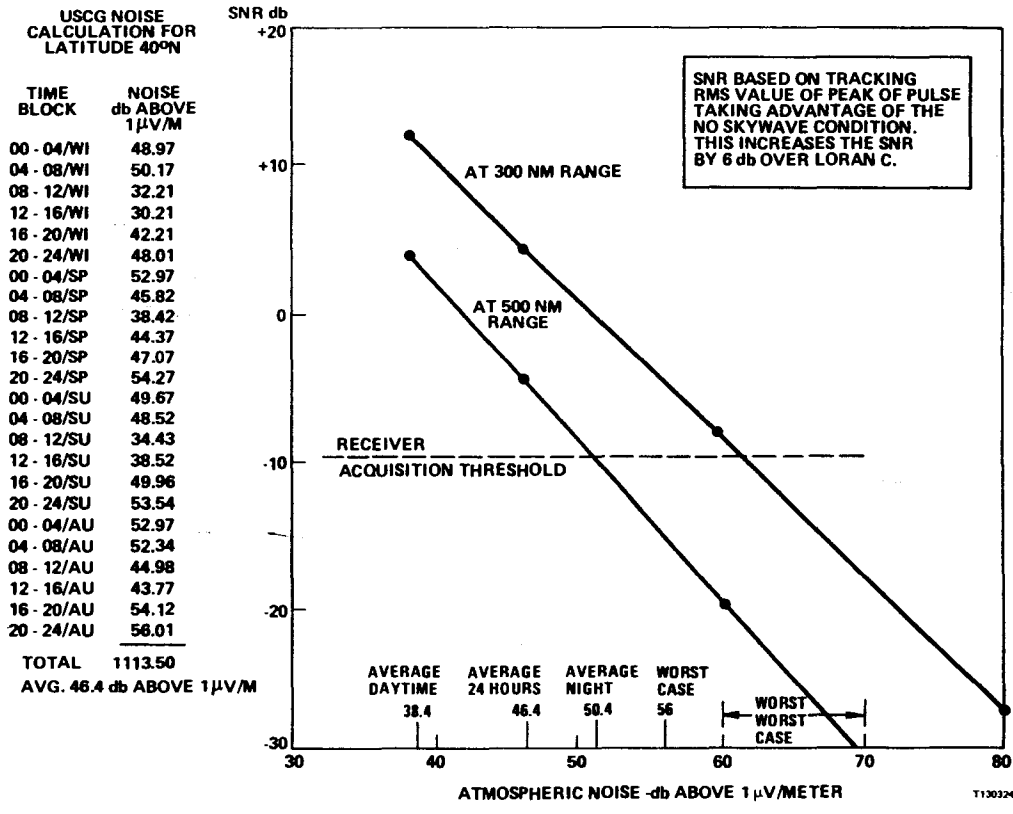


Figure 4. TRIPOD Loran Operating Range in European Noise Environment
 TRN-21 5KW Radiated Power
 (For TRN-38 30KW Radiated Power Raise Both Curves 8 db)

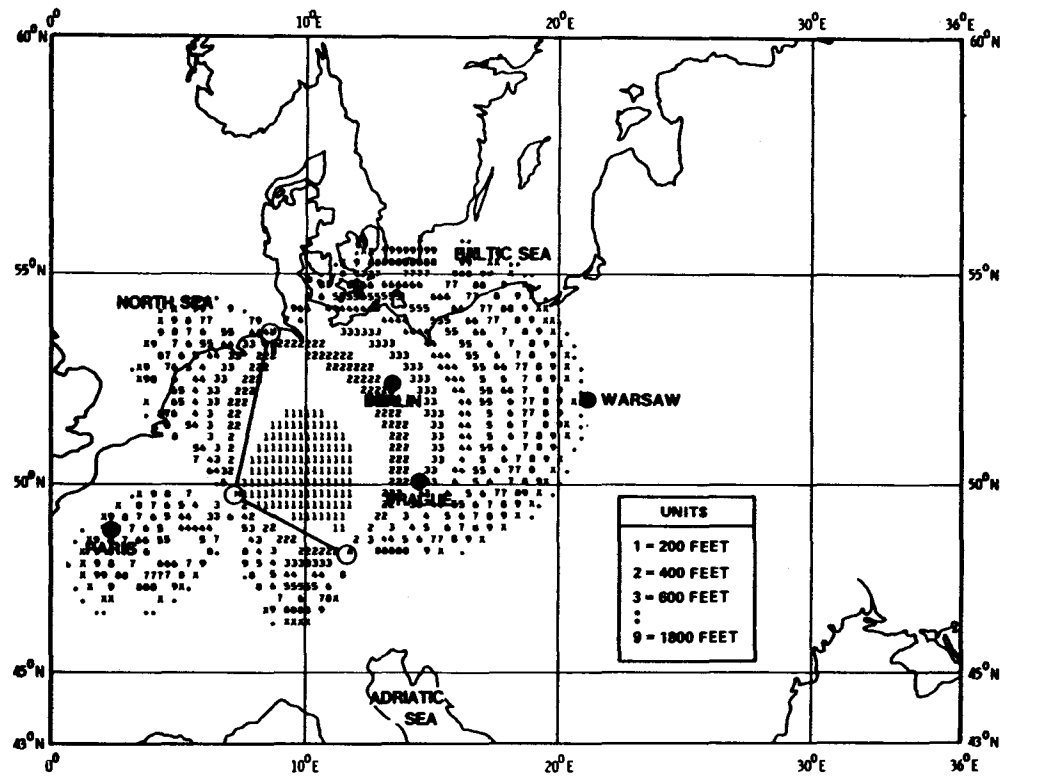


Figure 5. Central European Chain

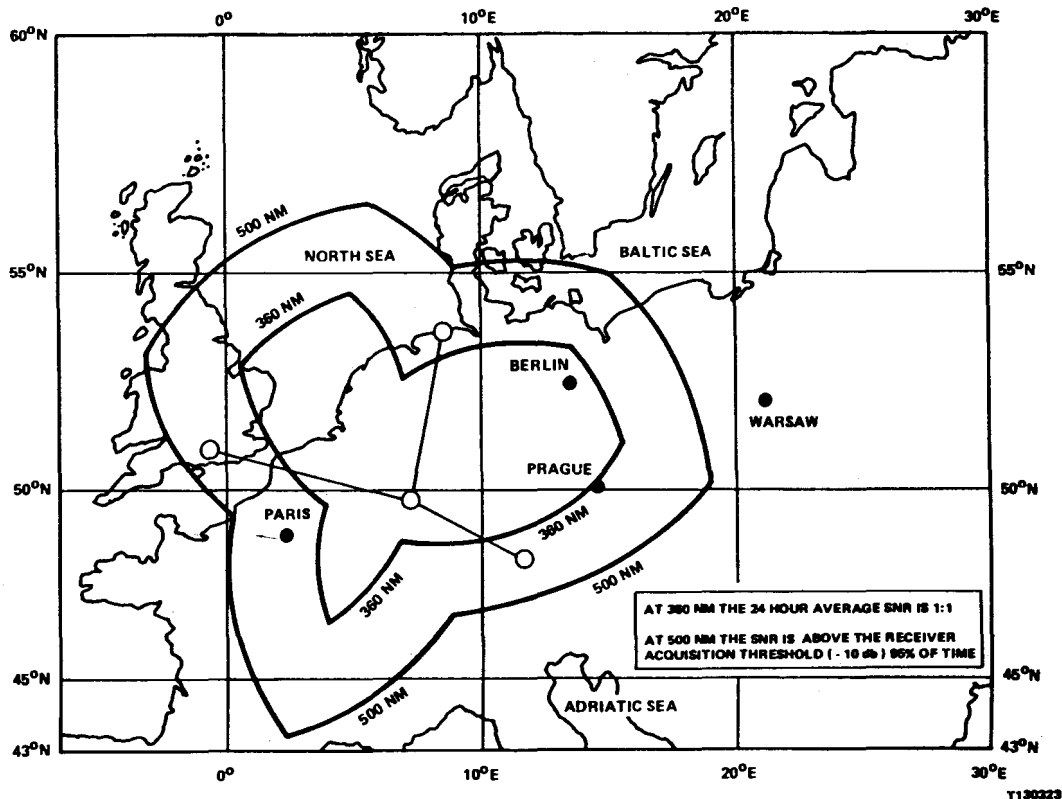


Figure 6. Central European Chain (Continued)

Second order tracking loops are used to insure that there will be no lag in the solution if the receiver is moving at a constant velocity relative to the transmitter. Obviously, if the receiver is in an aircraft that is turning a lag error will build up and when the aircraft again returns to a constant velocity this lag error will disappear. If the smoothing time is too large the receiver will lose lock. If the smoothing time is too short the receiver cannot extract the signal from the noise under conditions of poor SNR. The effective SNR improves proportionally to the square root of the smoothing time.

In order to have the SNR advantage of the longer smoothing time and not risk losing lock in turns an external velocity aid should be used. It can be integrated with the Loran sensor to blend their respective capabilities.

Rate Aiding

The integration of LORAN and rate aiding sensors has been practiced in countless applications for many years. Such integrations are undertaken either to improve the threshold performance of LORAN receivers, improve the solution accuracy or both. To improve both is most often the objective of integrating a velocity sensor with the receiver as is the case here. In terms of mechanization, the integrated sensors mutually offer three functions not found in unaided systems. Those functions are lag-free smoothing of the solution, dead reckoning of the smoothed solution when track is lost by the receiver and prepositioning of the tracking loops during signal outages. The smoothed solution seeks to usefully combine signal measurements

and velocity while estimating velocity sensor errors. The dead reckoning is commonly embodied in the algorithms of the velocity-aided solution. The tracking loop aiding serves to shorten the periods of track loss and improve the confidence of reacquisition without envelope errors.

There are many useful rate aiding sensors which may be integrated with a LORAN sensor. Chief among those for this application are air data/attitude and heading reference systems and inertial measurement units. These systems span a wide range of cost, computational complexity for both sensor management and solution, and performance. The simplest is an AHRS/air data system. The most expensive is a precision, gimbaled inertial sensor with a pressure altimeter. In between is a strapdown inertial sensor package of the sort used for weapon guidance, e.g., Harpoon, also with a pressure altimeter. All three may be characterized in terms of integrated system accuracy by their errors.

The AHRS/air data system can be a two-axis velocity sensor in a smoothed solution. Its principal error sources are wind, heading bias, altitude bias, and air speed errors due to air-frame structure, angle of attack and noise. The integrated solution can estimate wind and heading bias. The air speed sensor errors are virtually impossible to estimate effectively. The history of such integrations shows that all of the principal errors are either largest or changing fastest when the aircraft is performing strenuous maneuvers. At these very times, the LORAN receiver is most likely to lose lock. The estimation process then degrades significantly.

In level flight, such a system can achieve a CEP of better than 50 meters, but after 1-2 minutes of high-G (4+) turns and large attitude changes, the CEP can degrade to 200 meters or more. Even with large velocity sensor errors, the integrated system is still better than LORAN alone. Since the synergism between sensors is poor, there is little reason to use an adaptive, covariance type filter in the solution.

At the other end of the spectrum is the gimbaled IMU. Unlike the other velocity sensors, its principal errors are largely independent of environment. Those principal errors are angle biases, i.e., mislevel and heading errors. A dampened vertical fix requires the system to deal with pressure altitude bias. The precision and noise content of the velocity information is the same during combat maneuvers as during level flight. The smoothing time for signal measurement can be very long, so long that imperfections in the propagation corrections need to be accounted for in the measurement noise. The integrated solution can readily estimate the platform angle errors. Given a rigorous approach to propagation correction, the level flight CEP will be 25 meters or less. After 1-2 minutes of combat maneuvers, the CEP may degrade to 40 meters. If the LORAN receiver has all-attitude reception, the CEP will not degrade at all. The vertical fix will be the weakest part of the solution. Since the synergism between sensors is outstanding, a covariance filter is a worthwhile feature of the solution algorithms.

An inexpensive strapdown inertial sensor of the Harpoon type is a good compromise between the other two choices in both cost and performance. The dead reckoning performance over long periods of time is poorer than the gimbaled IMU. The smoothing time must accordingly be shorter. The principal error sources are more numerous than for the gimbaled IMU. Added to the angle errors, the principal error sources are G-sensitive gyro bias, scale factors and mounting misalignment; however, all these errors are readily estimable. In order to approach gimbaled IMU performance emphasis must be placed on the error estimation process. A simple error model, one which is manageable in a practical airborne minicomputer, can yield a CEP of 80 meters after 1-2 minutes of loss of Loran lock as might occur during strenuous maneuvers and be accurate to within 50 meters CEP in level flight. Any effective error model will utilize a covariance filter as part of the solution.

Clearly the quality and quantity of the signal measurements has an effect on the solution accuracy. A LORAN D chain using a short GRI will support better accuracy than a LORAN C chain using a long GRI, given the same signal-to-noise ratio at the sample point. Tracking the higher pulse rates of a LORAN D chain usually translates into less measurement noise for a fixed dynamic responsiveness than the equivalent situation under LORAN C coverage. Fortunately, the much higher broadcast power of LORAN C transmitters typically translates into a more generous sample point SNR, much better than LORAN D coverage provides. The exact signal environment, measurement noise and bandwidth, and CEP depend on the specific

coverage involved. All the estimated CEP's can be achieved in the groundwave coverage area on any existing chain in daylight with a GDOP factor less than three. In any case, no signal conditions will be encountered that make the AHRS/air data sensor perform as well as an inertial sensor in the integrated system under combat dynamics.

Table 1 summarizes the relative merits of the three aiding approaches considered. Figure 7 shows the information flow of an aided system.

Table 1. Aided Loran Navigation Configurations

Description	Advantages	Disadvantages
Loran/AHRS/Air Data Gimbaled AHRS	Simple Cheap	Poor Dynamic Performance
Loran/Gimbaled IMU/ Altimeter High Quality IMU	Superb Accuracy Good Dynamic Performance	Large Expensive Power Consumption
Loran/Strapdown IMU/ Altimeter Low Grade Instruments	Reasonable Accuracy Good Dynamic Performance	Much Computation Rapidly Degrades without Loran Data

ANTENNA

Much experimental and field evaluation work has been done to design a Loran antenna that provides good all attitude performance; e.g., 3-axis H-field ARN-101 antenna. Similarly, much work has been done to design a Loran antenna that will operate satisfactorily while installed in a pod mounted Loran set; e.g., balanced cavity E-field drone antenna. Then, there are a plethora of other designs which are satisfactory for modest maneuvers on most aircraft including: stubs, blades, long wires, towel-bars, and tail caps. Unfortunately, there have been no tests conducted on an antenna configuration designed specifically for the TRIPOD application. Unlike the drone antenna which was optimized for free flight, the TRIPOD antenna will only be used in captive flight. Furthermore, the maneuvers will be strenuous. This combination of requirements calls for special design considerations. In view of the limited surface area available on the TRIPOD and its captive location, it is unlikely that any practical antenna design will provide all attitude operation, hence, a tradeoff is in order. This tradeoff is between antenna design complexity and tolerable error resulting from loss of lock. A reasonable design objective appears to be to limit the Loran receiver loss of lock intervals to two to three minutes. This allows one to two minutes for the SNR to be below the tracking threshold (-16 db), roughly the duration one might expect for a strenuous maneuver and another minute for the receiver to return to track. The inertial system will restrain the error buildup and drive the Loran tracking loops when the receiver loses lock. When the SNR improves the receiver will return to track in approximately one minute. This would limit the total loss of lock interval to three minutes. The integration of the INS with the Loran can be mechanized to contain the error during this interval to less than 150 meters CEP. This is achievable and within the capabilities of the Loran receiver and INS contemplated for use in the TRIPOD.

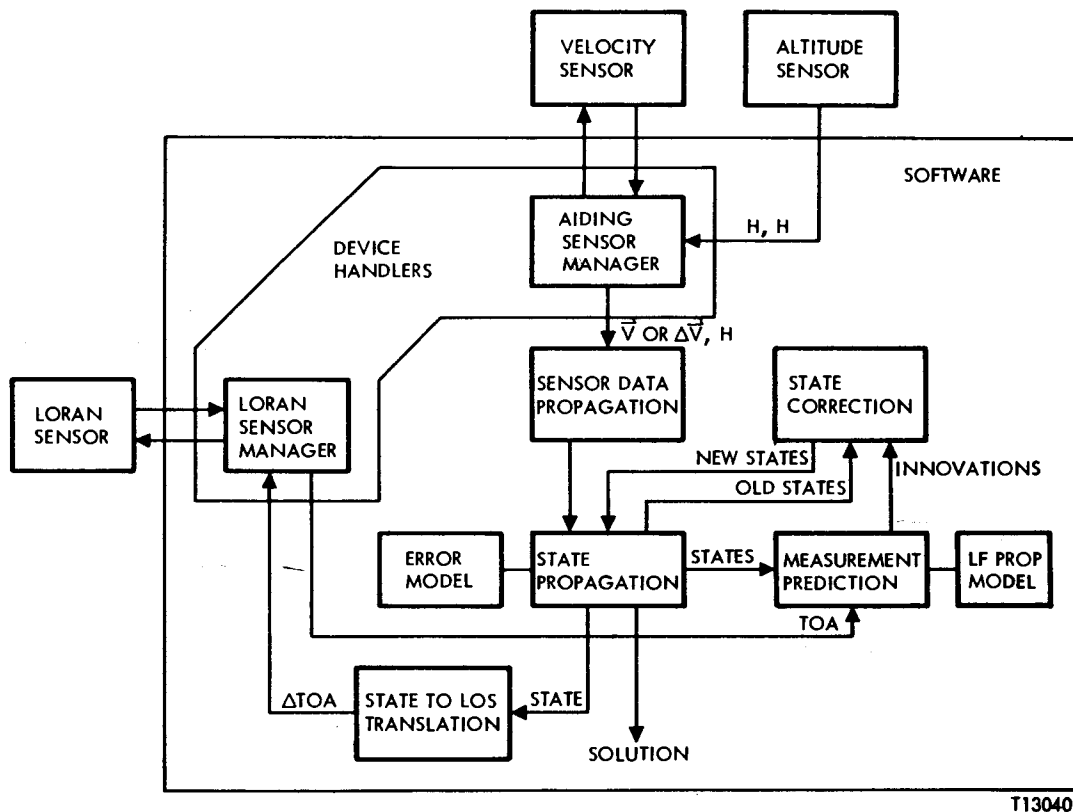


Figure 7. Aided Loran Navigation Functional Block Diagram

The choice of antenna will not finally be made until after the most promising ones are analyzed and scale model tests are conducted. Three types appear to be good compromise candidates: 2-axis H-field antenna, balanced cavity E-field antenna and a blade antenna.

The 2-axis H-field antenna mounted on the bottom of the TRIPOD would most likely work well in this application in spite of its known heading sensitivity in steep banked turns. The addition of the 3rd axis (the Z axis) reduces this heading sensitivity substantially in the ARN-101² application; however, there is no suitable place to install a 3rd axis on the TRIPOD so the alternative is to rely on the INS during certain flight attitudes.

The balanced cavity E-field antenna was tested extensively on a scale model drone which was designed for launch from a C-130 pylon.³ It consists of two separate cavity antennas, one on top and one on the bottom at the forward end of the fuselage. The area of each cavity is about 12 square inches and depth about 0.25 inches. Tests indicated that this antenna had satisfactory patterns in the captive mode, but the tests were limited to 30° roll and pitch. Additional tests would be necessary to examine the more extreme attitudes.

A blade antenna (bottom mounted) is also a candidate. Captive pattern tests on a scale model drone/C-130 combination indicated phase reversing nulls occurred at about 30° roll, but other than this it performed reasonable well.

The blade, being exposed to the airstream, is more susceptible to P-static than the balanced cavity; however, its relative simplicity and reasonably good performance warrant further consideration.

REFERENCES

1. Loran AVM Final Report No. DOT-TSC-1238, March 1977 U.S. Department of Transportation Systems Center, Cambridge, Massachusetts.
2. The AN/ARN-101 Loran Receiver, A. Gaunt and D. Gray, Lear Siegler, Incorporated, Grand Rapids, Michigan.
3. Loran Antenna Study Report for the Ryan 147 Drone Aircraft, Teledyne Micronetics, July 1972.

LORAN-C FLIGHT TESTING IN THE WESTERN UNITED STATES

Edwin D. McConkey and Thomas E. Scalise
Systems Control, Inc. (Vt)
Champlain Technology Industries Division
West Palm Beach, Florida

ABSTRACT

An FAA sponsored Loran-C flight test program was performed in the western United States during the summer of 1979. The purpose of the tests was to evaluate the use of Loran-C for non-precision approach applications in mountainous areas. Both operational and technical evaluations were performed. Three primary test sites were used during the tests. These were South Lake Tahoe, CA; Klamath Falls, OR; and Grand Junction, CO. Secondary sites were Reno Stead and Reno International Airports in Nevada. All test sites had high, rugged terrain located in the vicinity of the airport. Site selections were made to demonstrate specific Loran-C operational characteristics.

The flight test aircraft was the contractor's Piper Aztec. The Loran-C receiver/navigator used in the test was the Teledyne TDL-711 Micro-Navigator. The Micro-Navigator drove a course deviation indicator located on the cockpit control panel. The control/display unit for the navigator was operated by the co-pilot. The tests were flown in visual meteorological conditions with the pilot "under the hood" to simulate instrument conditions. Actual aircraft position was derived from a Remote Area Precision Positioning System (RAPPS) built by Sierra Nevada Corporation under FAA sponsorship. This system uses multiple range measurements from VCRTAC, DME and dedicated test beacons. An on-board data collection system was used to record and store Loran-C and RAPPS data.

The results of the tests indicated that the West Coast Loran-C chain and the receiver portion of the Micro-Navigator performed very well during the tests. Time difference data was available from the receiver throughout all the tests except for two brief instances when the Searchlight signal was lost. The tests did point out several areas where improvements in the navigation computer could be made. These include propagation modeling, track guidance computation and filtering, and ambiguity resolution. From an operational standpoint, the Micro-Navigator was easy to operate and produced stable, repeatable track and distance guidance. Improved propagation modeling, leading to a reduction in system bias errors, and improved guidance computation should

significantly improve the overall system accuracy to a level approaching or exceeding FAA area navigation requirements for non-precision approaches.

The results of these tests indicate in all likelihood during the 1980s Loran-C will increasingly find its way into the general aviation cockpit. There it can be used to aid pilots at locations where its wide-area, all-altitude coverage is needed for making low visibility approaches.

BACKGROUND

There are several civil air navigation operations which can utilize the long-range, low-altitude coverage of Loran-C. The most apparent applications are offshore helicopter flights to support oil and gas exploration and drilling operations and flights by general aviation aircraft to airfields in mountainous terrain where current navigation aids can not support low altitude instrument approach procedures. Because the Loran-C groundwave follows the contour of the earth and is not blocked by rolling or mountainous terrain, its signal can be received at all aircraft operational altitudes down to ground level. The current standard air navigation system is the VHF Omnidirectional Range (VOR) whose signals are line-of-sight limited. Therefore its signals are not capable of being received at low altitudes at distances far from the transmitter or in mountain valleys.

The Federal Aviation Administration (FAA) is sponsoring test programs to evaluate the use of Loran-C for non-precision approach applications in mountainous areas and for offshore helicopter operations. To date tests have been conducted in the western United States, Vermont, Gulf of Mexico, Appalachia, and the Northeast Corridor area from Boston to Washington, DC. This paper describes the tests and results of experimental non-precision approaches made in the western U.S. using the U.S. West Coast Chain.

OBJECTIVES

In preparing the West Coast Loran-C flight test plan, several objectives were considered important areas for experimentation.

Mountainous Terrain

It was important to evaluate Loran-C approaches in rugged terrain where at least one of the signals had to traverse mountainous terrain. It was also important that there be mountains in the vicinity of the airfield so that coverage and accuracy data could be obtained in areas where the VOR system could not support instrument approaches.

Area Navigation Procedures

Loran-C navigation is covered in the FAA regulatory process as an area navigation (RNAV) system. The document which covers RNAV operations in the U.S. is FAA Advisory Circular 90-45A, dated August 1978. The instrument approach procedures used in the tests were based on the guidelines and requirements described in this document.

Varying Loran-C Geometry

The accuracy of Loran-C navigation is dependent upon the geometry of the lines of positioning from the various transmitting stations. Therefore data from several combinations of stations at differing ranges from the aircraft were used to evaluate varying Loran-C geometry.

Loran-C Accuracy

The utility of Loran-C for non-precision approaches is closely tied to the accuracy of the system and the characteristics of the errors. Therefore it was necessary to measure and record several parameters from the Loran-C navigator to determine system accuracy and to isolate possible sources of error. Accuracy characteristics were then computed in terms of FAA RNAV standards.

Loran-C Operational Utility

Even when FAA accuracy standards are met, there are a number of operational requirements that must be satisfied to make Loran-C a useful navigation system for non-precision approaches. Among these concerns are system reliability, maintainability, compatibility with Air Traffic Control requirements, acceptable pilot workload, signal acquisition (reacquisition) time, etc. Some of these parameters are quantifiable and were measured during the test. Others are more qualitative in nature and for those, only pilot opinions and user acceptance of the Loran-C system can be used to determine the operational acceptability of Loran-C. Therefore, both qualitative and quantitative operational data were collected during the flight test.

Remote Area Approach Testing Procedure

In addition to the Loran-C tests that were performed, a preliminary assessment of the Remote Area Precision Positioning System (RAPPS) was performed for the FAA. This system uses distance measurements from the aircraft to multiple ground based transponders located at known positions of latitude and longitude to accurately determine the aircraft's position during the approach tests. The FAA must determine procedures which can be used to qualify approach procedures in remote areas where radar or other precision tracking instrumentation is not available. The RAPPS is under consideration as a means to solve this problem. The West Coast Loran-C tests were used to provide a preliminary evaluation and airborne acceptance test of RAPPS prior to more comprehensive testing at the FAA Technical Center in New Jersey. The experimental nature of these tests limited the amount of Loran-C data which could be used for conclusive accuracy results. These limitations are discussed in the data acquisition section of the paper.

LORAN-C COVERAGE

In the western U.S. Loran-C coverage is provided by the U.S. West Coast chain. The master station is located at Fallon in northwestern Nevada. The X secondary is located in central Washington near the town of George. The Y station is found in north central California at Middletown and the Z secondary is located in southwestern Nevada at Searchlight. The chain operates with a group repetition interval of 79300 microseconds.

The Fallon-Middletown-George triad (F-M-G) provides coverage to western Washington, Oregon and northern California. The Fallon-Middletown-Searchlight (F-M-S) triad provides coverage for southern California and the Fallon-George-Searchlight (F-G-S) triad provides coverage to the inland areas of Idaho, Montana, Colorado, Wyoming, Nevada, northern Arizona and states to the east where signal reception is available.

TEST LOCATIONS

Due to the limited scope of the tests and the experimental nature of the RAPPS equipment, only three sites were initially selected for approach testing. These sites were Lake Tahoe Airport, South Lake Tahoe, California, Runway 18; Kingsley Airport, Klamath Falls, Oregon, Runway 32; and Walker Field, Grand Junction, Colorado, Runway 16.

Subsequently, during the tests two additional test sites were established near Reno, Nevada; the operational base for the tests. A test approach procedure to Reno International Airport was established for Runway 16 and at Reno Stead Airport for Runway 26. Only limited tests were flown at these two sites. The Loran-C stations and the test sites are shown in Figure 1.

Two of the test site triad selections were outside of the normal Loran-C coverage area. The Klamath Falls site is nearly on the baseline extension from Searchlight causing poor geometrical relationships. This is confirmed by the very high 2-drms value for the F-M-S triad shown in Table 1. The Grand Junction location is in the poor geometry region of the F-M-G triad. Both of these locations have an expected 2-drms error that exceeds 1500 ft, the coverage limit defined by the U.S. Coast Guard.

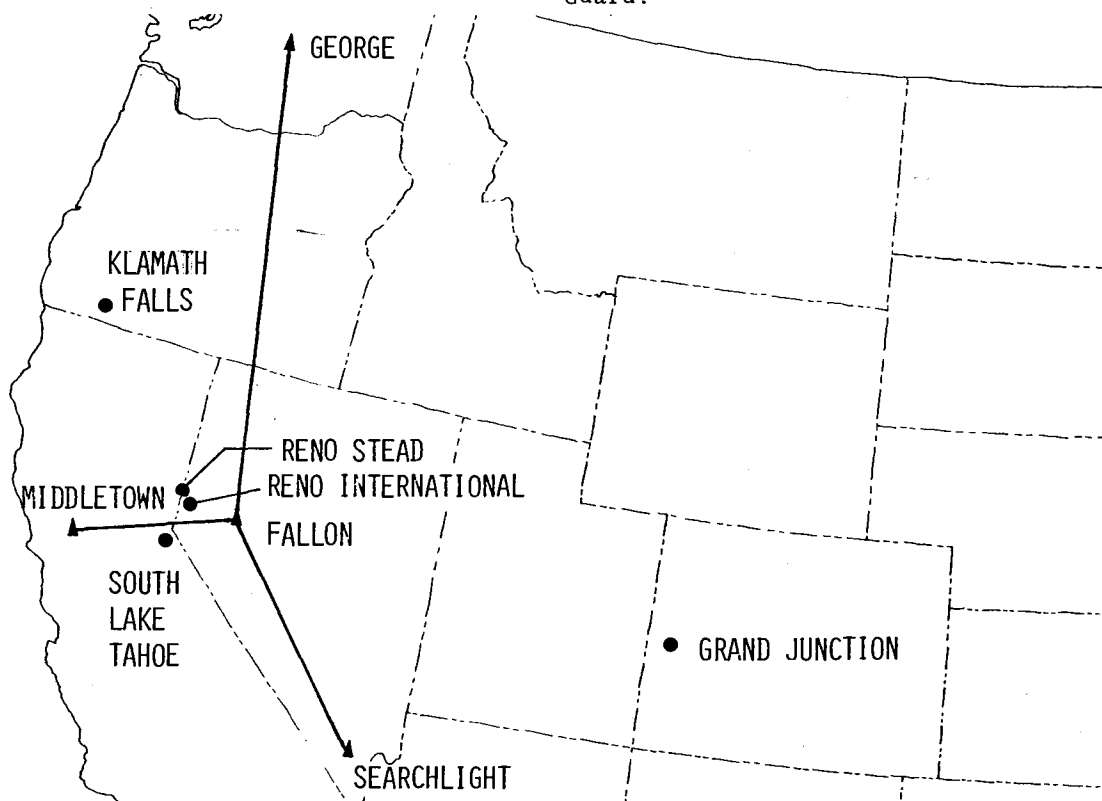


Figure 1. West Coast Loran-C Test Sites

Due to the limited number of test sites and the desire to collect information on both favorable and unfavorable fix geometry, two triads were selected for approach testing at each site. Table 1 shows the sites, triads utilized and expected 2-drms* accuracy for each site.

Table 1. Test Site Triads and Expected 2-drms Accuracy*

SITE	PRIMARY TRIAD	2 drms (feet)	SECONDARY TRIAD	2 drms (feet)
SOUTH LAKE TAHOE	F-M-S	205	F-M-G	335
KLAMATH FALLS	F-M-G	254	F-M-S	71981
GRAND JUNCTION	F-G-S	589	F-M-G	7904
RENO	F-M-G	217	F-M-S	299

*2drms accuracy based on a time difference accuracy of 0.1µs (1σ)

NON-PRECISION APPROACH PROCEDURES

The non-precision approach procedures used for the test were patterned after those used for area navigation (RNAV) procedures described in FAA Advisory Circular 90-45A. These procedures call for the use of straight-in approach paths which are defined by waypoints which are aligned with the runway. Figure 2 depicts the Loran-C non-precision approach procedure that was established for Lake Tahoe Airport, Runway 18.

Typically, four waypoints, spaced 5 nm apart, were used to define the procedure. The initial approach waypoint is the beginning point for the procedure. This waypoint is normally a part of the enroute airway system. The next waypoint is the intermediate way-

Mountainous Terrain

It was important to evaluate Loran-C approaches in rugged terrain where at least one of the signals had to traverse mountainous terrain. It was also important that there be mountains in the vicinity of the airfield so that coverage and accuracy data could be obtained in areas where the VOR system could not support instrument approaches.

Area Navigation Procedures

Loran-C navigation is covered in the FAA regulatory process as an area navigation (RNAV) system. The document which covers RNAV operations in the U.S. is FAA Advisory Circular 90-45A, dated August 1978. The instrument approach procedures used in the tests were based on the guidelines and requirements described in this document.

Varying Loran-C Geometry

The accuracy of Loran-C navigation is dependent upon the geometry of the lines of positioning from the various transmitting stations. Therefore data from several combinations of stations at differing ranges from the aircraft were used to evaluate varying Loran-C geometry.

Loran-C Accuracy

The utility of Loran-C for non-precision approaches is closely tied to the accuracy of the system and the characteristics of the errors. Therefore it was necessary to measure and record several parameters from the Loran-C navigator to determine system accuracy and to isolate possible sources of error. Accuracy characteristics were then computed in terms of FAA RNAV standards.

Loran-C Operational Utility

Even when FAA accuracy standards are met, there are a number of operational requirements that must be satisfied to make Loran-C a useful navigation system for non-precision approaches. Among these concerns are system reliability, maintainability, compatibility with Air Traffic Control requirements, acceptable pilot workload, signal acquisition (reacquisition) time, etc. Some of these parameters are quantifiable and were measured during the test. Others are more qualitative in nature and for those, only pilot opinions and user acceptance of the Loran-C system can be used to determine the operational acceptability of Loran-C. Therefore, both qualitative and quantitative operational data were collected during the flight test.

Remote Area Approach Testing Procedure

In addition to the Loran-C tests that were performed, a preliminary assessment of the Remote Area Precision Positioning System (RAPPS) was performed for the FAA. This system uses distance measurements from the aircraft to multiple ground based transponders located at known positions of latitude and longitude to accurately determine the aircraft's position during the approach tests. The FAA must determine procedures which can be used to qualify approach procedures in remote areas where radar or other precision tracking instrumentation is not available. The RAPPS is under consideration as a means to solve this problem. The West Coast Loran-C tests were used to provide a preliminary evaluation and airborne acceptance test of RAPPS prior to more comprehensive testing at the FAA Technical Center in New Jersey. The experimental nature of these tests limited the amount of Loran-C data which could be used for conclusive accuracy results. These limitations are discussed in the data acquisition section of the paper.

LORAN-C COVERAGE

In the western U.S. Loran-C coverage is provided by the U.S. West Coast chain. The master station is located at Fallon in northwestern Nevada. The X secondary is located in central Washington near the town of George. The Y station is found in north central California at Middletown and the Z secondary is located in southwestern Nevada at Searchlight. The chain operates with a group repetition interval of 79300 microseconds.

The Fallon-Middletown-George triad (F-M-G) provides coverage to western Washington, Oregon and northern California. The Fallon-Middletown-Searchlight (F-M-S) triad provides coverage for southern California and the Fallon-George-Searchlight (F-G-S) triad provides coverage to the inland areas of Idaho, Montana, Colorado, Wyoming, Nevada, northern Arizona and states to the east where signal reception is available.

TEST LOCATIONS

Due to the limited scope of the tests and the experimental nature of the RAPPS equipment, only three sites were initially selected for approach testing. These sites were Lake Tahoe Airport, South Lake Tahoe, California, Runway 18; Kingsley Airport, Klamath Falls, Oregon, Runway 32; and Walker Field, Grand Junction, Colorado, Runway 16.

Subsequently, during the tests two additional test sites were established near Reno, Nevada; the operational base for the tests. A test approach procedure to Reno International Airport was established for Runway 16 and at Reno Stead Airport for Runway 26. Only limited tests were flown at these two sites. The Loran-C stations and the test sites are shown in Figure 1.

Two of the test site triad selections were outside of the normal Loran-C coverage area. The Klamath Falls site is nearly on the baseline extension from Searchlight causing poor geometrical relationships. This is confirmed by the very high 2-drms value for the F-M-S triad shown in Table 1. The Grand Junction location is in the poor geometry region of the F-M-G triad. Both of these locations have an expected 2-drms error that exceeds 1500 ft, the coverage limit defined by the U.S. Coast Guard.

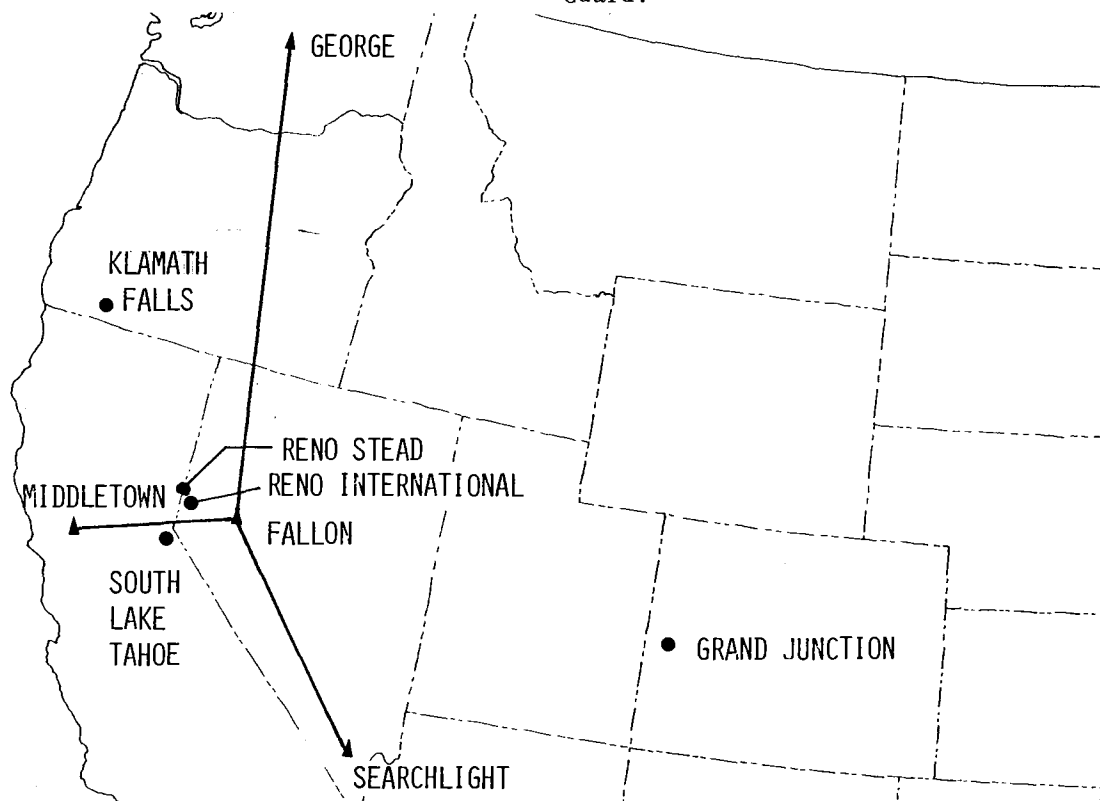


Figure 1. West Coast Loran-C Test Sites

Due to the limited number of test sites and the desire to collect information on both favorable and unfavorable fix geometry, two triads were selected for approach testing at each site. Table 1 shows the sites, triads utilized and expected 2-drms* accuracy for each site.

Table 1. Test Site Triads and Expected 2-drms Accuracy*

SITE	PRIMARY TRIAD	2 drms (feet)	SECONDARY TRIAD	2 drms (feet)
SOUTH LAKE TAHOE	F-M-S	205	F-M-G	335
KLAMATH FALLS	F-M-G	254	F-M-S	71981
GRAND JUNCTION	F-G-S	589	F-M-G	7904
RENO	F-M-G	217	F-M-S	299

*2drms accuracy based on a time difference accuracy of 0.1µs (1σ)

NON-PRECISION APPROACH PROCEDURES

The non-precision approach procedures used for the test were patterned after those used for area navigation (RNAV) procedures described in FAA Advisory Circular 90-45A. These procedures call for the use of straight-in approach paths which are defined by waypoints which are aligned with the runway. Figure 2 depicts the Loran-C non-precision approach procedure that was established for Lake Tahoe Airport, Runway 18.

Typically, four waypoints, spaced 5 nm apart, were used to define the procedure. The initial approach waypoint is the beginning point for the procedure. This waypoint is normally a part of the enroute airway system. The next waypoint is the intermediate way-

point. The segment between these waypoints is called the initial approach segment and provides a transition from the airway route to the approach path. In Figure 2 this path is aligned with the approach path. In actual applications, this path is aligned to provide an optimum transition from enroute to approach and its length is typically five to fifteen nm.

SOUTH LAKE TAHOE, CALIFORNIA
LAKE TAHOE-RNAV/LORAN-C RUNWAY 18

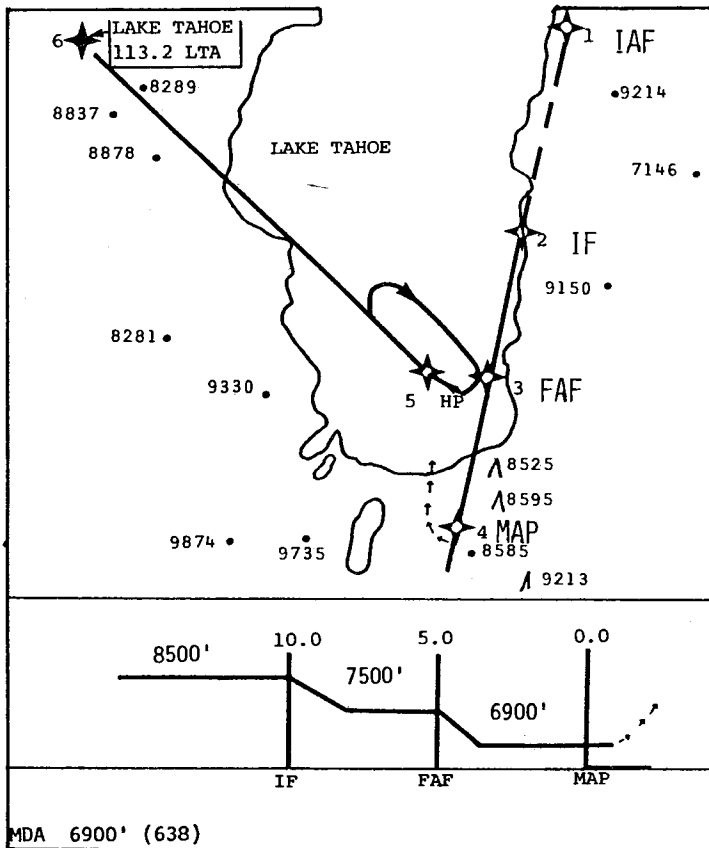


Figure 2. Loran-C Test Approach at South Lake Tahoe

The third waypoint in the approach is the final approach waypoint. The segment between the intermediate and final approach waypoints is called the intermediate segment and is used to align the aircraft with the final approach course. As shown in Figure 2, this segment is aligned with the final approach course whenever obstructions or operational considerations permit. This segment is usually 5 to 10 nm in length.

The fourth waypoint is called the missed approach waypoint. The segment from the final approach waypoint to the missed approach waypoint is called the final approach segment. This segment is typically 5 to 10 nm in length.

The waypoints also define the vertical path of the aircraft. Upon reaching a waypoint, the pilot can descend to the altitude specified for the next segment. These altitudes are shown on the vertical profile in Figure 2.

The approach terminates at the missed approach waypoint where the pilot either sees the runway and completes the landing or performs the missed approach procedure when the runway cannot be seen visually.

AIRBORNE EQUIPMENT

The flight test vehicle was a Piper Aztec, a twin engine, six place aircraft that is typical of those used at small airfields. The aircraft cruises at about 160 knots, and has a normal service ceiling of 18,000 feet.

The Loran-C receiver used in the test was a model TDL-711 Micro-Navigator manufactured by the Teledyne Systems Company and marketed by Offshore Navigation Inc. The Micro-Navigator comes in four physical units, the antenna with integral antenna coupler, the receiver/computer unit, the control/display unit (CDU) and the course deviation indicator (CDI). The antenna was a short vertical E-field antenna that was mounted on top of the aircraft above the copilots seat. The receiver/computer unit was mounted in the data acquisition system rack which was located in the cabin behind the pilot's and copilot's seat.

Due to space limitations on the instrument panel of the Aztec, the CDU was bolted to the front surface of the copilot's seat where it was accessible to only the copilot. The CDI, which provides the pilot with the primary left-right steering guidance, was mounted in the center of the instrument panel where it was visible to both pilots. The CDI also had a flag indicator which was pulled into view by the Micro-Navigator at times when the Loran-C unit was not providing satisfactory guidance information.

The CDU shown in Figure 3, is the operator's interface with the Loran-C system. The top third of the panel is devoted to display functions and the remainder contains control switches.

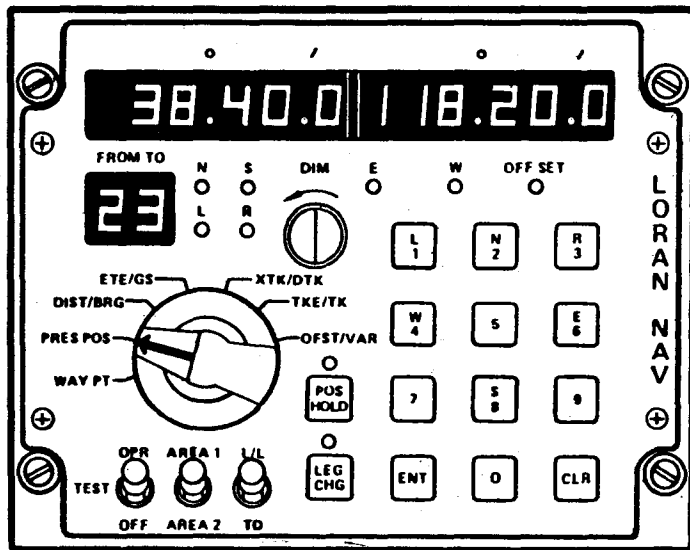


Figure 3 Micro-Navigator Control Display Unit

The information shown on the upper display is controlled by the large rotary data selector on the left side of the unit. Depending on the selector position, the following data is displayed:

- "WAYPT" : The selected waypoint position is displayed or the coordinates to be entered for the selected waypoint are shown.
- "PRES POS" : Displays present position or allows entry of present position for initialization.
- "DIST/BRG" : Displays distance to waypoint in the left window, and bearing to waypoint in the right window.
- "ETE/GS" : Shows time to go to the "TO" waypoint and present ground speed.
- "XTK/DTK" : Shows cross track distance on the left and desired track on the right.
- "TKE/TK" : Displays track angle error and track angle.
- "OFST/VAR" : Shows the current parallel offset distance (or allows selection of a new offset), and current magnetic variation (or entry of a new variation).

Data is entered into the processor through the twelve button keyboard on the right. Waypoints are selected by

depressing the "LEG CHG" (leg change) switch, selecting the "FROM" and "TO" waypoint, and depressing "ENT". No automatic leg change functions are provided. On the lower left are three toggle switches which perform on/off/test functions, triad selection, and determine whether waypoint coordinates are time difference or latitude-longitude. Latitude-longitude was used throughout these tests. One additional function, called "Area Calibration", is worthy of note. Predetermined latitude/longitude and time difference values for a calibrated point in the airport vicinity are entered into the processor through the keyboard. The processor then computes the difference between the time difference position and the latitude/longitude position

and applies this correction factor to all further position computations. This feature can, in theory, correct constant errors, or biases, in the vicinity of the calibration point.

When the processor detects a problem that affects guidance outputs, the decimal points on the upper display either blink or come on steady to alert the crew. The blinking display indicates that a selected station is not being received and that an alternate station has been selected and the system accuracy may be degraded. The solid lights occur during initialization, loss of station, and at other times when guidance is invalid.

During the tests the pilot used the CDI for primary, left/right steering guidance. The along track progress of the approach was achieved by setting the CDU mode selector in the DIST/BRG position which provides distance-to-waypoint information in the left display of the CDU. The copilot then provided distance callouts to the pilot at regular intervals during the approach.

DATA ACQUISITION SYSTEM.

An onboard microcomputer-based data acquisition system (DAS) was used throughout the approach tests. Loran-C data from the Micro-Navigator and RAPPS range data was processed and recorded by the DAS. The Loran-C parameters are shown in Table 2.

Data from RAPPS was used to track the aircraft and evaluate the accuracy of the Loran-C navigator. RAPPS operates at standard L-band DME frequencies and is compatible with standard TACAN and DME transponders. Range measurements

to these facilities and to carefully located portable beacons were made using a standard King KDM 7000 DME interrogator-receiver. This unit had a special indexing frequency selector which allowed the reception of ranges from up to six transponders. The system cycled through the selected frequencies pausing for one second on each to obtain its range data. The range was then passed to an Intel SBC-80 microcomputer for processing. One additional input from a NARCO AR-500 digital encoding altimeter was necessary to convert the DME slant range to ground range.

Table 2. Recorded Loran-C Parameters

REPLICA OF THE CDU DISPLAY INDICATIONS OF CDU SWITCH POSITIONS INDICATIONS OF CDU STATUS LIGHT INDICATORS LORAN DISTANCE TO WAYPOINT AND GROUND-SPEED LORAN TIME DIFFERENCES LATITUDE, LONGITUDE AND CROSS TRACK DEVIATION SIGNAL-TO-NOISE RATIO DATA AND STATIONS IN-TRACK STATION BLINK STATUS STATION ENVELOPE TRACK STATUS AND ENVELOPE NUMBERS PARALLEL OFFSET AND MAGNETIC VARIATION TRIAD IN TRACK

Real-time data presentation was available from a Tektronix 4051 graphics terminal. This unit provided real-time data entry and operator control. Position data was computed every six seconds in real-time from the RAPPS data and displayed on the terminal CRT. A CRT plot of the aircraft track was available during the flight.

The Micro-Navigator and the RAPPS data were formulated by the Intel SBC-80 and recorded on a Tandberg Model SCDR-3000 cartridge recorder, and a Tektronix Cartridge recorder. These data were used for detailed post flight data processing and analysis.

FLIGHT TEST SCHEDULE

A balanced schedule of flights was planned for each of the three primary test locations. One checkout flight and five data flights were planned using two triads at each location. This produced a total of 36 planned approaches.

Due to equipment problems at Grand Junction and failures to lock-on to valid latitude/longitude positions on the F-M-S triad at Klamath Falls, the

actual number of data flights at the three locations totaled only 21. These were supplemented by three approaches to Reno International Airport and two abbreviated approaches to Reno Stead Airport. Non-area calibration procedures were used on 21 approaches. Area calibration procedures were used on three approaches at South Lake Tahoe and two approaches at Grand Junction.

Two pilots were used during the tests. They shared the pilot/copilot role on an equal basis. This provided flight technical error data on two separate subjects which helped to broaden the data base and minimize individual pilot technique as a factor in the analysis.

DATA PROCESSING

A three step data processing procedure was developed for these tests. In the first step aircraft position was determined from the RAPPS data and was used as a standard by which the accuracy of the Micro-Navigator could be established. This step yielded system errors in both easting and northing components and along track/cross track components. In addition, data on flight technical error, which is the ability of the pilot to track the deviation signal, was processed in this step. The along track cross track error components are those used by the FAA to determine system accuracy compliance. The relationship between the error parameters are shown in Figures 4 and 5.

In the second step of data processing error budget data were derived. At this time, with the aid of the recorded parameters shown in Table 2, an assessment of where the errors were occurring in the Micro-Navigator was made. Among the areas investigated were:

- Coordinate Conversion
- Position to Track Conversion
- Propagation Modeling
- Spheroid Modeling

Analysis of these data were achieved by duplicating, in the data processing computer, the coordinate conversion and navigation processes performed by the Micro-Navigator.

The third data processing step was slanted toward possible error reduction through improved propagation modeling and reduced filtering of the navigation track parameters. These analyses were again performed by duplicating the functions performed by the Micro-Navigator but different propagation models and filter time constants were applied in the data processing computer.

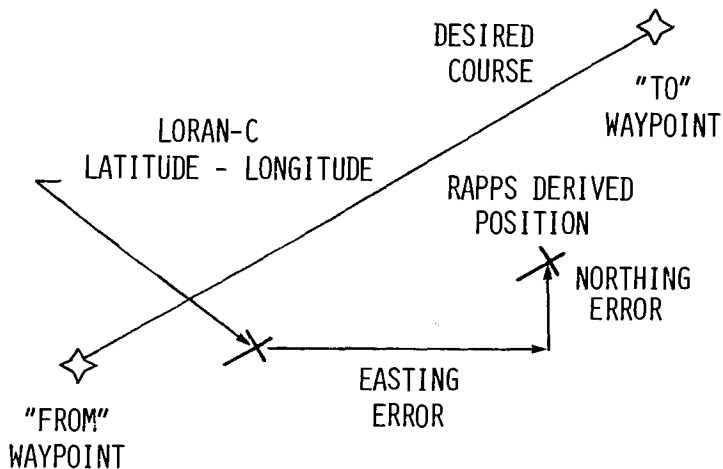


Figure 4. Position Error Parameters

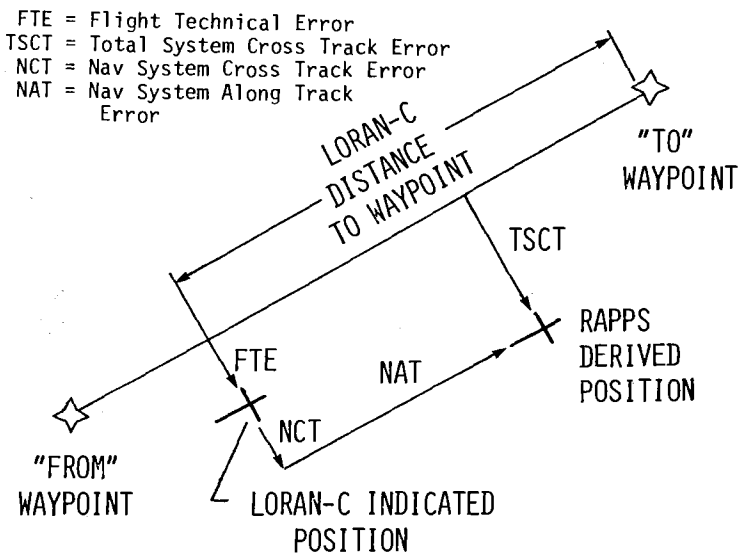


Figure 5. Track Error Parameters

Test Results-Reno International Airport

Reno International Airport was used for preliminary system checkout. A Loran-C approach procedure was developed for Runway 16 which is shown in Figure 6. On July 6, 1979, three approaches were flown using the F-M-S triad. During the initial phases of all three flights the Micro-Navigator showed invalid data flags in an area about 13 miles north of the airport. The only apparent source of possible interference in the area was a commercial broadcast station. At the runway threshold, the Micro-Navigator had positioned the aircraft within 500 feet of centerline, but indicated 1 mile to go to the threshold.

Data recordings were made during the

three approaches and the results are shown in Table 3. Of primary concern are large bias errors in the northing direction which also shows up as navigation along track error.

Test Results-South Lake Tahoe

Test flights were flown at South Lake Tahoe on July 7, 1979 and July 26, 1979 to Runway 18 (see Figure 2). On the 7th of July one flight each was made on the F-M-G triad and the F-M-S triad. Loran steering was stable and smooth throughout both approaches. On the F-M-S triad the Micro-Navigator had positioned the aircraft .12 mile right of the runway with 1 mile to go as the aircraft crossed the threshold. Using the F-M-G triad, the aircraft was slightly left of the runway with 0.0 miles to go as the aircraft crossed the threshold.

On the third flight on 7 July, the belt driving the right alternator broke and the power loss required shutting down the data recording system. The aircraft was sent to Reno Stead for repair.

On July 26th, the tests at South Lake Tahoe were resumed and completed. Ten approaches were flown in total. Five approaches were flown using the F-M-S triad. Loran guidance was good although at about 2.5 miles to threshold the Loran guidance veered slightly left and slowly corrected back to centerline at threshold.

Two approaches were flown using the F-M-G triad. Loran steering was generally good although at about 2.5 miles to threshold, the guidance again veered off centerline, this time to the right.

Three approaches were flown using the F-M-G triad in the area calibration mode. The calibration point was on the airport ramp at South Lake Tahoe. Loran guidance placed the aircraft close to the runway centerline, but the same tendency to veer right at the 2.5 miles to go point was still evident.

Results of the data processing for South Lake Tahoe are shown in Table 3. The TSCT data confirms the observations of left and right offsets for the F-M-S and F-M-G triads, respectively. The

Table 3. Position and Track Error Statistics With No Area Calibration

LOCATION/ TRIAD	NO. OF APPR'S.	PTS*	NORTHING		EASTING		PTS*	FTE		TSCT		NCT		NAT	
			\bar{X}	σ	\bar{X}	σ		\bar{X}	σ	\bar{X}	σ	\bar{X}	σ	\bar{X}	σ
RENO/FMS	3	56	.80	.16	-.11	.05	56	.11	.08	.01	.07	-.11	.05	.75	.16
STEAD/FMG	1	16	-.31	.11	.25	.13	16	.14	.35	.34	.19	.20	.22	.22	.13
STEAD/FMS	1	12	.86	.10	-.01	.18	12	.09	.14	-.76	.10	-.85	.10	-.18	.18
KLAMATH/FMG	6	249	-.02	.06	.15	.10	209	-.02	.16	.05	.15	.07	.12	.04	.06
TAHOE/FMS	6	225	.47	.12	-.15	.07	200	.09	.21	-.23	.20	-.33	.06	.39	.13
TAHOE/FMG	3	90	-.47	.12	.15	.12	86	.04	.14	.21	.12	.17	.08	-.48	.11
GRAND JUNCTION/FGS	1	41	-.36	.16	-.33	.28	36	.13	.15	-.07	.10	-.21	.20	.00	.08

*At some locations points for the track related parameters are fewer in number because data is unavailable during waypoint sequencing.

LEGEND: FTE = Flight Technical Error (pilot's track following error)
 TSCT = Total System Cross Track Error (FTE + NCT)
 NCT = Navigation System Cross Track Error
 NAT = Navigation System Along Track Error

RENO, NEVADA
 RENO INTERNATIONAL-RNAV/LORAN-C RUNWAY 18

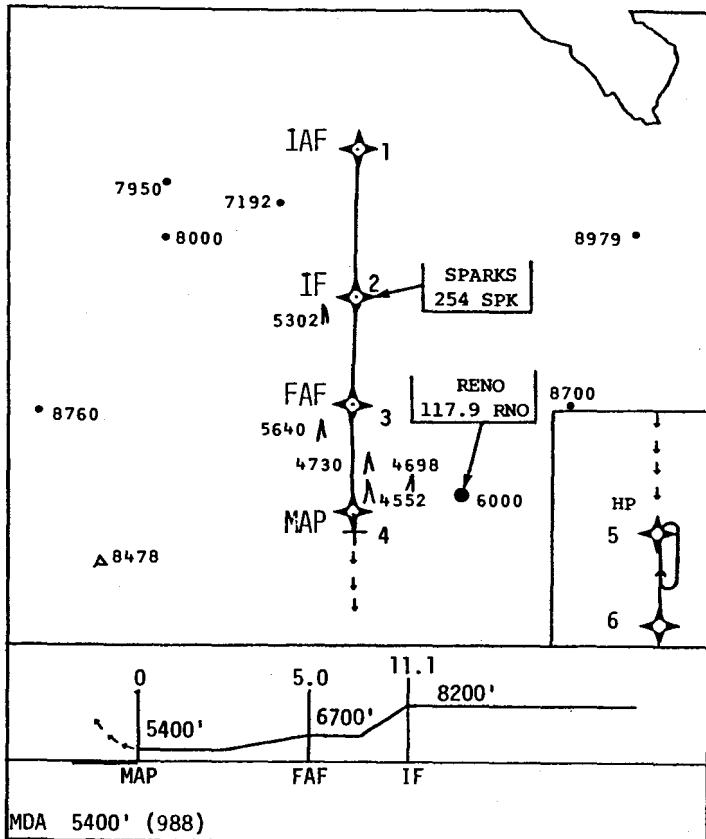


Figure 6. Loran-C Test Approach at Reno International

F-M-S data shows a mean TSCT error of -.23 nm (negative is left of track) while the F-M-G data shows a mean TSCT error of +.21 nm. Mean along track error for

both triads is comparable with 0.39 nm for F-M-S and 0.48 nm for F-M-G (a positive error means the aircraft is actually ahead of the indicated along track position).

Results of the data processing for the area calibrated flights are shown in Table 4. The calibration was definitely effective in removing the mean TSCT error to 0.03 nm. However, an along track error of -0.22 nm was observed. The calibration was effective in reducing a significant portion of the error, but some error still remained.

Test Results-Reno Stead Airport

After the aircraft alternator belt was repaired, two visual passes were made to Runway 26 at Reno Stead Airport. The F-M-S triad was used in the first pass. The aircraft was tracked 0.9 nm left of the centerline and indicated 0.1 nm to go at threshold. In the second pass the F-M-G triad was used and the Loran placed the aircraft 0.3 nm right of centerline with 0.1 nm to go on the distance display at threshold.

Data was recorded during these passes and the results of the data processing are shown in Table 3. These results

Table 4. Position and Track Error Statistics With Area Calibration

LOCATION/ TRIAD	NO. OF APPR'S.	PTS*	NORTHING		EASTING		PTS*	FTE		TSCT		NCT		NAT	
			\bar{X}	σ	\bar{X}	σ		\bar{X}	σ	\bar{X}	σ	\bar{X}	σ	\bar{X}	σ
TAHOE/FMG	3	143	-.19	.07	.00	.05	110	.08	.06	.03	.06	-.05	.04	-.22	.08
GRAND JUNCTION/FMG	2	58	.29	.10	-.54	.14	48	.09	.15	.25	.16	.16	.16	.60	.13

confirm the observations at threshold. A mean TSCT error of -0.76 nm was found using F-M-S and +.34 nm was measured using F-M-G. The measured along track errors are of the same magnitude but opposite in sign (-.18 nm for F-M-S versus +.22 nm for F-M-G).

It is of interest to compare the results of Reno International and Reno Stead which is about 7 miles north-northwest of Reno International. For the F-M-S triad the mean easting and northing errors are quite comparable, .80 vs .86 in northing error and -.11 vs -.01 in easting error. Since the runways are oriented nearly perpendicular to each other, the large northing error becomes cross track error at Stead and along track error at Reno International (+.75 nm) and TSCT at Stead (-.76 nm). These values are of equal magnitude and correspond in direction with the northing error value at both locations. This evidence is strongly supportive of a consistent bias error value in the Loran-C grid in the Reno area.

Test Results - Klamath Falls

On July 23rd, tests at Klamath Falls, Oregon; began with a ramp check of the Micro-Navigator position and a check-point whose coordinates were computed from USGS Quad Charts. Using the F-M-G triad, the primary triad for this area, the Micro-Navigator position agreed with the ramp location within 0.1 arc minute. The equipment would not lock onto the F-M-S triad so no position check could be obtained.

Two visual approaches were flown using Loran guidance. The equipment provided smooth guidance through the approaches. At threshold the Loran had placed the aircraft about 300' right of centerline with 0.1 nm to go showing on the distance display. An inflight acquisition of the F-M-S triad was unsuccessful.

On July 24th, six approaches, three by each pilot, were flown using the F-M-G triad. These flights were conducted in simulated IFR conditions with the pilot using an IFR training hood during the approach. The results were consistent with the visual flights of the day before. During one approach the Loran unit broke lock twice for about 30 seconds each time.

Results of the post flight data processing for Klamath Falls are shown in Table 3. The results are among the most accurate obtained during the test program. The northing and easting mean errors are small (-.02 nm and .15 nm, respectively). No accuracy data were available from the F-M-S triad as the receiver would not lock on to these stations. The reason for this problem became apparent in the error budget data analysis and is discussed in detail in that section.

Test Results - Grand Junction

On July 27, 1979, the aircraft was flown to Grand Junction, Colorado. En-route from Reno to Grand Junction, the Micro-Navigator was operated using the F-M-G triad. Initially, in the Reno area, the accuracy was good, but as the aircraft approached Grand Junction the accuracy deteriorated to about 10 nm at landing. This result was not totally unexpected as Grand Junction is near the Middletown-Fallon baseline extension.

The F-G-S/F-M-S PROM was placed in the Loran-C unit and a ramp check indicated errors of 0.5 minutes north and 0.7 minutes west with the F-G-S triad.

On July 28, 1979, flight tests were initiated. Using the F-M-G triad, an area calibration was attempted but the unit would not accept the calibration precisely as entered. A residual error of 0.2 minutes south and 0.7 minutes east was observed after calibration. In subsequent data processing, it was learned that this residual error probably occurred due to the resolution of the associated time difference correction of 0.1 μ s and the poor fix geometry.

A visual approach was flown using area calibration of the F-M-G triad. Guidance was good but not as steady as during previous tests. At the threshold the aircraft was 800 feet left of centerline with 0.5 nm to go.

The second approach was flown under simulated IFR conditions. Steering was similar to the visual approach. At threshold the unit broke lock.

Area calibration was deleted and the F-G-S triad was selected. A visual approach was flown and guidance was good.

At threshold the aircraft was 800 feet right of the runway centerline with 0.4 nm to go on the CDU display.

Shortly after beginning the next approach, the unit malfunctioned and no guidance was available. Shortly thereafter, the unit was deemed inoperable and the tests were terminated.

Initial data processing confirmed the errors observed in the static tests the day before. These results are summarized in Tables 3 and 4. Using the F-M-S triad, a mean northing error of -.36 nm and a easting error of -.33 nm was observed. These errors were not reflected in the track errors however. Data processing produced TSCT errors of -.07 nm and NAT errors of 0.00 nm. Analysis of this apparent incompatibility between position errors and track related errors was pursued further in the error budget analysis.

Accuracy Summary

The track oriented error statistics in Table 3 were aggregated and the results are summarized in Table 5. Also included in Table 5 are the accuracy requirements for non-VOR/DME RNAV systems as contained in FAA Advisory Circular 90-45A.

Table 5. Comparison of Test Results with AC 90-45A Criteria (nm)

	AC 90-45A Criteria (2σ)		Loran-C Test Results (2σ)	
	Cross Track	Along Track	Cross Track	Along Track
TSCT	0.60	-----	0.50	-----
FTE	0.50	-----	0.37	-----
NAV SYSTEM	0.30	0.30	0.49	0.71

LEGEND: TSCT = Total System Cross Track
FTE = Flight Technical Error

It is evident that the along track errors measured during the test exceed the stated requirements and cross track errors are close to the stated limit values. An extensive analysis was performed to isolate the sources of these errors and to determine if error reduction is possible.

ERROR BUDGET ANALYSIS

The error budget analysis was performed in a three step procedure. First, the recorded time difference values were converted to latitude/longitude values using an in-house coordinate conversion program. Several geoid and low frequency propagation models are available in the conversion program. Using the WGS earth model specified by the U.S. Coast Guard and a propagation model that contained only primary factor delays, the results

from the conversion model closely matched those recorded from the Micro-Navigator. The differences obtained were typically less than 100 feet.

It was determined that the lack of secondary factor terms was the reason that no lock-on could be obtained at Klamath Falls using the F-M-S triad. The time difference obtained by the Micro-Navigator exceeded that which was achievable using the propagation model in the unit. Therefore, the system continued to search for a position solution that would satisfy the time difference values being received. Since no such solution existed with that propagation model, the Micro-Navigator could not lock-on.

The second error budget analysis involved geographic to track orientation conversion. The track oriented errors and the easting/northing errors are related through the orientation of the flight path with respect to true north. This conversion was made in the post-flight analysis program and some significant deviations from those obtained in the Micro-Navigator were observed. Generally the differences between the Micro-Navigator results and the data acquisition program were small (less than 0.1 nm). However, in two instances the errors were much larger than expected. At Klamath Falls the cross track error was 0.19 nm and at Grand Junction the cross track error was 0.27 nm. The errors were correlated to some extent with large output filter time constants. However, the reasons for these relatively large coordinate conversion errors could not be fully explained.

The third step in the error budget processing consisted of resolving the easting/northing errors along the Loran-C lines of position and expressing the results as time difference errors. This step was performed as a preparatory step for the error reduction analysis. It was found in this analysis that there was a high correlation between the time difference errors and the distance difference between the corresponding stations. This analysis and the fact that apparently no secondary factor terms were used in the Micro-Navigator propagation model led to an attempt to reduce position errors through the use of improved propagation models.

ERROR REDUCTION ANALYSIS

The propagation model used in the Micro-Navigator did not use a secondary propagation factor. The result was a propagation velocity that was too high, especially at distances greater than several hundred miles from the transmitter. Several secondary propagation

factors corresponding to different surface conductivities were included in the data analysis program. These factors take the form:

$$SF = A/D + B + C \cdot D$$

where SF = secondary factor delay (μ s)
D = distance from transmitter (nm)

A,B,C are constants obtained from curve fits of data contained in Reference 1. These constants change with conductivity values.

Two equations are used, one for distances less than 50 nm and one for distances greater than 100 nm. Between 50 and 100 miles a blend of the two equations is used for continuity. Secondary factors for several conductivity values were evaluated. Based on large scale conductivity maps of the western U.S. and the amount of error reduction obtained, a conductivity value of 0.005 mho/meter appeared to provide a reasonable average value for the test area. The resultant time difference error reductions are shown in Table 6. The root-mean-square (RMS) value of the errors was calculated as a figure-of-merit. A 65% reduction in RMS error was achieved. Slight increases in the magnitude of error were observed at Lake Tahoe and Reno for the Middletown-Fallon TD. All other TD errors were reduced in magnitude.

Table 6. TD Error Reduction

	UNCORRECTED	.005 mho/m
STATION PAIR:	GEORGE-FALLON	
LAKE TAHOE	2.28 μ s	-1.39 μ s
STEAD	4.26	0.79
RENO	ND*	ND*
GRAND JUNCTION	1.94	0.24
KLAMATH FALLS	0.62	-0.24
STATION PAIR:	MIDDLETOWN-FALLON	
LAKE TAHOE	-0.44	-1.03
STEAD	2.54	1.64
RENO	0.24	-0.75
GRAND JUNCTION	2.29	0.87
KLAMATH FALLS	0.94	0.92
STATION PAIR:	SEARCHLIGHT-FALLON	
LAKE TAHOE	2.90	0.55
STEAD	3.12	0.37
RENO	3.11	0.38
GRAND JUNCTION	-1.37	-0.59
KLAMATH FALLS	3.35	0.27
RMS	2.41 μ s	0.85 μ s

*ND = No Data

A companion analysis was carried out by adjusting the propagation velocity to achieve a least mean square error. A propagation velocity of 299.232 meters/ μ s produced an RMS error of .83 μ s. This RMS value and the corresponding delay are very consistent with the results obtained using the conductivity value

of 0.005 mho/meter.

The assumption of a single conductivity value is simplistic and may not be applicable in many operational areas. Simple models are desirable from the computer mechanization standpoint. In these tests the simple model was effective in reducing the bias errors to a point where the accuracy standards of Advisory Circular 90-45A can be met. Tests in other areas are required to evaluate the propagation model problem.

OPERATIONAL RESULTS

Operational results are based on both quantitative data recorded during the tests and impressions or observations of the flight crew. These observations relate the experiences gained using the equipment to navigation operations that are typical of civil aviation.

While navigating with Loran-C, the crew came in direct contact with the CDU and the CDI. The operation of the CDU was logical and straightforward. The rotary data selector knob clearly described the parameters that were displayed or were to be entered into the navigator. The crew experienced neither difficulty in entering the waypoint data nor in sequencing from waypoint to waypoint along the flight path.

The Micro-Navigator uses programmable read-only memory (PROM) storage to define station locations and chain constants. Selection of chain constants is made through the AREA 1-AREA 2 toggle switch. This switch is inadequate for describing the useful coverage area of the triad in use. The CDU provided no annunciation of chain-in-use, stations-in-track, or triad-in-use. An inadvertent use of the wrong PROM through improper maintenance or an erroneous setting of the toggle switch could lead to confusion by the flight crew as to the actual triad-in-use. Annunciation of these parameters would provide the crew with positive identification of correct or incorrect stations.

The system provides no indication of deteriorating geometrical conditions caused by GDOP. Positive indication of poor geometry conditions should be incorporated in the functions of the navigator. The criteria should consider LOP crossing angles and operations near baseline extension areas where Loran-C position values are often inaccurate. Also, special Loran-C navigation charts would be helpful for identifying valid coverage areas.

The system provides only the display of blinking or steady decimal point

lights to indicate improper operation. These indications do not provide the pilot with any clues as to what corrective action should be taken. The pilot only knows that the navigation information is unreliable.

The Micro-Navigator uses time difference or latitude/longitude waypoints for route definition. These quantities can be easily entered incorrectly because they are a series of numbers. Procedures need to be developed to minimize the occurrence of these data entry errors. One effective method, if charted routes are used, is to step through the waypoints checking the displayed distance-bearing with values shown on the chart. Another means of cross checking is to use alternate navigation signals from VOR or NDB facilities to provide an independent position measurement. This method assures the crew that the aircraft is at the desired location indicated by the Loran-C prior to the commencement of the approach.

The pilots were favorably impressed with the steadiness of the CDI deflections. The oscillations that often accompany VOR and localizer deflections were not observed during the tests. The CDI sensitivity was +1.25 nm full scale with 0.25 nm gradation. The pilot's impressions of the deviation indications were borne out later in post-flight data reduction when small values of flight technical error were observed.

A large number of warning indications were observed during the test by the illumination of the decimal points on the CDU. No indications were available to the crew to identify the source of these warnings. Statistics on the break-lock and operational station outage time are presented in Table 7. An operational station outage is defined as the event when a station in the triad-in-use is not being received by the Micro-Navigator. During the tests, triad reliability was 99.8%. One 24 second operational station outage of the Searchlight station was observed at South Lake Tahoe. A second outage of the same duration was noted 10 minutes after the first. It occurred during an outbound leg and is not included in the approach statistics.

The reliability of the Micro-Navigator during the test was 94.5%. Post-flight analysis of the recorded data revealed some clues to the source of the break-lock problems. The data showed that problems were occurring at a point in the processing after time differences were being computed. Therefore, the problems were internal to the system processor and not in the Loran-C signals or the receiver portion of the processor.

Table 7. Break Lock Statistics

PARAMETER DESCRIPTION	VALUE
TOTAL APPROACH TIME	11922 seconds
OPERATIONAL STATION OUTAGE TIME	24 seconds
TRIAD RELIABILITY	99.8%
BREAK-LOCK TIME	650 seconds
NAVIGATOR RELIABILITY	94.5%
NUMBER OF FULL LENGTH APPROACHES	24
NUMBER OF BREAK-LOCKS	15
BREAK-LOCKS PER APPROACH	0.625
MEAN DURATION OF BREAK-LOCK	43 seconds
STANDARD DEVIATION OF BREAK-LOCK	24 seconds
LONGEST BREAK-LOCK	88 seconds
SHORTEST BREAK-LOCK	12 seconds

Since valid time differences were received throughout the tests, these break-locks should not be interpreted as Loran-C system problems but rather as problems with the specific mechanization of the unit that was tested.

CONCLUSIONS

The West Coast Loran-C chain provided stable, reliable signals which the airborne receiver could acquire and track at distances of up to 700 nm. Greater distances were not tested. The signals were available at all altitudes flown during the test.

The Micro-Navigator CDU was easy to operate and imposed no undue workload burdens on the crew. Improved annunciation of the chain-in-use and the triad-in-use would be useful in preventing erroneous triad selection. Warning indications of poor geometry areas should be incorporated in the navigator functions.

The CDI deflections produced by the Micro-Navigator were stable and very easy to interpret and use for course guidance. This stability produced flight technical error values that are considerably smaller than those observed for comparable VOR/DME RNAV tests.

The break-locks that occurred during the approaches were disconcerting to the flight crew. Software improvements in the navigation processor should correct many of these occurrences.

Propagation model errors caused the system performance to be outside the accuracy standards of Advisory Circular 90-45A. An improved propagation model

would have reduced the system errors to levels where the standards could have been met at the locations tested.

The system bias errors caused by the propagation model could produce erroneous guidance if an inappropriate triad was chosen. Procedures to verify the triad-in-use prior to starting the approach should be developed and utilized.

Area calibration procedures reduced the effects of the system bias errors at the two locations tested. The procedure does cause extra workload for the crew and data entry errors could produce erroneous guidance.

With modifications to the propagation model, the Loran-C system should be capable of supporting non-precision approaches in remote areas where other navigation aids are not available.

ACKNOWLEDGEMENTS

Much of the material for this paper was derived with the aid of associates at the Champlain Technology Industries Division of Systems Control, Inc. (Vt). Dr. Donald W. Richardson, President of the CTI Division, provided overall program management and participated as one of the subject pilots. Mr. Eric H. Bolz provided technical expertise in the areas of test planning, instrumentation coordination, data reduction system design and error analysis.

Mr. George H. Quinn and Mr. Frank W. Bassett of the Federal Aviation Administration, Systems Research and Development Service provided technical guidance for the program.

The views expressed in this paper are those of the authors and do not constitute an endorsement by the sponsoring agency.

REFERENCES

1. Jöhler, J.R., Kellar, W.J., and Walters, L.C., "Phase of the Low Radiofrequency Ground Wave", National Bureau of Standards Circular 573, U.S. Department of Commerce, Washington, D.C., June 26, 1956.

SESSION III
SIGNAL QUALITY ASSURANCE

A LORAN-C TRANSMITTER SIMULATOR

Kiyoshi Tamura, Kiyohiko Tatebayashi & Tadayuki Yamada
Laboratory, Japan Radio Co., Ltd.
1 - 1, Shimorenjaku 5-chome, Mitaka-shi, Tokyo, Japan

ABSTRACT

For total evaluation of Loran-C receivers, a testing equipment which can simulate actual receiving circumstances is necessary. We have developed a powerful tool for this purpose, the NJZ-89 Loran-C Transmitter Simulator.

The NJZ-89 Loran-C Transmitter Simulator generates groundwave and skywave signals of master and two slave stations. The groundwave signals cover the 0 to 99.99 msec GRI range in 10 usec steps and the 0 to 99.9999 msec time difference range in 0.1 usec steps. Time lags of the skywaves vary from 0 to 1999 usec. White noise that has a center frequency of 100 kHz and a 30 kHz bandwidth, cross-rate signals of other chains and interference signals on spot frequencies (10.2, 70, 85, 100, 112, 116, 128 kHz) can be superposed on the chain signals of interest. These signal levels are adjustable independently from 0 to 110 dB μ V in 1 dB μ V steps. In addition to the generation of these signals, special functions are available: the distortion over +19 usec of the groundwave pulse envelope and the uniform motion simulation of the receiving point at a velocity of 0 to 999 kt.

The NJZ-89 Loran-C Transmitter Simulator has played an important role in our Loran-C receiver development. It has also proved to be an effective tool for the training of the receiver operation and the examination of receiver sets in the factory.

INTRODUCTION

Of the radio navigation systems, the Loran system has earliest been put into practical use. The newest Loran-C system features a few transmitting stations covering a wide service area, and high position fix accuracy, allowing not only the individual uses on ships, aircraft and vehicles, but also the use as position fixing sensor in the marine and land traffic controls.

The Loran-C system determines a position based on the time differences of the radio signals transmitted from plural stations. Today, fully automatic Loran-C receivers capable of automatic signal recognition and acquisition, and automatic time difference measurement using a microcomputer are prevailing.

The Loran-C system has many indefinite factors such as the signal-to-noise ratio that is variable from 100/1 to 1/100 for each receiving position, the dynamic range of 1 : 10⁶, and mixture of skywaves that are homogeneous with the signals. The Loran-C receivers must adapt to these factors. However, it is impossible to check the receiver's functions under the combinations of these factors in the field. Therefore, a simulator which can simulate various Loran-C conditions in a way very close to the reality is required.

This paper describes the outline of the Loran-C system and the Loran-C simulator capable of simulating the sky conditions that the Loran-C receiver may encounter in reality.

LORAN-C SYSTEM^{1) 2) 3)}

Loran is the abbreviation of Long Range Navigation, one of the hyperbolic radio navigation systems. Two or more lines of position (LOPs) are obtained from the arrival time differences of the signals received from transmitting stations, and the position fix can be obtained from the intersections of LOPs, that are hyperbolas centered at the transmitting stations.

The Loran-C system consists of a chain of Loran-C signal transmitting stations; one master station (M-station) and slave stations (W, X, Y and Z stations). These stations transmit the same Loran-C signal in certain time differences.

The waveform of the Loran-C signal is a carrier frequency of 100kHz modulated with a pulse of about 250 μ S, as shown in Fig. 1. The master station transmits 9 pulses and each slave station transmits 8 pulses in certain group repetition intervals (GRI). Various chains can be distinguished by the differences of GRIs.

Fig. 2 shows the time relation of the Loran-C signals at a certain receiving point. At any receiving point within the Loran-C service area, the signal from the master station is first received and then the signals from the slave stations W, X, Y and Z are received in this order with predetermined coding delays with respect to the master signal.

In addition, the pulse signals of the master and slave stations are subject to the phase coding shown in Fig. 3. The phase codings for the master and slave stations are different in the first period (GRI A) and the second period (GRI B), but the phase coding for each slave station is the same within the same period.

The Loran-C receiver receives the Loran-C signals and measures the time differences between the first pulse from the M-station and the first pulse from the X-station (TDX in Fig. 2), or that from the Y-station (TDY in Fig. 2) in the order of micro-seconds and indicates the measured values. The user can obtain the position by means a Loran chart in which LOPs are drawn in certain time differences.

The service area of one Loran-C chain is within a radius of 1200 miles and the position fix accuracy is 50 to 360m. Fig. 4 illustrates the Loran-C chain for the Japanese Sea area.

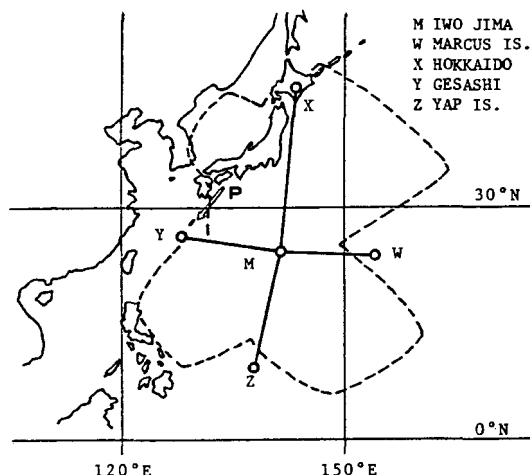


Figure 4. Northwest Pacific Chain (GRI 9970)

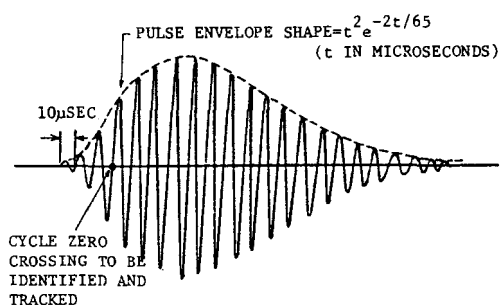


Figure 1. Loran-C Pulse

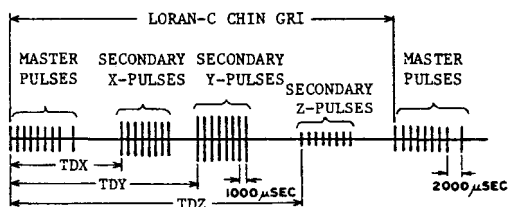


Figure 2. Example of Received Loran-C Signal

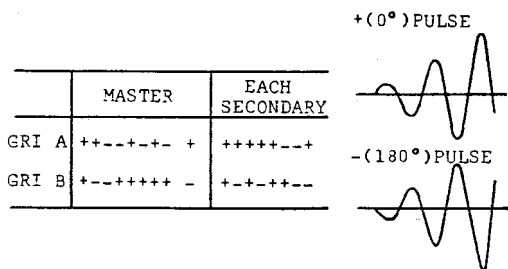


Figure 3. Loran-C Phase Codes

LORAN-C SIMULATOR

This simulator is designed to generate the Loran-C pulse signals and also various interference signals, and its block diagram is shown in Fig. 5.

Assuming a certain receiving point, GRI, time differences between the master and slave signals, and signal levels are keyed in from the keyboard. The input data are sent to the respective signal generators through the bus line. The display presents the data from the signal generators at any time.

The signal generators generate groundwaves and skywaves of the Loran-C pulses and other interference signals. These signals are combined by a combiner to generate an output signal. This simulator is designed to transfer data from or to the external through the I/O interface, allowing a mini-computer to control the signal generators. The configuration and operation of the main parts of each signal generator will be described below.

Loran-C Pulse Generation

There are two methods of generating the Loran-C pulse envelope; analog and digital methods.

The analog method simplifies the circuit configuration, being used for the generation of skywaves and cross-rate signal that require no envelope control.

The digital method permits accurate envelope control, being used for the generation of groundwaves.

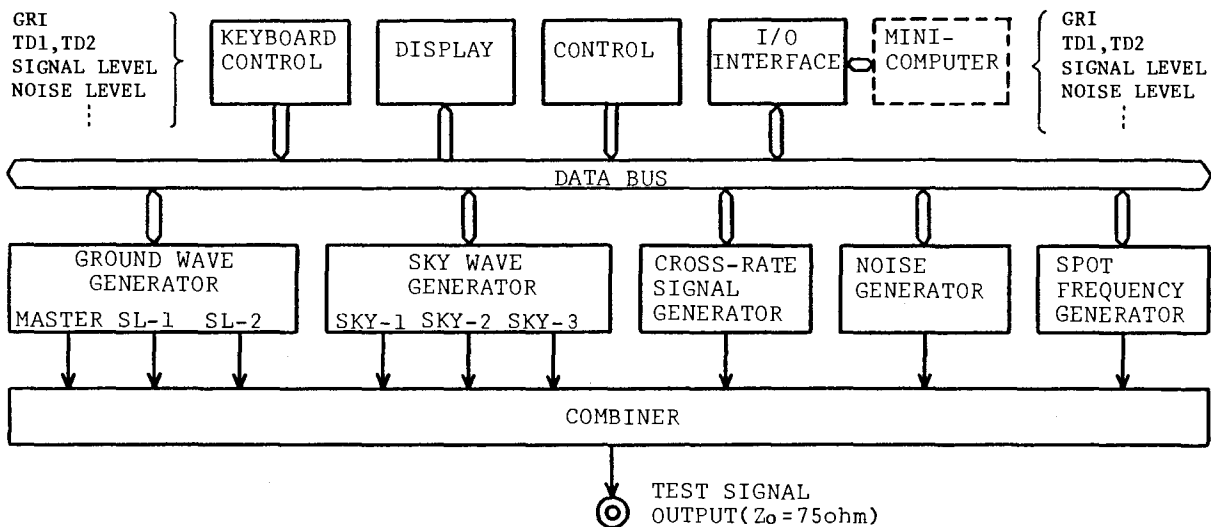


Figure 5. Block Diagram of the Loran-C Transmitter Simulator

Analog Method. When connecting first-order lag circuits (time constant T) in three-step tandem, the transfer function G(S) is given by

$$G(S) = \frac{1}{T^3} \left(\frac{1}{S + \frac{1}{T}} \right)^3 \quad (1)$$

When the impulse response is e_o ,

$$e_o(t) = \frac{t^2}{2T^3} e^{-\frac{t}{T}} \quad (2)$$

If $1/2T^3 = K$, and $T = 65/2$ in the above equation, it results in:

$$e_o(t) = Kt^2 e^{-2t/65} \quad (3)$$

The actual circuit configuration is shown in Fig. 6. The first order lag output of the impulse is obtained by switching the switch S and the envelope shown by the above equation is obtained by the two-step CR integrating circuit.

On the other hand, phase coding is performed by switching the polarity of the 100kHz carrier. As shown in Fig. 6, the 100kHz burst signal is obtained by closing the switch S2 in the + phase and by closing S3 in the - phase.

The burst signal and the envelope signal are balanced-modulated by a multiplier to produce a Loran-C pulse signal.

Digital Method. The pulse envelope generated at the actual transmitting station is within a certain margin based on the standard pulse form in Fig. 1, but the same envelope according to the

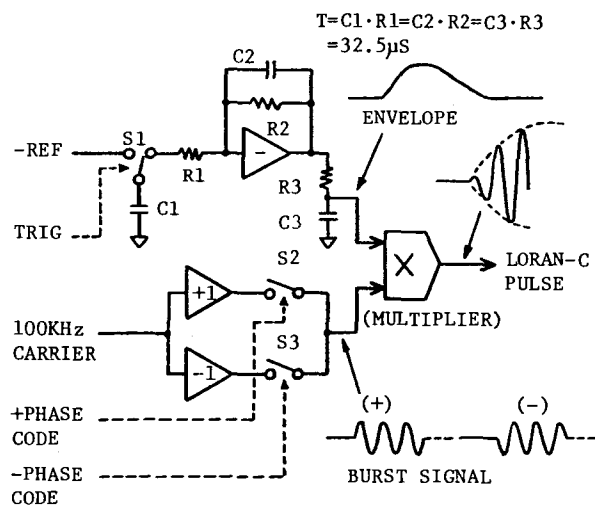


Figure 6. Loran-C Pulse Generator (Analog Type)

above equation is not necessarily received due to distortion in propagation to the receiving point.

In order to simulate this pulse envelope distortion, the digital method controls the rise characteristic of the envelope. The ROM stores the envelope data represented by the above equation, so that by changing the value of the read-out clock frequency f_R , the theoretical value or a value deviated from it can be obtained.

The envelope data in a range of 400 μ s from the start of the standard envelope are sampled in 1 μ s steps and the sample data are converted to 8-bit data that are stored in the ROM. The actual digital pulse generator is shown in Fig. 7.

The clock frequency f_R of the address counter for the ROM is:

$$f_R = \frac{30}{m} \text{ (MHz)}$$

When $m = 30$, $f_R = 1 \text{ MHz}$, and the standard envelope can be obtained. When changing the value of m , the point $30 \mu\text{s}$ after the start of the pulse is moved forwards and afterwards, as shown in Fig. 8, though the peak level is constant. This movement is herein called "envelope distortion". The value of m can be controlled within a range of 11 to 49 and the distortion is variable in $1 \mu\text{s}$ steps in a range of -19 to $+19 \mu\text{s}$. In Fig. 7 the low pass filter is used to smooth the step-wise output of the D/A converter.

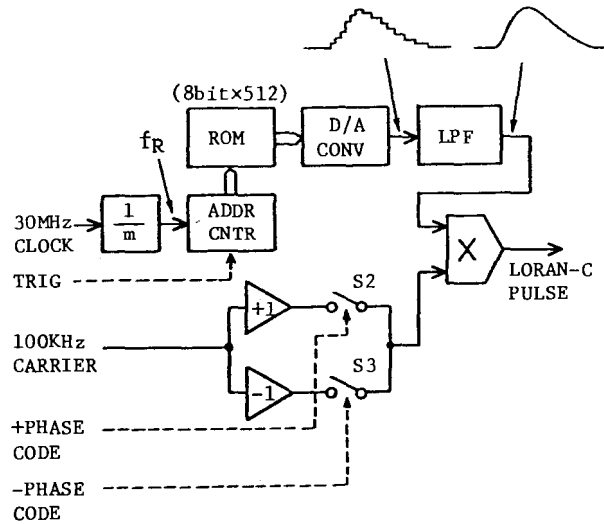
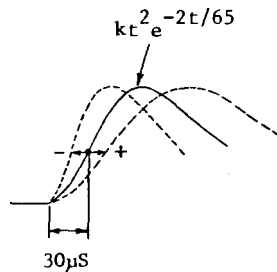


Figure 7. Loran-C Pulse Generator (Digital Type)

Groundwave Generation

The Loran-C waves consist of the groundwaves that propagate along the earth surface and the skywaves that are reflected on the ionosphere. The skywaves are unstable because they are dependent on the condition of the ionosphere. Thus, the groundwaves are used for normal position fixing. This simulator is also designed for the groundwaves as the signals from the master and slave stations (any pair of W, X, Y and Z.)



m	f_R (MHz)	ENVELOPE DIST (μs)
11	2.727	-19
20	1.5	-10
30	1.0	0
40	0.75	+10
49	0.612	+19

Figure 8. Envelope Distortion

Fig. 9 is a block diagram of the signal generators of the master station and the slave-1 and slave-2 stations. In this figure, logic gate 1 is a circuit to obtain the master phase code signal (Fig.3) at each GRI set by counting the standard clock of 10 MHz, and the carrier frequency of 100 kHz that is synchronized with that phase code signal. Logic gates 2 and 3 generate the phase code signals and the carrier frequencies for the slave stations with the time differences preset in reference to the GRI trigger set at logic gate 1.

These phase codes and 100 kHz carrier are fed into the digital Loran-C pulse generator to produce the master, slave-1 and slave-2 Loran-C pulse signals. These signals are adjusted in level by the programmable attenuators. Fig. 10 shows the master pulse waveforms generated by this simulator, and Fig. 11 shows the signal spectrum measured of the master signal.

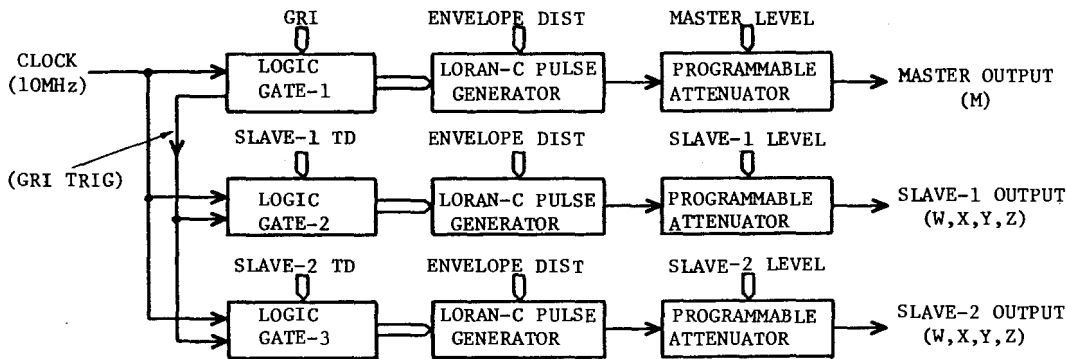
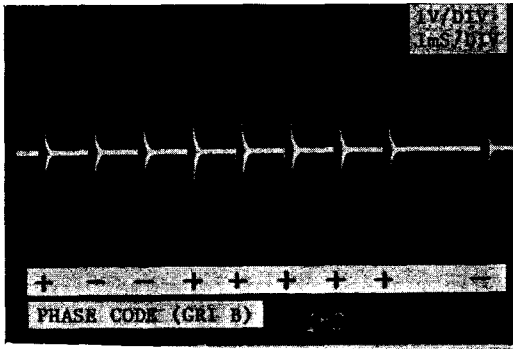


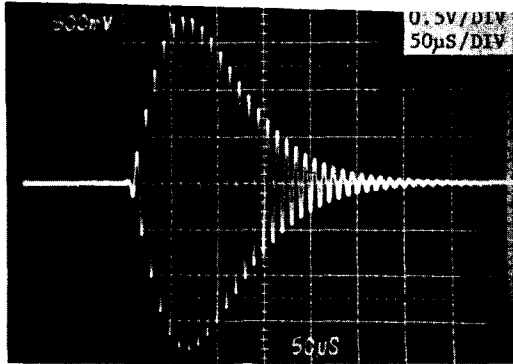
Figure 9. Loran-C Groundwave Generator



(a)

Skywave Generation

Since the skywave travels a longer distance than the groundwave, the skywave appears after the groundwave at the receiving point. The strength of skywave and its delay from the groundwave vary for each ionosphere condition, and the delay is within a range of approximately 35 to 1500 μ S. Two or more skywaves can be received in a complex mixed with the groundwaves. Thus, the signal pattern of the skywaves is the same of the groundwaves except that the skywaves arrive at the receiving point with a little delay after the groundwaves.



(b)

This simulator consists of three Loran-C pulse generators (analog-type) for skywave generation, each skywave being called skywave 1, skywave 2 and skywave 3, as shown in Fig. 12. Using the switches S1, S2 and S3, these skywaves are used as the master skywave, slave-1 skywave and slave-2 skywave. Fig.13 shows a signal waveform that is a complex of two skywaves mixed with a groundwave (master signal).

Figure 10. Master Pulse Waveforms

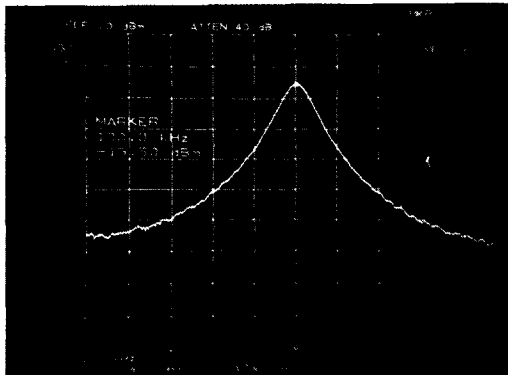


Figure 11. Spectrum of the Master Signal

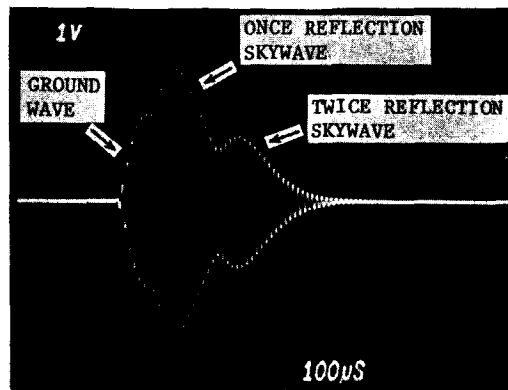


Figure 13. A Signal Waveform that is a Complex of Two Skywaves mixed with a Groundwave

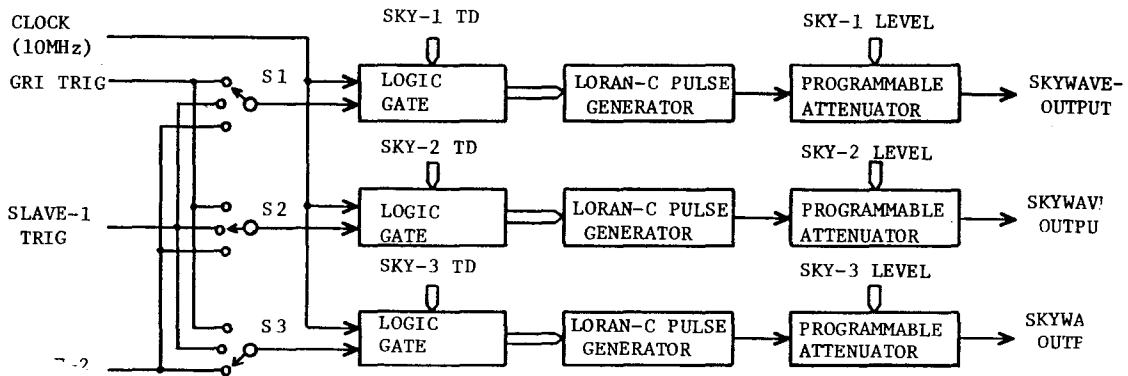


Figure 12. Loran-C Skywave Generator

Noise Generation

For evaluation of the Loran-C receiver on noise suppression, white noise is required. A white noise generator as shown in Fig. 14 allows generation of two noise in 30 kHz and 100 kHz bands and the simple S/N measurement.

Since the automatic Loran-C receivers are required normally operating at the S/N ratio of 0 dB or less, the test using those noise signals is an important requirement. The S/N ratio (SNR) of the Loran-C receivers is given by the following equation⁴⁾:

$$SNR = 20 \log_{10} \frac{E_s}{E_n},$$

where E_s is the signal level (equivalent to 50.6% of the peak) at 25 μ S from the building-up point of the Loran-C pulse and E_n is the effective value of the band-limited (30 kHz) noise. Fig. 15 shows noise spectrums generated by this simulator.

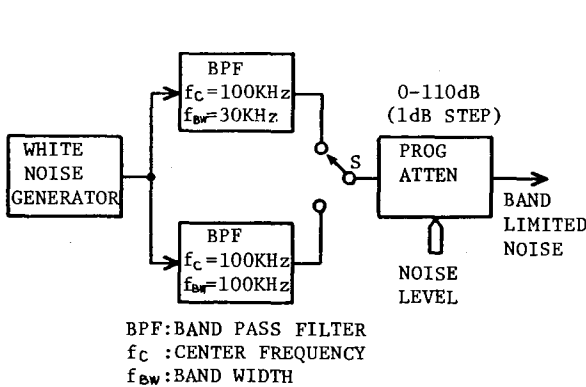


Figure 14. Band Limited Noise Generator

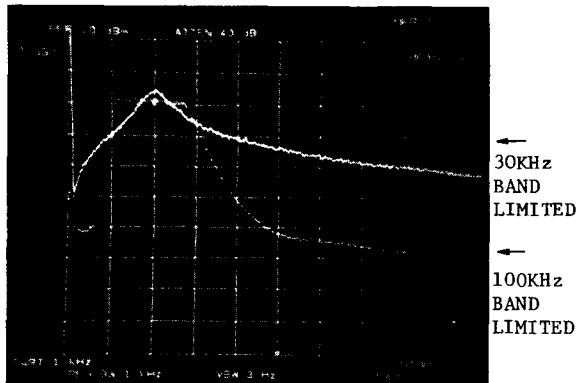


Figure 15. Spectrums of the Band Limited Noise

Generation of Other Interference Signals

Cross-Rate Signal. A signal from any other chain than the chain from which the signals are received is called "cross-rate signal". There is a sea area in which the cross-rate signal appears as interference signal. Therefore, this simulator is provided with a signal generator for generating other chains. The generator can control the GRIs, time differences and signal levels of slave-1 and slave-2.

Spot Frequency. There are other interference signals such as broadcasting radiowaves and Decca signals in the vicinity of the Loran-C frequency of 100 kHz. This simulator can also generate continuous waves of 10.2, 70, 85, 100, 112, 116 and 128 kHz individually or simultaneously, and control their signal levels. Fig. 16 shows the spectrum of the above signals simultaneously generated.

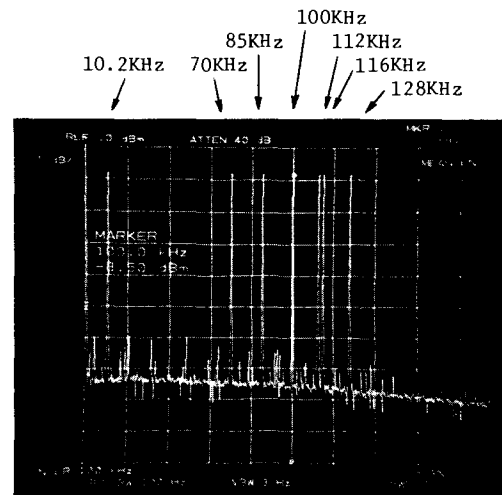


Figure 16. Spectrum of the Spot Frequency

Ship's Speed Control

The simulation of ship's speed control is available by automatically adjusting the time differences of slave-1 and slave-2. When the ship is traveling at 0 kt in the direction of the master station and at N kt in the direction of one slave station, the time difference varies according to the equation:

$$0.5144 \frac{N}{C} (\mu\text{S}/\text{sec})$$

where C is the velocity of light.

This simulator when setting the ship's relative speed N to each slave station, varies the time difference of slave-1 or slave-2 in Fig. 9 according to the above equation. The ship's speeds and TD variations are shown in Table 1.

The relative speed is presettable up to 999 kt, taking into account an application to aircraft.

Table 1. Ship's Speed and Time Difference Variations

Ship's speed (kt)	Time difference variation ($\mu\text{s}/10 \text{ sec}$)
10	0.17
20	0.34
30	0.51
35	0.60

SIMULATION

The simulation is performed by connecting the simulator to the Loran-C receiver as shown in Fig. 17. The following tests including normal operation of the receiver are made:

- (1) Basic operation test
- (2) S/N ratio
- (3) Dynamic range
- (4) Response and tracking characteristic
- (5) Receiver alarm functions and
- (6) Characteristics for each interference signals.

In addition, an actual ship's course can be preset to produce its circumstances, allowing the training for navigation by means of the Loran-C receiver.

An example of operation procedure for this simulator will be described below. The tracking characteristics will be tested, assuming that the ship is travelling from point P toward Station Y in Fig. 4.

The operation panel is shown in Fig. 18 and the key switch operations are illustrated in Fig. 19. Data input is made by function keys and data keys. The desired signal is available from the output BNC connector (75 ohms).

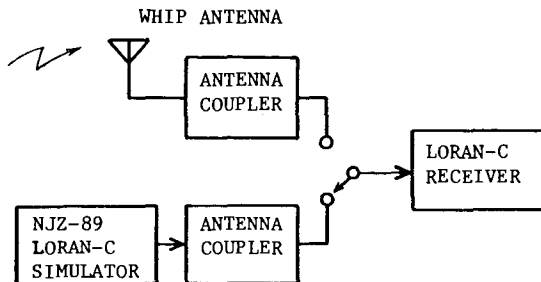


Figure 17. Simulation

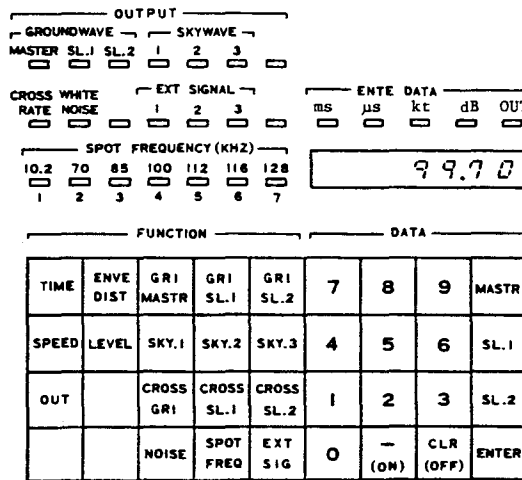


Figure 18. Operating Control Panel

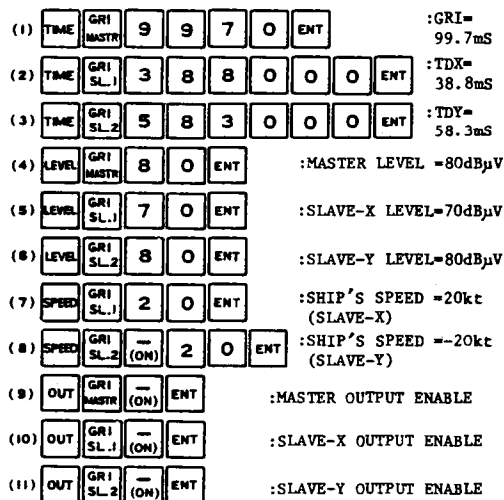


Figure 19. Key Switch Operations

CONCLUSION

The configuration, operation principle and an example of operation procedure of this Loran-C transmitter simulator have been described above. This simulator can simulate various Loran-C conditions in a simple way, which have been checked with actual Loran-C signals received from the actual transmitting stations. However, this simulator permits quantitative dynamic performance estimation on Loran-C receivers and applications to research and development of a new type of Loran-C receivers.

For Loran-C pulse generation, the analog and digital methods are available, ensuring the generation of the actual transmitting signals. However, some improvements will be necessary for 100 kHz carrier leak and others. Further, we must discuss the systems used for the actual transmitting stations in the future.

Finally, the appearance of this simulator is shown in Fig. 20 and its performance specifications are given in the Appendix. It is added that the output signals comply with RTCM⁴⁾.

REFERENCES

- 1) U.S. Coast Guard "Loran-C User Handbook", August 1974.
- 2) Kazuo Taguchi "The Newest Navigation Systems", Kaibun-do 1976.
- 3) Radio Beacon Committee of Japan "Radio Beacon" Vol. 1 1971.
- 4) RTCM Paper 255-77/SC 70-42.

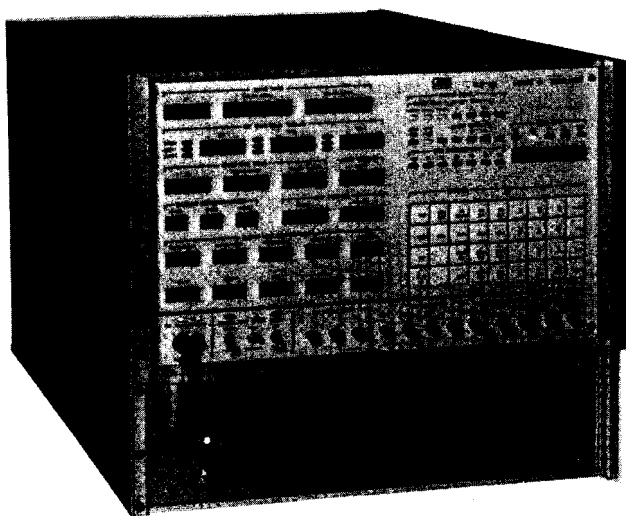


Figure 20. NJZ-89 Loran-C Simulator

APPENDIX

JRC MODEL NJZ-89 LORAN-C SIMULATOR

Features

- (1) This Loran-C Simulator has been designed and manufactured for the purpose of development and improvement of performance and characteristics of Loran-C receivers.
- (2) This Loran-C Simulator has advantageous functions for serving for training and familiarization of the operating procedures for Loran-C receivers that meet the basic Loran-C specifications under various receiving signal conditions.
- (3) The Loran-C Simulator is capable of producing various kinds of simulated Loran-C transmitting signals, allowing effective training for trainees such as ship crews.
- (4) All simulated Loran-C conditions are generated by switch operations from the keyboard on the front panel.
- (5) The Loran-C Simulator is designed to operate in two operation modes, manual and remote operations; the remote operation mode is available by programming all the functions used in the manual mode in a CPU or any other controller.

Specifications

- (1) Groundwave signal

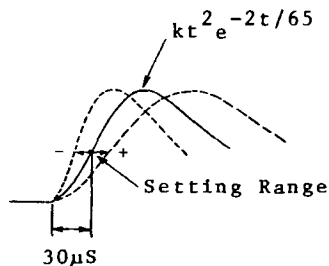
Carrier frequency: 100kHz pulse-coded
Signal output level: 0 - 110dB in 1dB steps;
Signal output consists of master, slave-1 and slave-2 signals whose levels are independently controlled.
(0dB = 1 μ Vrms)

GRI setting range: 0 - 99.99ms in 10 μ s steps
Time difference setting: 0 - 99.9999ms in 0.1 μ s steps for two slave stations.

- (2) Skywave signal

Number of signals: Three independent signals
Signal output level: 0 - 110dB in 5dB steps
Signal position: 0 - 1999 μ s time lag from the start of groundwave signal.

- (3) Simulated white noise
 Output level: 0 - 110dB in 1dB steps
 Bandwidth: 30kHz, 100kHz
 Center frequency: 100kHz
- (4) Simulated cross-rate signal
 Signal output level: 0 - 110dB in 5dB steps;
 Signal output consists of master, slave-1 and slave-2 signals whose levels are independently controlled.
 GRI setting range: 0 - 99.99ms in 10µs steps
 Time difference setting range: 0 - 99.99ms in 10µs steps for two slave stations.
- (5) Simulated interference signal
 Spot frequency: 10.2, 70, 85, 100, 112, 116, 128kHz
 Signal level: 0 - 110dB (for all spot frequencies); any spot frequency can be switched on/off independently.
- (6) Ship speed
 Speed range: 0 to +999kt in 1kt steps
- (7) Loran pulse envelope distortion (only for groundwave signal)
 Setting range: 0 ± 19µs
 Setting step: 1µs
- (8) Warming-up time
 Frequency stability: 5 x 10⁻⁹ for 20 minutes after power switch on
 5 x 10⁻¹⁰ 24 hours after power switch on
- (9) Display/control
 Control: Keyboard switch operation for function and data setting.
 Display: Digital readout (7-segment LED)
- (10) Output impedance (signal output)
 Signal output: 75 ohm
 Monitor signal: 1K ohm
- (11) External input signal (interference signal to be superimposed on the simulated output)
 Number of inputs: 3 channels
 Input impedance: 100K ohm
 Frequency range: 10 - 500kHz
 Input signal level: 0.84V_{pp} max. (110dB)
- (12) External clock signal input
 Frequency: 5MHz
- (13) Trigger signal output
 Signal timing: GRI x 1, GRI x 2
 Output impedance: 1K ohm
- (14) Control mode
 Modes: Manual and remote
- (15) Power requirements
 100/115/127/220V AC ± 20%,
 50/60Hz, single-phase,
 approx. 350VA
- (16) Dimensions and weight:
 Approx. 430(W) x 350(H)
 x 600mm(D); approx. 30kg



- (8) Warming-up time
 Frequency stability: 5 x 10⁻⁹ for 20 minutes after power switch on
 5 x 10⁻¹⁰ 24 hours after power switch on
- (9) Display/control
 Control: Keyboard switch operation for function and data setting.
 Display: Digital readout (7-segment LED)

OPERATION OF A REMOTE CONTROL SYSTEM AT LORSTA PORT HARDY, BC, CANADA

by

LCDR Ronald H. Frazier
U. S. Coast Guard Headquarters
Electronics Engineering Division
Washington, DC

LT George T. Gunther
U. S. Coast Guard
Electronics Engineering Center
Wildwood, NJ

LT Richard J. Sellers
U. S. Coast Guard
Electronics Engineering Center
Wildwood, NJ

I. ABSTRACT

A Remote Control System (RCS) for the Solid State Transmitter (SSX) has been developed and installed at LORSTA PORT HARDY, BC, CANADA. This system provides a watchstander at a remote location with the ability to control and monitor various parameters in an operational Loran-C transmitting station. The design, development, and integration of the RCS with existing station equipment are discussed along with a preliminary review of the operation of the system at PORT HARDY. The hardware design of this system allows for further expansion and improvements, and these will be discussed.

II. BACKGROUND

Many recent papers have discussed the new solid state equipment that has been developed and implemented at Loran-C transmitting stations by the U. S. Coast Guard. Solid state timing, control, and transmitting equipment coupled with semiautomatic (and in some cases automatic) chain control equipment have significantly reduced the personnel requirements at transmitting and control stations. Also, many of the monitor stations are now unmanned. In addition to having fewer personnel assigned to our stations, the need for watchstander intervention has been greatly reduced with the newest generation of equipment.

The authors, officers in the U. S. Coast Guard, were assigned to Coast Guard Headquarters, Washington, D. C., and the Electronics Engineering Center, Wildwood, NJ, during the work described. The opinions or assertions contained herein are the private ones of the writers and are not to be construed as official or reflecting the views of the Commandant or the Coast Guard at large.

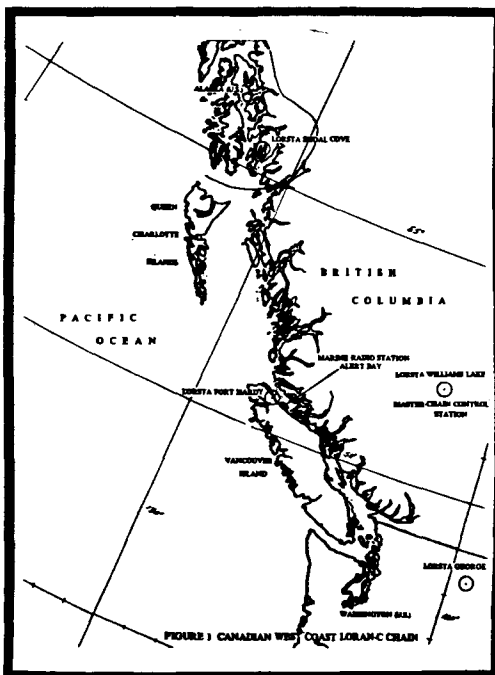
The process of removing personnel from the stations began with the Loran 70's Program and has slowly evolved over the last seven to ten years with additional improvements and personnel reductions. A large step was taken toward the "unmanning" process when the watchstander at a non-control type transmitting station was allowed to sleep during the night. Presently, the watchstander is available and on call in the event that he is needed for some immediate action. In some chains, only one watchstander is awake during the nighttime hours.

However, the need to further reduce operating and personnel costs continues to be a major problem with all government agencies. When the Canadian Coast Guard proposed (in 1979) to add a solid state transmitting station to the Canadian West Coast Loran-C Chain and man the station with only three persons, the need for a remote control set arose. The outstanding reliability and soft-failure features of the AN/FPN-64 Solid State Transmitter (SSX) assisted in the development of the RCS concept.

Our timeframe from the specification of the system to a required installation was approximately one year. This time constraint led to a requirement that all hardware be available from "off-the-shelf" sources where possible. A project to design, develop and install the first system at Port Hardy was assigned to the U.S. Coast Guard Electronics Engineering Center in November, 1978. The station installation at PORT HARDY was to begin in January, 1980, and our deadline for completion of the system was December, 1979. Due to delays in the completion of the station building, the RCS installation was postponed for several months. Our plans called for a field test at a similar type Loran-C station in the event that the RCS was

ready before it was to be installed. This field test was conducted from mid January, 1980 until mid February, 1980 at a single rated SSX-equipped secondary station; i.e. LORSTA RAYMONDVILLE, Texas. The results of this field test were invaluable as they identified several potential problems that were corrected prior to the installation of the equipment at LORSTA PORT HARDY.

The Canadian West Coast Loran-C Chain is shown in figure 1. Two new stations were added to the existing chain during the summer of 1980; the Loran-C Transmitting Station PORT HARDY and the Marine Radio Station ALERT BAY. The ALERT BAY station serves as the remote control station for LORSTA PORT HARDY.



III. DESIGN GOALS

The primary design goal for the Remote Control System was to provide the necessary controls to allow the operator to recover from equipment casualties by switching to independent redundant equipment using a computer with a video display. A station technician living near the transmitting station is on call on a twenty-four hour basis, and he visits the station within one hour after a call for assistance. A watchstander at the remote control station (Alert Bay) has the ability to keep the Loran-C signal on the air and in tolerance in the event of most casualties until the technician can respond. The remote control watchstander also has the ability to monitor the essential station

signal parameters. This feature assists the watchstander in making decisions when casualty recovery is necessary as well as in keeping records on the transmitting station's performance. In order to make the system easier to use with a normal watchstander, the system operation has to be simple and easy to use. It must verify operator entries, and inform the operator when an incorrect entry has been made. In order to meet the required deadlines and provide adequate support with minimum Coast Guard maintenance for the RCS, it was necessary to require that all equipment be available from commercial sources. The ability to expand the system hardware to meet future needs and the ability to accommodate future software improvements was required. A final design goal was to build in the capability for self testing the RCS and assisting a technician in troubleshooting the equipment.

IV. HARDWARE

The system consists of a Coast Guard designed station interface, commercial process control and monitoring equipment, data communications equipment and data processing equipment. Figure 2 shows an overall block diagram of the RCS along with some of the station equipment that is monitored/controlled by RCS.

State-of-the-art process control equipment that could be controlled by desktop computers and mini/microcomputers was investigated. After a careful examination of the design requirements, Hewlett Packard desktop computer equipment was chosen as the major control element used in RCS. Other equipment in the system was chosen to be compatible with existing transmitting station equipment. In the present RCS system, only one new custom printed circuit board was needed and this is the only module that must be supported by the Coast Guard depot repair facilities. All of the remaining equipment can be supported through commercial maintenance contracts.

All RCS equipment is capable of expansion. The data collection interface, an HP6940 Multiprogrammer, is a bussed card cage that can accommodate 15 printed circuit cards, each having an independent function. (Fifteen additional chassis with fifteen printed circuit cards each may be added for future expansion.) The present system uses one chassis and nine printed circuit cards. The desktop computers used, a HP9825S and HP9845B, can also have their memories expanded by twice their present size if future

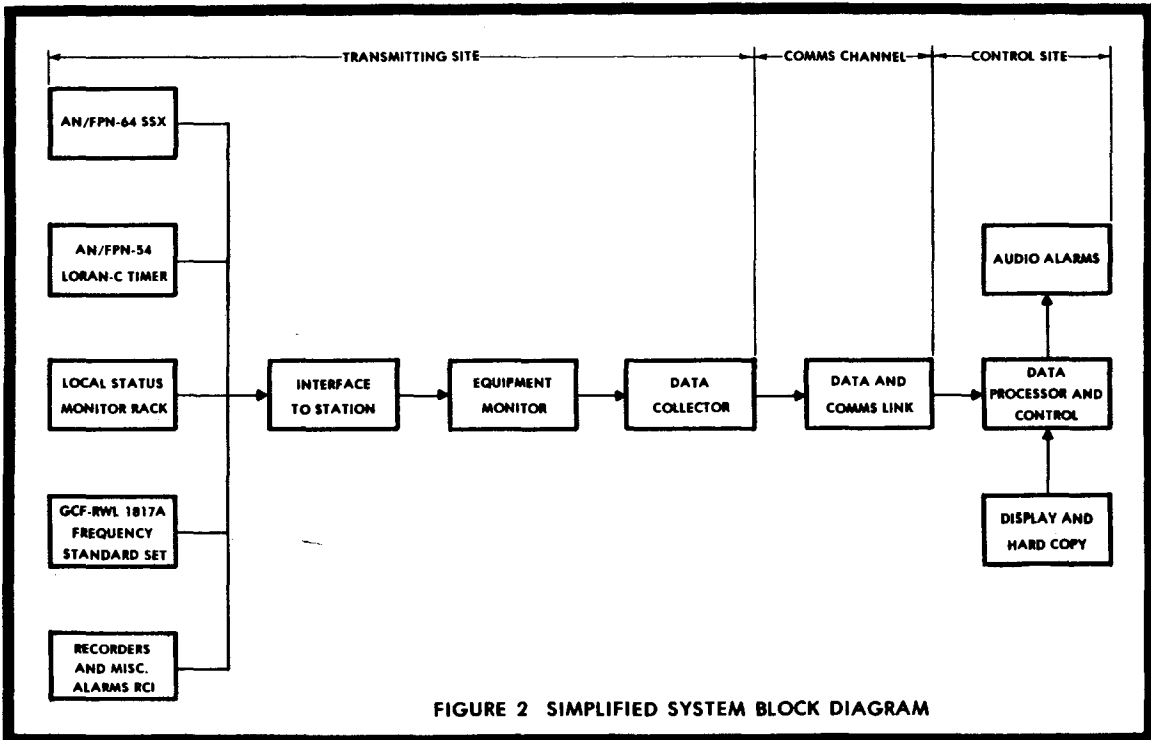


FIGURE 2 SIMPLIFIED SYSTEM BLOCK DIAGRAM

program improvements require it. The RCS hardware allows for a great deal of versatility and expandability. Diagrams of the system equipment are shown in figure 3a for the transmitting site and 3b for the control site.

V. SYSTEM DESIGN

Casualty control is defined as keeping the transmitted signal on air and in tolerance in the event of an equipment casualty. A watchstander

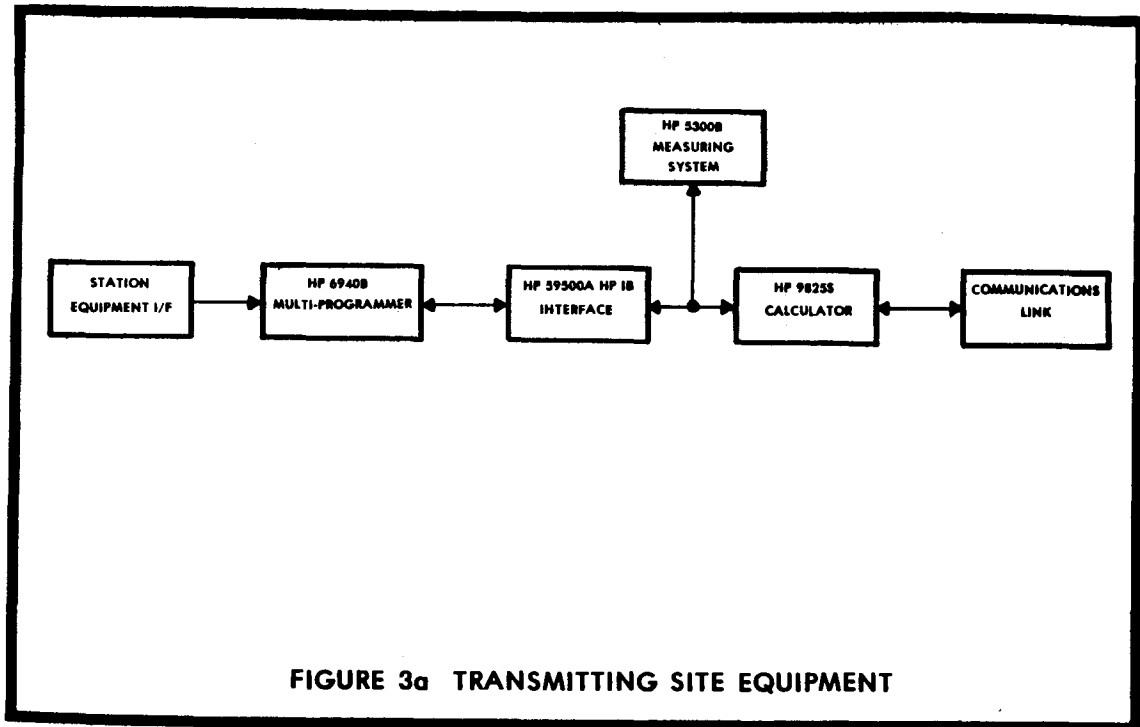
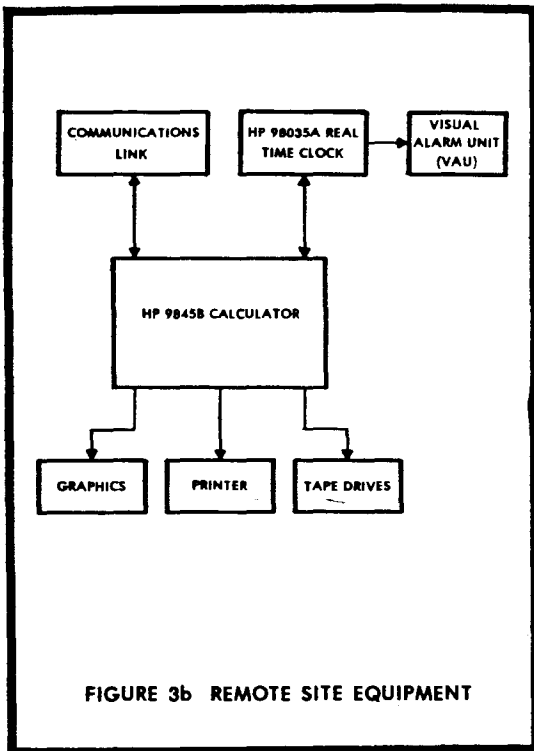


FIGURE 3a TRANSMITTING SITE EQUIPMENT



must be able to monitor all of the time of transmission indicators, pulse shape parameters, equipment status and environmental conditions and to be able to make decisions to maintain transmitting station operations.

On conventional transmitting stations, the on-site maintenance watchstander must be able to provide the capabilities summarized in Table 1.

!	WATCHSTANDER RESPONSIBILITIES	!
!	1. Switch timers	!
!	2. Switch Pulse Amplitude and Timing Controllers (PATCOs)	!
!	3. Insert Timing Adjustments	!
!	4. Initiate and stop blink	!
!	5. Turn off the transmitter in an emergency	!
!	6. Make standby and number three oscillator phase corrections	!
!	Table 1. Conventional Loran-C Station Watchstander Capabilities.	!

With the RCS system, the remote watchstander can do all of the casualty procedures listed except for the insertion of timing adjustments. In all Loran-C chains a watchstander at the Loran-C Chain Control Station has the

ability to make timing adjustments to all transmitting stations within the chain. This process is accomplished by sending a coded string of characters via the ADMIN/CONTROL teleprinter loop that connects all stations within the chain. The ability to make timing adjustments was not provided in the initial RCS as a teleprinter for the chain ADMIN/CONTROL loop was provided at the remote station in addition to the RCS equipment. This teleprinter allows the remote watchstander to insert small timing adjustments and to monitor the commands from the chain control station.

The inherent features of the computers make the system easy to use. The use of single keystroke was desirable for command entry while letting the operating system decide the propriety of the command. This was achieved by using the special function keys on the Hewlett Packard computers. To prevent the watchstander from becoming confused during an alarm condition, a clear, concise display showing necessary data and all alarms was needed. The CRT, thermal printer and graphics display of the HP9845B computer at the control site, are used to present data in two forms, graphical and numerical (some of this data is also saved on magnetic tape for retrieval at a later time if desired by the watchstander). Alarms and commands are displayed on the CRT and recorded on paper. If the watchstander is away from the console, a separate three-color audio/visual alarm unit is also provided to give him warning of an abnormality.

Implementation of the design goals required that an interface to the solid state transmitting station be developed that paralleled all existing alarm signals and timing waveforms. This would allow the RCS to be eliminated or bypassed without affecting the capability for normal unwatched station operations. In addition, unmanning the building requires that environmental alarms, not normally monitored by the timing and control equipment, be interfaced to the RCS system. The necessary control functions were achieved in the equipment by replacing mechanical switches with relay activated switches, thus allowing a relay closure to effect an equipment switch. However, all relay activated switches still allow for manual operations. Figure 4 is a functional block diagram of the RCS monitor and control functions.

The data monitored by the RCS is both analog and digital. Through the use of an A/D converter, switching logic and digital input cards, all the

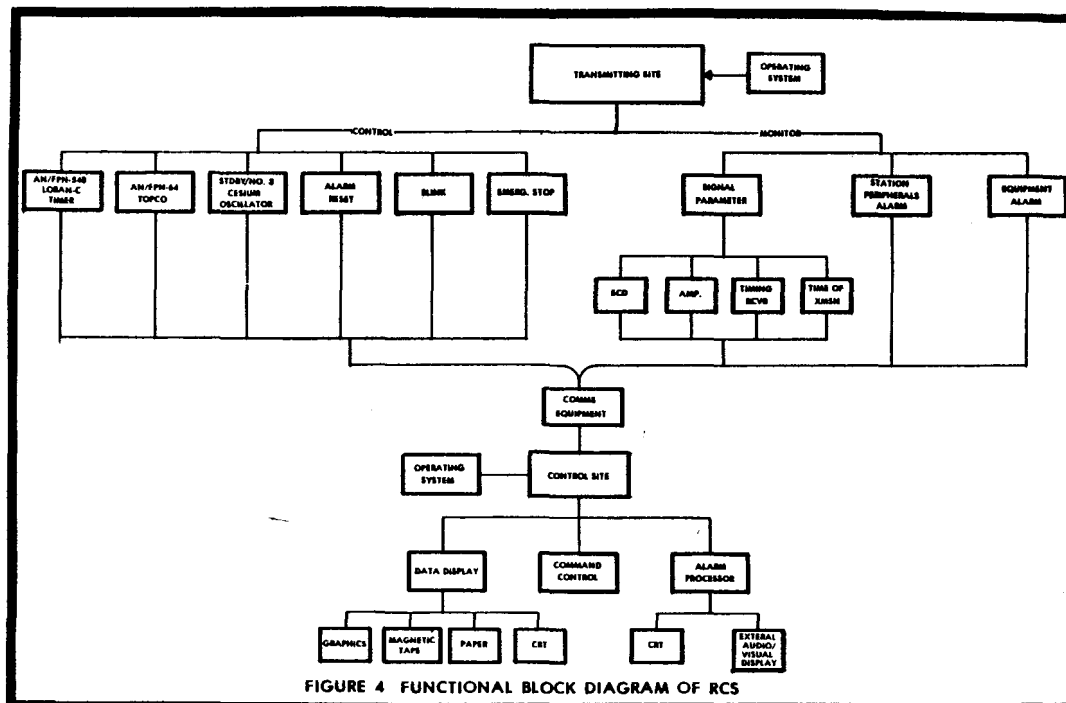


FIGURE 4 FUNCTIONAL BLOCK DIAGRAM OF RCS

data can be read by the transmitting site calculator (HP9825S). Alarms, being unpredictable, are captured by transition sensitive "event sense" cards that generate interrupts in the RCS operating system. Once data and/or alarms are processed by the transmitting site equipment, they are coded into a prescribed format and transmitted to the control site. At the control site, the information is decoded, displayed and saved by the control calculator (HP9845B). The system data interval is controllable by the watchstander (from 45 seconds to 10 minutes) and can be selected to meet operational requirements, i.e., a slower data rate for normal operations and a faster one for a casualty condition.

The RCS uses an asynchronous full-duplex ASCII communications protocol which operates at 110 baud. The purpose of RCS was to monitor transmitting station operations and not be tied up in communications. In order to minimize the amount of time spent communicating (maximizing time spent monitoring alarms), a two part scheme was implemented using code letters and control characters to indicate different types of data and alarms. Error detection is provided by a checksum and transmissions received in error are automatically retransmitted. If several errors occur in a row, a secondary routine is available, and this scheme corrects some errors via majority vote in an attempt to compensate for the poor communications channel.

In both cases, data is sent in blocks delimited by control characters. If the checksum method is being used, the block is followed by the checksum. If error correction is being used, the information block is repeated three times in a larger block and the correct transmission is derived from the majority of the three blocks (if possible).

The system has a plain talk communications routine that can be accessed from either computer. This routine allows for plain text transmissions between the two stations in the event that other means of communication are not available.

Self-test capability and some redundancy are built in to the RCS to insure its reliability. The transmitting site computer periodically checks all data and alarm input cards to ensure they are giving proper indications. At the control site, a time limit for receipt of data is set to ensure that communications are not lost. If either abnormality is encountered, an alarm is generated to alert the watchstander. A secondary check for the operator of the control site is a "watch dog timer" that will, unilaterally, alarm if the control calculator does not communicate with it within the maximum data interval. A Loran-C receiver and oscilloscope are also available to the watchstander for redundant confirmation of control commands and some signal parameters.

SYSTEM CAPABILITIES	
1.	Switch Loran-C Timer Sets.
2.	Stop the Solid State Transmitter (SSX) in case of emergency.
3.	Switch Pulse Amplitude and Timing Controllers (PATCOs) in SSX.
4.	Start and stop blink.
5.	Monitor all Status Alarm Unit (SAU) alarms.
6.	Monitor analog and digital station parameters.
7.	Monitor environmental alarms.
8.	Reset the Remote Control Interface (RCI) and SAU.
9.	Reset SSX Half-Cycle Generators (HCGs).
10.	Communicate in plain talk between stations

Table 2. Remote Control System capabilities.

VII. INSTALLATION

The RCS is now installed at Loran-C transmitting station PORT HARDY B.C., located at the northern end of Vancouver Island, British Columbia, Canada. The station is approximately 30 Km from Port McNeill, B.C., where the station personnel live. The control site is located at Canadian Coast Guard Marine Radio Station ALERT BAY, B.C. Alert Bay is an island located approximately 8 Km southeast of Port McNeill and is only accessible by ferry or air. The Marine Radio Station maintains a 24 hour radio watch and is suited to the additional responsibility of Loran-C watchstanding.

HARDY in photo 1. After field changes are installed in the timer, SSX transmitter and other transmitting station equipment, the installation and check-out of the RCS takes approximately four man days. The equipment at the remote control station, ALERT BAY, has been temporarily installed near the radio operator's console as shown in photo 2. The radio station will relocate to a new building in the near future, and all of the RCS equipment will be situated near the operator's console for easy access. Given that the communications link is installed and working properly, the control site equipment takes one man one day to install and test.

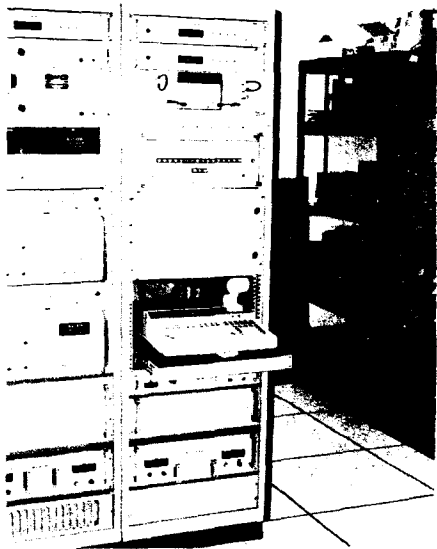


Photo 1. RCS Equipment Rack at LORSTA PORT HARDY, BC, CANADA

The transmitting station's RCS equipment is housed in a 19" rack, and shown as installed at LORSTA PORT



Photo 2. Control Room at Marine Radio Station, Alert Bay, BC, CANADA

Chain control communications for the station come via landline and microwave data circuits from Vancouver, B.C., to Alert Bay. From Alert Bay, the ADMIN/CONTROL circuit, RCS communications and voice telephone are sent via a frequency division multiplexed UHF channel to the Port Hardy station. Local communications at Alert Bay and Port Hardy use 60 ma., 130VDC, neutral current loop.

Installation and certification of the station were completed in August, 1980, and the remotely controlled Loran Station PORT HARDY (5990 Z) has been operational since 20 November 1980.

VII. FUTURE PLANS

Although the Remote Control System at LORSTA PORT HARDY is used with an operational Loran-C station, it will also be evaluated for future improvements to reduce the manning at other stations. Other plans may include adaptation of the system for older Coast Guard Loran-C transmitters. This would involve minor modifications to the station interface in the RCS. A final step in the remote control process would be to centralize the control of an entire chain with several remote control systems. This step can be realized by providing additional program memory to the existing HP9845B desktop computer.

SESSION IV
LAND VEHICLE APPLICATIONS

HYBRID LORAN-C FOR AUTOMATIC VEHICLE LOCATION FOR PRESENTATION AT WGA CONVENTION
BOSTON, 10/24/80

Dr. John Hovorka
Professor of Physics, Chmn., Science Division, Curry College, Milton, MA.
Lecturer, M.I.T., Cambridge, MA.

INTRODUCTION

Using LORAN-C to locate a land vehicle, as compared with locating a boat or a ship gives rise to a model for the operating region which differs from a mariner's view in the following way. For local vehicle location (e.g., police cars, ambulances), the operating region appears as a spatial field of usable signals perforated with some limited regions of totally unusable signals. Thus LORAN-C "holes" in the operating area are observed.

Let's take a look at some representative cases. In Fig. 1, as map of Cambridge and Boston shows both the starting-point of TSC's LORAN-C-equipped van and the most congested, high-rise, downtown business district of Boston. We traversed this region with LORAN-C recorded on an Epsco marine plotter, set for about 30 second averaging, moving at about 20 miles an hour except in heavy traffic. The recorder trace (Fig. 2), superimposed on the map, shows a clear departure from reality as we enter the downtown area, but presently recovers as we approach the Charles River to re-enter Cambridge.

But not every time. On another run (Fig. 3) LORAN-C carries us out into the harbor waters while the van is parked in Congress Street. Recovery is not achieved before returning to Cambridge. By contrast, in Cambridge and in Boston near the river, repeatability is very good indeed, a half-block or less (Fig. 4).

In a suburb like Newton, Massachusetts (map, Fig. 5) a superimposed trace is (except for a couple of glitches) immediately useful (Fig. 6).

LORAN-C by itself provides, roughly, 90-meter repeatable accuracy on land, adequate for many non-metropolitan applications. In metropolitan areas, two difficulties arise, and the accuracy is degraded: (1) shadowing of the radiation from one or more transmitters is caused by tall buildings and other obstructions, and (2) electromagnetic interfering street noise creates pockets where reception is poor. In addition, accuracy requirements rise in metropolitan areas because of the higher density of location identification points, such as street corners, and 15-meter repeatable accuracy is desirable.

To augment the LORAN-C system in coping with the metropolitan conditions, some form of dead-reckoning can be used. The two immediately most promising instrument sensors for dead-reckoning are vehicle odometers and accelerometers.

ODOMETERS

A dead-reckoning device currently being investigated as an augmentor for LORAN-C is the differential odometer. A ring of magnets is fastened to the brake drum of each front wheel of the vehicle, and Hall-effect pickoffs furnish a pulse-coded signal indicating wheel revolutions and distance along track for each wheel. There are two outputs: the difference in wheel revolutions is a measure of change in heading, and the sum of the wheel revolutions, divided by 2, is a measure of average distance along track. The advantage of odometer-indicated position over LORAN-C is that the odometer reading is always available, even when LORAN-C reception is poor. The disadvantages of odometers are that they need initialization for heading reference and start of track (this can be obtained from LORAN-C TD's), and that odometers drift, in a pattern that varies with tire wear, road crown, and other factors. However, LORAN-C can be regarded as a drift monitor; with suitable computational arrangements (described by Bowles, Hildebrand and Markey's paper later in this session) LORAN-C can, in conjunction with a differential odometer, have 15-meter repeatable accuracy as a reasonable design goal.

4.4.1.2 ACCELEROMETERS

Accelerometers for land-use in connection with LORAN-C have not yet been developed, but appear to this author to be the most promising form of augmentation. Two linear accelerometers are mounted in the vehicle near the LORAN-C electronics, with their input axes so oriented as to provide position data. These data may be either position in rectangular coordinates in the nominally horizontal plane, or indicated heading and distance along track, as described for the differential odometer. The advantage of an accelerometer package over odometers is that accelerometers, being mounted within the vehicle, can be serviced and maintained in a manner similar to other electronic maintenance. Odometers, since they are necessarily located on the wheels, need special care to avoid injury during tire changes, are likely to be hit by debris from the tires, are subject to severe shock as unsprung weight, and require long wiring runs on and within the vehicle. Speed and distance derived from accelerometers by integration will exhibit drift, in general; how this will compare with odometer drift is yet to be

determined. However, it is evident that accelerometers and LORAN-C are complementary modes of position indication with the possibility of greatly improved reliability, maintainability, and lower cost, as compared with odometers. The dynamic computation that controls the time-sharing of LORAN-C and accelerometers for optimum position-indication would probably be similar to that already being tested for sharing position indication between LORAN-C and odometers.

AUGMENTATION COMPUTER

The computer that controls the time-sharing between LORAN-C time differences and dead-reckoning sensor outputs is the crucial element in a high-accuracy metropolitan-based LORAN-C position-indicator.

The LORAN-C dead-reckoner combination is regarded, for computer-algorithm design purposes, as a single hybrid system. The hybrid system is dominated neither by LORAN-C nor by the dead-reckoner. LORAN-C is regarded as jittery, with time-correlated proximate time-difference errors, and unavailable as useful information for periods of a few seconds to several minutes. Dead-reckoners are regarded as constantly in state of drift with a variable level of accuracy. LORAN-C and dead-reckoner errors are uncorrelated. This fact justifies their being used to supplement each other as information sources.

The interfacing between the LORAN-C signal and the dead-reckoner must be worked out so that there is an automatic selection of the appropriate navigation data source. The LORAN-C hiatuses can be expected to require dead-reckoning for periods of several minutes, considerably longer than marine-receiver float-mode intervals. This optimal on-going data analysis and minimum-indicated position-error data computation is usually assigned to a real-time averaging-up-date computer, a special case of a Kalman filter.

In the metropolitan land use of LORAN-C, this computation is at the heart of the system in one sense, since ultimately, after receiver noise rejection has been optimized, the mode in which the remaining poor signal areas are to be traversed will be determined by the design of the dead-reckoning signal processor.

The work supporting this paper was performed while the author was a Faculty Fellow here at the Transportation Systems Center.

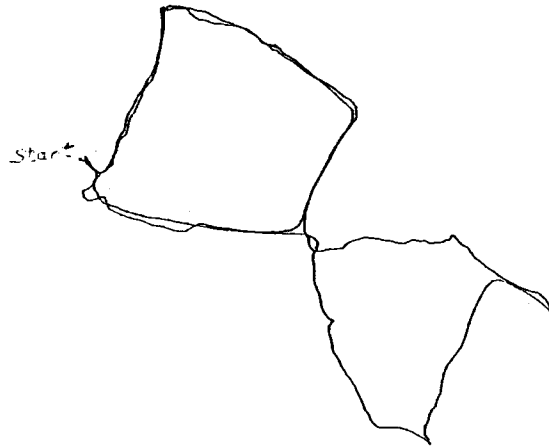
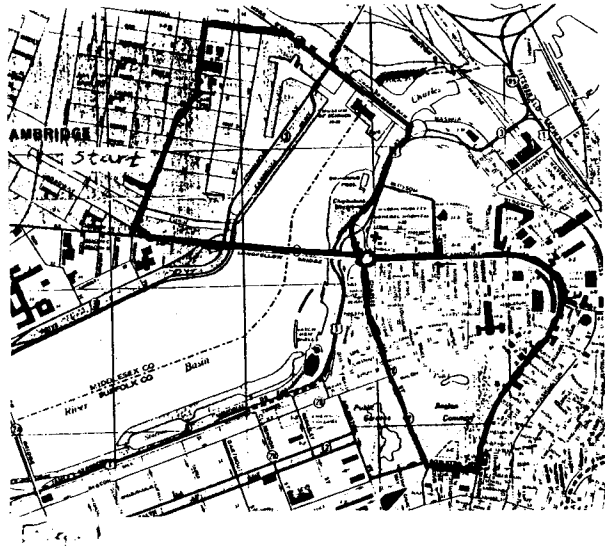


Fig. 2

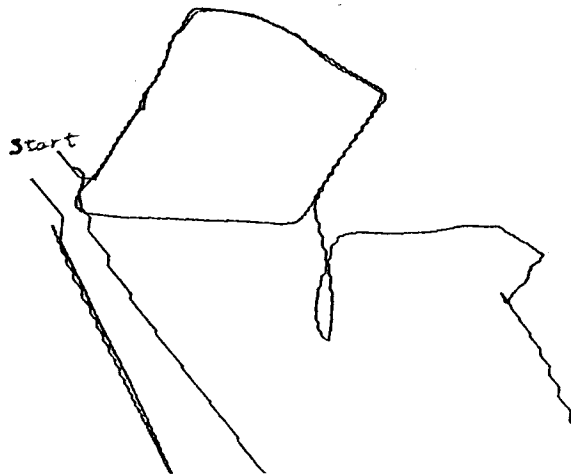


Fig. 3

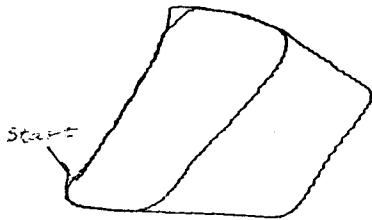


Fig. 4

CAR 54 -- WHERE ARE YOU?

Bahar J. Uttam and William F. O'Halloran

JAYCOR
300 Unicorn Park Drive
Woburn, Massachusetts

Abstract

Loran-C is a federally-operated radio-navigation system which has been used primarily as a marine and airborne navigation system for the coastal confluence region. The availability of Loran-C signals has led to considerable interest in Loran-C utilization by federal, state and local agencies. One of the applications is Automatic Vehicle Monitoring (AVM) which is being considered for use in law enforcement, fire prevention and emergency medical services (EMS). In this paper, a number of different available and proposed AVM system concepts are discussed, including use of Loran-C. Tradeoff factors for choosing a particular AVM system approach are presented. A hypothetical example is chosen involving AVM for a rural ambulance service, where Loran-C is an ideal candidate solution.

Introduction

Recently, there has been considerable interest in automatic vehicle monitoring (AVM) by law enforcement, emergency medical services (EMS) and fire prevention agencies (Ref. 1). The principal benefits which can be derived from knowledge of vehicle locations for these operations include reduced response time (with a corresponding reduction in loss of lives and property, and improvement in apprehension rate), increased safety, reduced radio channel congestion, and improved coordination between police, fire and EMS. Use of AVM also may lead to a better management of resources and possible savings in fuel. Recent trends towards the installation of multi-channel UHF communication systems, which can handle digitally encoded data transmissions, are particularly suited to supporting AVM system requirements. For large fleets of vehicles, AVM would be a useful adjunct to a computer-aided dispatch (CAD) system.

In order to be suitable for a wide variety of AVM applications, a candidate vehicle location system should be assessed in terms of the following:

- Sufficient accuracy to unambiguously assign the correct vehicle to each call.

- Minimum cost of procuring, installing and maintaining the system over its life-time.
- Adequate coverage over the user area, which should be easily expandable with future growth needs.
- Unlimited vehicle capacity within the capabilities of the communication system.
- Adequate update rates to keep location data current.
- Facilitate expansion to multi-user environments.

Basic Types of AVM Systems

A number of vehicle location systems have been proposed or are currently in use. A brief description of the major system concepts is presented below.

- Dead Reckoning - Dead reckoning AVM systems are based on determining the vehicle's distance and direction traveled from a known initial starting point. Direction and distance sensors such as a compass and odometer are used to measure the direction and distance traveled. The system is self-contained, allowing each vehicle in a fleet to determine its position independently. A disadvantage of a dead reckoning AVM system is that errors accumulate with time and provisions for resetting distance/direction are required.
- Proximity Location System - The proximity system is based on low-power "signposts" at known locations distributed over a user area. The signpost radiates coded messages to vehicles in the vicinity of the signpost. The message is then retransmitted to a base station location and the location of the vehicle with respect to the signpost can be determined. Inverse proximity is also possible where the vehicles transmit an ID code to the signpost. The number of signposts needed to provide coverage is proportional to the square of the spacing, which is determined by the accuracy requirements. As an example, the Washington, D.C. metropolitan area requires 5000 signposts (Ref.1). A disadvantage of this system is the number of signposts required, which could be expensive to install and maintain. Furthermore, this system is impractical for providing large area coverage.

- Multilateration Systems - Multilateration systems use three or more fixed receiver sites in a service area. The receiver at each site measures the times of arrival of synchronized signals from a polled vehicle. The times of arrival of the vehicle signals and those from a fixed site transmitter are transmitted to a base station for processing and determination of vehicle location. Vehicles can be polled individually or in groups. The disadvantages of this system are limited coverage area and the need for fixed-site transmitters and receivers.
- Loran-C Systems - Loran-C is a pulsed, hyperbolic, radionavigation system, operating in the 90-110 kHz frequency band, which has been selected as the U.S. Government - provided radionavigation system in the coastal confluence region. Loran-C coverage exists for the Northeast U.S., Southeast U.S., Great Lakes, and West Coast U.S. Most of inland United States has coverage, with the exception of the mid continent region. Since the signals are already available, no fixed-site equipment would be necessary to use Loran-C for AVM. The availability of Loran-C signals has led to considerable interest in Loran-C utilization by many federal, state and local agencies for a number of different AVM applications (Refs. 2 and 3).

AVM System Tradeoffs

The major issues involved in AVM system tradeoffs are

- Accuracy
 - localization repeatability
 - need for reset
 - gaps in coverage area
- Equipment Requirements (fixed site and vehicle)
 - cost
 - reliability/maintainability
 - vandalism
 - required coverage area
- Flexibility
 - growth potential
 - extension to multi-user environments

Based on the issues involved in the system tradeoffs, it is felt that Loran-C best meets the desired attributes of an AVM system for many applications. Loran-C has the following characteristics:

- Meets AVM system accuracy requirements
 - 50 to 150 feet repeatable accuracy
- Wide area coverage facilitates multi-user common-grid operation
 - provides common reference system for both terrestrial and airborne vehicles
- Vehicle capacity
 - limited only by vehicle-to-base communications systems
- Continuous update capability
- Cost effective system
 - eliminates large expenditures for off-vehicle equipment
 - small increment on large 'sunk costs'
 - low-cost commercial receivers available
- Operationally proven

In the near future, it is likely that the number of applications for AVM systems will increase, including those where Loran-C offers the best solution.

Sample Application of a Loran-C Based AVM System

To make more specific some of the above comments and descriptions of AVM systems, a possible sample application is now discussed. The example chosen is that of using Loran-C to provide AVM and accident location capability for an ambulance service operating in a rural area. This example is chosen because it is representative of an application where an AVM system could provide significant benefits. It is also an application that is ideally suited to utilizing Loran-C, both from a cost and operational standpoint.

The area chosen as a hypothetical example is Indiana County, in western Pennsylvania. Located about 50 miles east of Pittsburgh, Indiana County is a mostly rural area in the foothills of the Allegheny Mountains. A map of Indiana County is shown in Figure 1. Emergency Medical Services for the county are provided by the Citizens' Ambulance Service, which covers the nearly 800 sq. mile area with 13 ambulances. All emergency calls -- police, fire, EMS -- are received via the 911 emergency number at a central dispatching location. Ambulances are dispatched from one of five locations in the county as shown in Figure 1.

Automatic Vehicle Monitoring could provide significant benefits to the dispatching of EMS in an area such as Indiana County. Currently, a considerable fraction of the telecommunication traffic is devoted to ascertaining locations of ambulances, which may be returning to home base from a call or enroute to a routine transport call. Significant time may be spent on the road under these circumstances due to the fairly large area being covered, thus leading to uncertainties in ambulance locations and radio channel congestion due to "Where are you?" questions.

Another problem often encountered in rural areas is lack of adequate street address information to locate the caller. In some instances, addresses may be out of sequence or missing altogether. The ability to pinpoint the location of calls from public telephone booths would also be useful in quickly identifying accident locations. An improved command and control system based on better vehicle monitoring and accident location could enhance EMS dispatching.

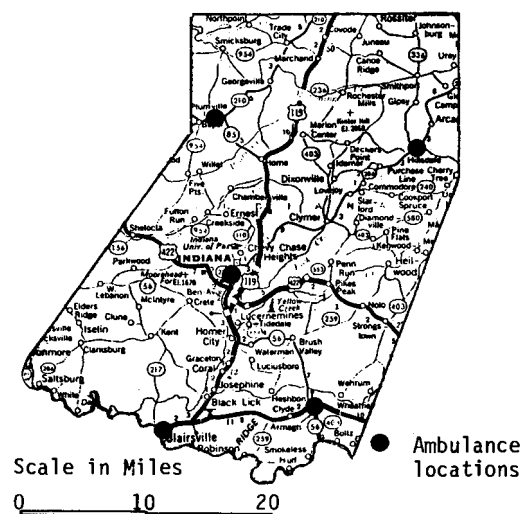


Figure 1 - Indiana County, Pennsylvania

The existing command and control system is ideally suited to the addition of an AVM and accident location capability. Countywide communications are provided via a 4-channel VHF-FM system. Three microwave towers at strategic locations allow complete radio contact coverage to be maintained with each ambulance, equipped with 5 watt portable radios. Thus, if each mobile unit were equipped with a position location system, the status and location of each unit could be continuously monitored by the central dispatcher, either by voice reporting or by automatic repeaters interfaced with the portable radios.

Because of the common central dispatching for EMS, fire and police, a unique opportunity exists for improving coordination between all three activities by addition of an AVM system. In addition to better resource management and improved dispatch efficiency, a potentially important benefit of an AVM system would be improved accident location and rendezvous, particularly in rural areas. Locations transmitted from the first emergency vehicle on the scene could be used to help other vehicles "home in" on the correct location.

For serious accidents or disasters, the need may arise to coordinate with other agencies. For example, Pittsburgh's Allegheny General Hospital supports a unique helicopter-based emergency system known as Life Flight. In life-threatening emergencies, especially if large numbers of casualties are involved, the Life Flight helicopter can quickly mobilize medical personnel to the scene in order to provide onscene life support to the patients. Life Flight services a radius of 130 miles around Pittsburgh, which includes Indiana County.

Experience has shown that it is often difficult to direct the helicopter to the scene of an emergency along ground routes. Furthermore, helicopter navigation is often impaired, especially during poor weather and over hilly terrain, when normal VOR navigation may become unusable. An enhanced ability to navigate and rendezvous the Life Flight emergency helicopter with on-scene ambulance or police units could perhaps save vital minutes in times of emergency.

For the kinds of vehicle and accident location problems described for Indiana County, Loran-C would be the natural choice as the basis of a candidate AVM system. Some of the reasons favoring this choice are as follows:

- The wide-area coverage required would make other AVM systems prohibitively expensive.
- The county is located in an area of good Loran-C signal coverage
- No high-rise urban areas exist which might interfere with Loran-C reception.
- Loran-C would be ideal as a Life Flight helicopter navigation aid, leading to better coordination with local Loran-C equipped ambulances.
- Loran-C provides a common grid for caller location identification.

Regarding the first point above, it is unrealistic to consider installation of sufficient transmitting equipment to provide a self-contained AVM system (e.g., signposts or multilateration) which would cover the nearly 800 sq. miles of Indiana County. With Loran-C, only low-cost receivers must be procured. A

minimal system could depend on voice communication of TD (or lat/lon) information to the dispatcher via existing telecommunication links. A more automated system would directly interface the vehicle Loran-C receivers to the telecommunications system to send digitally encoded position information either on request from the dispatcher or at preset intervals.

While no Loran-C experiments have yet been performed in Indiana County, the region is centrally located within the coverage areas of the Northeastern U.S. chain. The county contains some hilly areas but the topography is generally mild, which should result in good Loran-C signal strengths. Some experimentation will be necessary to choose the best station pair combinations for the region.

Previous experiments with Loran-C reception in large urban areas have sometimes encountered reception and/or multipath caused by signal interference with large metallic structures. Reception problems can be aggravated if there are very long overland paths between the station and user. Signal reception problems such as these should not be major factors in Indiana County.

The Loran-C AVM benefits could be extended if emergency helicopters, such as Life Flight, were equipped with Loran-C Receivers. Loran-C is routinely used by oil company helicopters servicing oil platforms in the Gulf of Mexico. A Loran-C navigation system with waypoint display capabilities, such as the Teledyne TDL-711, would provide excellent backup to VOR for general helicopter navigation, as well as provide a natural mechanism for the helicopter to rendezvous with a Loran-C equipped ambulance. With both units operating in the Loran-C common grid, the helicopter could fly a direct path to the accident location without the requirement to follow dispatcher directions based on highway landmarks. Substantial savings in helicopter response times could be realized this way.

With the existing Loran-C grid, additional benefits could be derived by instituting a caller location identification system. Certain locations, such as phone call boxes or some rural households, could be surveyed by one of the mobile units and stored for future references. Any point within the coverage area could be identified by its Loran-C coordinates. A quick means of providing the dispatcher with Loran-C coordinate information could reduce the amount of conversation needed to trace the caller location and would facilitate both the dispatcher's and the ambulance's response to the call.

Summary

The application of automatic vehicle monitoring (AVM) to terrestrial applications, such as police, fire and emergency medical services (EMS), has been discussed. Descriptions of the various approaches to AVM systems including Loran-C were discussed, along with the tradeoff factors required in selecting an

AVM system. It was shown that the capabilities required to provide an AVM system for a centrally-dispatched, emergency medical service for a large rural area can be best met using Loran-C positioning. The attributes of such a system have been described using the Citizens' Ambulance Service of Indiana County, Pennsylvania as a hypothetical application.

References

1. Carter, David A., "Automatic Vehicle Monitoring: A Life Saver," Proceedings of the IEEE Transactions of Vehicular Technology, 1980.
2. Wiseman, R.L. and Veronda, C.N., "The Costs and Benefits of a Mid-Continental Expansion of Loran-C," Department of Transportation, Report No. DOT-TSC-79-3, March, 1979.
3. O'Halloran, W.F. and Uttam, B.J., "Use of Loran-C in AVM and C² Systems", Proceedings of Carnahan Conference on Crime Countermeasures, 1980.

"TWO LAND VEHICLE TRACKING SYSTEMS"

Jacob Parness
The MITRE Corporation
McLean, VA 22101

ABSTRACT

This paper describes field and laboratory activities undertaken in demonstrating and studying two land vehicle tracking systems using LORAN-C. Traditional use of LORAN-C has been restricted to marine applications. This study found that LORAN-C receivers which meet the minimum performance standards established by the Radio Technical Commission for Marine Services (RTCM) will not reliably and accurately track vehicles on land. More stringent performance standards are needed for LORAN-C receivers used in land vehicle tracking.

The findings from two Department of Transportation sponsored LORAN-C programs are presented. In one, the LORAN Demonstration Laboratory (LDL), a specially equipped van was tracked in real-time as it travelled in the Washington, D.C. area. In the other, for the Philadelphia Health Management Corporation (PHMC), two emergency rescue ambulances were tracked in real-time from the Headquarters of the Philadelphia, PA Fire Department.

INTRODUCTION

This paper describes brief field and laboratory activities undertaken in demonstrating two LORAN-C land vehicle tracking systems. The results* are based upon findings of two recent U.S. Department of Transportation (DOT) sponsored LORAN-C vehicle tracking programs. The first program was the LORAN-C Demonstration Laboratory (LDL), sponsored by the National Highway Traffic Safety Administration (NHTSA) and Federal Highway Administration (FHWA). The LDL vehicle is a specially equipped van which was tracked in real-time as it travelled in the Washington, D.C. area. In the other program, developed for the Philadelphia Health Management Corporation (PHMC) under NHTSA and U.S. Department of Health, Education, and Welfare (HEW) support, two emergency rescue ambulances were tracked in real-time from the Headquarters of the Philadelphia, PA Fire Department. Both programs utilized a modified, miniature LORAN-C receiver manufactured by Teledyne Corporation (Model 701).

* Based upon studies conducted by the author and published as MITRE Reports MTR-79W00349 and DOT HS-805-446.

BACKGROUND

During the Second World War, the Massachusetts Institute of Technology developed LORAN-A as a long-range radio navigation system for use as an aid to marine and aeronautical navigation over large expanses of water (Reference 1). Use of LORAN-A was initially limited to the military, overseas airlines and shipping companies because of the high cost of LORAN receivers and the extensive training required to operate the receivers. LORAN-A was also somewhat limited in use by radio signal distortion caused by ground interference over large land masses.

LORAN-C, operating at lower frequencies than LORAN-A, is the second modification to the initial system. It was developed in the late 1950's and is currently in use over much of the world's coastal areas. Use of LORAN signals over land areas was considered to be a bonus by-product of the LORAN-C system. Two significant developments that have made LORAN-C feasible for terrestrial applications are: 1) lower frequency carrier waves which minimize ground wave attenuation, and 2) the development of receivers that are compact, easy to use, and relatively inexpensive.

During the past 10 years, government and industry (References 2 and 3) have investigated the potential use of real-time LORAN-C systems to locate vehicles in and around cities. However, successful LORAN-C system operations have proven much more difficult in cities than at sea because of the more adverse radio spectrum environment. In addition to propagation anomalies introduced by structures and terrain (References 4 and 5), strong interfering signals are present which are generated by industrial machinery, power lines, vehicle ignition systems, and other radio signal sources. These signals often degrade the performance of land vehicle tracking systems based on LORAN-C. The degree of degradation depends, among other things, upon the receiver's performance characteristics.

The LORAN-C receiver Minimum Performance Standards (MPS) developed for marine receivers (Reference 6) are not sufficient to produce reliable, accurate vehicle tracking in the terrestrial environment. Successful LORAN-C terrestrial applications require a receiver with more stringent performance characteristics.

In view of the above, the programs described in this paper were directed to further characterize the terrestrial environment and receiver performance requirements.

LORAN-C Vehicle Tracking Concept

The basic LORAN-C vehicle tracking approach consists of measuring the intersection of two lines of constant time difference (referred to as TDA and TDB throughout this paper) derived from the difference in signal arrival times from one master and two secondary LORAN-C transmitters. A groundwave propagated mode LORAN-C signal is the primary navigation signal utilized which is normally usable over water at distances of up to a thousand miles. Usable terrestrial range is less than that over water but typically can be up to 400-500 miles from the transmitters.

The accuracy potential of LORAN-C vehicle tracking system depends upon two key parameters; receiver location and accuracy. Small crossing angles introduce geometric errors (Geometric Dilution of Position - GDOP) as the hyperbolic lines become more nearly parallel (Reference 1) in the coverage grid. Gradient* factors also introduce geometric errors.

The second factor is the receiver's ability to accurately measure TDA and TDB values by "locking" onto a specified cycle of the received master and secondary pulses. "Locking on" refers to the state of a receiver after it has acquired and is tracking the correct cycle and is properly measuring time difference values. Factors which can introduce errors into the time difference measurements are 1) a low signal-to-noise ratio (SNR), 2) phase or envelope slope contamination of the signals due to geographic and man-made structures, 3) receiver processing characteristics and 4) ionosphere reflections (skywaves).

LORAN-C Terrestrial Vehicle Tracking System

In a typical real-time vehicle tracking system, time difference data is transmitted from a suitably equipped vehicle to a central location and converted into tracking display outputs. For the purpose of this paper, a terrestrial LORAN-C tracking system is defined as one which contains three basic elements. They are: 1) a vehicular mounted LORAN-C receiving system, 2) a communications data link for real-time transmission of the TDA and TDB data to the central location, and 3) central equipment which can receive and process the TDA and TDB values and display the vehicle's location on suitable maps.

* A measure of the divergency of LORAN-C lines of position as their distance from the transmitting stations increase. Typical gradients range from 50 to 500 feet/0.1 μ sec.

TERRESTRIAL LORAN-C ACTIVITIES

LDL and PHMC Programs

The purpose of the LDL and PHMC programs has been described elsewhere (Reference 7). Both systems employ real-time LORAN-C tracking technology. The LDL project, designed and implemented by MITRE, uses a demonstration van equipped with a Teledyne Microlocator 701 receiving system. A low band (40MHz) data link is used to relay TDA and TDB data to a base station located at the Headquarters Facility of the U.S. Department of Transportation in Washington, D.C. The range of the data link is approximately 20 miles. The TDA and TDB values are automatically converted to x and y coordinates and displayed on an area map at the Operations Center. The LDL system has been used extensively in the Washington, D.C. area for demonstration purposes to various federal and local agencies. It has also served as a roving testbed to measure and modify the performance characteristics of several LORAN-C receivers, and to gather data on LORAN-C signal parameters and radio spectrum characteristics in the northeast U.S. corridor, including Washington, D.C., Philadelphia and New York City.

MITRE also designed and implemented a similar emergency medical services vehicle tracking system for PHMC. Two ambulances were equipped with receiving systems similar to that of the LDL. A Teledyne 701 receiver was mounted in each ambulance and coupled to a 108 inch whip antenna which was bent over to allow for operation at hospitals with low roof overhangs. A data link between the ambulances and the Philadelphia Fire Department Headquarters operated on a UHF narrow-band FM channel with a nominal range of 10-15 miles. The ambulances were assigned to the northeast portion of Philadelphia, which consists primarily of 1-3 story dwellings with some industry. Extensive overhead power line systems are prevalent in the area, supporting electric power distribution to consumers, electric buses, and electric railroads. Therefore, the area contains many sources of radio frequency noise.

In the initial stages of the PHMC program, technical problems that prevented the receivers from locking onto the East Coast LORAN-C chain (9930) were a troublesome occurrence. During September 1979, this chain was reconfigured to become the new Northeast U.S. LORAN-C chain (9960). The new chain provided stronger signals to the test areas, and the relocation of the chain monitor station to Sandy Hook, New Jersey, provided for a more stable and accurate LORAN-C grid in the test areas. Test measurements from the Philadelphia project discussed in this paper were derived from the weaker 9930 chain.

Investigations were required to isolate the additional contributions to receiver performance problems from 1) receiver characteristics, 2) interference from in-band signals, 3) interference from out-of-band signals and 4) installation limitations. A discussion of these areas follows.

The Terrestrial Environment: Signal-to-Noise Ratio (SNR)

The SNR is defined as the ratio of the RMS signal level to the RMS value of noise at the sampling point (3rd cycle). The SNR of LORAN-C signals as received in the vehicle depends upon the following factors:

- 1) absolute signal level (at the sampling point)
- 2) other signals present in the receiver's passband
- 3) noise level in the passband
- 4) receiving system design

LORAN-C Signal Levels

LORAN-C groundwave signal level is a function of the distance between the vehicle and the transmitter sites, the nature of the terrain between the vehicle and the transmitter sites and local structures and geographic features. Predicted groundwave signal levels as a function of distance and terrain have been extensively studied and are summarized in References 8 and 9.

Other Passband Signals

SNR is also affected by strong man-made signals. Although all observed signals of this type were licensed and required to adhere to limits on their radiation, their levels were sometimes large enough within the passband to reduce the receiver's sensitivity and locking performance (Reference 10). Carrier communication signals of electric utilities operating in the LORAN-C signal spectrum are sometimes encountered near high voltage power lines.

Noise

A third factor is man-made noise. Impulse noise, common in the 100 KHz band, is generated by many sources in a city (e.g. vehicles, rotating machinery, solid state industrial controls, traffic signals). Traffic and some automobile equipment (e.g. DC to DC converters) can radiate signals at a sufficient level to disturb a LORAN-C receiver's performance. Atmospheric noise was not studied in this program and is not considered to be a major factor in system operational performance.

SNR values measured during the LDL and PHMC programs varied as a function of the vehicle's location within a city but were generally consistent in different cities having similar distance to the weakest secondary transmitter signal. SNR data was gathered in Philadelphia using the SNR test position on the Teledyne 701 receiver. Nominal SNR of the three transmitters on the 9930 chain varied between +5 and -3dB. Distances between Philadelphia and the LORAN-C transmitters were between 280 and 690 miles.

LORAN-C Receiving System Design

LORAN-C receivers are complex, and their use requires other elements of the system to be matched properly for successful performance.

A typical vehicle installation consists of 4 basic elements. One, the antenna, consists of a 1 to 3 meter steel whip mounted in such a location as to minimize its capacitive reactance. Since any short (compared to a wavelength) vehicle-mounted antenna exhibits low resistance and high capacitive reactance, a coupler is employed to provide noise attenuation, passband filtering and impedance matching to a 50 Ohm coaxial cable.

Within the receiver, individual manufacturers use different signal processing techniques, time constants, etc., to process LORAN-C signals. The Teledyne 701 receiver employs a hard limited, microprocessor controlled digital design. It operates in a differential* envelope mode to determine proper cycle selection.

Typical LORAN-C receiver performance characteristics include the following:

- o sensitivity/selectivity (measure of receiver's ability to lock on to desired signals, eliminating those which are out-of-band)
- o dynamic range (range of signals that can be processed in the receiver)
- o ECD range (range of ECD values for which the receiver will initially achieve lock and stay in lock)

* Compares the envelope of the secondaries to the measured slope of the master.

- o lock-on time (time taken for the receiver to initiate proper tracking of the LORAN signals)
- o dead reckoning time (time after a receiver has lost signal before it starts the acquisition, settle and track process over again)

The sensitivity of a LORAN-C system is controlled by the combined characteristics of the receiver and antenna coupler, including front-end bandwidth, noise and gain characteristic and receiver signal processing and averaging technique. Typical marine LORAN-C receiver specifications state a -10dB SNR performance at 5-7 minute lock-on time. Based upon laboratory tests with the Teledyne 701 receiver, the 3dB coupler/receiver bandwidth of a LORAN-C receiver should be set to about 23-25 kHz to maximize the SNR characteristics. At this bandwidth, the lock-on sensitivity of a Teledyne 701 receiver was measured to be about -2dB SNR over a range of $\pm 3\mu\text{sec}$ ECD offset. Once the receiver was locked-on, its tracking sensitivity (minimum SNR at which it continues to maintain proper track) was measured to be -7dB. When tracking below this value, receivers were observed to lose lock. The receiver must then re-acquire if the "lost signal" time was greater than the dead reckoning time.

Typically, signal dynamic range of 25dB was observed in the street tests. The dynamic range capability of the Teledyne 701 receiver exceeded signal variations encountered in the tests. Thus, dynamic range is not considered to be a very critical receiver characteristic unless a receiver is operated in close proximity to one of the several continental LORAN-C transmitter sites or the source of a strong interfering signal.

To prevent cycle slip, a LORAN-C receiver must tolerate a wide range of ECD. In addition, it is essential that no skywave signals be introduced at the sampling point. Trade-offs were studied between sampling the pulse at the third cycle (no skywave contamination) versus sampling the pulse at a later cycle yielding a higher SNR reading at the expense of skywave contamination and envelope distortion. It was found that skywave contamination increases the range of ECD observed on incoming signals, which already possess local phase variations and initial ECD offset. This added ECD range often exceeded the receiver's ECD limits and resulted in loss of lock or cycle slip.

Interference from out-of-band signals was also examined. One source (an 88 kHz high-power, narrow band transmitter located in Annapolis, MD) reduced the receiver's sensitivity by several dB. When properly

adjusted, successful operation occurred in the presence of this interfering signal as long as the vehicle was greater than approximately 10 miles away from the transmitter.

Bench tests indicated that the narrow band notch filters (which are manually controlled) did not adversely affect the receiver's accuracy or ECD characteristics if they were adjusted outside the LORAN-C band (below 90 or above 110 kHz). However, for the Teledyne 701, a LORAN-C simulator was required to recalibrate the receiver's ECD characteristics (slope and centering) after the notch filters were altered from previously calibrated settings. The simulator generated the LORAN-C master, secondary A and B signals with programmable ECD, SNR and TDA, TDB variations. Retuning and recalibration were also required for mismatched antennas (capacitive component).

Allowable LORAN-C signal lock-on times for terrestrial applications depend upon the user application and the amount of "lost track time" which can be tolerated. As an example, the receiver used for PHMC ambulance tracking possessed a lock-on time of less than 2 minutes, which, based upon emergency rescue vehicle applications tests was considered satisfactory by users.

Dead Reckoning Time (DR) is the time that a receiver holds its last reading after losing lock before it re-initializes the signal, acquisition, search and track process. The Teledyne 701 DR time was programmed (in the microprocessor internal to the receiver) for about 2 minutes which appeared to be satisfactory for the LDL and PHMC users.

Findings of LDL and PHMC Programs

The key findings of the MITRE study were:

- 1) A properly designed, adjusted and installed LORAN-C system can be used to successfully and reliably track a vehicle in terrestrial settings in places such as north-east Philadelphia and Washington, D.C.
- 2) Accuracy for the PHMC system is typically 1-2 city blocks based upon display observations. Tests in Washington, D.C. showed accuracies within 300 feet for 85% of all tests.

* The inaccuracies of the display cartography and processing algorithm are included in these results.

- 3) Areas were found in which tall buildings and local noise degrade SNR below the receiver's capability to track.
- 4) The key elements which determine system performance are SNR, ECD range, and lock-on time.
- 5) System coverage is primarily limited by the SNR sensitivity of the Teledyne 701 receiver when properly installed to eliminate self-generated vehicle noise.
- 6) The receiver must be capable of processing signals over a wide ECD variation range.
- 7) Special purpose test equipment, including a variable ECD LORAN-C simulator, is needed to set up such systems.
- 8) A combination of bench and driving tests can be used to predict the performance of a LORAN-C vehicle tracking system in any given city.

Both the LDL and PHMC programs demonstrated that a modified off-the-shelf small LORAN-C receiver can provide wide area coverage in terrestrial settings. During the January-July 1979 period, the LDL van logged over 8000 miles of travel in the north-east U.S. LDL coverage was good over most of the terrain covered. PHMC results showed that the system maintained lock over about 80% of the distance travelled in the north-east part of Philadelphia, PA. As mentioned earlier, the LORAN-C chain used here was significantly weaker than the current north-east LORAN-C chain.

Both systems experienced loss of coverage or degraded accuracy only in 1) areas with large carrier communication signals on power lines, or very noise power lines (possibly due to arcing insulators), and 2) downtown areas of cities with building heights above 10-15 stories.

Both projects independently determined that three key LORAN-C parameters are SNR, ECD range, and lock-on time. Other important parameters are: DR time and immunity to impulse noise. The data indicated that the ECD in local situations will vary up to about 2.0 μ sec and this range must be properly processed in a terrestrial LORAN-C receiver. Based on conversations with the Coast Guard and LORAN-C equipment manufacturers, state-of-the-art receiver designs are capable of achieving up to ± 5 μ sec ECD range with a lock-on sensitivity of about -5dB SNR. Lock-on time at these conditions will be about 5 minutes. However, this condition requires that the cycle sampling point be adjusted so that no skywave signals are present. Otherwise ECD variations have been observed which will exceed the receiver's capability to maintain proper cycle selection.

Key technical performance characteristics for terrestrial LORAN-C systems are suggested below in the areas of: SNR, ECD, lock-on time, DR, and impulse noise immunity. Experience with data link performance and base station computer/display design was also developed but these factors are beyond the scope of this paper.

Suggested Minimum Performance Characteristics

Table 1 presents suggested minimum LORAN-C terrestrial receiving system performance characteristics derived from the LDL and PHMC programs and discussions with Coast Guard and industry personnel. The characteristics listed (only a partial list for user procurement purposes) are in the same format for ease of comparison as the Radio Technical Commission for Marine (RTCM) standards for marine LORAN-C type receivers.

Based upon the LDL and PHMC experience, it is also suggested that future users consider the additional set of minimum performance characteristics (also compared to RTCM where applicable) which are presented in Table 2.

TABLE 1

SUGGESTED MINIMUM LORAN-C RECEIVER PERFORMANCE CHARACTERISTICS

PARAMETER	MARINE RTCM	SUGGESTED TERRESTRIAL
1. ECD Range	$\pm 3.8 \mu\text{sec}$	$\pm 3.8 \mu\text{sec}^*$
2. Minimum SNR @ specified lock on time	0dB	-5dB at max ECD (Lock on referenced to 3rd cycle
3. Lock on time	7.5 min @ a) -10dB SNR b) ECD +2.4-3.8 -2.4-3.8 c) Level 110-120 dB/ $\mu\text{V}/\text{meter}$ - 14-25dB/ $\mu\text{V}/\text{meter}$ d) differential signal level 60-80dB	Less than 2 minutes @ a) -5dB SNR b) ECD $\pm 3.8 \mu\text{sec}$ c) Level 110-120 dB/ $\mu\text{V}/\text{meter}$ - 14-25dB/ $\mu\text{V}/\text{meter}$ d) differential signal level 60-80dB
4. Effects of Skywave	None specified	Should track the 3rd or 4th cycle when the receiver is within the groundwave coverage region so as not to introduce skywave created ECD variations
5. ECD sensitivity to antenna capacitance	None specified	Less than 0.05 $\mu\text{sec}/\text{pF}$. after initial adjust- ment of ECD
6. ECD sensitivity to notch filters	None specified	None as long as they are placed outside the LORAN-C band (90-110 kHz)

* with complete installation including the antenna and antenna coupler

TABLE 1

(CONCLUDED)

PARAMETER	MARINE RTCM	SUGGESTED TERRESTRIAL
7. Dead Reckoning time	None specified	Programmable up to 5 minutes
8. Immunity to impulse noise	None specified	Typical street power line impulse noise peaks at 40 dB above the LORAN- C signal should result in a change in the receiver's SNR performance by less than 2 dB
9. Tunable notch filter	None specified	At least two inde- pendently controlled filters with 40 dB peak attenuation. Receiver-recalibration should not be re- quired when adjusted outside the LORAN-C band (90-110 kHz)

TABLE 2

ADDITIONAL MINIMUM LORAN-C RECEIVER AND INSTALLATION
PERFORMANCE CHARACTERISTICS

PARAMETER	MARINE RTCM	SUGGESTED TERRESTRIAL
1) Signal level	25-116 dB/ μ V/m	Same
2) Differential signal level	0-60dB	Same
3) Accuracy	0.3 μ sec	Same (but may be degraded for some less accurate user application)
4) Dynamic tracking	Up to 16KT and 3KT/min. acceleration	Up to 70 mph, typical vehicle acceleration on straight roads and on rapid turns
5) Internal receiver noise	None specified	2 μ volts equivalent (antenna input at coupler)
6) Vehicle noise level	None specified	Less than 2 μ volts equivalent (antenna input at coupler)
7) Vibration	None specified	Electrical performance of the system - especially the notch filter settings - should be stable when mounted in a vehicle
8) Front-End Selectivity	None specified	Should be designed to afford maximum attenuation to out of band signals

CONCLUSIONS

With many aspects of transportation safety and control undergoing rapid change, wide-area vehicular tracking technology is likely to become a useful and cost-effective future transportation aid. LORAN-C holds promise for meeting many of these vehicle tracking needs in areas such as law enforcement, public transportation security, and public and private large fleet operations. Key to the successful deployment of such high technology systems will undoubtedly be careful overall system design, suitable receiver specifications, reliable hardware and appropriate installations.

The information and experience gained from the LDL and PHMC LORAN-C vehicle tracking programs should be helpful to designers and users of future LORAN-C based automatic vehicle monitoring systems. Key receiver performance characteristics for terrestrial use relate to street level signal-to-noise (SNR) ratios, ECD range and receiver lock-on time.

Special care must be taken to ensure proper design, adjustment and grounding of all LORAN-C and data link equipment in the vehicle. In addition, proper test equipment and trained personnel are needed to set up and maintain equipment of this complexity.

There are currently no published and accepted minimum receiver performance characteristics for users of terrestrial LORAN-C. Therefore, it is recommended that a government/industry/university standards group be established to serve the needs of LORAN-C terrestrial users and to develop suitable receiver specifications. It is hoped that the suggested performance characteristics discussed in this paper would be an input to these deliberations.

REFERENCES

1. Department of Transportation, Coast Guard, "LORAN-C User Handbook," CG-462, August 1974.
2. Department of Transportation, "The Costs and Benefits of a Mid-Continent Expansion of LORAN-C," DOT-TSC-RSPA-79-3, March 1979.
3. Teledyne Corp., "Automatic Vehicle Monitoring System," Final Report DOT-UT-72, July 1972.
4. Johler, R. J., "LORAN-C, D. Phase Corrections Over Irregular, Inhomogenous Terrain-Simplified Computer Methods," U. S. Department of Commerce Institute for Telecommunication Science, ESSA Report ERL 1160ITS83, April 1969.
5. Johler, R. J., Horowitz, S., "Propagation of LORAN-C Ground and Ionospheric Wave Pulses," U. S. Department of Commerce, Institute for Telecommunication Science, OT Report 73-20, January 1973.
6. Radio Technical Commission for Marine Service, "Minimum Performance Standards (MPS) Marine LORAN-C Receiving Equipment," Report of Special Committee No. 70, December 1977.
7. El-Sawy, A. A., Feuerstein, J. W., Mayer, R. P., "LORAN-C Tracking of Land Vehicles Using Microcomputers," presented at IEEE Vehicle Technology Group Annual Conference, March 1978, Denver, Colorado.
8. Advisory Group for Aerospace Research and Development, "Medium Accuracy, Low-Cost Navigation: LORAN-C versus the Alternatives," ITT Avionics Division, presented at 30th Technical Meeting of the Avionics Panel, September 1975.
9. Veronda, C., "Bibliography and Comments on LORAN-C Ground Wave Propagation," U. S. Department of Transportation, DOT-TSC-RSPD-77-2, December 1977.
10. U. S. Coast Guard, "LORAN-C Interference List," January 1979.

A HYBRID LORAN/DIFFERENTIAL ODOMETER SYSTEM FOR LAND VEHICLE NAVIGATION

W. M. Bowles and R. R. Hildebrant
Department of Aeronautics and Astronautics
Massachusetts Institute of Technology
Cambridge, Massachusetts 02139

ABSTRACT

Loran C is an attractive navigation system for a variety of land vehicles because it is relatively inexpensive and available in many areas. However, it suffers in a land environment (particularly urban) because of localized sources of interference, such as traffic lights or rotating machinery, and because of severe warp of the hyperbolic grid due to large metal objects (building frameworks, powerlines, etc.) Occasionally these problems cause Loran C to perform poorly in urban environments.

Another system which has been proposed for this same navigation task is based on the differential odometer. The differential odometer is actually two odometers - one on each front wheel. The average of these odometer outputs indicates the vehicle's forward speed. The difference between them is proportional to the rate-of-change of the vehicle's heading. Given proper initial conditions then, in theory, the vehicle position may be computed.

Problems arise with the differential odometer system, as with any dead-reckoning system, because there tend to be scale factor errors in both speed and heading rate. These errors cause the position computed by a differential odometer alone to become increasingly inaccurate as the vehicle moves away from its initial point.

In this paper a hybrid design is presented which makes optimum use of the differential odometer and Loran C sensors. The resulting system possesses the good features of both of these systems and the deficiencies of neither. The algorithm presented is simple enough to be implemented in a microprocessor.

Simulation results are presented.

I. INTRODUCTION

This paper presents a design for a hybrid navigation system for use in land vehicles such as buses, taxicabs or police cars. The navigation system incorporates measurements from two different position sensing devices in a way which largely overcomes the difficulties with each.

The position sensors forming the heart of this system are a differential odometer and a Loran C receiver. The differential odometer is comprised of two odometers - one on each front wheel. When cornering, the outer front wheel traverses a longer path than the inner one and thus its rotation rate is larger. The difference between the wheel rates (hence the name, differential odometer) will indicate the turning rate of the vehicle. Speed is obtained by averaging the front wheel turning rates. Theoretically then, the differential odometer, with proper utilization, could be used to determine a land vehicle's position, since it indicates both heading and speed. In practice, however, problems arise in using this instrument as a position indicating system. One difficulty stems from the need to integrate the turning rate, as indicated by the differential odometer, in order to obtain a heading angle. Provision must then be made to initialize the heading. This is a serious operational problem.

Another, and perhaps more fundamental, problem is that the relation between differential tire rotation rate, which the differential odometer measures, and the actual rate of change of heading may not always be known. Slight changes in tire pressure, wind loading and road camber alter this relation substantially. A typical drift rate between actual heading and heading indicated by a differential odometer is $10^\circ/1000$ ft. The differential odometer provides an accurate position indication only if the initial condition is good, and if the distance traveled is relatively short.

The general operating principles of Loran C may be familiar to the reader, but there are two problems with Loran C which are unique to the urban environment. The first is called grid warp. Grid warp is a deviation of the true Loran C grid from the theoretical hyperbolae. Marine users are familiar with such deviations and know to calibrate their sets by taking readings at a known location and shifting the theoretical curves to compensate. The grid warp observed on land is too severe for the marine approach to be successful. These warps are highly localized (usually less than 500 feet) and very severe (500 feet on the average and often as large as 1500 feet).

The second problem Loran C faces in an urban environment is loss of lock due to signal shadowing from buildings and due to localized noise sources such as traffic lights and rotating machinery.

Neither the differential odometer nor the Loran C receiver will suffice for land navigation. The differential odometer drifts badly and the Loran C suffers from localized but large errors. On the other hand, the differential will, if properly initialized, give a smooth and accurate position indication for a short time, and the Loran C, aside from these pockets of large error, will give a consistent and reasonably accurate indication of position.

The design we present here combines these two sensors to yield a navigation system that exploits the good features of both. The system operates by using Loran C, when it is not shadowed, to continually calibrate and initialize the differential odometer. When the Loran C falls out, the differential odometer is used to coast through the disturbance.

In the following sections, the design for a complete hybrid land navigation system is developed. Section 2 gives the mathematical model for the sensors. Section 3 describes the initialization algorithm and section 4 gives the tracking algorithm. Section 5 discusses some simulation results and section 6 summarizes and indicates where future work is required.

II. MATHEMATICAL MODELS

The differential odometer measures true heading rate plus an error. Let $(d/dt)\phi_m$ be the heading rate measured by the differential odometer, $(d/dt)\phi_e$ be the true heading rate and $(d/dt)\phi_e$ the error heading rate. Then

$$\frac{d\phi_m}{dt} = \frac{d\phi_t}{dt} + \frac{d\phi_e}{dt} \quad (2.1)$$

The error heading rate depends on a scale factor we shall denote by $\alpha(t)$, and on the vehicle speed, $V(t)$. This is shown below:

$$\frac{d\phi_e}{dt} = V(t) \alpha(t) \quad (2.2)$$

The scale factor $\alpha(t)$ is called the differential odometer drift rate and it will be assumed to satisfy

$$\frac{d\alpha(t)}{dt} = n(t) \quad (2.3)$$

where $n(t)$ is a white noise. Thus, the scale factor is expected to behave as a random walk. Justification for this

stochastic model lies in the very unpredictable and random condition of the road and the variability of wind forces on the vehicle. More accurate models of the differential odometer can easily be incorporated into the analysis when field test studies of the instrument become available.

We shall assume that the speed measured by the differential odometer is accurate. The measured velocity will be denoted by $v_m(t)$.

The Loran C measures two ΔT 's and these measurements are corrupted with noise. The ΔT 's will be sampled at a rate of about once every ten seconds and it will be assumed that the noise on the ΔT measurements is uncorrelated from sample to sample. The Loran C measurements will be denoted by $Z_1(t_i)$ and $Z_2(t_i)$ and satisfy

$$\begin{bmatrix} Z_1(t_i) \\ Z_2(t_i) \end{bmatrix} = \begin{bmatrix} \Delta T_1(t_i) \\ \Delta T_2(t_i) \end{bmatrix} + \begin{bmatrix} M_1(t_i) \\ M_2(t_i) \end{bmatrix} \quad (2.4)$$

That is, at each sample time t_i , the Loran C receiver measures a pair of $\Delta T_1(t_i)$ and $\Delta T_2(t_i)$, corresponding to the vehicle's true position, corrupted with noises $M_1(t_i)$ and $M_2(t_i)$.

Summarized below are the main variables important in the hybrid design:

$\begin{bmatrix} \Delta T_1(t) \\ \Delta T_2(t) \end{bmatrix}$	- ΔT 's corresponding to the vehicle's true position at time t
$\phi_m(t)$	- heading measured by the differential odometer
$\phi_e(t)$	- heading error in the differential odometer
$\alpha(t)$	- differential odometer scale factor error
$v_m(t)$	- speed measured by the differential odometer
$\begin{bmatrix} Z_1(t_i) \\ Z_2(t_i) \end{bmatrix}$	- Loran C measured ΔT pair at sample time t_i

These are related to one another through the following system of equations:

$$\frac{d}{dt} \begin{bmatrix} \Delta T_1(t) \\ \Delta T_2(t) \end{bmatrix} = \begin{bmatrix} C_{11} & C_{12} \\ C_{21} & C_{22} \end{bmatrix} \begin{bmatrix} \cos(\phi_m - \phi_e) \\ \sin(\phi_m - \phi_e) \end{bmatrix} v_m(t) \quad (2.5)$$

$$\frac{d\phi_e}{dt} = \alpha(t) v_m(t) \quad (2.6)$$

$$\frac{d}{dt} \alpha(t) = n(t) \quad (2.7)$$

$$\begin{bmatrix} z_1(t_i) \\ z_2(t_i) \end{bmatrix} = \begin{bmatrix} \Delta T_1(t_i) \\ \Delta T_2(t_i) \end{bmatrix} + \begin{bmatrix} M_1(t_i) \\ M_2(t_i) \end{bmatrix} \quad (2.8)$$

The parameters C_{ij} depend on the Loran C transmitter geometry. In particular, if $\alpha_m, \alpha_{s1}, \alpha_{s2}$ are the bearings to the master, first slave and second slave, respectively, then

$$\begin{bmatrix} C_{11} & C_{12} \\ C_{21} & C_{22} \end{bmatrix} = \begin{bmatrix} \cos \alpha_{s1} & -\cos \alpha_m & \sin \alpha_{s1} & -\sin \alpha_m \\ \cos \alpha_{s2} & -\cos \alpha_m & \sin \alpha_{s2} & -\sin \alpha_m \end{bmatrix} \quad (2.9)$$

It will be assumed here that the vehicle operates in a small enough region such that the bearing angles remain nearly constant and the C_{ij} do not change.

III. INITIALIZATION

We shall eventually be interested in using an Extended Kalman Filter to provide a hybrid navigation solution. One step in the derivation of this filter requires a small angle approximation in the heading error. The details of this will be provided later, but for now it is sufficient to note that when first starting out, the system has no knowledge of true heading. This is because the differential odometer measures only changes in heading and cannot independently determine the initial vehicle heading angle. The differential odometer can do no more than guess the initial heading, which would surely result in a large initial heading error. Determining this heading is further complicated by the fact that heading error builds with distance traveled.

In order for the Extended Kalman Filter (presented in this section) to operate properly, a reasonable guess for the initial heading and scale factor must be generated. The purpose of this section is to develop an initialization algorithm which will generate initial estimates of heading and scale factor.

We will begin by manipulating the Loran Measurement of position into a form that is suitable for estimating the initial heading and scale factor and then develop a simple Kalman Filter to do so. Depicted in Figure 3.1 are the elements that will compromise our basic measurement for initialization. The true ground track described by the vehicle and a "phantom" ground track generated by the differential odometer are both plotted. The system always assumes it

starts out in the east direction. Its true heading is determined only after initialization. Also, the initialization algorithm assumes that the drift rate $\alpha(t)$ is a constant.

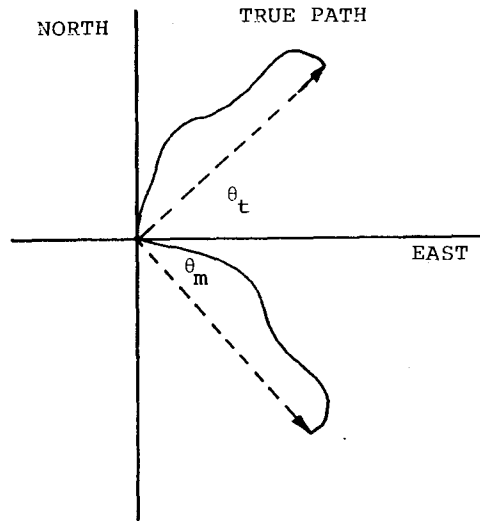


Figure 3.1

The information needed to estimate both ϕ_e and α is contained in the angle between vectors drawn from the origin to the end points of our two paths. We use Loran position information to measure ϕ_t and we integrate the velocity and heading from the differential odometer to measure θ_m . In terms of θ_t and θ_m , named the true and measured angles, our basic measurement is

$$F(t) = \theta_t(t) - \theta_m(t) + n_1 + n_2 \quad (3.1)$$

where the noise, n_1 , is a zero mean, non-gaussian error in position as measured by the Loran receiver, and n_2 is a zero mean noise due to the differential odometer. We will assume that n_2 is negligible when compared with n_1 and that n_1 is white and gaussian.

We must now relate the measurement, $F(t)$, to the quantities we wish to estimate, ϕ_e and α . The angle θ_m may be expressed as follows:

$$\theta_m = \text{ARCTAN} \frac{x_m}{y_m} \quad (3.2)$$

where x_m, y_m = measured east and north position components of the vehicle

u_m = unbiased measured heading rate

and

$$\begin{aligned}\frac{dx_m}{dt} &= v_m(t) \sin \phi_m \\ \frac{dy_m}{dt} &= v_m(t) \cos \phi_m \\ \frac{d\theta_m}{dt} &= u_m(t) + v_m(t)\alpha \quad (3.3)\end{aligned}$$

After changing the independent variable from time, t , to distance, s , and employing the trigonometric identity, $\tan 1/2 x = [1 - \cos(x)]/\sin x$, we obtain (with some manipulation:

$$\theta_m = \frac{1}{2} \alpha s + \frac{1}{2} \int \frac{u_m}{v_m} ds \quad (3.4)$$

The true quantities may be treated in the same way to obtain

$$\theta_t = \text{ARCTAN} \frac{x_t}{y_t} \quad (3.5)$$

$$\begin{aligned}\frac{dx_t}{dt} &= v_t(t) \sin \phi_t \\ \frac{dy_t}{dt} &= v_t(t) \cos \phi_t \\ \frac{d\phi_t}{dt} &= u_t(t)\end{aligned} \quad (3.6)$$

where ϕ_t = true vehicle heading at time t ,
and

$$\theta_t = \phi_t(0) + \frac{1}{2} \int \frac{u_t}{v_t} ds \quad (3.7)$$

Now, by definition

$$\phi_e = \phi_m - \phi_t \quad (3.8)$$

and

$$\begin{aligned}\frac{d\phi_e}{dt} &= \frac{d\phi_m}{dt} - \frac{d\phi_t}{dt} \\ &= v_m + u_m - u_t \quad (3.9)\end{aligned}$$

For now, assume that the unbiased heading rate and the velocity as measured by the differential odometer are accurate measurement of the true values ($u_m = u_t$; $v_m = v_t$). In general, these assumptions will be very good. Eqn. (3.8) then yields

$$\frac{d\phi_e}{dt} = v_t \alpha \quad (3.10)$$

or, with distance as the independent variable

$$\frac{d\phi_e}{ds} = \alpha \quad (3.11)$$

The angle θ_t may now be expressed in terms of ϕ_e and α as follows. Since $\phi_m(0) = 0$ (by assumption, i.e., the phantom path starts out in the east direction), Eqn. (3.8) yields

$$\phi_t(0) = -\phi_e(0) \quad (3.12)$$

and integration of Eqn. (3.11) gives

$$-\phi_e(0) = -\phi_e(t) + \alpha s \quad (3.13)$$

Substituting Eqns. (3.12) and (3.13) into Eqn. (3.7) results in

$$\theta_t = -\phi_e(t) + \alpha s + \frac{1}{2} \int \frac{u_t}{v_t} ds \quad (3.14)$$

Now combining Eqns. (3.14), (3.4), and (3.1), we have our measurement in the desired form.

$$F(t) = -\phi_e(t) + \frac{1}{2} \alpha s + n_1 \quad (3.15)$$

This, together with equations describing the behavior of $\phi_e(t)$ [Eqn. (3.11)] and α (assumed constant) are the ingredients we need to construct a Kalman Filter for their estimation. The necessary equations in discretized form are outlined below.

Outline for Initialization Filter

System Model:

$$\phi_e(k+1) = \phi_e(k) - \alpha(k) \Delta s(k) \quad (3.16)$$

$$\alpha(k+1) = \alpha(k)$$

or

$$x(k+1) = A(k) x(k) \quad (3.17)$$

where

$$x(k) = \begin{bmatrix} \phi_e(k) \\ \alpha(k) \end{bmatrix} \quad A(k) = \begin{bmatrix} 1 - \Delta s(k) \\ 0 & 1 \end{bmatrix} \quad (3.18)$$

Measurement:

$$F(k) = -\phi_e(k) + \frac{1}{2} \alpha(k) s(k) + n_1(k) \quad (3.19)$$

or

$$F(k) = H(k) x(k) + n_1(k) \quad (3.20)$$

where

$$H(k) = -1 + \frac{1}{2} s(k) \quad (3.21)$$

Initial Conditions:

$$\hat{\phi}_e(0) = 0 \quad \hat{\alpha}(0) = 0 \quad (3.22)$$

$$E\{[\phi_e(0) - \hat{\phi}_e(0)]^2\} = \pi^2/3$$

$$E\{[\phi(0) - \hat{\phi}(0)]^2\} = \left(\frac{\pi}{100 \cdot 180}\right)^2 \quad (3.23)$$

$$E\{n_1(k) n_1(m)\} = \begin{cases} R & k=m \\ 0 & k \neq m \end{cases} \quad (3.24)$$

State estimate extrapolation:

$$\hat{x}^-(k) = A(k) \hat{x}^+(k) \quad (3.25)$$

Covariance extrapolation:

$$P^-(k) = A(k-1)P^+(k-1)A^T(k-1) \quad (3.26)$$

State update:

$$x^+(k) = \hat{x}^-(k) + K(k) [F(k) - H(k)\hat{x}^-(k)] \quad (3.27)$$

Error covariance update:

$$P^+(k) = P^-(k) - K(k)H(k)P^-(k) \quad (3.28)$$

Kalman gain:

$$K(k) = P^-(k)H^T(k) [H(k)P^-(k)H^T(k) + R]^{-1} \quad (3.29)$$

Hand-over Criterion

As the initialization filter is running along obtaining new measurements and making ever better estimates for ϕ_e and α , it must be decided when these estimates are good enough to hand operation off to the tracking filter. Poor estimates will cause the tracking filter to converge very slowly or not at all. Very precise estimates bring about an inordinate delay in the time when the improved position estimates of the tracking filter are available. Plotted in Figure 3.2 is an envelope of convergence below which the tracking filter will estimate ϕ_e to within a tenth of a radian within one minute.

IV. TRACKING ALGORITHM

After the heading sensor has been initialized, the job of tracking ΔT 's, the differential odometer error and drift rate is handled by a continuous - discrete Extended Kalman Filter (EKF). This version of the filter propagates

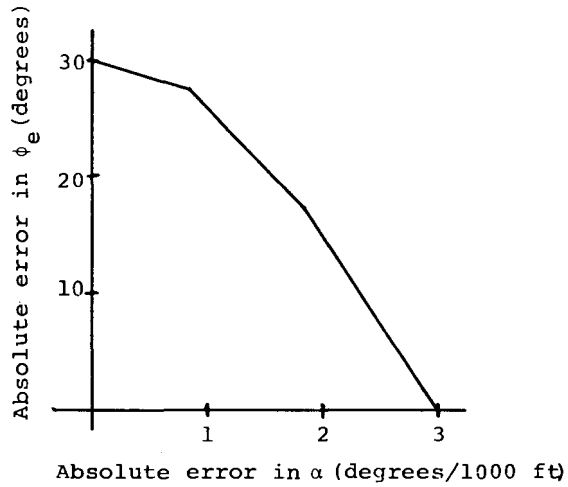


Figure 3.2

states as continuous time functions, but includes measurements at discrete times. This format is chosen because it gives continuous time estimates of the Loran C ΔT 's which are necessary for accurate reporting to headquarters, but it only requires Loran C measurements at discrete times. The Loran C measurements cannot be included continuously, because they are time correlated. That is, since they are the output of a low pass filter they do not have white noise corrupting them. However, if the Loran sampling period is chosen sufficiently long, then successive samples may be considered to be corrupted by independent noises.

The first step in developing the EKF is to obtain a set of linearized perturbation equations from the system state equations (2.1)-(2.3). Those equations are summarized here:

$$\frac{d}{dt} \begin{bmatrix} \Delta T_1 \\ \Delta T_2 \end{bmatrix} = \begin{bmatrix} C_{11} & C_{12} \\ C_{21} & C_{22} \end{bmatrix} \begin{bmatrix} \cos(\phi_m - \phi_e) \\ \sin(\phi_m - \phi_e) \end{bmatrix} v_m \quad (4.1)$$

$$\frac{d}{dt} \phi_e = \alpha(t) v_m(t) \quad (4.2)$$

$$\frac{d}{dt} \alpha(t) = n(t) \quad (4.3)$$

In these equations ϕ_m and v_m are the heading and velocity indicated by the differential odometer. Suppose now that nominal trajectories for the ΔT 's, $\phi_e(t)$, and $\alpha(t)$ are given. Denote these nominal trajectories by $\Delta T_1(t)$, $\Delta T_2(t)$, $\phi_{en}(t)$ and $\alpha_n(t)$. If the perturbations

$$\begin{bmatrix} \delta \Delta T_1 \\ \delta \Delta T_2 \\ \delta \phi \\ \phi \alpha \end{bmatrix} = \begin{bmatrix} \Delta T_1 - \Delta T_{1n} \\ \Delta T_2 - \Delta T_{2n} \\ \phi_e - \phi_{rn} \\ \alpha - \alpha_n \end{bmatrix} \quad (4.4)$$

are sufficiently small, they satisfy

$$\frac{d}{dt} \begin{bmatrix} \delta \Delta T_1 \\ \delta \Delta T_2 \\ \delta \phi_e \\ \delta \alpha \end{bmatrix} = A(t) \begin{bmatrix} \delta \Delta T_1 \\ \delta \Delta T_2 \\ \delta \phi_e \\ \delta \alpha \end{bmatrix} \quad (4.5)$$

where

$$A(t) = \begin{bmatrix} 0 & 0 & v_m [C_{11} \sin(\phi_m - \phi_n) - C_{12} \cos(\phi_m - \phi_n)] & 0 \\ 0 & 0 & v_m [C_{21} \sin(\phi_m - \phi_n) - C_{22} \cos(\phi_m - \phi_n)] & 0 \\ 0 & 0 & 0 & v_m(t) \\ 0 & 0 & 0 & 0 \end{bmatrix} \quad (4.6)$$

Since these perturbations satisfy a linear equation, they can be estimated using a Kalman Filter. A so-called, continuous-discrete filter is chosen for reasons which were mentioned earlier.

The estimated states solve the non-linear equations:

$$\frac{d}{dt} \begin{bmatrix} \hat{\Delta T}_1 \\ \hat{\Delta T}_2 \end{bmatrix} = \begin{bmatrix} C_{11} & C_{12} \\ C_{21} & C_{22} \end{bmatrix} \begin{bmatrix} \cos(\phi_m - \phi_e) \\ \sin(\phi_m - \phi_e) \end{bmatrix} v_m \quad (4.7)$$

$$\frac{d}{dt} \hat{\phi}_e = \hat{\alpha} v_m(t) \quad (4.8)$$

$$\frac{d}{dt} \hat{\alpha}(t) = 0$$

The error covariance of the perturbation states satisfies the linear equation

$$\dot{P} = AP + PA^T + Q \quad (4.9)$$

where

$$Q = \begin{bmatrix} 0 & 0 & 0 & 0 \\ 0 & 0 & 0 & 0 \\ 0 & 0 & 0 & 0 \\ 0 & 0 & 0 & q \end{bmatrix} \quad (4.10)$$

and q is the variance parameter of the Brownian Motion driving the drift rate process. These equations are used to propagate the states between Loran C

measurements. When a Loran C measurement is taken, the perturbation states are updated as follows:

$$\begin{bmatrix} \delta \Delta T_1 \\ \delta \Delta T_2 \\ \delta \phi_e \\ \delta \alpha \end{bmatrix}^+ = \begin{bmatrix} \delta \Delta T_1 \\ \delta \Delta T_2 \\ \delta \phi_e \\ \delta \alpha \end{bmatrix}^- + P^- H^T R^{-1} \begin{bmatrix} \Delta T_{1m} - \Delta T_1 \\ \Delta T_{2m} - \Delta T_2 \end{bmatrix} \quad (4.11)$$

The (-) superscripts denote values prior to incorporation of the measurement, and the (+) superscripts denote quantities after the update. The states themselves are updated after a Loran fix by the formula

$$\begin{bmatrix} \Delta T_1 \\ \Delta T_2 \\ \phi_e \\ \hat{\alpha} \end{bmatrix} = \begin{bmatrix} \Delta T_1 \\ \Delta T_2 \\ \phi_e \\ \hat{\alpha} \end{bmatrix}^- + \begin{bmatrix} \delta \Delta T_1 \\ \delta \Delta T_2 \\ \delta \phi_e \\ \delta \alpha \end{bmatrix} \quad (4.12)$$

The covariance is updated by

$$P^+ = P^- - P^- H^T (HPH^T + R)^{-1} HP^- \quad (4.13)$$

In these equations the matrix H is given by

$$H = \begin{bmatrix} 1 & 0 & 0 & 0 \\ 0 & 1 & 0 & 0 \end{bmatrix} \quad (4.14)$$

and the matrix R is the covariance matrix for the jitter on the Loran C measurements. The initial conditions for these equations are either received from the initialization routine, or from the Loran C set.

V. SIMULATION RESULTS

Single Run Discussion of Events

Figure 5.1(a) displays two curves, one of which is smooth and represents the ground track of a vehicle. The vehicle is traveling along a segment of the Mystic Valley Parkway north of Somerville, Massachusetts, and through some of the housing areas adjacent to the Parkway. The Loran transmitters are in the Los Angeles configuration and the SNR is zero dB on all channels. The differential odometer is initialized with a 90° heading error, and a drift rate of 10°/1000 ft. The hybrid tracking algorithm, of course, does not know what the initial heading error or drift rate is. The algorithm begins operation believing that the heading error and drift rate are both zero.

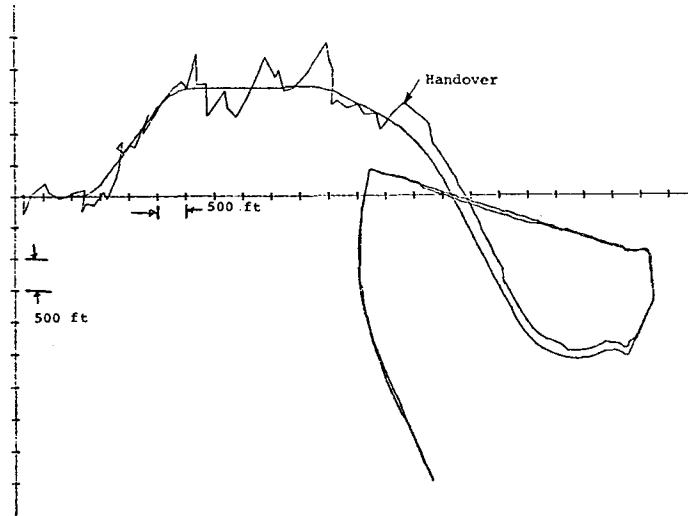


Figure 5.1(a) Vehicle Track

While the initialization routine is acquiring the drift rate and heading angle, the system displays the Loran C output. As time and distance from the start grow, the initializer grows more and more confident of the heading error and drift rate numbers which it is generating. When its confidence in these quantities reaches a predetermined level, the algorithm initializes the EKF which then begins its task of estimating position. This point is marked "Handover" on Figure 5.1(a). The EKF then generates the ΔT 's. The filter takes as its starting point a Loran C fix. A new Loran C measurement is incorporated into the navigation solution approximately every ten seconds. The precise navigation update rate depends on the Loran C tracking loop natural frequencies. At

the tracking loop natural frequency used to generate this plot (.2 rad/sec.), the navigation filter incorporates a measurement every 10.5 seconds. The incorporation of a measurement manifests itself as a discontinuity in the estimated vehicle path. Just after handover, the estimated trajectory parallels the true trajectory until the first Loran C measurement. It then steps closer to the true trajectory and runs parallel again until the second measurement. The estimated trajectory continues in this way, stepping closer and closer to the true vehicle position. Figure 5.1(b) shows the position errors versus time for this run. Notice how small the errors are at the end of the run.

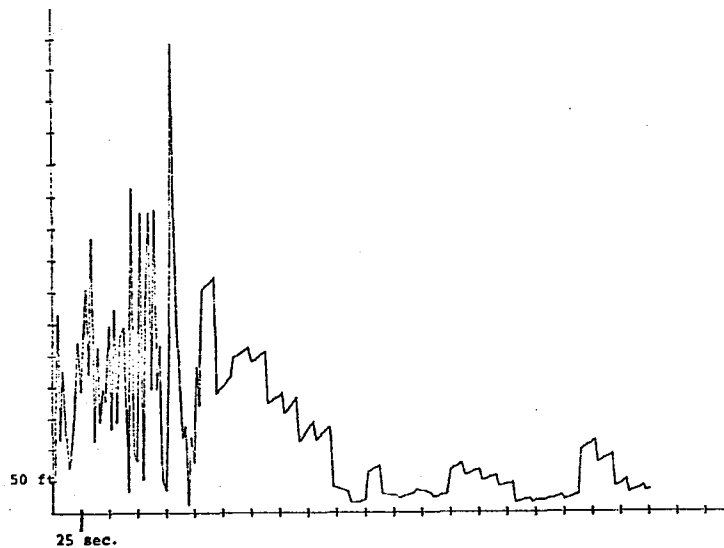


Figure 5.1(b) Position Error vs. Time

VI. A DISCUSSION OF RESULTS

We have presented a design for a hybrid land navigation system using Loran C and a differential odometer. The simulation results show a marked improvement over Loran C stand-alone performance.

The greatest uncertainty in what we have presented is in the differential odometer model. Actual test results are required to determine the true differential odometer model. Until those are obtained this uncertainty cannot be resolved. The model we have chosen is, however, reasonable and we expect that performance results will not change substantially when a more accurate model is used.

LORAN-C POSITIONING TESTS IN NEW YORK

Walter N. Dean
Verdes Engineering Co.
26619 Shorewood Road
Rancho Palos Verdes, California 90274

ABSTRACT

A series of measurements was made in Monroe County, NY, to determine the feasibility of using Loran-C as a vehicle monitoring system in that area. Approximately 200 sets of readings were taken in a 200 square mile area, using a Micrologic ML-320 Loran Navigator, and the positions compared with topographic maps. With bias removed, 83 percent of the fixes had an error of less than 500 feet.

INTRODUCTION

The Loran-C Demonstration Project in New York State selected eastern Monroe County as its site to test loran for vehicle location. A survey of the area was made using a Micrologic ML-320 navigator in a passenger car. A total of 200 data points were taken and analyzed. The results indicate that a system using only loran for positioning can be used to provide vehicle location satisfactory for EMS, police and traffic record services.

NEW YORK LORAN COVERAGE

New York State has something few others can claim - a Loran-C Master station in the center of the state. This can be regarded as a mixed blessing, as we discovered in analyzing the application of loran to vehicle location in New York.

When the Loran-C Demonstration Project was conceived, loran coverage in New York was as in figure 1, with the Master at Carolina Beach, and secondaries at Nantucket and Dana. Signal strengths were adequate, and the geometry provided repeatable accuracies in the order of 200 feet. Progress, in the form of the new Seneca master and the Northeast (9960) chain changed all that. Now instead of one, there are six M-S combinations of stations, with the possibility of retaining the old geometry with a receiver that can be master independent, using XYZ secondaries. Figures 2-7 give a graphic picture of what has happened to New York's loran coverage. The five counties shaded, the candidates for the demonstration project, each uses a different combination of stations for best coverage. There is one advantage, however - highly adequate master signal strength.

MONROE COUNTY TESTS

Monroe County, which includes the city of Rochester, was selected on the basis of a variety of factors, and it was determined that the experiment would be limited to the eastern half of the county. A major question arose as to whether a useful system could be assembled using loran only without augmentation. To help answer this question, a survey was conducted in the area.

The instrumentation used for the survey was a Micrologic ML-320 Loran-C Navigator, which is a combined loran receiver and coordinate converter. It was mounted in a passenger car with the antenna coupler and 52 inch whip antenna mounted on the left rear bumper. Data were taken by stopping the car at a recognizable location, usually an intersection, and recording two TDs, Lat/Lon, SNR and envelope numbers for the two secondaries. Data recording usually took less than a minute.

The dots on figure 8 show the approximate locations of most of the data points. An attempt was made to make this a representative sample of the area, with about 20% of the points in the "downtown" area, 40% in urban/suburban and 40% in rural areas. Rochester's downtown is not as severe as, say, Manhattan in that the buildings are not as tall, so the effects, as expected, are not as severe. However, significant signal loss was observed. The downtown did not contain significant noise or interference sources, so the loran performance was limited by the noise figure of the receiver. This is a significant observation which indicates a design factor not considered significant in marine receivers.

The secondary stations used were W and Z, which was seen in figure 4 to provide the best geometry. Interestingly, the MW lines are nearly east-west, while the MZ lines run nearly north-south. The W signal is the weakest, although the range is less than to Z, because the propagation path is over the mountains of New Hampshire and Vermont, which should also cause the phase of the signal to be retarded more than the others.

The ML-320 calculates latitude and longitude, based on a velocity of propagation slightly slower than over seawater. Therefore it was expected that

the calculation of position would have a bias error. Both TDs will be higher than they would be over seawater, so the calculated position should be east and south of the true, especially south, because of the direction of the MW LOP.

DATA ANALYSIS

The data were first analyzed by finding the latitude and longitude of each data point from 7½-minute topographic maps of the area. The differences between the lat/lon determined by the ML-320 and the map positions were then calculated. As expected, there were bias errors in the differences.

It was observed that the biases were slightly different in the southwest quadrant of the area. This was expected, because the LOPs are non-linear in the area. The data were therefore segregated into the two areas and the mean and standard deviations of the lat/lon differences calculated. The results were, in minutes of arc:

	Latitude		Longitude	
	Mean	S.D.	Mean	S.D.
S.W. Quadrant	0.44	0.057	0.06	0.041
Rest of County	0.35	0.051	0.03	0.049

The mean values were then subtracted from the latitude and longitude readings, and the residual error converted to distance in feet. Figure 9 shows the distribution of the resultant position errors. It should be noted that these errors include both map errors and coordinate conversion errors, in addition to the Loran-C error. The roundoff error in the ML-320 is about 75 feet. The map error can be estimated at 50-100 feet.

TIME DIFFERENCE BIAS

In retrospect, it seemed apparent that the bias error in the time differences should be relatively constant over the county area. Therefore, a method was devised to calculate the bias and remove it. Using the ML-320 in its calculator mode, the map position for each data point was converted to loran time difference. The TD actually measured at that point was subtracted from the calculated value and the residuals for the 200 points analyzed.

As expected, the measured TD's were higher than the calculated values; by 2.5 microseconds for MW and 0.8 usec for MZ. As also expected, because the W signal is weaker, the standard deviation of the MW residuals was higher; 0.36 usec compared with 0.29 usec for MZ.

The TD biases were subtracted from each measurement, and the lat/lon

recalculated. These new values were then subtracted from the map locations, and the distance error for each calculated. The results are analyzed in Figure 10. As can be seen, the percent of fixes with error less than 200 feet has increased substantially from 36 to 44 percent.

The histogram shows that 9 of the 200 fixes had errors of over 1000 feet. These obviously require further attention. Some are known to be related to local phenomena such as power lines with interference.

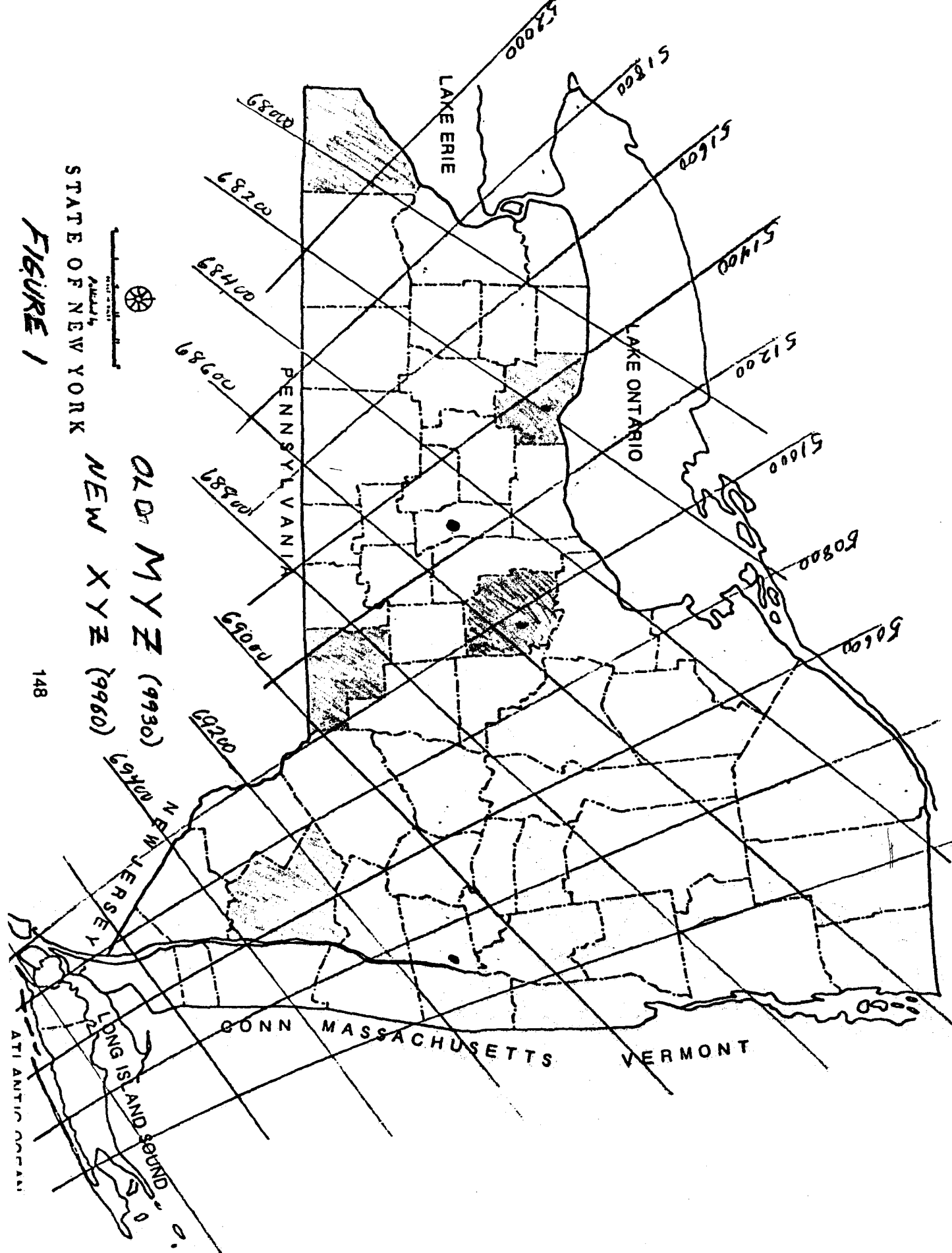
Even without interference, or with the interference notched out, phase distortions can be caused by power lines. These must be mapped, so that a first-order correction can be applied to readings in the affected areas. The magnitude of this task has not yet been evaluated fully, but the preliminary evidence indicates that it is by no means as formidable as some have been led to believe.

DATA EVALUATION

Examination of the details of the TD bias correction shows no systematic variation over the county. This indicates that the one correction does the job as well as possible - the propagation paths do not change enough as one moves from one end of Monroe County to the other to cause a significant difference in secondary phase correction. This is not surprising. The distance change is not great, 30 miles or so, and the ground conductivity in the area is relatively homogeneous and average in value.

CONCLUSIONS

The principal conclusion to be drawn from the preliminary calibration is that there is no significant loran grid warpage which cannot be removed by a simple bias correction, and once this is done, nearly all position data can be used without further correction. A few small areas of significant distortion can be either ignored or compensated for by further calibration.



STATE OF NEW YORK
FIGURE 1

OLD MYZ (9930)
 NEW XYZ (9960)

LONG ISLAND SOUND
 ATLANTIC OCEAN

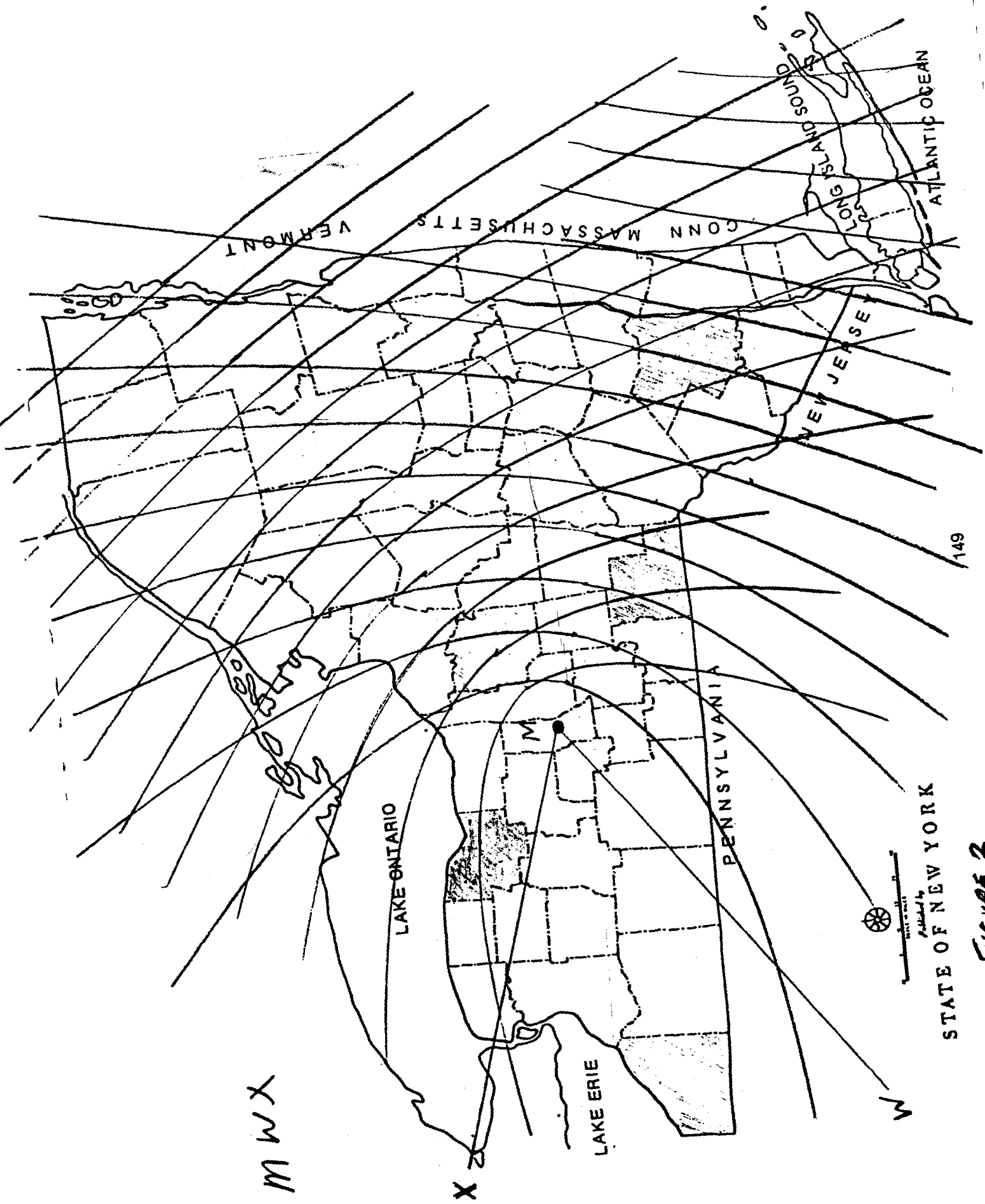
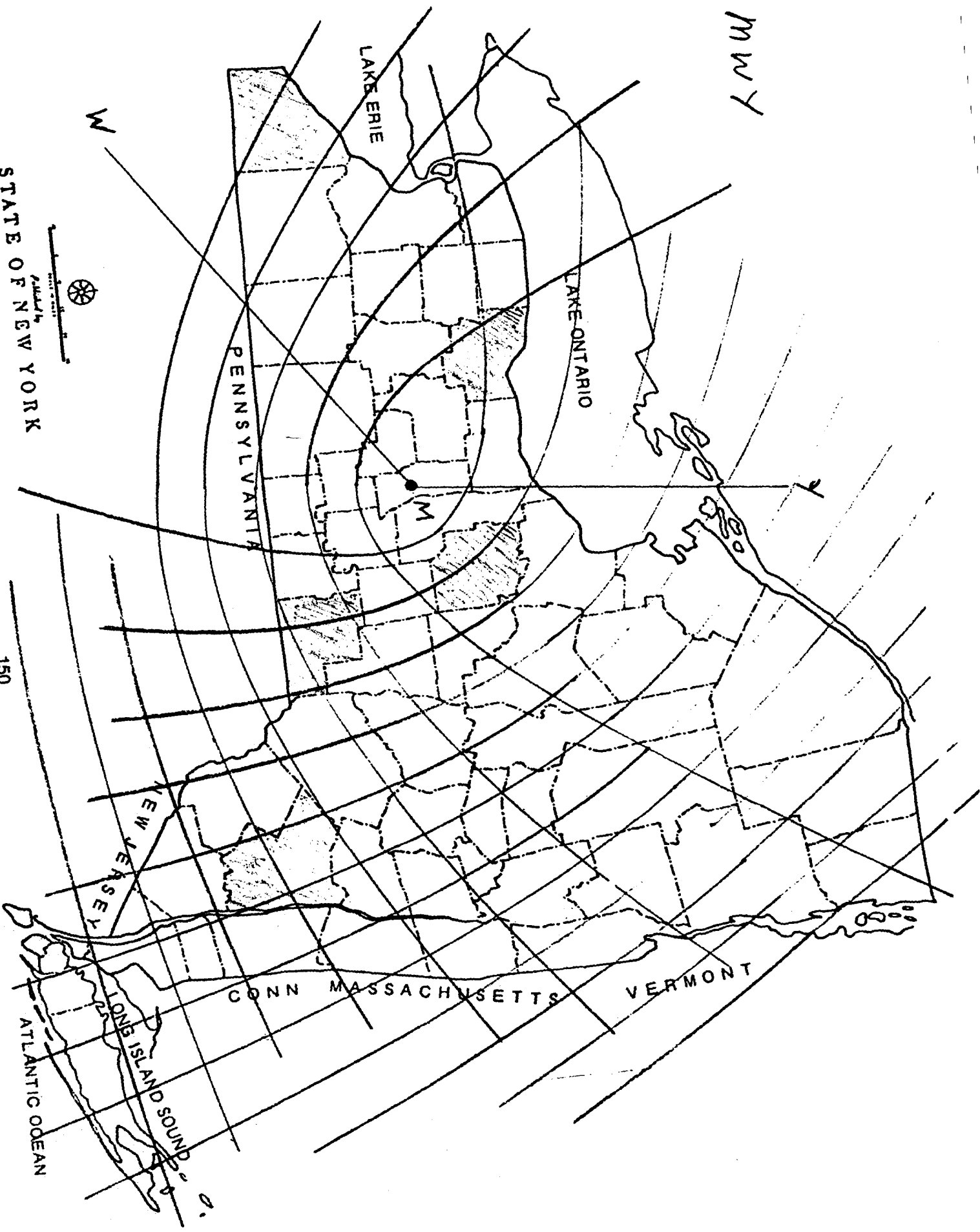


FIGURE 2

MWY



STATE OF NEW YORK

FIGURE 3

150

CONN MASSACHUSETTS VERMONT

N

E

LAKE ERIE

LAKE ONTARIO

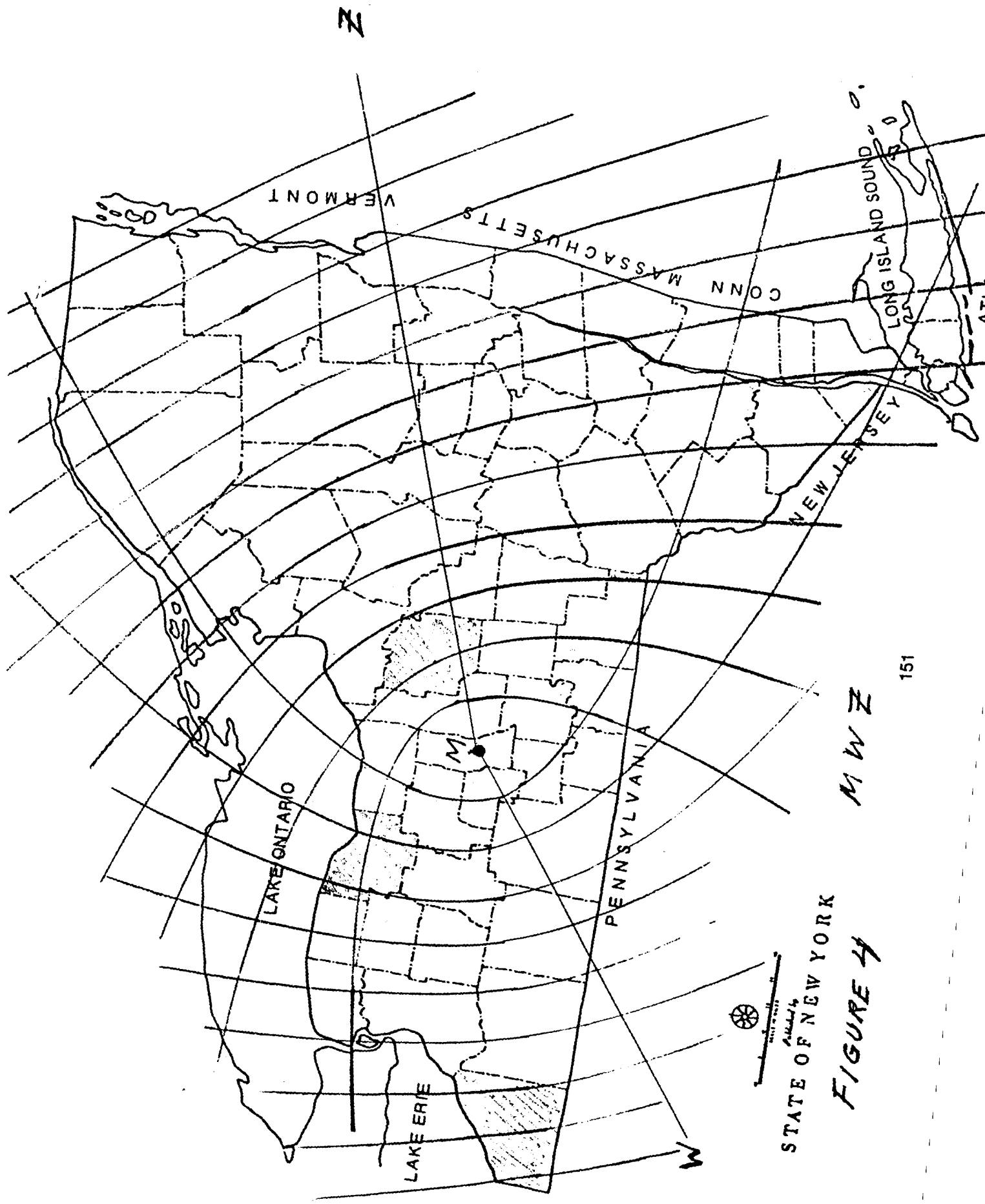
PENNSYLVANIA

NEW JERSEY

LONG ISLAND SOUND

ATLANTIC OCEAN

M



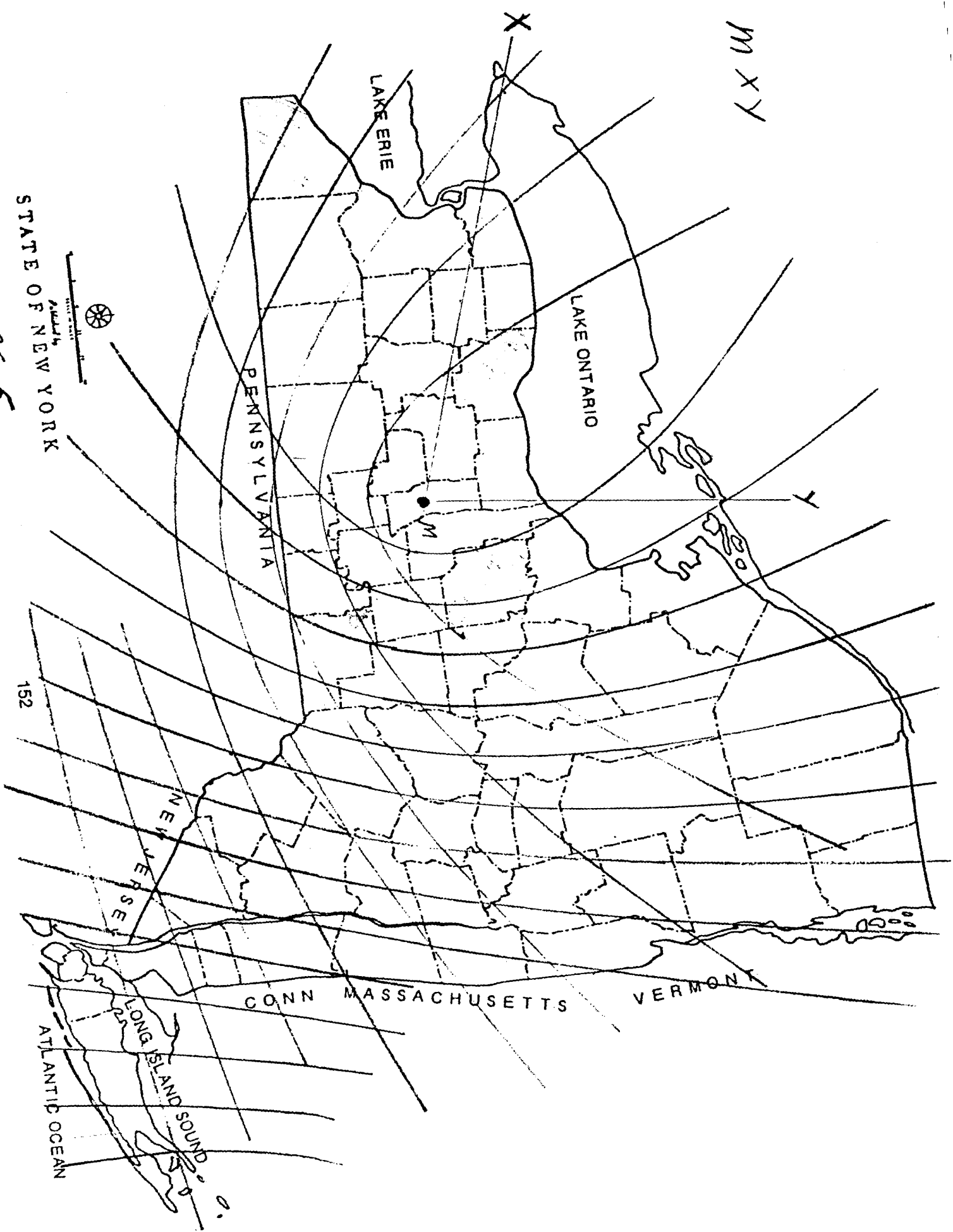
STATE OF NEW YORK

FIGURE 4

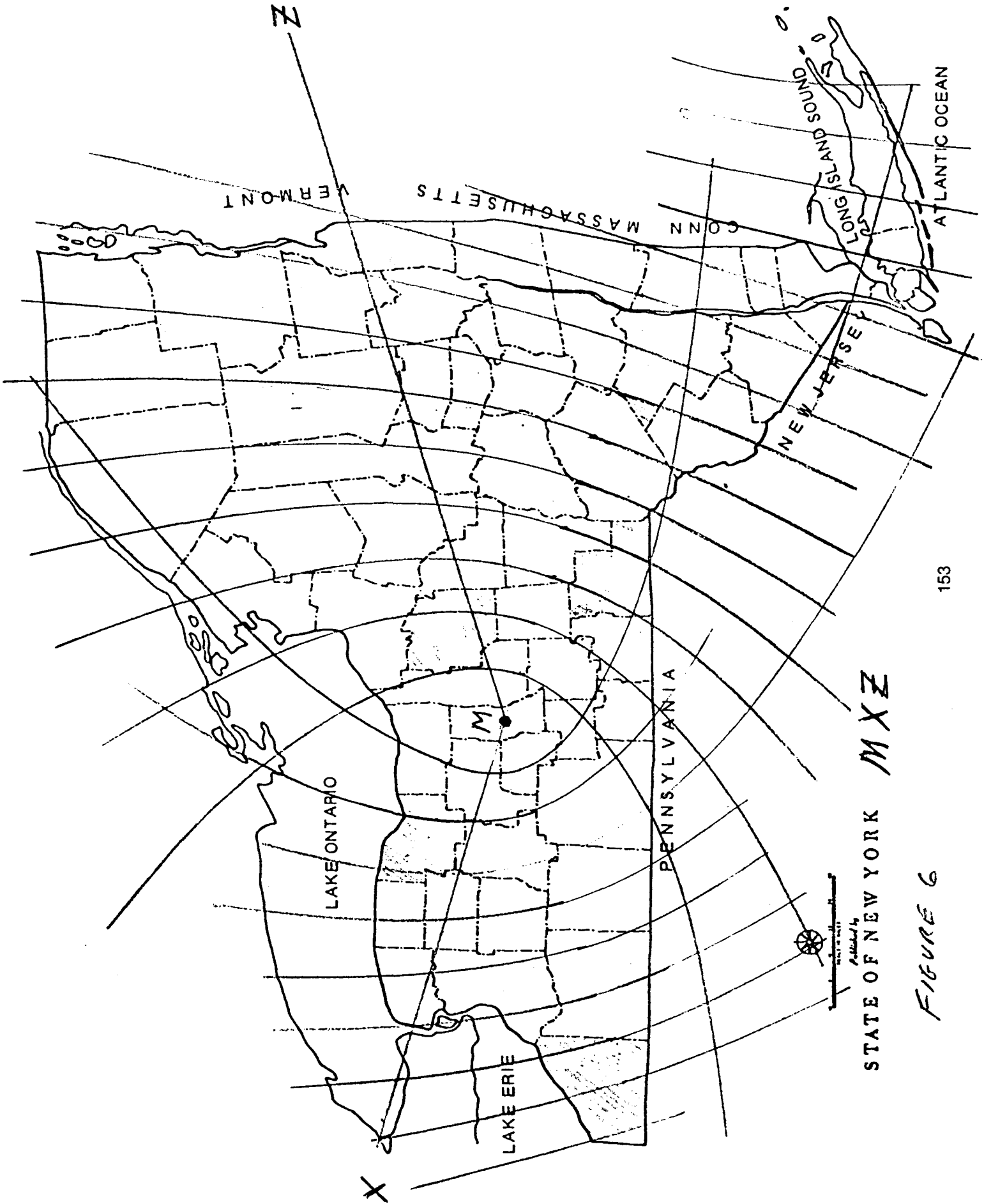
M W Z

FIGURE 5

STATE OF NEW YORK
Assembled by

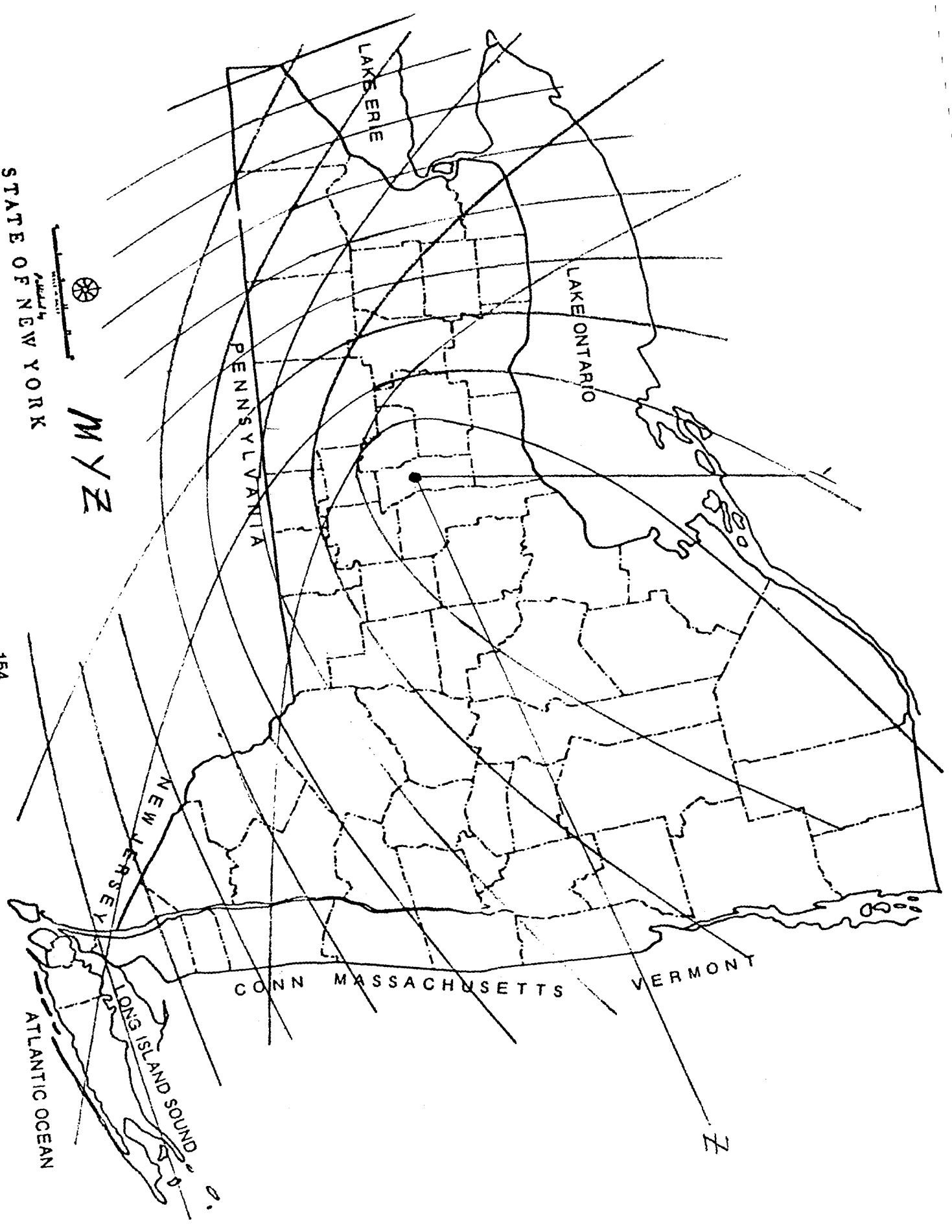


152



STATE OF NEW YORK *MXZ*

FIGURE 6



STATE OF NEW YORK

FIGURE 7

M Y Z

154

Z

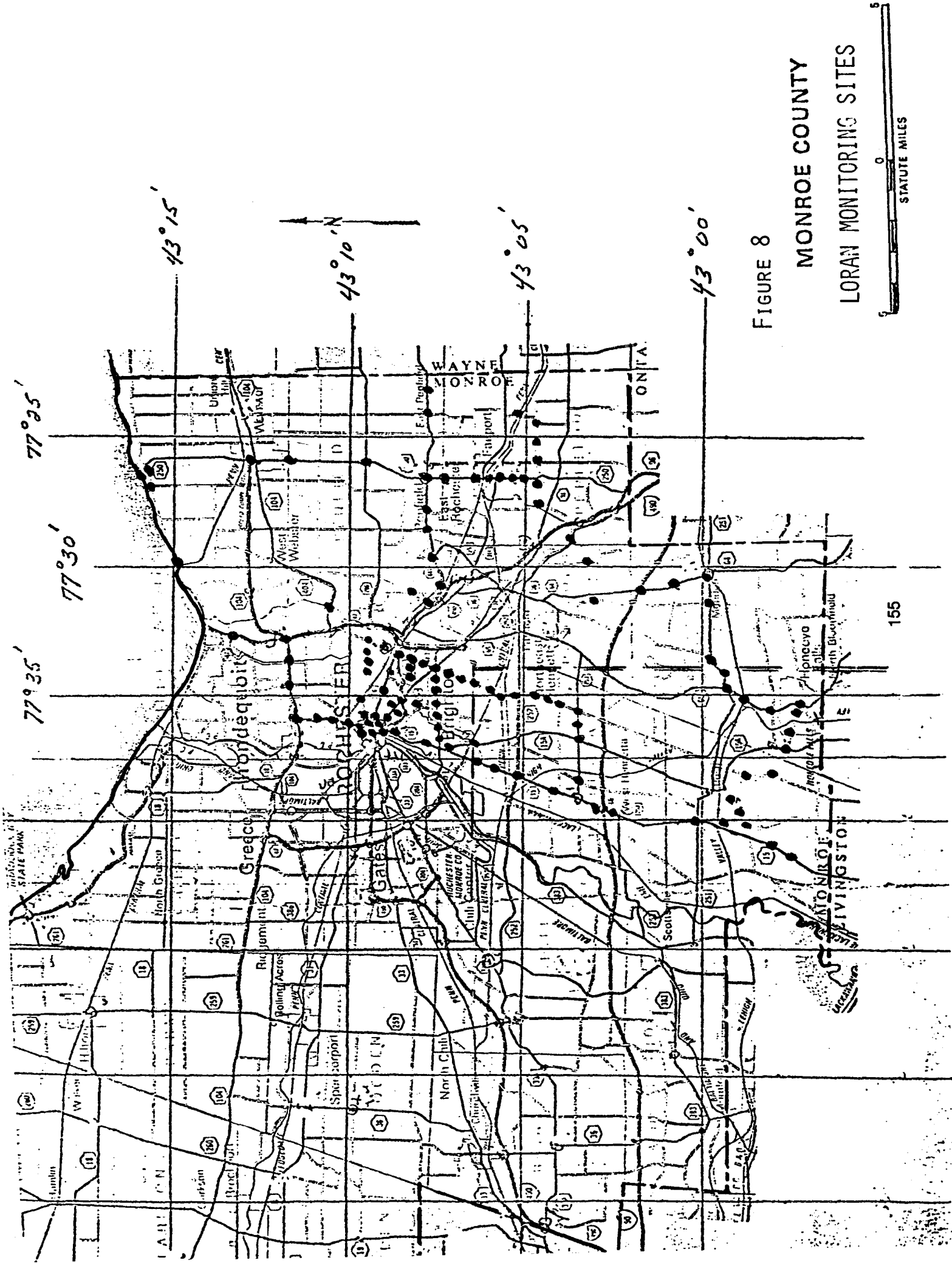
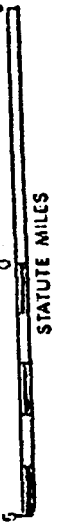


FIGURE 8

MONROE COUNTY
LORAN MONITORING SITES



LORAN-FIX ACCURACY
 EASTERN MONROE COUNTY
 LAT/LON CORRECTED

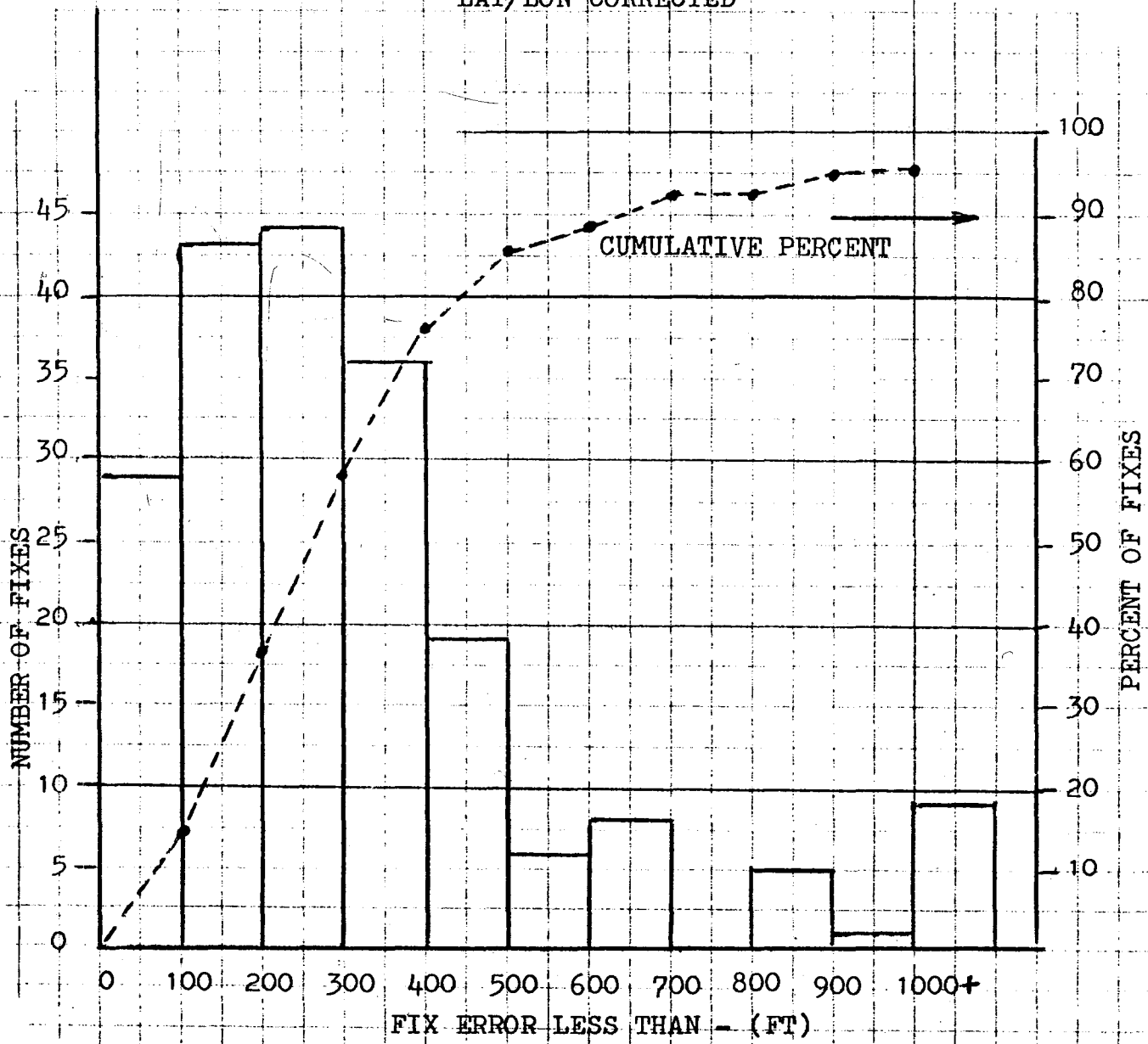


FIGURE 9

LORAN FIX ACCURACY
 EASTERN MONROE COUNTY
 TD CORRECTED

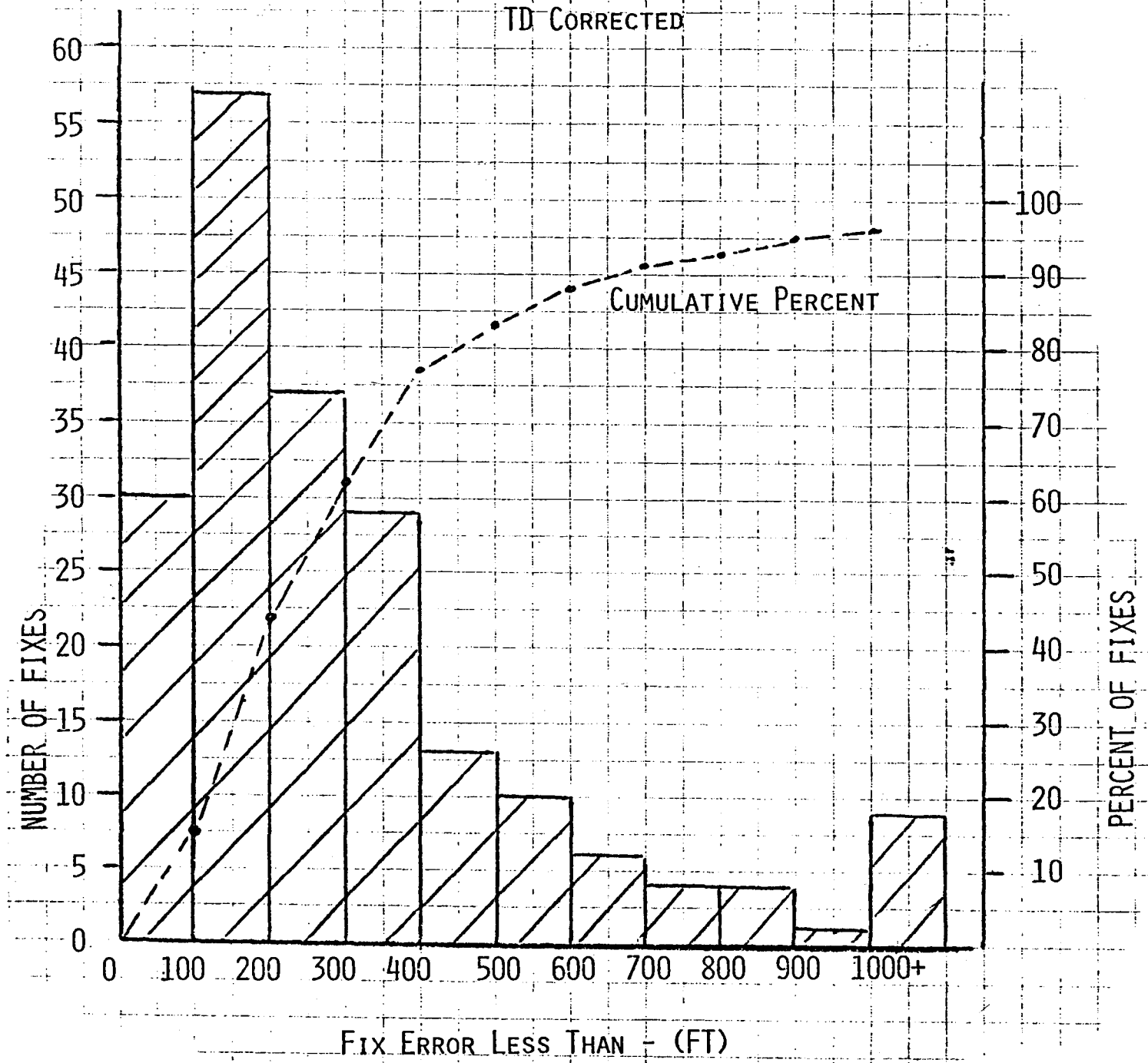


FIGURE 10

CONVENTION SCENE AND AWARDS



BAHAR UTTAM PRESENTS THE PRESIDENT'S AWARD TO CAPT DON FELDMAN.



LLOYD HIGGINBOTHAM RECEIVING THE OUTSTANDING SERVICE AWARD FOR HIS WORK AS CHAIRMAN OF THE 1979 WGA CONVENTION.



SPEAKER'S BREAKFAST WAS SERIOUS BUSINESS FOR HONKERS AMBROSINO, BERTSCHE, SCHROEDER, McCONKEY, AND HOPKINS.



LUNCHEON SPEAKER RADM RICHARD BAUMAN SHARING A JOKE WITH KARL SCHROEDER AND JOHN HOPKINS.



THE ORIGINAL LORAN MAN, JACK PIERCE, ADDRESSED US AT THE BANQUET.



WALT DEAN RECEIVES THE MEDAL OF MERIT FROM BAHAR UTTAM.



THE BEST PAPER AWARD FOR 1979 WENT TO JACK LIGON AND C.R. EDWARDS.



LCDR RON FRAZIER PREPARES HIS SESSION NOTES WITH KIYOSHI TAMURA AND KIYOHICO TATEBAYASHI.

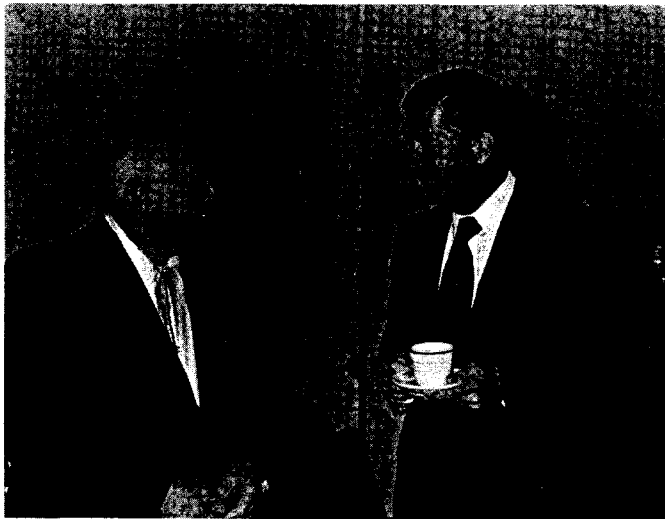


— AND DANCING ALL NIGHT WITH THE LIGHTS OF BOSTON IN THE BACKGROUND.

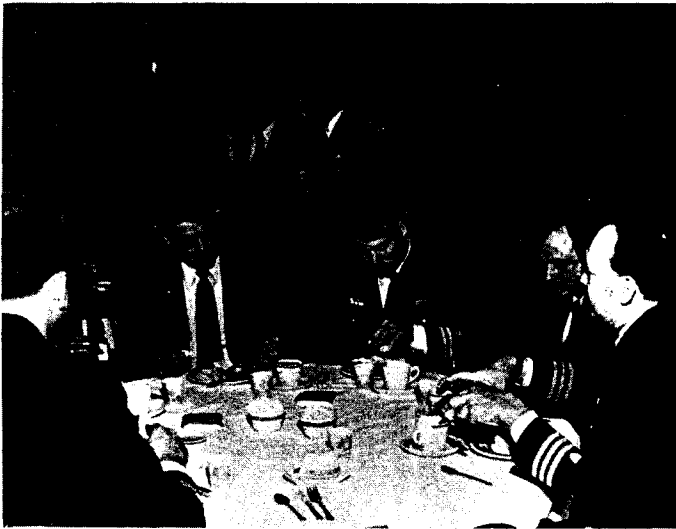


CONVENTION CHAIRMAN BILL RICE DOING HIS THING.

BAHAR UTTAM RECEIVED THE OUTSTANDING SERVICE AWARD FROM THE NEW PRESIDENT BARNEY AMBROSINO.



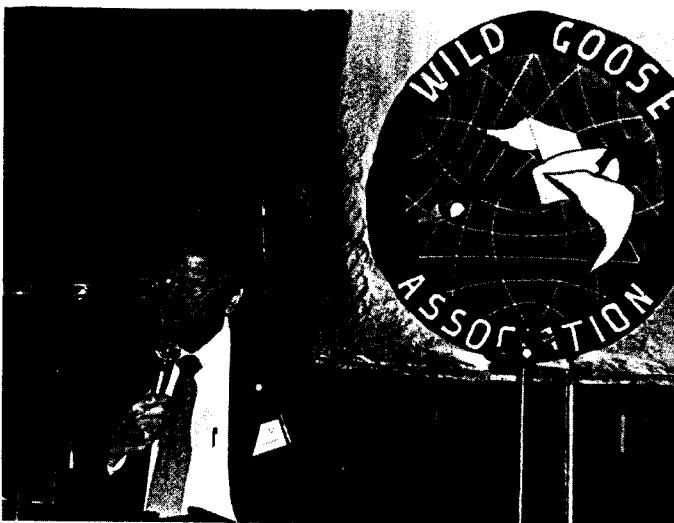
HAROLD DAHL AND JOHN HOPKINS ENJOY A CHAT.



PAPER DISCUSSIONS AT BREAKFAST FOR CDR BILL MOONEY, LCDR RON FRAZIER, LT GEORGE GUNTHER, JACK LIGON, AND LT DICK SELLERS.



A SUMPTUOUS BANQUET MEAL IN ART-NOUVEAU SURROUNDINGS.



BARNEY AMBROSINO PERFORMS HIS FIRST OFFICIAL ACT AS THE NEW PRESIDENT.



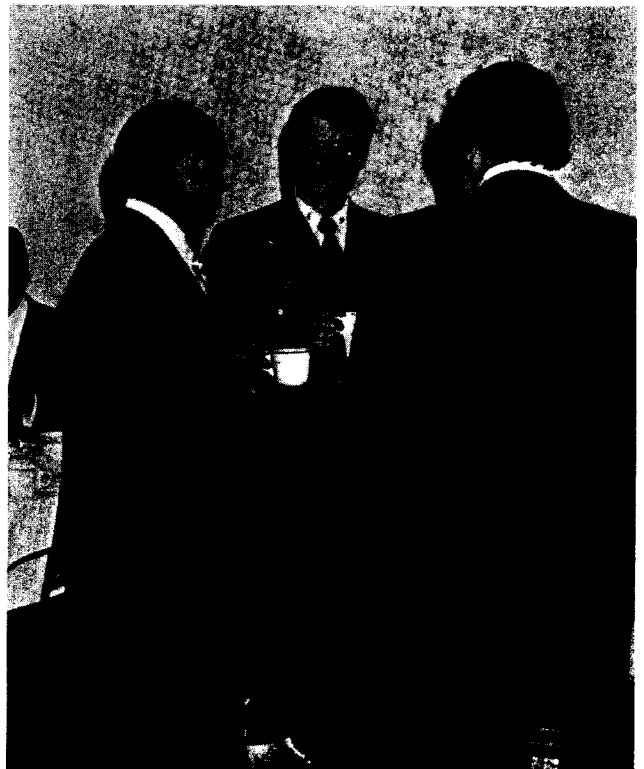
LCDR PERRY CAMPBELL AND CWO WALT GRAVES CARRY ON OLD COAST GUARD TRADITIONS.



GRACE AND JIM VAN ETTEN DANCE THE NIGHT AWAY.



PRESIDENT BAHAR UTTAM OPENS THE PROCEEDINGS.



ED McCONKEY, LCDR RON FRAZIER, AND BILL O'HALLORAN ENJOY COFFEE BEFORE SESSION OPENING.

REGISTERED ATTENDANCE
WILD GOOSE ASSOCIATION 9th ANNUAL TECHNICAL SYMPOSIUM
BOSTON, MASSACHUSETTS
OCTOBER 22-24, 1980

ATTENDEES

Members

Dalton Szelle
Sperry
Great Neck, NY 11020

Andrew Sedlock
USCG
USCGHQ
Washington, D.C.

W. Schorr
USCG
Lantarea, USCG
Governors Island, NY 10004

Mr. Rockwell
Sperry
Great Neck, NY 11020

W. H. Parker
Del Norte Technology
1100 Pamela
Eules, TX

Jack M. Ligon
USCG
5078 Coleridge Dr.
Fairfax, VA 22032

James D. Kelly
TASC
1 Jacob Way
Reading, MA 01867

Thomas J. Gilmartin
USCG EECEN
Wildwood, NJ 08260

Bruce Francis
Austron Navigation, Inc.
1800 Old Meadow Road, Ste 102
McLean, VA 22102

Richard Fitch
Spillsbury Comm. Systems
120 East Cordova St.
Vancouver, BC V6A1LI

Harald Dahl
Dahl Loran Service
46 N. Water St.
New Bedford, MA 02740

Robert Erikson
FAA Technology Center
Atlantic City, NJ

R. F. Dugan
USCG
CGR&D Center
Groton, CT 06340

Lt. T. M. Drown
USCG
1513 Perrell Lane
Bowie, MD 20716

LCDR Jim Doherty
USCG
Hq. (G-EEE)
Washington, D.C.

Lewis W. Campbell
ASEC
102 Hilldale Road
Ashland, MA 01721

Lester Brodeaur P.E.
Sanders Associates
95 Canal St.
Nashua, NH 03060
MS1-6244

James H. Black
Holbrook Industries, Inc.
600 River St.
Grand River, Ohio 44045

Walter J. Ambrose
Sperry Corp.
26 Dumbarton Drive
Huntington, NY

Walter N. Dean
Verdes Eng.
26619 Shorewood Road
Ranchos Palos Verdes, CA 90274

Peter H. Dana
Austron Navigation
8330 Burnet Road
Austin, TX

Mr. D. Feldman
USCG
Washington, D.C. 20593

F. W. Mooney
USCG
407A Governors Island
New York, NY 10004

C. J. Pannell
Sperry Gryoscope
9 Gates Avenue
Plainview, NY 11803

Don Naples
USCG
8714 Center Road
W. Springfield, VA 22152

S. P. Plusch
USCG
Washington, D.C.

Robert D. Bronson
Morrow Electronics, Inc.
4746 Ridge Dr. N.E.
Salem, Oregon 97303

Stephen Roth
Morrow Electronics
4740 Ridge Dr. NE
Salem, Oregon 97303

W. Polhemus
PAI
Cambridge, VT

Ken Foret
ONI
Box 3504
Horadan, CA

Bill O'Halloran
JAYCOR
300 Unicorn Park Drive
Woburn, MA 01801

Carter P. Pfallger
334-C Newton St.
Brookline, MA 02167

Jim Murdock
New York State DMV
Empire State Plaza
Albany, NY 12228

Ronald S. Warren
TASC
6 Jacob Way
Reading, MA 01864

Aylmre R. Trivers
USCG
17 Green Valley
East Lyme, Ct 06333

Jimmie L. Toms
Austron Navigation, Inc.
1800 Old Meadow Road #102
McLean, VA 22102

Mr. William F. Rice
ITT AVIONICS DIV.
54 Middlesex Turnpike
Bedford, MA 01730

Mr. J. VanEtten
ITT AVIONICS DIV.
390 Washington Avenue
Nutley, NJ 07110

Mr. Vernon L. Johnson
ITT AVIONICS DIV.
500 Washington Avenue
Nutley, NJ 07110

David H. Amos
USCG
67 Storybrook Road
Westford, MA 01886

William J. Becker
TRACOR, Inc.
1601 Research Blvd.
Rockville, MD 20850

Mr. B. Ambroseno
EPSCO
411 Providence Hwy.
Westwood, MA 02890

Mr. Garry Perchik
ITT AVIONICS DIV.
390 Washington Avenue
Nutley, NJ 07110

Barry J. Irwin
US Geological Survey
53 Eel River Road
E. Falmouth, MA 02536

Karl R. Schroeder
USCG
USCG Headquarters G-DST-1
Washington, D.C. 20593

Robert W. Merriam
Merriam Instruments Inc.
697 Tillinghast Road
E. Greenwich, RI 02818

J. F. Roeber
Commandant (E-DST-1)
USCG
Washington, D.C. 20593

Frederick H. Raab
Green Mountain Radio Research Co.
240 Staniford Rd.
Burlington, VT 05401

Daniel Blitz
Sanders Associates, Inc.
Nashua, NH 03061

Harold O. Holland
HWH Electronics
4215 Gulf Blvd.
St. Pete Beach, Florida 33706

W. F. Heathcock
Gould Inc.
2908 Cullen St.
Ft. Worth, TX 76107

CDR H. T. Sherman
USCG
Coast Guard Pacific Area (PTL)
630 Sansone St.
San Francisco, CA 94126

Gary Burrell
King Radio Corp.
400 N. Rogers Road
Olathe, Kansas 66062

Gene Grillot
King Radio Corp.
400 N. Rogers Road
Olathe, Kansas 66062

John Burns
Raytheon Marine Co.
676 Island Pond Road
Manchester, NH 03103

Mr. R. A. Vanina
International Navigation
Suite 532 Bowen Building
815 15th St. NW
Washington, D.C. 20005

Billy J. Watkins
Watkins Associates
Box 205
N. Dayton Station
Dayton, Ohio 45404

John M. Beukers
Beukers Labs.
Flowerfield Building #7
St. James, NY 11780

Capt. Jon C. Uithol
USCG
2100 2nd St. S.W.
Washington, D.C. 20593

Jerry Setliff
Texas Instruments
Box 225080 MS 3107
Dallas, TX 75266

Roger W. Hassard
USCG Activities Europe
Box 50
FPO NY, NY 09510

R. E. Burke, Jr.
USCG
Box 50 FPO
NY, NY 09510

David H. Gray
Canadian Hydrographic Service
605 Booth St.
Ottawa, K1A056 Canada

W. Kohl
USCG
4313 Southwood Dr.
Alexandria, VA 22309

L. Higginbotham
4 Townsend Road
Acton, MA 01720

Robert L. Frank
16500 N. Park Drive
Southfield, MI 48075

Mr. Roland A. Moody
MITRE Corp.
Box 208
Bedford, MA 01730

Johnnie Walker
E-Systems Inc.
9 Meriam St.
Suite 22
Lexington, MA 02173

Gordon Shillito
USCG EELEN
Wildwood, NJ 08260

Lindon U. Cockroft
Wild Goose Assn.
12819 Belhurst Lane
Bowie, MD 20715

Capt. W. M. Flanders
5 Abbott Bridge Drive
Andover, MA 01810

George T. Gunther
USCG
USCG EECEN
Wildwood, NJ 08260

Bahar J. Uttam
JAYCOR
300 Unicorn Park Drive
Woburn, MA 01801

Ronald Frazier
USCG
G-EEE
2100 2nd St. S.W.
Washington, D.C. 20593

Mr. J. Kaub
Teledyne Systems Company
19601 Nordhoff St.
Northridge, CA 91324

L. Cortland
Teledyne Systems Company
19601 Nordhoff St.
Northridge, CA 91324

Mr. E. J. Hird
DECCA NAVIGATION SYSTEMS
8841 Monard Drive
Silver Springs, MD 20910

Mr. R. H. Griffith
Hartman Systems
360 Wolf Hill Road
Huntington Sta. NY 11746

Mr. A. H. Goldman
Hartman Systems
360 Wolf Hill Road
Huntington Station, NY 11746

P. F. Barry
Hartman Systems
360 Wolf Hill Road
Huntington Station, NY 11746

Mr. J. A. Regan
Sperry
1164th St.
Garden City, NY 11530

Mr. P. D. Abranson
DOT
TSC
Kendall Square
Cambridge, MA 02142

Maurice J. Moroney
DOT-TSC
Kendall Square
Cambridge, MA 02142

Mr. G. Haroules
DOT-TSC
Kendall Square
Cambridge, MA 02142

Mr. Franklin MacKenzie
DOT-TSC
Kendall Square
Cambridge, MA 02142

Mr. William Wade
DOT-TSC
Kendall Square
Cambridge, MA 02142

Mr. C. Duncombe
DOT-TSC
Kendall Square
Cambridge, MA 02142

Mr. Joseph Lovecchio
DOT-TSC
Kendall Square
Cambridge, MA 02142

Mr. Carl Andren
DECA Navigation
8841 Monard Drive
Silver Springs, MD 20910

R. Duane
DECA Navigation
8841 Monard Drive
Silver Springs, MD 20910

Mr. J. Flynn
ADL
54 Middlesex Turnpike
Bedford, MA 01730

NON-MEMBERS

Barry Kane
US Coast Guard
New London, CT

Walter Graves
USCG
c/o Commander (Atl), USCG
Atlantia Area
Governors Island, NY 10004

Ed Goudie
Canadian Coast Guard
St. Anthony, NFLD
Canada

LCDR Bob Danforth
USCG
Commander (G-EEE-4)
Washington, D.C. 20593

John J. Anthony
USCG
Washington, D.C.

Mr. James M. Foltz
TASC
6 Jacob Way
Reading, MA 01864

Mr. Jim McCullough
Woods Hole Oceanographic
Woods Hole, MA 02543

Capt. J. N. MacDonald
USCG
Atlantic Area
Governors Island, NY 10004

Mr. Robert M. Bowles
US Geological Survey
Quissett Campus
Woods Hole, MA 02543

Mr. Jim Dodd
US Geological Survey
Bldg. B Quissett Campus
Woods Hole, MA 02543

A. W. Marshal
ONI
Box 23504
New Orleans, LA 70183

D. G. Currier
c/o USCG
Electronics Eng. Center
Wildwood, NJ 08260

Gregg Keary
USCG
Electronic Engineering Center
Wildwood, NJ 08260

Robert J. Weaver
USCG
USCG Loran-C Station
Romulus, NY 14541

Burt Thomas
USCG
Atlantic
Governors Island, NY 10004

Walter E. Tanner
29 Barney Hill Road
Wayland, MA 01778

Donald E. Meyers
Megapulse Inc.
8 Preston Ct.
Bedford, MA 01730

Erishman Natarjan
MIT
Cambridge, MA

William R. Bertsche
Electech Associates
Box 178
North Stonington, CT 06359

NEW MEMBERS

-7-

Edwin D. McConkey
Systems Control Inc. (Vt.)
2326 S. Congress Avenue
West Palm Beach, Florida 33406

Paul Arnstein
USCG
Comdt. (G-EEE)
Washington, D.C. 20593

Mr. William A. Meiman, Jr.
USCG
2100 2nd St. S.W.
Washington, D.C. 20593

Lt. William R. Phillips
USCG
Headquarters COMDT (G-EEE-4TP64)
Washington, D.C. 20593

Ronald Frazier
USCG
G-EEE/4TP64
2100 2nd St. S.W.
Washington, D.C. 20593

Paul Miller
USCG
USCG EECEN
Wildwood, NJ 08260

Richard L. Ryan
USCG
Electronics Eng. Center
Wildwood, NJ 08260

Kiyoshi Tamura
Japan Radio Co.
5-1-1 Shimorenjaku
Mitakashi, Tokyo, Japan

Kiyohiko Tatebayashi
Japan Radio Co. Ltd.
5-1-1 Shimoenjaku
Mitakashi, Tokyo Japan

Phil Llewellyn
Raytheon Marine Co.
676 Island Pond Road
Manchester, NH 03103

Robert Schelllhase
USCG
G-NRN-1
Washington, D.C. 20593

Larry E. Sartin
ASEC
11 Cummings Road
Merrimack, NH 03054

Gary Running
Canadian Coast Guard
Tower A
Place De Ville
Ottawa Canada

Robert H. Reust
USCG R&D Center
Avery Point
Groton, CT 06340

John F. Pillsbury
USCG
971 Carol Avenue
Capt May, NJ 08204

Stan Lehman
USCG
Box 3-5000
Juneau, AK

Ronald D. Lapp
USCG
42 Woodridge Circle
Gales Ferry, CT 06335

Dr. J. B. Langley
ADL
Acorn Park
Cambridge, MA 02140

Robert C. Imler
USCG
Electronics Engr. Center
Wildwood, NJ 08260

Leon DePalma
TASC
One Jacob Way
Reading, Mass. 01867

Everett J. Anderson
USCG
R&D Center
Avery Point
Groton, CT 06430

Charles Baltzer
Austron Navigation Inc.
1801 Fountain Ridge Road
Chapel Hill, NC 27514

P. W. Campbell
USCG
c/o Commander (ATL)
Atlantic Area
Governors Island
New York, NY 10004

Gene Wong
MITRE Corp.
1820 Dolly Madison Blvd.
McLean, VA

Richard J. Sellers
117 W. Hollywood Avenue
Wildwood Crest, NJ 08261

W. E. Hoover
1 Haystack Lane
Sandwich, MA 02563

Hugh F. Rice
Sperry
Marcus Avenue
Great Neck, NY

G. R. Goodman
USCG
Honolulu, Hawaii

Paul M. Creamer
TASC
1 Jacob Way, Reading, MA 01864

Carter P. Pfallzer
MIT
334-C Newton St.
Brookline, MA 02167

Eugene Waldendziewicz
Digital Strategies
17 Wildwood St.
Burlington, MA 01803

John Canniff
DOT/TSC
Kendall Square
Cambridge, MA 02142

Mr. John Gakis
DOT/TSC
Kendall Square
Cambridge, MA 02142

Anthony Passera
DOT/TSC
Kendall Square
Cambridge, MA 02142

Mr. John Morris
DOT/TSC
Kendall Square
Cambridge, MA 02142

Peter Mauro
DOT/TSC
Kendall Square
Cambridge, MA 02142

RENEWALS

Ed Bregstrone
USCG
2607 Central Avenue
Alexandria, VA 22302

CDR Dave Carter
USCG
DOT/NHTSA (NTS-13)
Washington, D.C. 20590

S. N. Samaddar
USCG
2100 2nd St. S.W.
Washington, D.C. 20593

